DESIGN, SYNTHESIS AND CHARACTERIZATION OF HYBRID MATERIALS PRODUCED BY GRAFTING OR MIXING HYBRID POLYHEDRAL OLIGOMERIC SILSELSQUIOXANES ONTO NATURAL RUBBER AND STARCH FILMS

A thesis submitted in fulfilment of the requirements for the degree of Doctor of Philosophy

Isaac Rubens Martinez Pardo

M. Eng. (PolyEng) Honours
The National Autonomous University of Mexico

School of Science

College of Science, Engineering and Health

RMIT University
Melbourne, Australia

December 2018

DECLARATION

I certify that except where due acknowledgement has been made, the work is that of the author alone; the work has not been submitted previously, in whole or in part, to qualify for any other academic award; the content of the thesis is the result of work which has been carried out since the official commencement date of the approved research program; any editorial work, paid or unpaid, carried out by a third party is acknowledged; and, ethics procedures and guidelines have been followed.

The work described in this research project was carried out in the School of Applied Sciences, RMIT University since the official date of commencement of the program.

Isaac Rubens Martínez Pardo December 2018

ACKNOWLEDGMENTS

Thanks to my beautiful wife Rocío, sweet love of my life. Thank you for joining me in this adventure of life, thanks for all the happiness, support, trust, patience and love.

I am thankful to the National Council of Science and Technology of Mexico (Consejo Nacional de Ciencia y Tecnología, CONACyT) for trust, support and sponsoring my Ph.D. studies.

Thanks to Emeritus Professor Dr. Robert Arthur Shanks for gave me the opportunity to study at RMIT, for gave me all his time, guidance, teachings, life model and great talks.

I am thankful to Professor Benu Adhikari, for all the academic support, his personal advice, his trust and help to develop my tutoring skills.

Thanks to Dr Raju Adhikari, for all the support, trust, friendship and the opportunity to collaborate with him.

Thanks to my father Isaac and mother in law Teresa, where many others never trusted on us you always remain unconditional. For all your love, advise and patience, I thank both of you from the bottom of my heart.

Thanks to my friends and colleagues for all the support and friendship, Ing Kong, Firoozeh Pourjavaheri, Farzad Mohaddes, Michael Czajka, Bo Wang. Specially to Tai Ling and Nabeen Dulal we lived together great adventures during the Ph.D.

TABLE OF CONTENTS

COVER……I

DECLARATION…..……...II

ACKNOWLEDGMENTS ……III

TABLE OF CONTENTS ……...…….……IV

PUBLICATIONS….……...……VIII

LIST OF FIGURES……...…….……IX

LIST OF TABLES ……..……XIV

GENERAL ABBREVIATIONS AND NOMENCLATURE…….....XV

ABSTRACT...……1

1 INTRODUCTION 3

1.1 Background 3
1.2 Aim 5
1.3 Research hypothesis 5
1.4 Research questions 6
1.5 Objectives 6
1.6 Contributing to or advancing the body of knowledge 7
1.7 Outline of the thesis 7
1.8 References 8

2 LITERATURE REVIEW 10

2.1 Starch 10
2.1.1 Starch structure 10
2.1.2 Thermoplastic starch films 11
2.1.3 Plasticisation of starch 13
2.1.4 Starch retrogradation 13
2.2 Natural Rubber 14
2.2.1 Epoxidized natural rubber 18
2.3 Polyhedral oligomeric silsesquioxanes. 19
2.3.1 POS synthesis 20
2.3.2 Mono-substituted POS 21
2.3.3 Single corner incomplete POS and corner-capping 21
2.4 Polyhedral oligomeric silsesquioxane into starch and natural rubber in the literature 22
2.4.1 POS with starch 23

2.4.2 POS with Natural rubber or ENR50 24
2.4.3 Conclusion of polyhedral oligomeric silsesquioxane into starch and natural rubber in the literature 26
2.5 References 26
3 CHARACTERISATION TECHNIQUES 31
3.1 Fourier-transform infrared spectroscopy 31
3.2 Halogen moisture analyser 32
3.3 Contact angle goniometer, static sessile drop method 33
3.4 Universal testing machine 35
3.5 Dynamic mechanical analysis 37
3.6 Differential Scanning Calorimeter 41
3.7 Molecular modelling 42
3.7.1 Topology method Synthia. 42
3.7.2 Molecular mechanics/dynamics 46
3.8 References 51
4 THERMOPLASTIC STARCH NANOHYBRID FILMS MODIFIED WITH POS 53
4.1 Introduction 53
4.2 Materials 54
4.3 Methods 55
4.3.1 Functionalization of nanohybrid POS 55
4.3.2 Identification of functional and reactive groups 56
4.3.3 Preparation of starch-plasticizer, starch-plasticizer-nano additive slurries 56
4.3.4 Determination of moisture content 58
4.3.5 Determination of wettability kinetics 58
4.3.6 Determination of mechanical properties 58
4.3.7 Determination of glass transition temperature by dynamic mechanical analysis 58
4.3.8 Statistical analysis 59
4.4 Results and Discussion 59
4.4.1 Identification of functional and reactive groups and indication of reaction completion 60
4.4.2 Moisture content in the films 61
4.4.3 Contact angle of the films 61
4.4.4 Tensile stress–strain behaviour of the films 63
4.4.5 Thermomechanical transition of the films 65
4.5 Conclusion 66
4.6 References 67

5 RHEOLOGICAL CHARACTERIZATION OF THERMOPLASTIC STARCH FILMS MODIFIED WITH POS 68

5.1 Introduction 68
5.2 Material and methods 71
5.2.1 Materials 71
5.2.2 Preparation of starch films and functionalization of POS nanohybrids 71
5.2.3 Determination of dynamic mechanical properties 72
5.2.4 Main differences between the proposed method and traditional methods. 77
5.2.5 Generalized time temperature superposition models 78
5.3 Results and Discussion 79
5.4 Conclusions 84
5.5 References 85
6 MOLECULAR MODELING OF POS-NATURAL RUBBER AND ENR50 87

6.1 Introduction 87
6.2 Methods 88
6.2.1 Topology method 88
6.2.2 Modelling size selection 88
6.2.3 Geometry optimisation of repeating units and molecules 89
6.2.4 Polymers and amorphous cell constructions 90
6.2.5 Relaxation of the amorphous cells 91
6.2.6 Mechanical Properties Calculation 92
6.2.7 Estimation of the glass transition temperature and melting temperature 92
6.2.8 Estimation of the Coefficient of Thermal Expansion 97
6.3 Results and Discussion 97
6.3.1 Comparison of reported properties, amorphous cells and the group contribution method 100
6.3.2 T_g comparison of amorphous cell and group contribution method 102
6.4 Conclusions 102
6.5 References 103
7 SYNTHESIS AND CHARACTERIZATION OF POS-ENR50 HYBRID 105

7.1 Introduction 105
7.2 Materials and Methods 106
7.2.1 Materials 106
7.2.2 Synthesis and characterisation of NR, ENR50 and ENR50 hybrid 106
7.2.3 Epoxidation of natural rubber 108
7.3 Results and Discussion 108

7.3.1 Confirmation of reaction through FTIR 108
7.3.2 Thermal transitions estimated by DSC 109
7.3.3 Thermo mechanical characteristics obtained by DMA. 110
7.4 Conclusions 115
7.5 References 115
8 CONCLUSIONS, REMARKS AND FUTURE WORK 117
8.1 Conclusions and remarks 117
8.2 Future work 119
9 APPENDIX 121
9.1 Thermoplastic starch-nanohybrid films with polyhedral oligomeric silsesquioxane 121
9.2 Natural rubber with polyhedral oligomeric silsesquioxane, nanocomposites, and hybrids compared by molecular modeling 129
9.2.1 Cover 129
9.2.2 Article 130

PUBLICATIONS

Martinez-Pardo, I., Shanks, R.A., Adhikari, B. and Adhikari, R., 2017. Thermoplastic starch-nanohybrid films with polyhedral oligomeric silsesquioxane. *Carbohydrate polymers*, 173, pp.170-177. See in appendix 9.1.

Martinez-Pardo, I., Shanks, R.A., Adhikari, R. and Adhikari, B., 2018. Natural Rubber with Polyhedral Oligomeric Silsesquioxane, Nanocomposites, and Hybrids Compared by Molecular Modeling. *Macromolecular Theory and Simulations*, p.1800026. See in appendix 9.2.

Pourjavaheri, F., Jones, O., **Martinez Pardo, I.**, Sherkat, F., Gupta, A. and Shanks, R., 2017. Keratin bio-composites with polysiloxane thermoplastic polyurethane. In *75th Annual Technical Conference of the Society of Plastics Engineers* (pp. 672-678). Society of Plastics Engineers.

Dulal, N., Shanks, R., Gengenbach, T., Gill, H., Chalmers, D., Adhikari, B. and **Martinez, I.P.**, 2017. Slip-additive migration, surface morphology, and performance on injection moulded high-density polyethylene closures. *Journal of colloid and interface science*, *505*, pp.537-545.

Pourjavaheri, F., Jones, O.A., Czajka, M., **Martinez-Pardo, I.**, Blanch, E.W. and Shanks, R.A., 2018. Design and characterization of sustainable bio-composites from waste chicken feather keratin and thermoplastic polyurethane. *Polymer Composites*, *39*, pp.E620-E632.

Shanks, R.A. and **Pardo, I.R.**, 2018. Cellulose Solubility, Gelation, and Absorbency Compared with Designed Synthetic Polymers. *Cellulose-Based Superabsorbent Hydrogels*, pp.1-26.

LIST OF FIGURES

Figure 1.1 Stress-strain behaviour of ceramic, organic, polymer and hybrid materials..... 3

Figure 1.2 The increase of surface area of a cubic substance with one millilitre (mL) volume when is divided in cubes with side divisions from 1000 nanometre to 1..... 4

Figure 2.1 Amylose and amylopectin structures..... 10

Figure 2.2 Starch organization architecture in scales of orders of tens [1]..... 11

Figure 2.3 Microscopic picture of soluble corn starch granules under polarized light. The Maltese cross is an indication of crystaline structure 12

Figure 2.4 Isomers of poly(isoprene)..... 15

Figure 2.5 Structure of two polymeric chains of natural rubber after vulcanization with sulphure 16

Figure 2.6 NR epoxidation reaction..... 18

Figure 2.7 ENR50 a) random structure b) Van der Waals surface indicating H-bonding acptor/donator sites 18

Figure 2.8 Comparation between a) buckminsterfullerene, b) Octa methyl POS and c) adamantane. Carbon, oxigen and silicon atoms are grey, red and yellow respectible, the The Van der Waals surface is colored to give sence of deep 20

Figure 2.9 Hydrolytic condensation of RSiY3 to produce POS 21

Figure 2.10 Synthesis of single incomplete corner POS..... 21

Figure 2.11. Functionalization of an incomplete POS with (3-aminopropyl) triethoxysilane (APTES) 22

Figure 2.12 Schematic diagram of the graphene oxide coupled with POS and used in a composite hydrogel with starch..... 23

Figure 2.13 Schematic representation of POSS starch grafting reaction 24

Figure 2.14 Schematic representation of the process to dispersed POS-rectorite hybrid into natural rubber. Tooked from Zhao [83] 25

Figure 2.15 Scheme of polyisoprene-like POS copolymer synthesis by ROMP. Took from Seurer [86] 25

Figure 3.1 Schematic representation of the seven principal steps in FTIR instrument measurement. Images adapted from a [1], b [2], c [3] d [4] and e [5] 31
Figure 3.2 Tension and flexion deformation of methylene group. The arrows indicate movements in the plane, plus and minus signs indicate movements perpendicular to the plane (up and down respectable). Figure adapted from Pardo [7] 32
Figure 3.3 Schematic representation of a halogen moisture analyser running at different stages of a test 33
Figure 3.4 Principal parameters of halogen moisture analyser changes over time 33
Figure 3.5 Young's equation parameters in a contact angle of a droplet on a solid surface 34
Figure 3.6 Goniometer simplified diagram 35
Figure 3.7 Picture of a universal testing machine 36
Figure 3.8 Example of uniaxial deformation of a cylinder due to a force F with initial length (L_0) 37
Figure 3.9 a) Stimulus-response sinusoidal curves of DMA test. b) Simple schematic of components of DMA instrument with cantilever testing geometry, adapted from Menard [13] 38
Figure 3.10 Representations of strain-stress behaviour of different materials a) elastic material, b) viscoelastic material and c) viscous material 38
Figure 3.11 Idealized DMA scan, took from Menard [17] 40
Figure 3.12 Key test modes, characterization and results of DMA, adapted from Kawak [18] 41
Figure 3.13 Schematic representation of a typical differential scanner calorimeter 42
Figure 3.14 Block diagram of power compensation DSC instrument, adapted from Höhne [20] 42
Figure 3.15 Schematic representation of connectivity indices calculations 45
Figure 3.16 Multi-scale theoretical and computational methods used for materials model development and computer simulations, took from Stan [23] 47
Figure 3.17 Schematic procedure of molecular mechanical molecular modelling 48
Figure 3.18 Different cells for a) crystalline isotactic styrene, b) amorphous styrene, c) crystalline poly(ethylene) and d) amorphous poly(ethylene) 49
Figure 3.19 Geometry optimization data change over steps for a) energy and b) its convergence parameters 50

Figure 3.20 Anneal dynamic data change over time for a) energy and b) cell length 51
Figure 4.1 Molecular illustrations of thermoplastic films, the surface is coloured accordin to its hydrogen bonding nature, green for acceptor, pink for donor and pure white for neither. a) molecules of starch, glycerol and water, b) Van der Waals surface of starch, glycerol and water, c) Van der Waals surface of POS, starch, glycerol and water. 54
Figure 4.2. Epoxy-POS functionalization reaction with either Erucamide or Jeffamine to produce POS nanohybrids 56
Figure 4.3 General schematic representation of thermoplastic starch film production after gelatinization 57
Figure 4.4 Hydrogen bonding receptor surface of molecules in the starch film systems, their Van der Waals surface coloured according to its hydrogen bonding nature, green for acceptor, pink for donor and pure white for neither 59
Figure 4.5 FTIR spectra of Eru-POS and Jeff-POSS and their precursors a) Jeff-POSS, b) Eru-POS, c) expanded details of Jeff-POSS and d) expanded details of Eru-POS 61
Figure 4.6 a) 10th order polynomial fitting of the average wettability profile of the films; the error bars represent the standard deviation and b) characterization of the initial and late behaviour of the control film by linear fitting 62
Figure 4.7 a) Stress-strain curves of starch–additive films b) expanded view of the NH_2-POS first offset yield 64
Figure 4.8 a) E', E'' and tan(δ) of Jeff-POS film. b) Schematic representation of the calculated T_g at different frequencies 66
Figure 5.1 Sequential shifting of selected isothermal modulus-versus-time curves of the control film, a) Initial experimental data T_r of 25 °C ($a_T = 1$); b) first shift below T_r, from left to right ($a_T > 1$); c) first shift above T_r from right to left ($a_T < 1$); d) consecutive shift below T_r; e) consecutive shift above the T_r; f) resulting master curve 73
Figure 5.2 a) example of fitting equivalent to a power law model of the control film; b) original area between fitting functions within the limits of the overlapping region and area optimization function; c) shift factor obtained for the control film at a reference temperature of 20 ˚C. Comparison between: d)

original isothermal modulus-versus-time curves from -100 ˚C to 93 ˚C and e) all the curves shifted throw 25 ˚C that construct a single master curve 75
Figure 5.3 a) calculation of T_g for the control film using tan(δ) at different frequency scans with polynomial fitting and base lines. Schematic aT modelling for b) WLF and c) Arrhenius equations .. 77
Figure 5.4 Schematic representation of generalised time-temperature superposition model for thermorheologically complex materials. 79
Figure 5.5 a) Schematic plot and equations used to model T_g, b) Predicted T_g at an expanded interval of frequencies and c) rubbery state temperature range 81
Figure 5.6 Master curves of the different films for the a) elastic modulus and b) viscous modulus. Resulting shift factors c) for the different films, d) comparison of the shift factors of the control film and models 82
Figure 6.1. Mechanical properties predicted by the group contribution method, a) NR, b) ENR50 and c) ENR50 reacted with 50 phr of POS 89
Figure 6.2 Extended simulation for the NRPhy01 density 93
Figure 6.3 Extended simulation for the NRPhy01 (time scale in $\log_{10}$) 94
Figure 6.4. Estimation of T_g, a) single temperature ρ_∞ calculation using the frames dynamic relaxation fitting an asymptotic function, b) estimation of T_g by solving the intersection of two fitting functions 94
Figure 6.5 Linear and quadratic curve fitting of a diagram density vs Temperature for a exemplified material 96
Figure 6.6 Linear and quadratic fitting comparation to determine a thermal transition in a diagram density vs temperature for natural rubber predicted by Synthia 96
Figure 6.7 Change due temperature of a) calculated volumes for NR, b) α_v for NR 97
Figure 6.8 a) to g) Topology method and amorphous cell calculated properties, h) difference of the properties with respect to the reported properties; all reported B, E, ρ, T_g, αv, ν and G for NR are found at [14][15][16]; the reported ENR50 ρ, T_g are found at [17][18][19] 101
Figure 6.9. NR temperature dependency of some topology method properties and density from AC102
Figure 7.1 Reaction between ENR50 and NH_2POS to produce the hybrid 107

Figure 7.2 Chemical reaction between NR and 3-chlorobenzene-1-carboperoxoic acid yielding ENR 108

Figure 7.3. Fourier transform infrared (FTIR) spectra of precursors (NH_2-POS and ENR50) and hybrid (product)..... 109

Figure 7.4. DSC thermograms of precursors and hybrid nano-composite materials 110

Figure 7.5 Tan(δ) DMA curve of NR (STR5L), ENR50 and Hybrid material. 111

Figure 7.6 Elastic modulus (E') for STR5L, ENR50 and the Hybrid. The blue dash line highlighted in yellow marks the ENR50 main thermo-mechanical characteristics of ENR50. 112

Figure 7.7 a) Characteristic β, α and rubbery plateaus comparison in $\log_{10}$ scale for all the materials and b) values of T_g and T_β from E' curves from DMA for all materials 113

Figure 7.8 The a) loss modulus (E") and b) complex modulus (E^*) of NR, ENR50 and their hybrid product 113

Figure 7.9 Scaled detailed comparation of the loss modulus (E'') of hybrid product to the storage modulus (E') of precursor materials (STR5L and ENR50) 114

Figure 7.10 Properties change due to the POS content 114

LIST OF TABLES

Table 2.1 Composition of fresh natural rubber latex. Adapted from Li [30] 14

Table 2.2 Epoxidation percentage versus glass transition temperature 18

Table 2.3 Keywords used in electronic databases 23

Table 3.1 Infrared band division recommended by international commission on illumination 31

Table 4.1 Film wettability (θc) and water resistance from 0 to 5 min. 63

Table 4.2 Tensile mechanical properties of films 64

Table 4.3 Thermo-mechanical transition temperatures of the films 66

Table 5.1 Dynamic mechanical properties of different films. Mean (standard deviation) 80

Table 5.2 WLF constants, f and α at the T_g and Tr of the control film at different temperatures intervals (inadequate values predicted by the model and R2 below 0.9 are between parenthesis) 83

Table 5.3 Arrhenius and WLF constants, f and α at the T_g and Tr at their valid interval. * indicates that the full range of data was used for calculation 84

Table 6.1 Structure and composition of the materials and code names 91

Table 6.2 Complementary predicted properties from amorphous cell molecular dynamics 98

Table 6.3 Complementary predicted properties from the topological method 99

GENERAL ABBREVIATIONS AND NOMENCLATURE

Aa_T: temperature-independent pre-exponential factor for the shift factors

AC: amorphous cell

A_g: temperature-independent pre-exponential factor for the glass transition

ACMD: amorphous cell molecular dynamics

APTES: (3-aminopropyl) triethoxysilane

ASTM: American Society for Testing and Materials

a_T: shift factors

ATR: attenuated reflectance

α_g: coefficient of thermal expansion at glass transition temperature

α_r: coefficient of thermal expansion at reference temperature

α_v or av: coefficient of volumetric thermal expansion

B: bulk modulus

β and β^v: bond indices

COMPASS: condensed-phase optimized molecular potentials for atomistic simulation studies

Control film: modified thermoplastic glycerol plasticized starch film

C_1, C_2, C_3: coefficients and constants of the asymptotic function

C_{1i}^r, C_{2i}^r WLF constants or viscoelastic coefficients at the reference temperature

DMA: dynamic mechanical analyser

DP: Degree of polymerization

DSC: differential scanning calorimeter

δ: simple atomic index

δ^v: second atomic index

ΔEa_T: apparent activation energy of the shift factors.

ΔE_g: apparent activation energy of glass transition

E: Young's modulus

ENR: epoxidized natural rubber

ENR50: natural rubber with a 50 % mol of random epoxidized natural rubber

FTIR: Fourier transformed infrared

phr: part per hundred

Epoxy-POS film: modified thermoplastic glycerol plasticized starch film with Epoxy-POS

Epoxy-POS: 1-(3-glycidyl)propoxy-3,5,7,9,11,13,15-isobutylpentacyclo[9.5.1.1^{3,9}.1^{5,15}.1^{7,13}] octasiloxane

Erucamide docos-13-enoic acid

Eru-POS film: Modify thermoplastic glycerol plasticized starch film with Eru-POS

Eru-POS: functionalized of Epoxy-POS with Erucamide in the epoxy ring

E': elastic modulus

E'': viscous modulus

E*: complex modulus

f: free volume fraction

f_g: free volume fraction at the glass transition temperature

f_r: free volume fraction at the temperature of reference

Jeffamine: O-(2-Aminopropyl)-O′-(2-methoxyethyl)poly(propylene glycol) 500

Jeff-POS film: modified thermoplastic glycerol plasticized starch film with Jeff-POS

Jeff-POS: functionalized of Epoxy-POS with Jeffamine M-600 in the epoxy ring

FTIR: Fourier transform infrared

FT: Fesko and Tschoegl

gWLF: generalized Williams–Landel–Ferry model

LVDT: linear variable differential transformer detector

M: mass

mer: polymeric repeating unit

Mw: weight average molar mass

μ: shear modulus

N_H: number of bonded hydrogens

NH_2-POS film: modified thermoplastic glycerol plasticized starch film with NH_2-POS

NH_2-POS: 1-(3-amino) propyl-3,5,7,9,11,13,15-isobutylpentacyclo[9.5.1.1.^{3,9}.1^{5,15}.1^{7,13}] octasiloxane

NR: natural rubber

NRChem: Code name for simulated natural rubber with POS chemically attached

NRPhy: Code name for simulated natural rubber with POS physically mixed

NPT: constant moles, pressure and temperature

NVE constant moles, volume and energy

N_{wr}: normalise water resistance ratio respect to the control film

p: p-value of statistics hypothesis test

PBC: periodic boundary conditions

POS or POSS™: polyhedral oligomeric silsesquioxane

POS-NH2: 1-(3-amino)propyl-3,5,7,9,11,13,15- isobutyl pentacyclic[9.5.1.1^{3,9}.1^{5,15}.1^{7,13}]octasiloxane

ν: Poisson's ratio

v_g: frequency of the glass transition temperature

R: universal gas constant

R^2: coefficient of determination

ρ: density

ρ_∞: density of the test materials at infinite relaxation time

SSMS: synthetic simultaneous multifrequency scans

SSR: sum of squared residuals

STRL5: Standard Thai Rubber L5

t: time

T: temperature

tan(δ): loss angle or dissipation factor or tangent to the δ angle

T_g: glass transition temperature

THF: oxolane or tetrahydrofuran

T_m: melting temperature

T_r: temperature of reference

TTSP: time-temperature superposition principle

T_0: reference temperature

τ_i: response times

θ(T) Heaviside step functions or unit step function

θ_c: contact angle

V: volume

WLF: Williams–Landel–Ferry model

wr: water resistant as area under a θc versus time plot

0χ, 0χυ: zeroth-order connectivity indices

1χ, 1χυ: first-order connectivity indices

Z: atomic number

Zν: number of valence electrons

ABSTRACT

The advantage of using nanomaterials as structure-property modifying agents is that they have substantially different physicochemical properties than those of their macroscale or bulk counterparts. Among nanomaterials, silica-based polyhedral oligomeric silsesquioxanes (POS or POSS™) have shown to improve several physicochemical properties such as hydrophobicity and thermal stability when they are incorporated in polymers through chemical reaction or physical mixing. POS are highly versatile materials as they enable alteration or tailoring of the pendant groups. For this reason, POS are gaining popularity in polymer industry. However, their technological potential has not been adequately utilised in many important applications such as modifying the surface of starch films to introduce hydrophobicity and improving thermo-mechanical properties of natural rubber (NR).

Starch films have intrinsic natural affinity for water on their surface as well as in the bulk. This affinity is due to the hydroxyl groups in starch structure. This high affinity for water is the main reason that starch-only films are not used widely in packaging applications. It is a technological challenge to introduce any hydrophobic agent into hydrophilic matrix of starch. However, because of unique nature of POS, they can be tailored to physically mix with starch to increase hydrophobicity and avoid dispersion and segregation problems.

Natural rubber, so far, is one of the most versatile elastomeric materials with quite wide application including in medical devices, adhesives and tyres. Nevertheless, its weak thermo-mechanical stability and relatively low temperature resistance have limited its applications. POS is capable of improving the above-mentioned properties as observed in other elastomers such as polyurethanes and non-elastomeric materials such as epoxy resins.

In this context, the overall objectives of this research were to increase the hydrophobicity of thermoplastic starch films and improve the thermo-mechanical properties of NR. These two desired characteristics were brought to starch and NR by tailoring different POS and then incorporating them into NR and starch films by chemical grafting or physical mixing.

To achieve above mentioned objectives, optimal formulation and synthesis of hybrids and composites of NR, epoxidized NR or thermoplastic starch with POS were carried out by chemically grafting or physically dispersing POS. The performance of chemical grafted hybrid and physically mixed composite was compared, in terms of physical, thermal and mechanical properties, using data obtained from chemical experiments and molecular modelling.

As part of this research, a new integrational method was developed to construct time-temperature master curves. Generalized time-temperature superposition models were proposed for rheologically complex materials and two computational techniques were developed to reduce the computational time/cost of calculations. The first technique estimated density of the test materials at infinite relaxation time and the second involved determination of minimum number of atoms to simulate materials in amorphous cell molecular dynamics.

This study contributes in advancing the body of knowledge and helps broaden the application of POS in developing water-repellent starch films, high-performance rubbers, hybrid materials and nanocomposites from starch and natural rubber. This study also outlines the advantages and limitations of incorporating POS into NR physically as nanofiller and chemically as hybrid, which will open up new applications for these materials.

1 INTRODUCTION

1.1 Background

Organic and inorganic materials have their specific intrinsic properties which dictate the range of products in which they can be satisfactorily used. When a ceramic (inorganic) material is chemically combined with a polymeric organic material, a hybrid material is obtained. Hybrid materials possess much better thermal, mechanical or physical properties compared to their source materials due to synergism and these properties cannot otherwise be obtained from the individual components [1].

Therefore, polymers or ceramic materials cannot be used alone in many applications because of their intrinsic limitations. As shown in Figure 1.1, the ceramic materials normally have high ultimate strength (stress at which it breaks) but they are brittle due to low ductility. In contrary, polymeric materials normally yield at lower stress and have a much greater ultimate strain (strain at break) than a ceramic material but their ultimate strength is normally much lower.

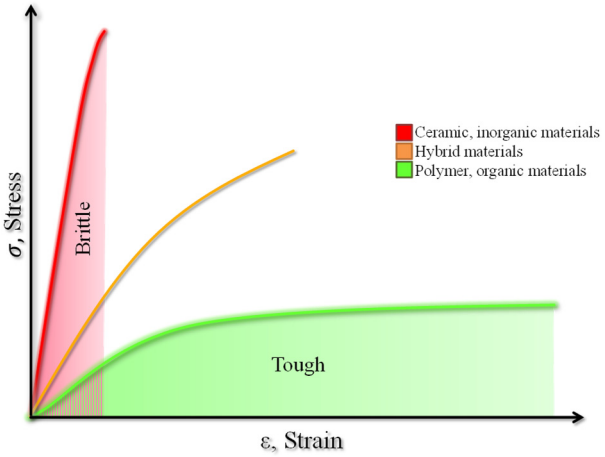

Figure 1.1 Stress-strain behaviour of ceramic, organic, polymer and hybrid materials

For instance, the melting point of silica is more than 1600 °C [2] and materials such as glass or a ceramic are hard (650 kg/mm^2= 63.77 MPa) [3]. Both of these properties are highly desirable; however, ceramic materials are brittle due to low ductility. In contrary, natural rubber (NR) is ductile and soft (27.5 Shore A ≈ Young's modulus of 1.35 MPa) [4, 5]; this is the main reason why globes, children's toys, tubes and even mattress are produced using NR. However, the NR cannot stand more than 350 °C [6] without decomposing.

In fact, neither the ceramic materials nor the polymers can be used alone in all desirable applications. One of the approaches to solve this problem is to make a physical mixture, laminate or in general make a composite. The composites or laminates produced in this way possess desirable properties of both ceramic and polymeric material and works reasonably well in many practical cases. However, this approach is constrained by the intrinsic natural incompatibility among the materials used and the area available for interaction (Figure 1.2). A more desirable approach of addressing this issue or overcoming the incompatibility problem is to develop or induce covalent bond between a ceramic material and an organic polymer to obtain a hybrid material.

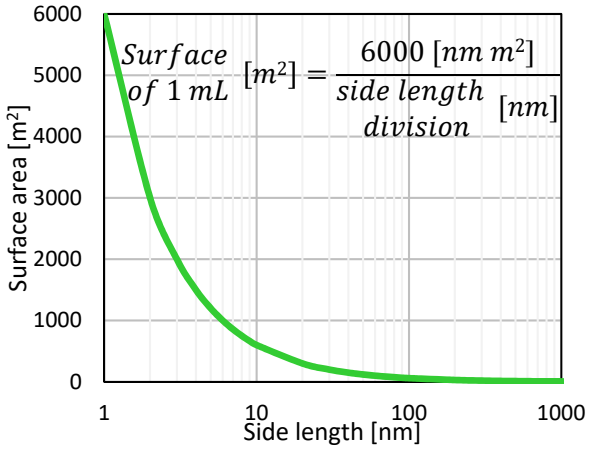

Figure 1.2 The increase of surface area of a cubic substance with one millilitre (mL) volume when is divided in cubes with side divisions from 1000 nanometre to 1.

When it comes to performance, the chemical approach has advantage over the physical one, because the increase in the area of interaction and the attachment of adequate number of pendant groups cannot be achieved even when the nanoparticles are used. Due to the poor compatibility and lower strength of physical bonds the composites or laminates are not strong enough to synergistically enhance their properties. It is possible to chemically bond two or more materials that are naturally incompatible to develop hybrid materials. For example, the polystyrene and polybutadiene are by nature immiscible, yet it is possible to develop or induce covalent bonds between these two through polymerization.

In many thermoset and thermoplastic polymers, polyhedral oligomeric silsesquioxanes (POS or POSS™) [7] are used as nanofillers or crosslinkers. So far there are just a handful of peer reviewed publications dealing with the application of POS together with natural rubber or polyisoprene obtained from natural rubber to develop hybrid materials [8, 9]. In the case of using POS to modify starch, there

is a similar dearth of published literature in public domain [10, 11]. The hybridization of natural rubber with POS would be of practical significance and is technologically feasible as POS has been used together with some synthetic rubbers that contained polyisoprene in their main chain [12]. The main aim of blending POS with starch is not just to improve the thermal and mechanical properties but also to bring about some degree of hydrophobicity.

In this context, the aim, research hypotheses, research questions and objectives of PhD study were as follows.

1.2 Aim

To design and synthesise hybrid-polymers or composites, using Natural rubber (NR) or epoxidized natural rubber (ENR) and thermoplastic starch films containing polyhedral oligomeric silsesquioxanes (POS or POSS™) as attached substituents or dispersed compounds through chemical synthesis underpinning by molecular modelling. The physical, thermal and mechanical properties of the chemically synthesised hybrids and physically blended composite materials were compared.

1.3 Research hypothesis

a) A custom or purpose designed POS can bring about desirable physical, thermal and mechanical properties in NR and thermoplastic starch films.
b) The time-temperature superposition principle can be applied to rheologically complex materials by imposing some simple constraints. Thus, master curves can be constructed using a proposed integrational method and thermoplastic starch films can be modelled as rheologically complex materials.
c) Grafting an amino substituted POS into NR is possible by epoxidizing the NR first by a click reaction.
d) A topological method can be used to determine the minimum number of atoms required in a molecular dynamic simulation that predicts the thermo-mechanical properties to a realistic scale of an experimental system.

In the basis of the above hypotheses, this study sought to answer the following research questions.

1.4 Research questions

a) Can discrete chemical bonding or interaction be formed and identified between substituted POS and the substrate (NR or starch films)?

b) Will POS substituents provide a distinct and defined molecular change that will show enhanced performance relative to dispersed compositions?

c) Is it possible to find simple constraints that allow scientist and engineers to use the time-temperature superposition principle to rheologically complex thermoplastic starch films?

d) Will POS behave as a bulk constituents or nano-particulate fillers in NR? Is there a difference between molecules or hybrids attached by covalent bonds and physically mixed composite materials?

1.5 Objectives

The specific objectives of this study were as follows.

a) Design and synthesise novel nanohybrid materials that are compatible with starch and which can increase the water resistant of the thermoplastic starch films.

b) Measure the thermo-mechanical properties and wettability kinetics of thermoplastic starch films with and without POS.

c) Construct master curves using the proposed integrational method together with constrains to be imposed when applying the time-temperature superposition principle to rheologically complex thermoplastic (e.g. starch films).

d) Chemically graft the purpose designed POS to natural rubber and prove that the proposed click reactions were achieved.

e) Use the topology method to determine the minimum number of atoms needed in a molecular dynamic simulation that can predict alike properties to realistic scale experiments.

f) Measure and compare the thermal and thermo-mechanical characteristics of the NR, the epoxide NR and the NR hybrids and use these data to validate the models.

1.6 Contributing to or advancing the body of knowledge

The advantage of using nanomaterials as structure-function modifying agents is that their physicochemical properties are substantially different from those of their macroscale or bulk counterparts. Among nanomaterials, silica-based POS have shown to improve several properties when they are incorporated in various polymers through chemical reaction or physical mixing. POS have great versatility as they allow altering or tailoring of pendant groups. For this reason, POS are gaining popularity in the polymer industry. However, their potential or promise is not well utilised in many desirable applications such as: surface modification (by increasing hydrophobicity) of starch films and improving thermo-mechanical properties of natural rubber (NR). This study has contributed in advancing the fundamental knowledge and also helped broaden the application of POS in developing water repellent starch films, high-performance rubbers, hybrid materials and nanocomposites of rubber and starch. In addition, new analytical and mathematical models are developed in this study for realistically constructing master curves for rheologically complex materials. The models and the simulations developed in this study will significantly reduce the computational time/cost in molecular modelling.

1.7 Outline of the thesis

This thesis is organised in eight chapters. **Chapter 1** presents the background and broader research context and documents the aim, objectives and underpinning research questions. The hypotheses used to guide the research are also documented. The contributions made by this thesis to the body of knowledge are also outlined.

Chapter 2 presents the literature review on the most relevant physicochemical properties of tested materials. This chapter makes critical appraisal and summarises what is out there and what is gap in knowledge and provides context to the remaining chapters. Firstly, it reviews the available literature on POS and their interaction with starch even though they are scarce. Secondly, it reviews the available literature on the hybrid and composite materials of POS in natural rubber (NR) or epoxide natural rubber (ENR). This chapter also outlines the gap in the knowledge which this thesis has endeavoured to fill.

Chapter 3 presents the working principle of the main instruments or methodologies used in this work.

Chapter 4 documents the characteristics and process developed to produce thermoplastic starch-POS films by adding custom-designed POS. The measurement and quantification/prediction of surface hydrophobicity (by wettability kinetics) of starch-POS hybrid films were performed by measuring the contact angle of water on the films, aiming to increase of the surface water resistance.

Chapter 5 describes an integrational method to construct master curves. This method used synthetic simultaneous multifrequency scans to avoid variation in intrinsic temperature control and better predicts the glass transition and melting temperatures. It also presents generalised time–temperature superposition models, developed in this thesis, for rheologically complex materials. The procedure and models are applied to thermoplastic starch-POS hybrid films.

Chapter 6 document the outcomes of simulations of NR and ENR with POS at different concentrations. These simulations were carried out using amorphous cell molecular dynamics (ACMD) and a topology method similar to group additivity contribution method. Pre-calculations using topology methods were proven useful to determine the optimum number of atoms required in ACMD that predicted benchmark real-life thermo-mechanical properties. Materials densities at infinite relaxation time were used to estimate Tg using asymptotic and quadratic polynomial functions.

Chapter 7 presents the detail of the chemical reaction-based method used to synthetize novel hybrids of ENR with POS. Different methods were used and documented to confirm the reaction and characterisation of the physicochemical properties of ENR-POS hybrid materials.

Chapter 8 presents overall conclusions drawn from the findings of four experimental chapters. This chapter also outlines the new knowledge created in this work and recommends some important future works.

APPENDIX presents the refereed journal papers published from this thesis.

1.8 References

1. Seurer, B., *Synthesis and characterization of novel thermoplastic elastomers employing polyhedral oligomeric silsesquioxane physical crosslinks*. 2008: ProQuest.
2. LLC., S.-A.C., *Silica, Material Safety Data Sheet*, in *Material Safety Data Sheet*. 2013, Sigma-Aldrich Co. LLC.

3. Yamane, M. and J. Mackenzie, *Vicker's hardness of glass.* Journal of Non-Crystalline Solids, 1974. **15**(2): p. 153-164.
4. Arroyo, M., et al., *Morphology/behaviour relationship of nanocomposites based on natural rubber/epoxidized natural rubber blends.* Composites science and technology, 2007. **67**(7): p. 1330-1339.
5. Mix, A. and A. Giacomin, *Standardized polymer durometry.* Journal of Testing and Evaluation, 2011. **39**(4): p. 696-705.
6. Fernández-Berridi, M.J., et al., *Pyrolysis-FTIR and TGA techniques as tools in the characterization of blends of natural rubber and SBR.* Thermochimica acta, 2006. **444**(1): p. 65-70.
7. Hartmann-Thompson, C., *Applications of polyhedral oligomeric silsesquioxanes*. Vol. 3. 2011: Springer.
8. Puhala, A.S., et al., *Rubber compound containing a polyhedral oligomeric silsesquioxanes*. 2005, Google Patents.
9. Zhao, Y., et al., *Toughened elastomer/polyhedral oligomeric silsesquioxane (POSS)-intercalated rectorite nanocomposites: Preparation, microstructure, and mechanical properties.* Polymer Composites, 2017. **38**(S1): p. E443-E450.
10. Bastola, K.P., et al. *Synthesis of poss-starch derivatives as effective fillers for developing high performance composites*. in *International SAMPE Technical Conference*. 2013.
11. Ata, S., S.L. Banerjee, and N.K. Singha, *Polymer nano-hybrid material based on graphene oxide/POSS via surface initiated atom transfer radical polymerization (SI-ATRP): Its application in specialty hydrogel system.* Polymer, 2016. **103**(C): p. 46-56.
12. Hayakawa, T., et al., *Fabrication of hierarchically ordered hybrid structures over multiple length scales via direct etching of self-organized polyhedral oligomeric silsesquioxane (POSS) functionalized block copolymer films.* Polymer journal, 2006. **38**(6): p. 567-576.

2 LITERATURE REVIEW

This chapter systematically reviews the literature on physicochemical characteristics of starch, natural rubber (NR), epoxidated natural rubber (ENR) and polyhedral oligomeric silsesquioxanes (POS), focussing on their application in synthesising nanohybrid and nanocomposite materials. The available literature on synthesis and characterisation of NR (ENR)-POS and starch-POS nanohybrid and nanocomposite materials is reviewed both on experimental and theoretical prediction aspects. This literature review identifies the gap in knowledge on the abovementioned aspects. This identified gap in knowledge forms the basis for experimental and modelling research undertaken in subsequent experimental chapters.

2.1 Starch

2.1.1 Starch structure

Starch is a carbohydrate consisting of a large number of glucose units joined by glycosidic bonds (Figure 2.1). It consists of linear amylose α (1,4)-glucopyranoside and amylopectin that has additional α (1,6) branches. Depending on a plant, starch generally contains 20 to 25% amylose and 75 to 80% amylopectin by weight. Starch is renewable and is abundantly available in nature.

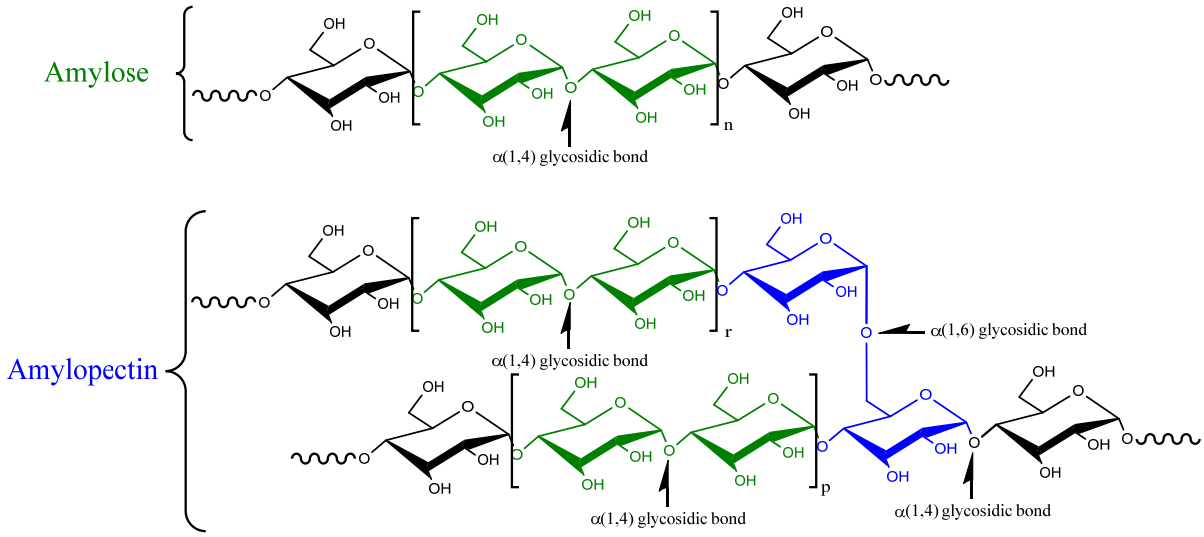

Figure 2.1 Amylose and amylopectin structures

Amylose and amylopectin are fundamental building blocks of starch. As polymer starch ramify from the granules' focal core or Hilum; amylose form branches and amylopectin form nodes as in a complex

dendrimer. Amylose forms clusters of double helical structure (Figure 2.2 a) clusters while the amylopectin allows the propagation of the double helix over specific directions. The clusters of amylopectin aggregate to form lamellae or crystalline domains (Figure 2.2 b) and the amylose guides these lamellae to form super helix (Figure 2.2 c) with amorphous domains in between . Thus, a starch granule consists of alternating crystalline and amorphous regions (Figure 2.2 d) which can be easily observed through a microscope (Figure 2.2 e, Figure 2.3).

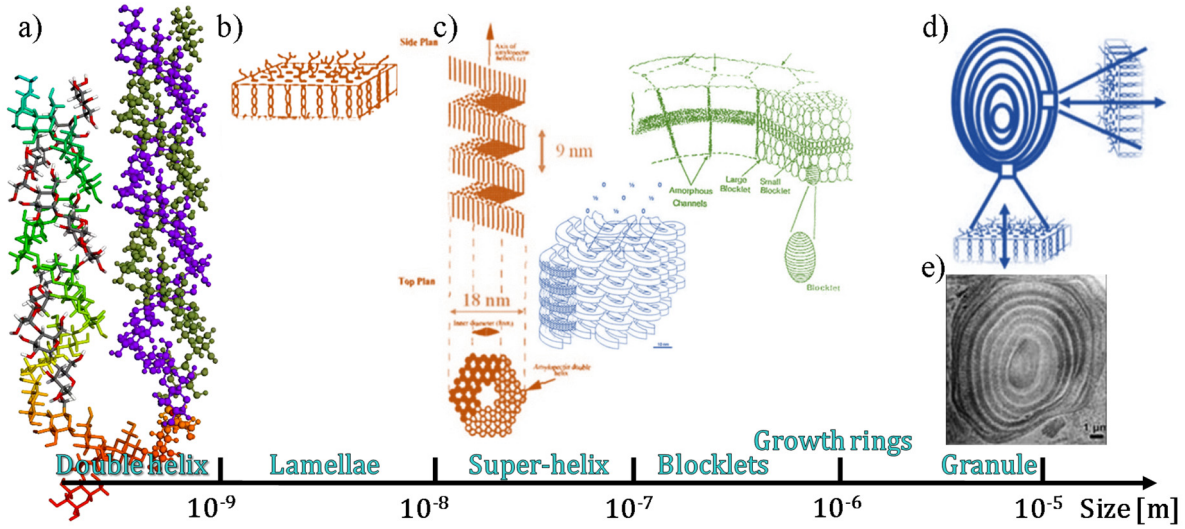

Figure 2.2 Starch organization architecture in scales of orders of tens [1]

2.1.2 Thermoplastic starch films

Starch is the energy storage material found in plants in the form of crystalline granules [2] and is primarily used as food. It can be sustainably produced worldwide in large quantities [3]. In terms of film forming or packaging material, it is biodegradable and possess respectable mechanical properties. About half of starch production is for non-food applications such bioplastics, papers, adhesives and biofuels [4]. This widespread use of starch is due to its desirable oxygen barrier and mechanical characteristics, biodegradability, non-toxic nature and having renewable resource. However, it lacks desirable water resistance (water repellence) and water barrier properties. Native starch is usually modified by physical and chemical means to meet industrial needs [5]; with one of these applications being manufacture of flexible packaging films.

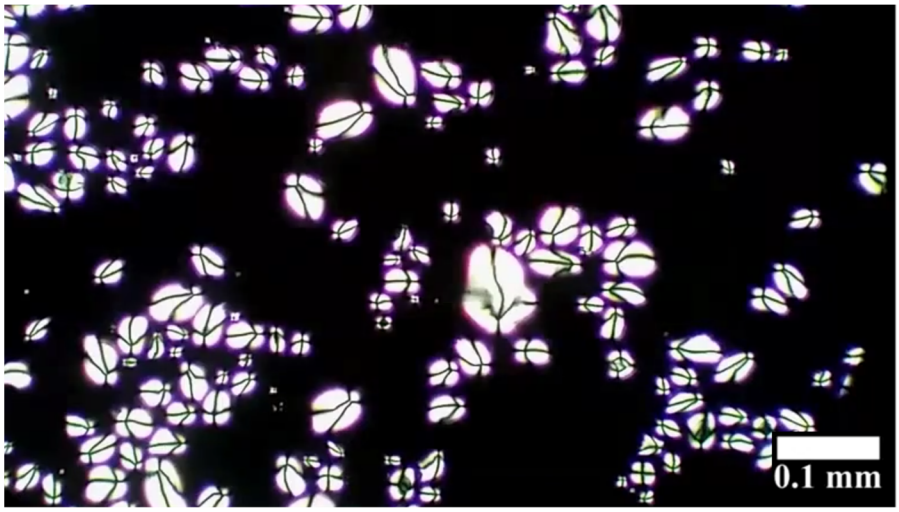

Figure 2.3 Microscopic picture of soluble corn starch granules under polarized light. The Maltese cross is an indication of crystaline structure

Starch granular and crystal structure must be disrupted by a process called gelatinization to convert it into a thermoplastic material. Extrusion and solution casting methods are most commonly used to produce flexible films from thermoplastic starch [6]. In the extrusion method, starch and appropriate amounts of plasticizers are extruded into films. In solution casting, aqueous dispersion of gelatinized starch containing appropriate amounts of plasticizers is cast to form a film. In the final stage of production, extruded and solution cast films are dried at mild temperature and air flow. The gelatinization process involves heating, hydration and dissolution of granular–crystalline starch [7]. The dissolution involves hydration of amorphous amylopectin and semi-reversible disruption of double helical structures of amylose.

The starch films are transparent and smooth. Nevertheless, due the hydrophilic nature of amylopectin and amylose, hydrogen bonds are formed when starch interacts with atmospheric moisture and facilitates the re association of starch into partially ordered (retrograded) structures [8].

Water plasticizes the amorphous regions at temperatures above its glass transition temperature (T_g) [9]. This feature influences the mechanical performance, storage condition, shelf stability, and applicability of the films. Therefore, two of the most important parameters that determine the usability of starch films are the melting temperature (T_m) and the T_g which are first and second order transitions, respectively. The first transition converts solid into liquid and the second transition transforms the glassy state into rubbery one.

2.1.3 Plasticisation of starch

Starch films can be produced without using any plasticizer other than water, but the resulting material is very brittle [10]. For this reason, plasticisation of starch using plasticisers other than water is necessary to increase the elongation at break. A plasticiser increases the intermolecular spacing [11] by increasing the intermolecular hydrogen bonding of itself and the OH groups of starch while decreasing the intramolecular hydrogen bonding of the hydroxyl groups on the carbons 2, 3 and 6 in the glucose residue [12]. The increase of intermolecular space increases the free volume, which leads to higher molecular mobility. The plasticisation lowers the T_g, increases the elongation at break and reduces the probability of starch re-crystallisation [13]. This process is called plasticization.

Water is the plasticiser with higher impact on thermoplastic process, because its big dipole moment easily attracts OH groups in starch. Unfortunately, due its readily evaporating nature it is not practical to use water as plasticiser in applications requiring longer stability as storage humidity can have substantial impact on it. This is the reason why polar molecules such ass polyols and amides are used plasticisers [14]. Some of the most used polyols are ethylene glycol and similes[15], glycerol, maltitol[10], sorbitol [16] and xylitol[17]. Some of the monosaccharides are fructose galactose glucose and mannose [18, 19] and sucrose [20]. Examples of amide plasticizers are acetamide ethylene bis formamide [21], ethanolamine [22], formamide [23] and urea[24].

Because water is a good plasticizer, the absolute humidity or relative humidity prevailing in the ambient affects the properties of starch-based films. However, moisture absorption-desorption isotherm models such as Brunauer-Emmet-Teller (BET), Flory-Huggins or Guggenheim-Anderson-deBoer (GAB) can be reliably used to correlate moisture content versus relative humidity data [25].

2.1.4 Starch retrogradation

The initial crystalline starch structure is disrupted by the plasticisers during the process of plasticisation. This process is partially reversable and when reverted, it is called retrogradation. Retrogradation is one of the main causes of quality deterioration such as brittleness in starch and starch-based films. V-type crystals of amylose are formed in excess moisture [26] during the processes such as retrogradation,

ageing or staling, causing the thermoplastic starch to become brittle. Plasticisers listed above and co-solvents such as hydroxypropylation are added to avoid or minimise retrogradation.

Plasticisers are able to retard retrogradation because a single helical structure of amylose tends to form helical inclusion complexes with adequate complexing agents (e.g. water or glycerol). This inclusion of complexes prevents or minimise formation of new double helical structures of amylose; thus, the formation of semicrystalline structure is prevented. Plasticisers reduce T_g, increase the flexibility and retard ageing of films all of which are desirable for good quality films. Water, xylitol and glycerol are the most commonly used plasticisers to produce starch films [27]; however, additives such as monoacyl lipids, emulsifiers, alcohols induce formation of left-handed amylose single helices [28].

2.2 Natural Rubber

Natural rubber (NR) is a natural polymer derived from milky colloidal suspension of many plants like *Cryptostegia grandiflora*, Guayule (*Parthenium argentatum*), *Hevea brasiliensis*, *Parthenium argentatum*, *Solidago virgaurea* and *Taraxacum kok saghyz* [29], NR also contains small percentage of impurities of other compounds such as resins, proteins, salts and sugar (Table 2.1).

Table 2.1 Composition of fresh natural rubber latex. Adapted from Li [30]

Component	Quantity [%]
Isoprene	30 to 35
Proteins	1.0 to 1.5
Resinous components	1 to 2
Other carbohydrates	1
Mineral components	1
Water	59.5 to 66.0

Chemically speaking, rubber or elastomeric hydrocarbon polymer present in the milky suspension is polyisoprene with a molecular mass between 100,000 to 1,000,000 [g/mol]. Depending on the strain or variety of the plant a type of isomer is predominant, poly(isoprene) isomers are 1,4 (cis or trans), 1,2 (Vinyl) or 3,4 (Figure 2.4). The most commercially available natural rubber comes from the Hevea tree which contains approximately 97 % of cis-1,4 poly(isoprene) isomer. The double bond in isoprene provides rigidity to the polymeric matrix and the isomer cis makes it geometrically asymmetric which leads to a rapid reversible stress-strain response [31].

Even though the most important constituent component on natural rubber is poly(isoprene) many times the name poly(isoprene) is reserved for the polymer obtained from non-natural resources, referred as synthetic rubber. This difference in the source of poly(isoprene) is important when comes to allergies. The allergy to latex is directly correlated to the presence of natural proteins and that is why a person can be allergic to natural rubber but not to synthetic natural rubber.

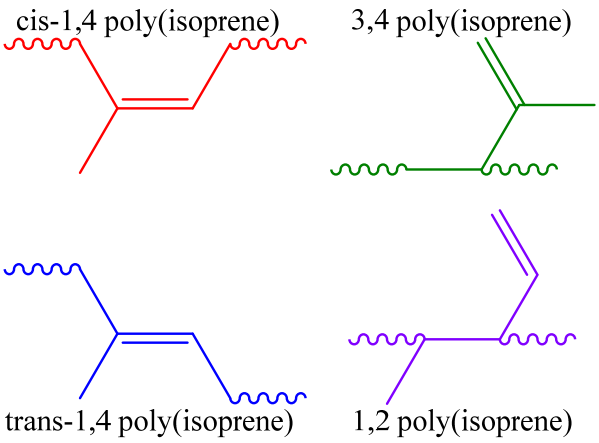

Figure 2.4 Isomers of poly(isoprene)

In order for the natural rubber to be used commercially, it is necessary to physical or chemically modify it to customize its properties. In general, some degree of chemical reaction to produce compounds is necessary for which a number of materials can be used to obtain specific effects. The most important are listed below.

1. Accelerators: They are used to change the rate of vulcanisation, normally to increase it. The most commonly used accelerators are amine dialkyl dithiocarbamate and metallic.
2. Antioxidants: two types of antioxidants agents are used, amine and phenolic type. The first can promote staining due to its resinous nature, for that reason the seconds are most commonly used.
3. Stabilisers / surfactants: They help to incorporate immiscible additives, promote foaming and crosslinking.
4. Thickeners: They are normally used during processing to modify the viscosity. Carboxymethyl cellulose and poly(vinyl alcohol) are the most commonly used for this purpose.

Curing or vulcanising agents are the most important compounding agents. Sulphur is most widely used not only for natural rubber but to almost any diene rubber. The sulphur reacts with the double bond of

the rubber forming mono, di and poly sulfidic linkages, and crosslinks the polymeric chains (Figure 2.5). It is also possible to use colloidal sulphur, tetramethylthiuram disulfide or butyl xanthogen disulphide for the same purpose.

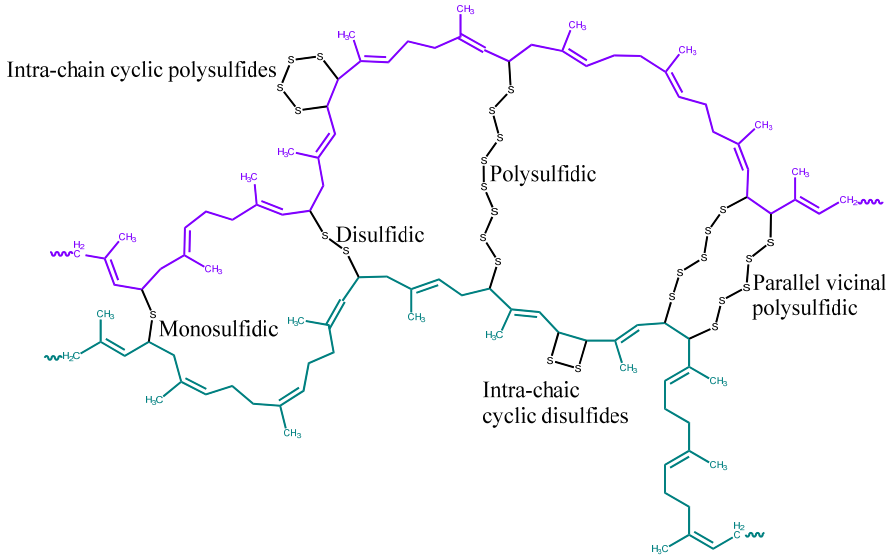

Figure 2.5 Structure of two polymeric chains of natural rubber after vulcanization with sulphure

Fillers and pigments: some of them are added just to lessen cost but many of them can improve abrasion tear, hardness, rupture or stiffness among other properties. Carbon black is by far the most commonly used reinforcing filler [32]. However, there are many more very important compounds that be excellent fillers such as carbon nanotubes, clays, calcium carbonate, metal particles, POS and silicas [33]. The fillers can be found in micrometre and nanometre scales. The most relevant fillers in this work are the POS which when incorporated in polymeric materials can improve , heat evolution, mechanical properties, service temperature and surface hardening among others [34]. POS are molecular forms of silica that are chemically functionalised to tailor polar and nonpolar characteristics and chemical reactivity. POS are known to be promising fillers compared with particulate silicas and carbon black, as they offer better processability, dispersion and avoid agglomeration [35, 36].

The physical mixture of inorganic or organic materials with NR can alter the property of the mixed product by transferring some characteristics of the filler to the material. However, the effectiveness of this transfer depends upon their intrinsic compatibility and their surface interactions [37]. Regardless, the physical mixing of nanoparticles provides much weaker interactions between the components of the mixture than the interactions achieved by chemical bonding.

The use of nanofillers to reinforce NR has high expectation because nanofillers have shown in many cases an enhancement of the mechanical properties [38]. In this context, conventional inclusion of inorganic fillers includes both inorganic and organic compounds such as carbon black and silica is achieved by dispersion [39]. The products obtained in this way have comparable tensile strength, but lower tensile modulus than exhibited by silica composites [40]. With current demand for fillers from renewable resources, organic fillers have become more widely used, especially in the form of fibres, although these inorganic fillers are somewhat lessen performance [41]. There are several studies where a synergetic contribution using hybrid fillers (organic–inorganic) appears to enhance mechanical properties as well as increasing thermal and physico-chemical properties [42-44].

Physical or chemical addition of nanofillers onto polymers may lead to changes in T_g that is the most significant transition or relaxation observed for amorphous polymers [45]; even small changes in T_g leads to considerable change in density, bulk modulus, tensile modulus and shear modulus [46]. Therefore, property prediction is an important factor to consider in the design, modification and production of polymer composites current or new applications. Hence a comparison of the mechanical and thermal properties using molecular dynamics of physical mixtures compared with chemical hybrids is important for design and synthesis of nano-composites, where both possibilities are of interest and estimation of properties such as T_g is essential.

Natural rubber (NR) is a versatile elastomer with well-balanced mechanical properties[47]. Due to its large strain at break and low stress-strain hysteresis NR has applications in the automotive [48], electronics [49], rubber goods industries [32] as well as in pressure sensitive adhesives [50, 51].

In addition to its industrial importance, NR is dynamically flexible, which is an advantage for simulations because local dynamics occur under 100 ps [52]. While experimental results for mixtures are preferred, molecular modelling is used to predict structure and properties of similar materials because it eliminates the need for synthesis of each material, confirming proposed hypotheses, while obtaining principally new results [53].

2.2.1 Epoxidized natural rubber

Epoxidized natural rubber (ENR) is an elastic material with a higher density and T_g than natural rubber. The T_g of ENR varies depending of its epoxidation percentage (Table 2.2).

Table 2.2 Epoxidation percentage versus glass transition temperature

Epoxidation mol percentage [%]	Commercial name	T_g [ºC]
10%	ENR10	-60
25%	ENR25	-46
47%	-	-26
50%	ENR50	-20
75%	-	-9
100%	-	18

ENR come from NR epoxidation (Figure 2.6) and it possesses improved properties such as oil resistance and gas permeability and hence broadens the range of applications while providing potential for further chemical modification.

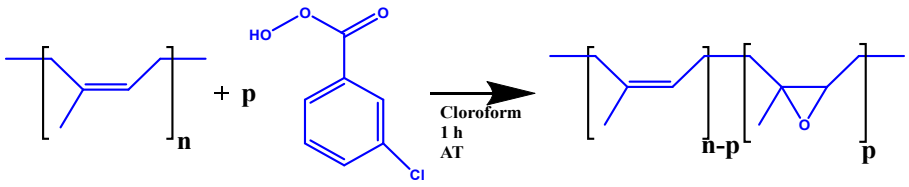

Figure 2.6 NR epoxidation reaction

Commercial levels of epoxidation are 10, 25% and 50%. The strain-induced crystallisation diminishes at epoxidation levels up to 95%, the degree of crystallinity diminishes at epoxidation levels above 50%. As in the case of NR, it can be vulcanized by conventional methods making use of double bounds or by using the epoxy ring (Figure 2.7).

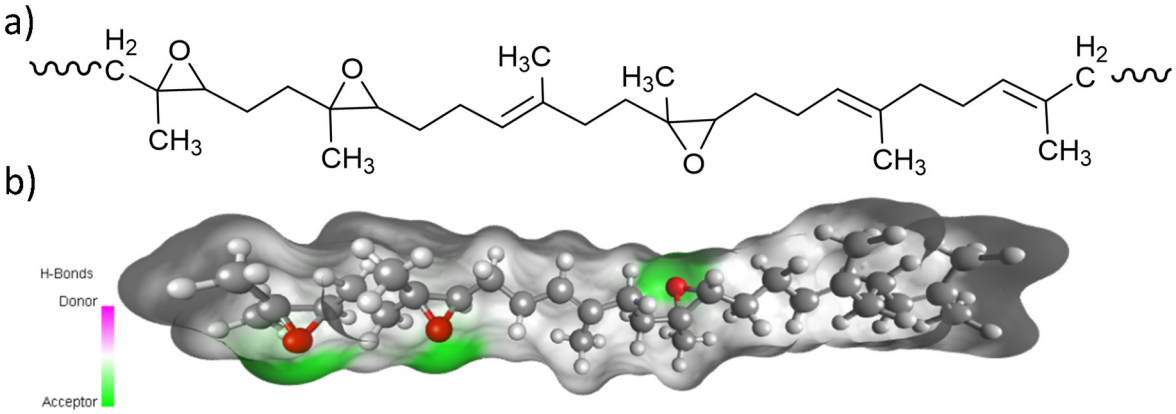

Figure 2.7 ENR50 a) random structure b) Van der Waals surface indicating H-bonding acptor/donator sites

2.3 Polyhedral oligomeric silsesquioxanes.

Combined materials made from two or more constituent materials with significantly different physical or chemical nature, produce a material with characteristics different from the individual components. Drisko and Sachez [54] define this kind of materials in two classes. If the interaction is through weak bonds, such as van der Waals, hydrogen bonding, or ionic bonds, the material is categorized as the class I hybrid. If covalent or ionocovalent bonding occurs between the inorganic and organic components, it is considered to be the class II. In this work, for the sake of convenience, hybrid class I will be addressed as composites and hybrid class II just as hybrids.

POS are well defined organic-inorganic nano hybrid materials. The word polyhedral means "many faces" derived from ancient Greek words πολύς (polús) - "many or much" and ἕδρα (hédra) – "face of a geometrical solid". Similarly, oligomer means "small individual parts" and comes from the ancient Greek words ὀλίγοι (olígoi) - "few" and μέρος (méros) - "part". Lastly silsesquioxane means that silicon oxygen and hydrocarbon groups are linked, where sil means silicon, sesqui indicates that each silicon atom is connected in average to "one and a half oxygens" and "ane" indicates that each Si atom is bounded to one hydrocarbon group.

Materials with 50 % or more of particles with surface, internal structure or external dimensions between 100 nm and 1 nm can be consider nano-materials [55-58]. Hence POS are individual molecules based on Si-O Linkages forming a cage having at their vertex a silicon atom where the oxygen-silicon-oxygen bonds have angles different from 90° (Figure 2.8 b). As many zero-dimension (0D) nanomaterials like fullerenes and adamantane, POS are in the scale of nanometres (Figure 2.8) but their actual size depends on the substituent in the vertex. Unlike other types of nano-silica like fumed silica or precipitated silica, POS have discreet molecular mass, can be liquid, can melt and recrystallized, can be characterized in solution by spectrographic techniques nuclear magnetic resonance (NMR) or Fourier transformed infrared (FTIR).

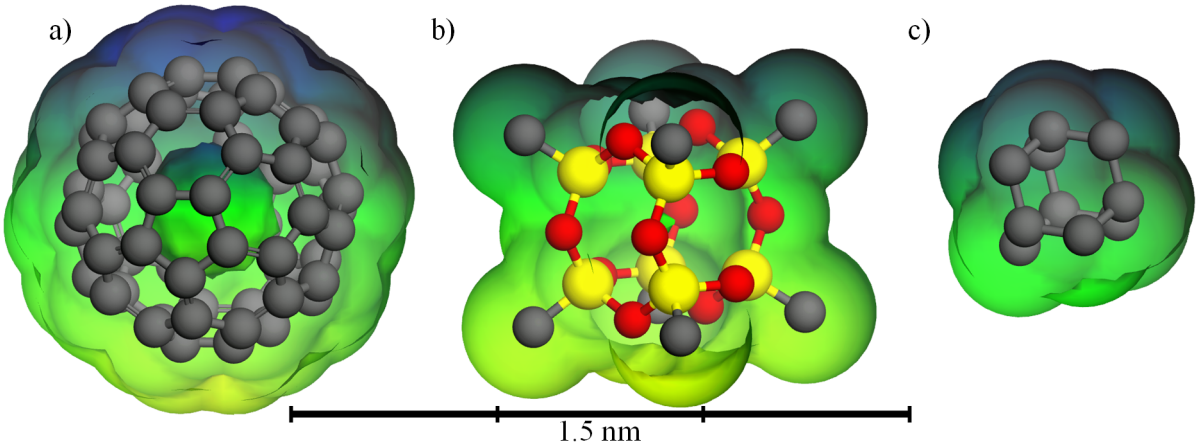

Figure 2.8 Comparation between a) buckminsterfullerene, b) Octa methyl POS and c) adamantane. Carbon, oxigen and silicon atoms are grey, red and yellow respectible, the The Van der Waals surface is colored to give sence of deep

Oxidic or siliceous fillers are reacted with organo-silanes to modify their surface characteristics [59, 60], producing organic-inorganic hybrids. The intention to modify them, is to enhance performance or compatibility in a variety of polymeric matrix. The organic part is the responsible to prevent agglomeration and increase the compatibility. These kinds of modifications are not "perfect" because the hole surface cannot be cover. The principal impediments are the stoichiometry (there is not a single molecular weight), natural occurrences of impurities of the surface and there are not practical prior or post purifications.

POS are nano-hybrid molecules but because its shape (pseudo rounded cube or cubic sphere packing) some of their properties evokes those of molecules and it could be considered as the smallest silica particle with "perfect" even treated surface.

2.3.1 POS synthesis

Most common synthesis route to produce octo-functionalized POS is a hydrolytic condensation of a trialkoxy silane functionalized, $RSiX_3$ [61] (Figure 2.9), where R and X are substituents, benign the first highly stable and the second the highly reactive. It is most used POS have a general chemical formula is $(RSiO_{1.5})_{2n}$.

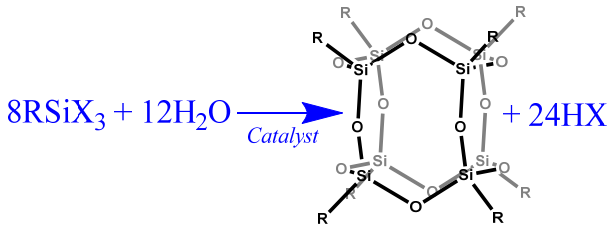

Figure 2.9 Hydrolytic condensation of RSiY3 to produce POS

2.3.2 Mono-substituted POS

The second most used POS are the so called "mono-substituted POS". Its general formula is $R'R_7Si_8O_{12}$ where R commonly are hepta-substituents like isobutyl, glycidyl, methacrylic, isooctyl or phenyl among others and R' is a different custom organic substituent for further chemical functionalization. The hepta-substituents have normally two main functions: prevent agglomerations and give compatibility to the polymeric matrix. The eight-substituent group normally is used to perform further chemical reactions which ultimates gives tremendous flexibility to POS.

2.3.3 Single corner incomplete POS and corner-capping

Many mono-substituted POS can be obtained directly from hydrosilylation [62-64], but corner-capping reaction is preferred over hydrosilylation because single incomplete corner POS are commercially available.

Similar synthesis steps to obtain complete POS must be carry out to obtain single corner incomplete POS (Figure 2.10), but some factors have to be taken to afford incomplete cage over complete. For example: bulky peripherical groups give preferences to incomplete cages; polar solvent or solvent with high dipole moment and high dielectric constant are able to stabilize incomplete condensed POS through interaction with the OH groups.

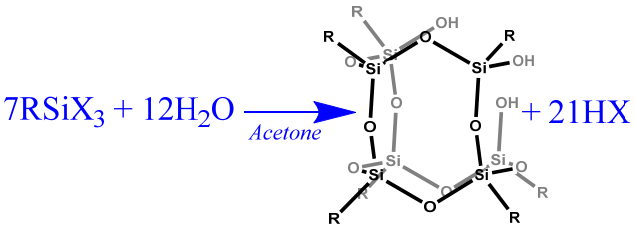

Figure 2.10 Synthesis of single incomplete corner POS

The corner-capping reaction consist basically to take a single incomplete corner POS and complete it by a silylation. The silylation consist in adding a coupling agent in the form of Y_3Si-R'where Y normally is a halogen, acetoxy or alkoxy group (Figure 2.11).

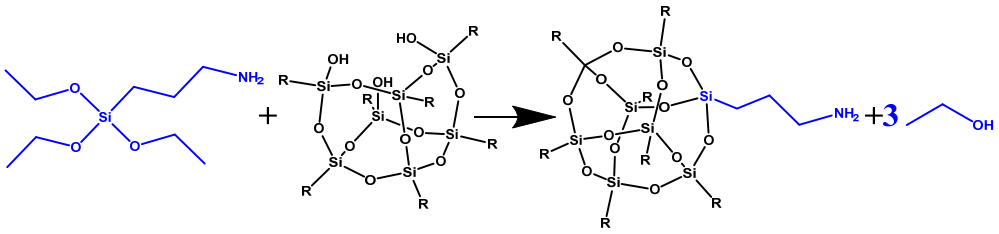

Figure 2.11. Functionalization of an incomplete POS with (3-aminopropyl) triethoxysilane (APTES)

This path gives the POS its ability to be customize through further chemical reaction and can lead to virtually unlimited types of POS since there are just a few tens commercially available.

The most interesting features that makes POS an ideal material to produce nano composites and hybrids with polymers [65] are: nano size area of interaction and dimensions, does not tent to form aggregates, do not agglomerate, its peripherical groups can be costume to change compatibility and it is possible to customize it to make specific reactions like grafting, polymerization, crosslinking and copolymerization among others. All this features allow POS to have countless applications in fields like fire retardance [66], packaging [67, 68], catalyst [69, 70], drug delivery[71, 72], sensors [73, 74], fuel cell membranes [75, 76]

2.4 Polyhedral oligomeric silsesquioxane into starch and natural rubber in the literature

Comprehensive review was performed using databases accessed through RMIT library and Google Scholar using keywords in Table 2.3. The words POSS and POS were partially and rarely used because they match false-positives articles containing words like "possible" or "polyorganosiloxanes (POSs)" among others.

Table 2.3 Keywords used in electronic databases

Keyword strings input
"Natural rubber" "Polyhedral oligomeric silsesquioxane"
Polyisoprene "Polyhedral oligomeric silsesquioxane"
"Poly(isoprene)" "Polyhedral oligomeric silsesquioxane"
"2-Methyl-1,3-butadiene" "Polyhedral oligomeric silsesquioxane"
"2-Methylbuta-1,3-diene" "Polyhedral oligomeric silsesquioxane"
"2-Methylbuta-1,3-diene" POSS
ENR550 "Polyhedral oligomeric silsesquioxane"
"epoxidized natural rubber" "Polyhedral oligomeric silsesquioxane"
Starch "Polyhedral oligomeric silsesquioxane"
Amylopectin "Polyhedral oligomeric silsesquioxane"
Amylose "Polyhedral oligomeric silsesquioxane"

2.4.1 POS with starch

The inclusion of POS into starch either by chemical or physical means is scarce reported in the literature.

2.4.1.1 Starch-POS non-covalent bond

So far, only one scientific work has studied some aspects of graphene oxide attached to POS that is introduced into semi-interpenetrating polymer network synthetized from acrylamide in the presence of starch by using free radical polymerization [77].

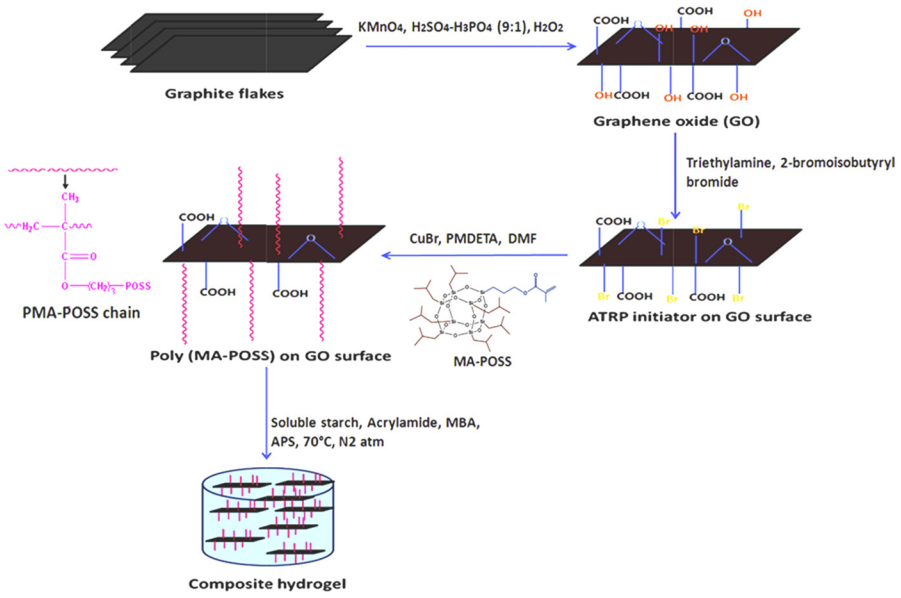

Figure 2.12 Schematic diagram of the graphene oxide coupled with POS and used in a composite hydrogel with starch

2.4.1.2 Starch-POS covalent bond

In the patent US 10,011,706 B2 [78] it is reported a reaction between starch and glycidyl isobutyl POSS using aluminium triflate under reflux (Figure 2.13).

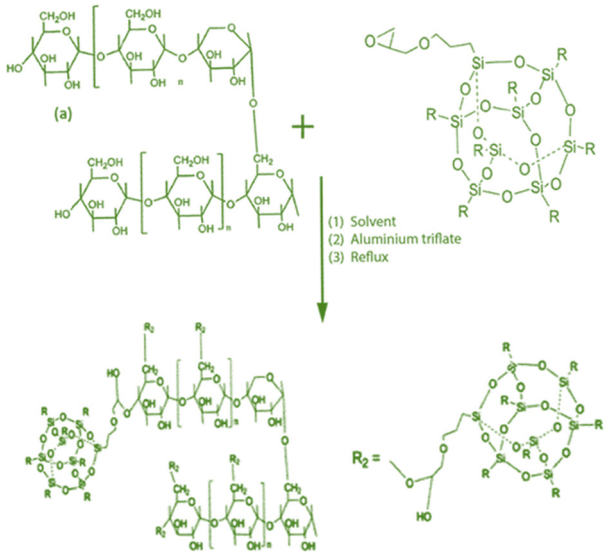

Figure 2.13 Schematic representation of POSS starch grafting reaction

2.4.2 POS with Natural rubber or ENR50

Comprehensive books about elastomers and fillers mark as promising the use of POS into elastomeric materials like NR [39, 79-81]. Never the less, the inclusion of POS into NR or ENR either by chemical or physical means are few. NR and ENR50 was taken into account since both were use in this dissertation and ENR50 is a direct modified polymer from NR.

2.4.2.1 Non-covalent bond of NR or ENR with POS

As representative of non-covalent bond between ENR or NR with POS two works were found, the first a hybrid POS dispersed in ENR50 to develop a composite solid polymer electrolyte (SPE) film [82]. The second a POS-rectorite hybrid dispersed in NR (Figure 2.14).

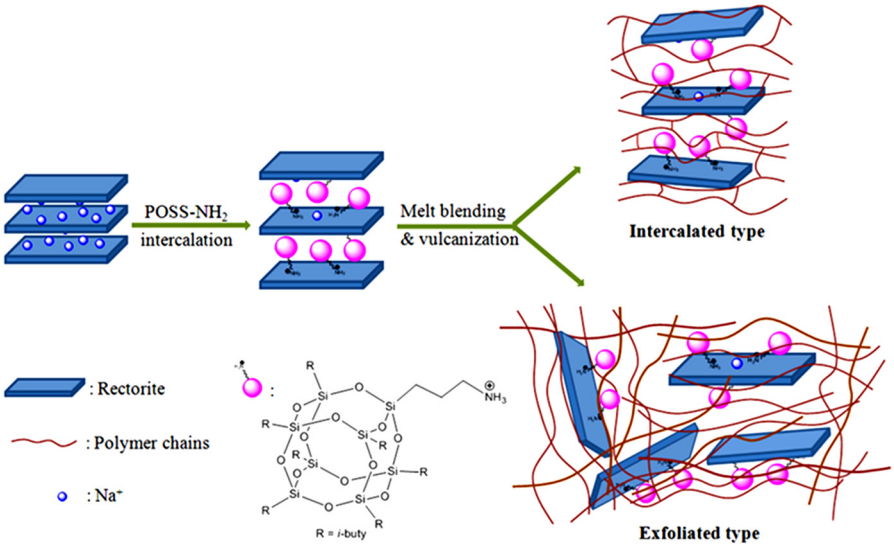

Figure 2.14 Schematic representation of the process to dispersed POS-rectorite hybrid into natural rubber. Tooked from Zhao [83]

There is also patent related to rubber compound containing POS, it tries to mention every single possible POS that they could cover regardless of its chemical properties, for this reason this patent is cited in this section of non-covalent bounding [84].

2.4.2.2 Covalent bond of NR or ENR with POS

There is just one scientific paper that use NR in conjunction with POS, in particular Octavinyl-POS is used as cross linker agent in NR [85] for vulcanization. There is also another scientific paper but NR or polyisoprene is not used directly, in the paper, ring opening metastasis polymerization (ROMP) is used to synthetize a copolymer of cyclopentyl periphery-POSS with polyisoprene from non-natural rubber or isoprene but from 1,5-dimethyl-1,5-cyclooctadiene (Figure 2.15).

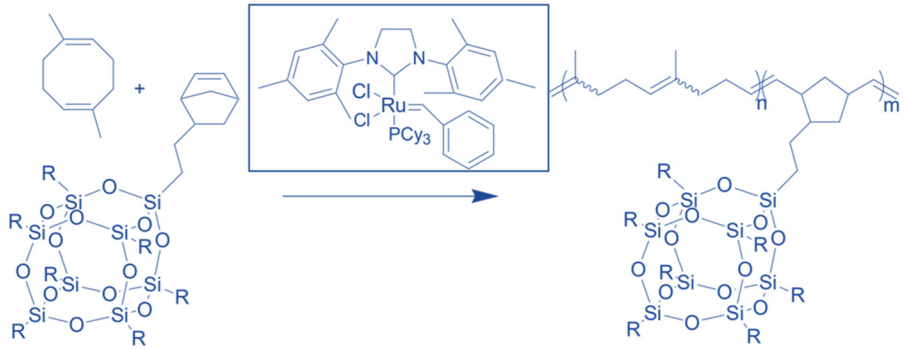

Figure 2.15 Scheme of polyisoprene-like POS copolymer synthesis by ROMP. Took from Seurer [86]

The only scientific paper that use ENR50 and a POS, is the one that used an incomplete cyclopentyl trisilanol-POS grafted to ENR50 through a reflux reaction using Tin (II) chloride dihydrate ($SnCl_2\ H_2O$) as catalyst [87].

What is more often found in the literature are patents which mention the monomer that constitute natural rubber which have some interaction with POS. In [88] the polyisoprene monomer is use as moiety for a POS photoinitiator which could function as initiator and nanofiller, in [89] the monomer is use as a copolymer in a crystal nucleation agent for crystalline polymers and in [90] it is use as coupling agent of bifunctional POS in a rubber composition.

In the patent [91] natural rubber, polyisoprene and POS are used as part of the composition of a vulcanized rubber that can be used for the manufacture of tyres.

The most closed related patent to the present work is [84] which graft POS to the main polymeric chain of NR using a thiol functional group and the double bond in the isoprene.

2.4.3 Conclusion of polyhedral oligomeric silsesquioxane into starch and natural rubber in the literature

Most of the patents do not make emphasis in the couples NR-POS but those that make it are related to tyre industry, these reveals that there is industrial interest in this work. The deep research reveals that this dissertation presents novel work regarding POS and NR because there are very few works related and none with our specific reactions. There are so few literatures related to starch and POS that almost all related work presented in this dissertation is novel.

2.5 References

1. Pérez, S. and E. Bertoft, *The molecular structures of starch components and their contribution to the architecture of starch granules: A comprehensive review*. 2010: Weinheim. p. 389-420.
2. Rindlav-Westling, Å. and P. Gatenholm, *Surface composition and morphology of starch, amylose, and amylopectin films.* Biomacromolecules, 2003. **4**(1): p. 166-172.
3. Kim, J.R. and A.N. Netravali, *Self-healing starch-based 'green'thermoset resin.* Polymer, 2017. **117**: p. 150-159.
4. Ceseracciu, L., et al., *Robust and biodegradable elastomers based on corn starch and polydimethylsiloxane (PDMS).* ACS applied materials & interfaces, 2015. **7**(6): p. 3742-3753.
5. Chen, C.-J., Y.-C. Shen, and A.-I. Yeh, *Physico-chemical characteristics of media-milled corn starch.* Journal of agricultural and food chemistry, 2010. **58**(16): p. 9083-9091.
6. Jiménez, A., et al., *Edible and biodegradable starch films: a review.* Food and Bioprocess Technology, 2012. **5**(6): p. 2058-2076.

7. Ebnesajjad, S., *Handbook of biopolymers and biodegradable plastics: properties, processing and applications.* 2013.
8. Yao, Y., J. Zhang, and X. Ding, *Partial β-amylolysis retards starch retrogradation in rice products.* Journal of agricultural and food chemistry, 2003. **51**(14): p. 4066-4071.
9. Biliaderis, C., et al., *Thermal behavior of amylose-lipid complexes.* Carbohydrate Polymers, 1985. **5**(5): p. 367-389.
10. Zhang, Y. and J.H. Han, *Plasticization of Pea Starch Films with Monosaccharides and Polyols.* Journal of Food Science, 2006. **71**(6): p. E253-E261.
11. Janjarasskul, T. and J.M. Krochta, *Edible Packaging Materials.* Annu. Rev. Food Sci. Technol., 2010. **1**(1): p. 415-448.
12. Muscat, D., et al., *Comparative study of film forming behaviour of low and high amylose starches using glycerol and xylitol as plasticizers.* 2012.
13. Guilbert, S., B. Cuq, and N. Gontard, *Recent innovations in edible and/or biodegradable packaging materials.* Food Additives and Contaminants, 1997. **14**(6-7): p. 741-751.
14. Ahmed, J. and J. Ahmed, *Starch-based polymeric materials and nanocomposites chemistry, processing, and applications*, ed. J. Ahmed. 2012, Boca Raton: CRC Press.
15. Róz, A.L.D., et al., *The effect of plasticizers on thermoplastic starch compositions obtained by melt processing.* Carbohydrate Polymers, 2006. **63**(3): p. 417-424.
16. Wang, L., R.L. Shogren, and C. Carriere, *Preparation and properties of thermoplastic starch-polyester laminate sheets by coextrusion.* Polymer Engineering & Science, 2000. **40**(2): p. 499-506.
17. Chaudhary, D., Y. Dong, and K.K. Kar, *Hydrophilic plasticized biopolymers: Morphological influence on physical properties.* Materials Letters, 2010. **64**(7): p. 872-875.
18. Zhang, Y. and J.H. Han, *Sorption Isotherm and Plasticization Effect of Moisture and Plasticizers in Pea Starch Film.* Journal of Food Science, 2008. **73**(7): p. E313-E324.
19. Smits, A.L.M., et al., *Interaction between dry starch and plasticisers glycerol or ethylene glycol, measured by differential scanning calorimetry and solid state NMR spectroscopy.* Carbohydrate Polymers, 2003. **53**(4): p. 409-416.
20. Galdeano, M.C., et al., *Effects of plasticizers on the properties of oat starch films.* Materials Science & Engineering C, 2009. **29**(2): p. 532-538.
21. Yang, J.H., J.G. Yu, and X.F. Ma, *Preparation of a Novel Thermoplastic Starch (TPS) Material using Ethylenebisformamide as the Plasticizer.* Starch - Stärke, 2006. **58**(7): p. 330-337.
22. Huang, M., J. Yu, and X. Ma, *Ethanolamine as a novel plasticiser for thermoplastic starch.* Polymer Degradation and Stability, 2005. **90**(3): p. 501-507.
23. Ma, X. and J. Yu, *Formamide as the plasticizer for thermoplastic starch.* Journal of Applied Polymer Science, 2004. **93**(4): p. 1769-1773.
24. Ma, X. and J. Yu, *The plastcizers containing amide groups for thermoplastic starch.* Carbohydrate Polymers, 2004. **57**(2): p. 197-203.
25. Suriyatem, R. and P. Rachtanapun, *Prediction Modeling for Moisture Sorption Isotherms of Rice Starch/Carboxymethyl Cellulose from Durian Rind Blend Films.* Applied Mechanics and Materials, 2013. **431-431**(Mechanical Engineering, Industrial Materials and Industrial Electronics): p. 32-36.
26. Bernazzani, P., et al., *Evaluation of the phase composition of amylose by FTIR and isothermal immersion heats.* Polymer, 2008. **49**(19): p. 4150-4158.
27. Muscat, D., et al., *Comparative study of film forming behaviour of low and high amylose starches using glycerol and xylitol as plasticizers.* Journal of Food Engineering, 2012. **109**(2): p. 189-201.
28. Pérez, S. and E. Bertoft, *The molecular structures of starch components and their contribution to the architecture of starch granules: A comprehensive review.* Starch-Stärke, 2010. **62**(8): p. 389-420.
29. Bonner, J. and A. Galston, *The physiology and biochemistry of rubber formation in plants.* The Botanical Review, 1947. **13**(10): p. 543-596.
30. Joseph, R., *Practical guide to latex technology*. 2013, S.l.]: S.l. : Smithers Rapra.

31. Shanks, R., *Linear and non-linear viscoelastic behaviour of natural rubber composites from micro- to nanoscales*, C.H.C.L.A.P.J.J. S. Thomas and H.J. Maria, Editors. 2014, Royal Society of Chemistry (London, United Kingdom).
32. Jo, J.O., et al., *Development of nanocomposite with epoxidized natural rubber and functionalized multiwalled carbon nanotubes for enhanced thermal conductivity and gas barrier property.* Materials & Design, 2015. **83**: p. 777-785.
33. THOMAS, S., *Natural rubber-based composites and nanocomposites: state of the art, new challenges and opportunities.* Natural Rubber Materials: Volume 2: Composites and Nanocomposites, 2013. **8**: p. 1.
34. Li, G., et al., *Polyhedral oligomeric silsesquioxane (POSS) polymers and copolymers: A review*, in *J. Inorg. Organomet. Polym. Mater.* 2001. p. 123-154.
35. Arroyo, M., et al., *Morphology/behaviour relationship of nanocomposites based on natural rubber/epoxidized natural rubber blends.* Composites science and technology, 2007. **67**(7): p. 1330-1339.
36. Ketkaew, R. and Y. Tantirungrotechai, *Dissipative Particle Dynamics Study of SWCNT Reinforced Natural Rubber Composite System: An Important Role of Self-Avoiding Model on Mechanical Properties.* Macromolecular Theory and Simulations, 2018: p. 1700093.
37. Rajasekar, R., et al., *Development of nitrile butadiene rubber–nanoclay composites with epoxidized natural rubber as compatibilizer.* Materials & Design, 2009. **30**(9): p. 3839-3845.
38. Ismail, H., A. Ramly, and N. Othman, *Effects of silica/multiwall carbon nanotube hybrid fillers on the properties of natural rubber nanocomposites.* Journal of Applied Polymer Science, 2013. **128**(4): p. 2433-2438.
39. Pothen, L., C.H. Chan, and S. Thomas, *Natural Rubber Materials, Volume 2-Composites and Nanocomposites*. 2013: Royal Society of Chemistry.
40. Hashim, A.S., N. Kawabata, and S. Kohjiya, *Silica reinforcement of epoxidized natural rubber by the sol-gel method.* Journal of Sol-Gel Science and Technology, 1995. **5**(3): p. 211-218.
41. Lopattananon, N., D. Jitkalong, and M. Seadan, *Hybridized reinforcement of natural rubber with silane-modified short cellulose fibers and silica.* Journal of Applied Polymer Science, 2011. **120**(6): p. 3242-3254.
42. Haq, M., et al., *Hybrid bio-based composites from blends of unsaturated polyester and soybean oil reinforced with nanoclay and natural fibers.* Composites Science and Technology, 2008. **68**(15): p. 3344-3351.
43. Huda, M., et al., *The effect of silane treated-and untreated-talc on the mechanical and physico-mechanical properties of poly (lactic acid)/newspaper fibers/talc hybrid composites.* Composites Part B: Engineering, 2007. **38**(3): p. 367-379.
44. Zhao, Y., et al., *Toughened elastomer/polyhedral oligomeric silsesquioxane (POSS)-intercalated rectorite nanocomposites: Preparation, microstructure, and mechanical properties.* Polymer Composites, 2015.
45. Porter, D., *Group interaction modelling of polymer properties*. 1995: CRC Press.
46. Sharma, P., S. Roy, and H.A. Karimi-Varzaneh, *Validation of Force Fields of Rubber through Glass-Transition Temperature Calculation by Microsecond Atomic-Scale Molecular Dynamics Simulation.* The Journal of Physical Chemistry B, 2016. **120**(7): p. 1367-1379.
47. Lee, C.-W., et al., *A novel synthetic route to natural rubber/montmorillonite nanocomposites using colloid stabilization–destabilization method.* Composites Part A: Applied Science and Manufacturing, 2011. **42**(11): p. 1826-1832.
48. Omnès, B., et al., *Effective properties of carbon black filled natural rubber: Experiments and modeling.* Composites Part A: Applied Science and Manufacturing, 2008. **39**(7): p. 1141-1149.
49. Ponnamma, D., et al., *Free-volume correlation with mechanical and dielectric properties of natural rubber/multi walled carbon nanotubes composites.* Composites Part A: Applied Science and Manufacturing, 2015. **77**: p. 164-171.
50. Skeist, I., *Handbook of adhesives*. 2012: Springer Science & Business Media.
51. Gazeley, K. and W. Wake, *Natural rubber adhesives*, in *Handbook of adhesives*. 1990, Springer. p. 167-184.
52. Moe, N.E. and M. Ediger, *Molecular dynamics computer simulation of polyisoprene local dynamics in dilute toluene solution.* Macromolecules, 1995. **28**(7): p. 2329-2338.

53. Mittal, V., *Modeling and prediction of polymer nanocomposite properties*. 2012: John Wiley & Sons.
54. Drisko, G.L. and C. Sanchez, *Hybridization in Materials Science – Evolution, Current State, and Future Aspirations.* European Journal of Inorganic Chemistry, 2012. **2012**(32): p. 5097-5105.
55. Taniguchi, N., C. ARAKAWA, and T. KOBAYASHI. *On the basic concept of'nano-technology'*. in *Proceedings of the International Conference on Production Engineering, 1974-8*. 1974. The Japan Society of Mechanical Engineers.
56. Potocnik, J., *Commission recommendation of 18 October 2011 on the definition of nanomaterial.* Off. J. Eur. Union L, 2011. **275**: p. 38-40.
57. Lövestam, G., et al., *Considerations on a definition of nanomaterial for regulatory purposes.* Joint Research Centre (JRC) Reference Reports, 2010: p. 80004-1.
58. ISO, T., *27687 Nanotechnologies-Terminology and definitions for nano-objects.* Nanoparticle, nanofibre and nanoplate, 2008.
59. Scholl, T., *Surface-modified, oxidic or siliceous fillers and their use*. 1998, US Patent 5,780,531.
60. Korth, K., et al., *Silane-modified oxidic or siliceous filler, process for its production and its use*. 2007, US Patent 7,186,768.
61. Hartmann-Thompson, C., *Applications of polyhedral oligomeric silsesquioxanes*. Vol. 3. 2011: Springer.
62. Calzaferri, G. and R. Imhof, *Dalton communications. Synthesis of the first organometallic monosubstituted octanuclear silasesquioxane.* Journal of the Chemical Society, Dalton Transactions, 1992(23): p. 3391.
63. Lin, W.-J., et al., *Synthesis and Optoelectronic Properties of Starlike Polyfluorenes with a Silsesquioxane Core.* Macromolecules, 2004. **37**(7): p. 2335-2341.
64. Knischka, R., et al., *Silsesquioxane-Based Amphiphiles.* Langmuir, 1999. **15**(14): p. 4752-4756.
65. Li, G., et al., *Polyhedral oligomeric silsesquioxane (POSS) polymers and copolymers: a review.* Journal of Inorganic and Organometallic Polymers, 2001. **11**(3): p. 123-154.
66. Zhang, W., G. Camino, and R. Yang, *Polymer/polyhedral oligomeric silsesquioxane (POSS) nanocomposites: An overview of fire retardance.* Progress in Polymer Science, 2017. **67**: p. 77-125.
67. Martinez-Pardo, I., et al., *Thermoplastic starch-nanohybrid films with polyhedral oligomeric silsesquioxane.* Carbohydrate Polymers, 2017. **173**: p. 170-177.
68. Ayandele, E., B. Sarkar, and P. Alexandridis, *Polyhedral oligomeric silsesquioxane (POSS)-containing polymer nanocomposites.* Nanomaterials, 2012. **2**(4): p. 445-475.
69. Tang, S., et al., *Recoverable organorhodium-functionalized polyhedral oligomeric silsesquioxane: a bifunctional heterogeneous catalyst for asymmetric transfer hydrogenation of aromatic ketones in aqueous medium.* Chem. Commun., 2012. **48**(50): p. 6286-6288.
70. Li, W., et al., *Immobilization of isolated FI catalyst on polyhedral oligomeric silsesquioxane-functionalized silica for the synthesis of weakly entangled polyethylene.* Chem. Commun., 2016. **52**(74): p. 11092-11095.
71. Nair, B.P., D. Vaikkath, and P.D. Nair, *Polyhedral oligomeric silsesquioxane-F68 hybrid vesicles for folate receptor targeted anti-cancer drug delivery.* Langmuir : the ACS journal of surfaces and colloids, 2014. **30**(1): p. 340-347.
72. John, U., et al., *First step towards a model system of the drug delivery network based on amide-POSS nanocarriers.* RSC Adv., 2017. **7**(14): p. 8394-8401.
73. Hartmann-Thompson, C., et al., *Hydrogen-bond acidic polyhedral oligosilsesquioxane filled polymer coatings for surface acoustic wave sensors.* Journal of applied polymer science, 2007. **104**(5): p. 3171-3182.
74. Narikiyo, H., et al., *Development of the optical sensor for discriminating isomers of fatty acids based on emissive network polymers composed of polyhedral oligomeric silsesquioxane.* Bioorganic & Medicinal Chemistry, 2017. **25**(13): p. 3431-3436.
75. Chhabra, P. and V. Choudhary, *Polymer nanocomposite membranes based on sulfonated poly(ether ether ketone) and trisilanol phenyl POSS for fuel cell applications.* Journal of Applied Polymer Science, 2010. **118**(5): p. 3013-3023.

76. Elumalai, V. and D. Sangeetha, *Anion exchange composite membrane based on octa quaternary ammonium Polyhedral Oligomeric Silsesquioxane for alkaline fuel cells.* Journal of Power Sources, 2018. **375**: p. 412-420.
77. Ata, S., S.L. Banerjee, and N.K. Singha, *Polymer nano-hybrid material based on graphene oxide/POSS via surface initiated atom transfer radical polymerization (SI-ATRP): Its application in specialty hydrogel system.* Polymer, 2016. **103**(C): p. 46-56.
78. Mohan, M.S., K. Mishra, and R.K. Vaidyanathan, *System and method for synthesis of POSS-graphene oxide derivatives as effective fillers for developing high performance composites*. 2018, Google Patents.
79. Kodal, M. and G. Ozkoc, *Micro and Nanofillers in Rubbers*. 2013 ed, ed. P.M. Visakh, A.K. Chandra, and A.P. Mathew. Vol. 11. 2013, Berlin, Heidelberg: Berlin, Heidelberg: Springer Berlin Heidelberg. 303-356.
80. Strankowski, M., *Nonlinear viscoelasticity in Three Dimensional filler reinforced rubber composites and nanocomposites*, in *Non-Linear Viscoelasticity of Rubber Composites and Nanocomposites*. 2014, Springer. p. 59-83.
81. Stephen, R. and S. Thomas, *Nanocomposites: state of the art, new challenges and opportunities.* Rubber Nanocomposites: Preparation, Properties, and Applications, S. Thomas and R. Stephen Eds., John Wiley & Sons, singapore, 2010: p. 1.
82. Mei, H., et al., *The grafting reaction of epoxycyclohexyl polyhedral oligomeric silsesquioxanes with carboxylic methoxypolyethylene glycols and the properties of composite solid polymer electrolytes with the graftomer.* Journal of Applied Polymer Science, 2017. **134**(7): p. n/a-n/a.
83. Zhao, Y., et al., *Toughened elastomer/polyhedral oligomeric silsesquioxane (POSS)-intercalated rectorite nanocomposites: Preparation, microstructure, and mechanical properties.* Polymer Composites, 2017. **38**(S1): p. E443-E450.
84. Puhala, A.S., et al., *Rubber compound containing a polyhedral oligomeric silsesquioxanes*. 2005, Google Patents.
85. Zhao, L., et al., *Morphology and thermomechanical properties of natural rubber vulcanizates containing octavinyl polyhedral oligomeric silsesquioxane.* Composites Part B, 2018. **139**: p. 40-46.
86. Seurer, B., *Synthesis and characterization of novel thermoplastic elastomers employing polyhedral oligomeric silsesquioxane physical crosslinks*, E.B. Coughlin, A. Crosby, and H. Winter, Editors. 2008, ProQuest Dissertations Publishing.
87. Rosniza, H. and A.B. Mohamad. *The Structural Studies of Oxirane Ring Opening Reaction in Epoxidized Natural Rubber (ENR-50) by SnCl2. 2H2O and the Formation of ENR/TiN Complex Hybrid*. in *Advanced Materials Research*. 2013. Trans Tech Publ.
88. Wang, F., F. Wang, and C. He, *Photoinitiators functioned as both initiators and nanofillers*. 2018, Google Patents.
89. Coughlin, E.B., Y. Nozue, and S. Seno, *Crystal nucleating agents, crystalline polymer composition, methods of manufacture thereof, and articles thereof*. 2012, Google Patents.
90. Robert, P., et al., *Plasticizing system for a rubber composition*. 2012, Google Patents.
91. Crutchley, G., *Rubber Composition Comprising a Polyhedral Oligomeric Silsesquioxane Additive*. 2007, Google Patents.

3 CHARACTERISATION TECHNIQUES

3.1 Fourier-transform infrared spectroscopy

Fourier-transform infrared spectroscopy (FTIR) quantifies the infrared absorption/transmittance capacity of the sample. It consists of three basic elements (infrared source, interferometer and detector) that produce the spectrograph within seven principal steps of the measurement (Figure 3.1).

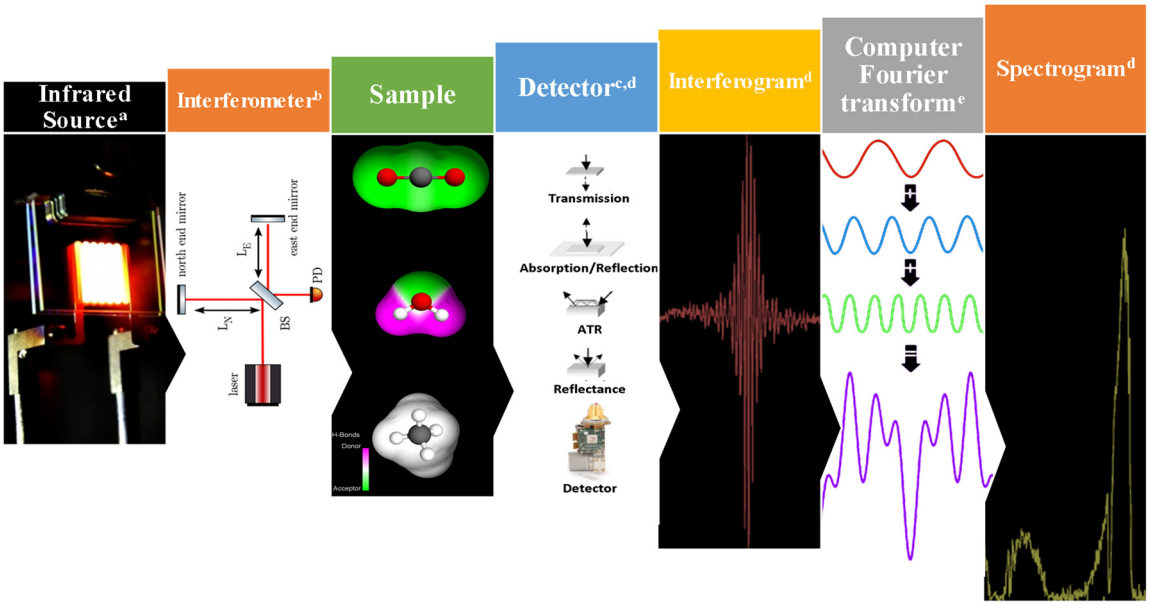

Figure 3.1 Schematic representation of the seven principal steps in FTIR instrument measurement. Images adapted from a [1], b [2], c [3] d [4] and e [5]

The infrared radiation arranges from wavelength of 700 nm to 1,000,000 nm (1 mm), for its study and application. International commission on illuminations has divided the infrared radiation in three different bands: IR-A, IR-B and IR-C [6] (Table 3.1).

Table 3.1 Infrared band division recommended by international commission on illumination.

Band name	Wavelength interval [µm]	Frequency [THz]
IR-A	0.7 to 1.4	215 to 430
IR-B	1.4 to 3	100 to 215
IR-C	3 to 1000	0.3 to 100

The covalent bonds between atoms in a molecule are in constant vibrations and this vibration can be of two types: tension or flexion. The tension vibration is due to a continuous change in the interatomic distance along the axis of connection between two atoms. The flexion vibration is characterized by a change in an angle between two bonds and can be divided into four types: snipping, rocking, flapping

and twisting. Any change in the amplitude of this vibrations is reflected in the spectrogram as an absorption peak (Figure 3.2).

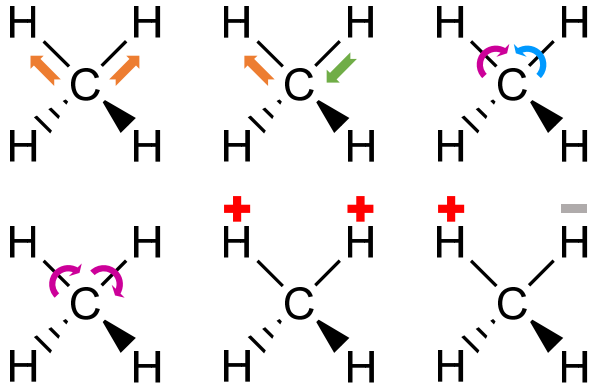

Figure 3.2 Tension and flexion deformation of methylene group. The arrows indicate movements in the plane, plus and minus signs indicate movements perpendicular to the plane (up and down respectable). Figure adapted from Pardo [7]

The infrared radiation vibrates at the same vibration interval as the molecules. So, if a molecule is irradiated with an infrared radiation, it will absorb those frequencies radiation that are exactly equal to the vibration frequencies of the different bonds that constitute the molecule. The absorbed radiation at of each type of bond are specific to each wave length. The infrared spectrum of a compound is the representation of the absorption that occurs in the infrared region as a function of the frequency of the radiation. The amount of radiation absorbed is measured as a percentage of transmittance. Because each functional group has a characteristic absorption at a single wavelength, it is possible to identify the functional groups that constitutes a specific molecule or compound.

3.2 Halogen moisture analyser

As any thermo-gravimetric analysis, the method is based in measure the mass change of the probe over time. Particularly in this method the change of mass is due to the radiation from a halogen lamp which irradiates the probe evenly with accurate control of its temperature (Figure 3.3). All the mass loss independently from the composition is interpreted as moisture content. The main advantage of this methods over using electrical resistance drying systems is the saving on time trails [8, 9].

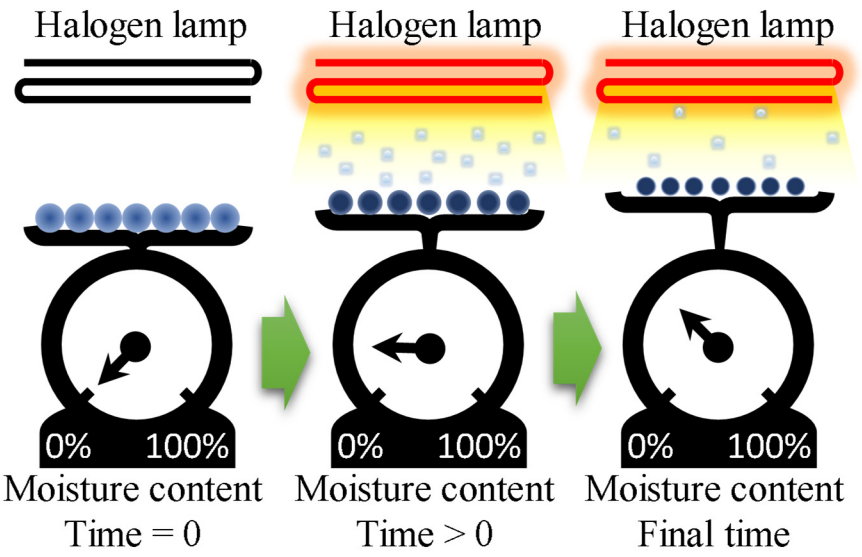

Figure 3.3 Schematic representation of a halogen moisture analyser running at different stages of a test

The most important parameter of the instrument along with the temperature is its set up to switch off criteria when the test is completed as a true dry weight can only be obtained at infinite time. For this reason and depending greatly on the type of the sample the switch-off criteria is based on the mean weight loss per time interval (Figure 3.4). A shorter time is preferred over a longer time for slow-drying sample with a low moisture content.

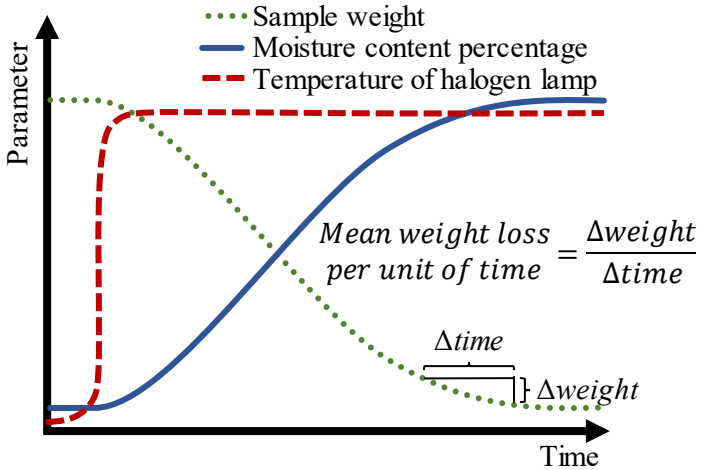

Figure 3.4 Principal parameters of halogen moisture analyser changes over time

3.3 Contact angle goniometer, static sessile drop method

Is generally agreed that the contact angle method is the most practical method used to measure the surface energy (liquid- solid, vapor-solid) or surface tension [10]. The technic is based in the equilibrium between three components to be involved in the measurement.

The wetting phenomena of the system can be understood and study from the Young's equation (1).

$$\gamma_{lv}\cos\theta_Y = \gamma_{sv} - \gamma_{sl} \qquad (1)$$

Where γ_{lv} is the liquid-vapor surface tension, θ_Y is the Young's contact angle, γ_{sv} is the solid-vapor surface tension and γ_{sl} is the solid-liquid surface tension (Figure 3.5).

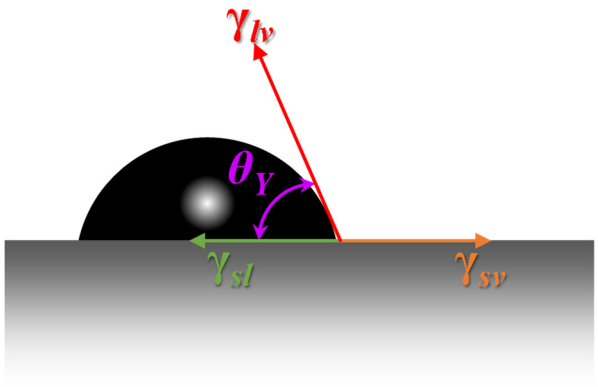

Figure 3.5 Young's equation parameters in a contact angle of a droplet on a solid surface

Experimentally only the liquid-vapor and the contact angle can be directly measure, for this reason, additional information is needed to determine the others surfaces tensions.

Experimentally observed contact angle at equilibrium is different from the Young's contact angle unless following constrains are fulfil:

1. Ideal solid surface is needed, or in other words a contact angle hysteresis shall not occur.
2. Solid surface shall not be a chemically heterogeneous solid.
3. The solid surfaces must be "smooth".
4. No swelling, penetration or chemical reaction shall occur.

The measurement of the contact angle falls in the category of tensiometric techniques. It measures the energies at interface(s) that determines adsorption and adhesion and it is sensitive enough up to 0.5 nm of surfaces [11].

The sessile drop technique is a method where a droplet of liquid with a known surface energy is placed over the surface of the solid of interest with unknow surface energy. The shape of the drop and the

surface as a base line is used to calculate the contact angle. The contact angle is the arc between the tangent of the drop and the solid surface at the edge of the droplet.

A goniometer is simply an apparatus for measuring an angle, in this case the sessile drop contact angle. A syringe is used to deposit a droplet over the surface of the solid of interest. A camera is pointed parallel to the surface plane to take image(s) of the droplet. Normally a source of light is placed parallel but opposite to the camera is placed pointing in the direction of the drop. The camera is used for image acquisition (Figure 3.6). The image is analysed either manually or automatically using a computer.

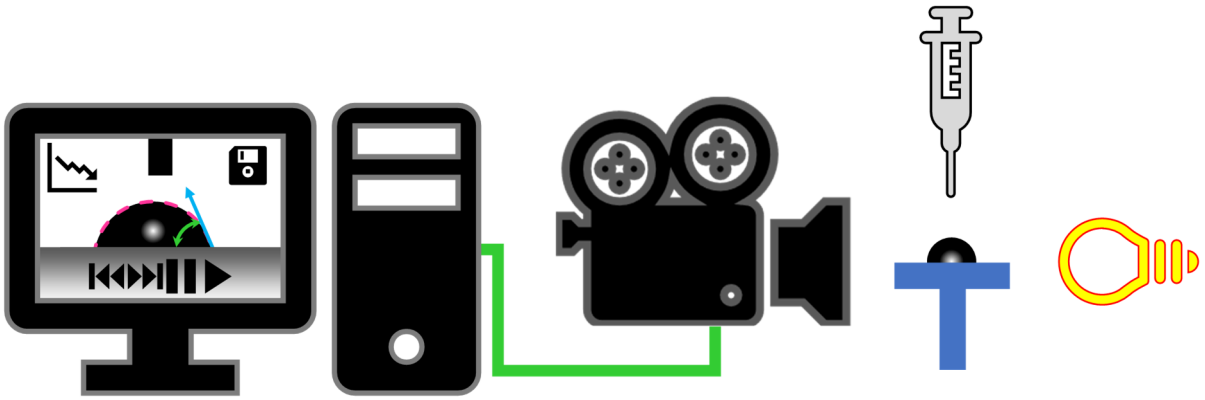

Figure 3.6 Goniometer simplified diagram

3.4 Universal testing machine

Universal testing machines are known by many names such as universal tester, universal mechanical testing machine, material testing machine or Instron, the later due to the great popularity of the manufacturer.

The main components of a universal testing machine are shown in Figure 3.7 and are:

1. Base: it is the lower surface of the instrument, normally it is a very resistant rigid steel plate. Over its surface it has the space necessary to allocate the accessories for the test fixtures and the frame is permanent mounted over it.
2. Frame: It confines the main body of the instrument, it is rigid and forms the main support of the cross head and encloses the mechanical parts that move the cross head.
3. Cross head: It is mounted on the load frame and moves vertically, it also tracks the strain during the test and gives support to the load cell.

4. Load cell: It is used to measure the stress during the test and have the space necessary to fit in the opposite part of the accessories for the test fixtures.
5. Test fixtures: Depending on the type of the test, the fixtures vary and they are fixed to the base and to the load cell.
6. Display and control unit: They are used for calibration, programming the test, setting limits, setting parameter and displaying results.

Figure 3.7 Picture of a universal testing machine

Depending on the accessories, set-up and the programming it is used to determine many mechanical characteristics/properties of materials like Young's modulus, modulus of elasticity, ultimate elongation at break, adhesion force, coefficient of friction, bulk modulus, yield stress, ultimate stress among many others. Beside the custom test that can be performed in the machine, the most measured tests are for tensile, compression, torsion, shear and bending force.

The universal testing machine works on the principle of strain-stress during compression, shear or elongation of a material. For example, a uniaxial direct stress (σ_x) and direct strain(ε_x) in *x* direction in can be related in the hook's law by the Elastic modulus or Young's modulus (E) equation (2).

$$\boldsymbol{\sigma_x = E\,\varepsilon_x} \qquad (2)$$

Notice that E can be determine experimentally using the universal testing machine [12], with the reference to Figure 3.8, σ and ε can be expressed as equations (3) and (4) respectable.

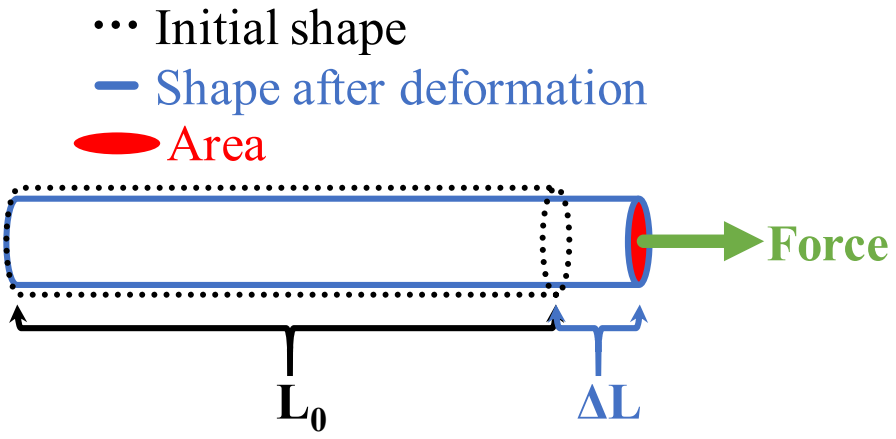

Figure 3.8 Example of uniaxial deformation of a cylinder due to a force F with initial length (L_0)

$$\sigma = \frac{Force}{Area} \quad (3)$$

$$\varepsilon = \frac{\Delta L}{L_0} \quad (4)$$

3.5 Dynamic mechanical analysis

A dynamic mechanical analyser or DMA is an instrument to measure and analyse the material's response to an oscillating force. When this force is applied to a material, the force causes a sinusoidal stress which intrinsically generates a sinusoidal strain. Normally, under small oscillatory deformations, both the strain and the stress will oscillate sinusoidally shifted by a phase angle δ but with the same frequency (Figure 3.9 a). A standard device apply an oscillatory force using its motor (Stress), which cause a sinusoidal strain, the movements can be monitored using either optical encoders, linear variable differential transformer detector (LVDT) or force balanced transducers [13] (Figure 3.9 b).

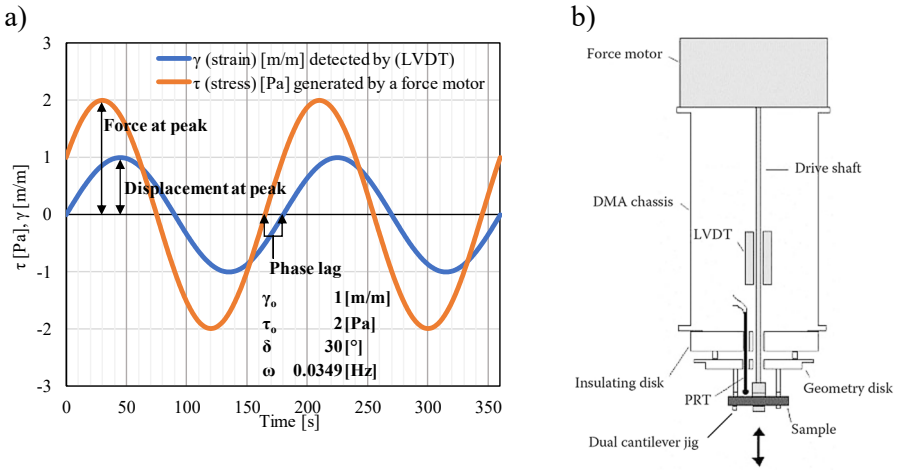

Figure 3.9 a) Stimulus-response sinusoidal curves of DMA test. b) Simple schematic of components of DMA instrument with cantilever testing geometry, adapted from Menard [13]

If the phase angle (δ [º]) or face lag (ΔT [s]) is equals to zero, the material could be considered a completely ideal elastic material. If δ is equal to 90º (tan(δ)=1) then the material could be considered as completely ideal viscous material [14]. Because the previous mentioned angles results are atypical for most of the materials, most materials can be considered in major or minor measure visco-elastic materials (Figure 3.10).

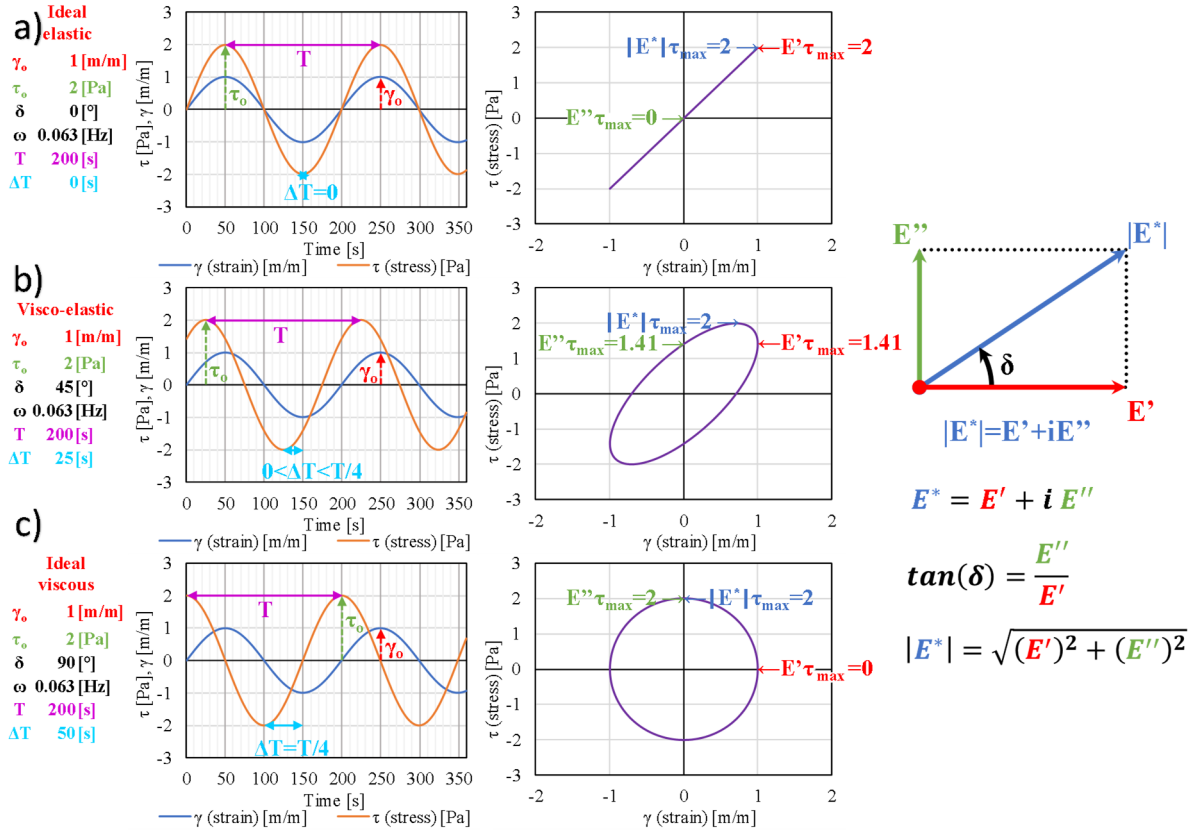

Figure 3.10 Representations of strain-stress behaviour of different materials a) elastic material, b) viscoelastic material and c) viscous material

Based in this principle, it is possible to measure properties like modulus, viscosities and damping. The sinusoidal generated and recorded curves in Figure 3.9 a and Figure 3.10 can be expressed as equations (5) and (6).

$$\gamma = \gamma_0 \sin(\omega t) \quad (5)$$

$$\tau = \tau_0 \sin(\omega t + \delta) \quad (6)$$

Normally the stress curve is decomposed in two sinusoidal functions, equation (7) , one in synchrony with the strain in equation (8) and the other 90º asynchronous as equation (9).

$$\tau = \tau' + \tau'' \quad (7)$$

$$\tau' = \tau'_0 \sin(\omega t) \quad (8)$$

$$\tau'' = \tau''_0 \cos(\omega t) \quad (9)$$

Macosko [15] use trigonometry to show that:

$$\tan(\delta) = \frac{\tau''_0}{\tau'_0} \quad (10)$$

Because of the decomposition, it is possible to suggest a synchronous elastic dynamic modulus (G', equation (11)) respectable to the strain and the 90º asynchronous viscous equivalent G'' in equation (12).

$$G' = \frac{\tau'_0}{\gamma_0} \quad (11)$$

$$G'' = \frac{\tau''_0}{\gamma_0} \quad (12)$$

From equations (10) to (12) is possible derive equation (13).

$$\tan(\delta) = \frac{G''}{G'} \quad (13)$$

It is known that the prime and double prime in G' and G'' are notation that indicates parts of a complex number and can be express as equation (14).

$$G^* = G' + i\,G'' \quad (14)$$

Also Macosko [15] used the identity in equation (15) to represent γ and τ' in equivalent terms to equation (14) to finally lead to equations (16) and (17).

$$e^{i\delta} = \cos(\delta) + i\sin(\delta) \tag{15}$$

$$\tau = G'\gamma_0 \sin(\omega t) + G'\gamma_0 \sin(\omega t) \tag{16}$$

$$\frac{\tau_0}{\gamma_0} = G^* = \sqrt{G'^2 + G''^2} \tag{17}$$

Beside the ability of DMA to mechanically characterize a material it can also test those mechanical properties in a range of temperatures, which make this instrument the best option to characterize the thermo-mechanical properties and behaviours of materials.

As shows in Figure 3.11 the sensitivity of DMA instruments are in a state of the art where is possible to measure the β γ transitions [16] in standard instruments.

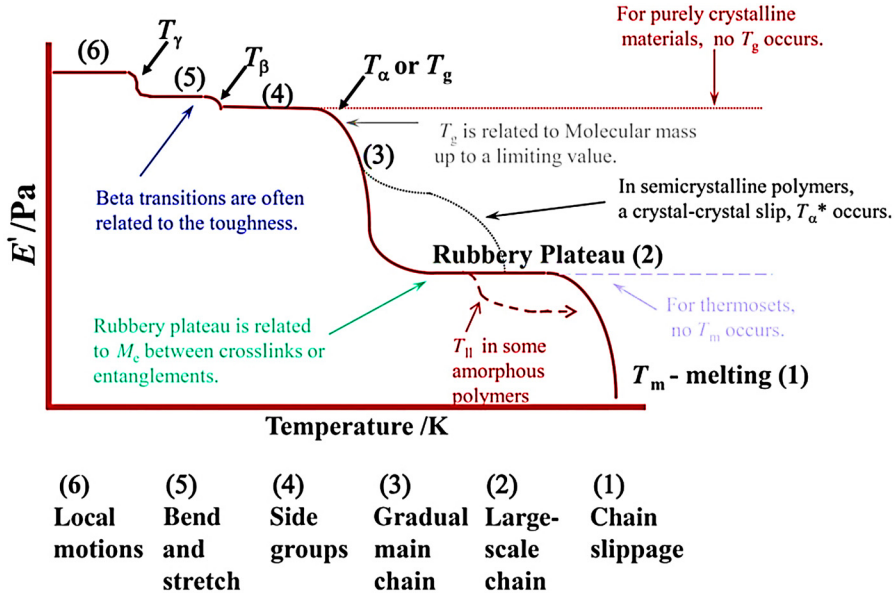

Figure 3.11 Idealized DMA scan, took from Menard [17]

There are a wide variety of test that can be performed in the instrument, each test mode has particular stress/strain profile to measure different properties or characteristics (Figure 3.3).

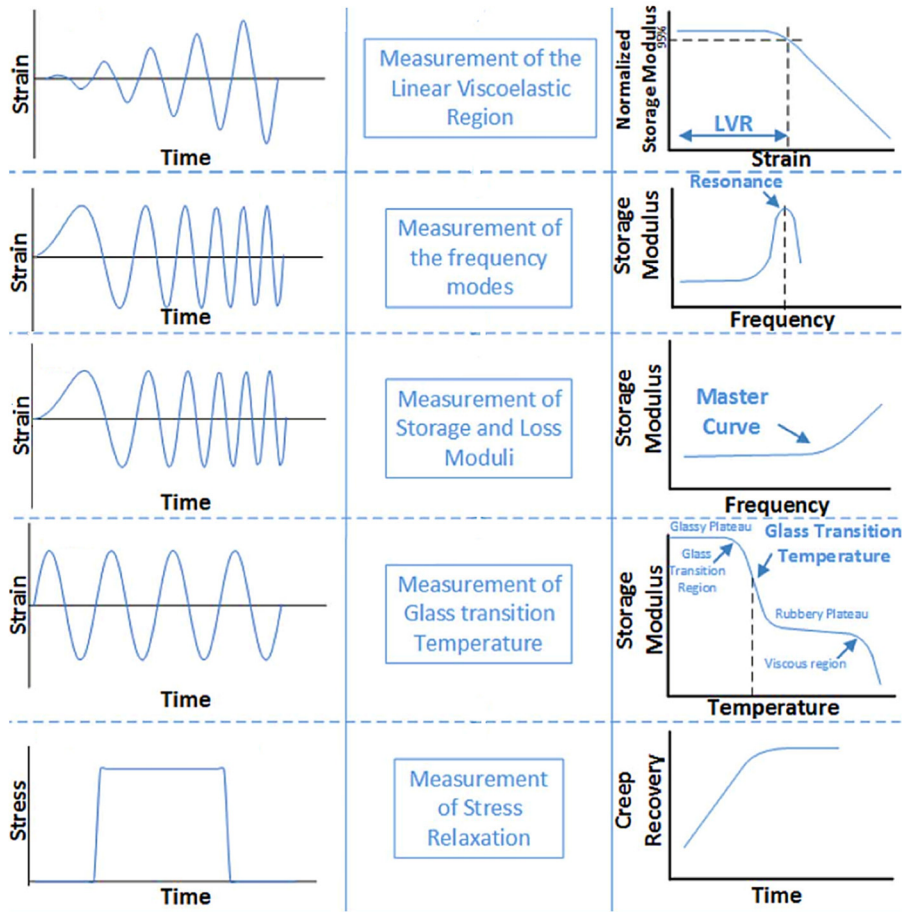

Figure 3.12 Key test modes, characterization and results of DMA, adapted from Kawak [18]

3.6 Differential Scanning Calorimeter

The differential scanning calorimeter, it is a technique in which a temperature sweep is made with a certain heating ramp [k/min]). With this ramp it is possible to quantify the heat difference that a material absorbs with respect to a reference. It is a technique used to understand the thermal behaviour of materials under heating ramp or heat rates [19].

The devices consist of two independent microfurnaces, inside a thermostatic metallic block normally made of aluminium. Each microfurnaces have enclosed one heater and one temperature sensor (Figure 3.13).

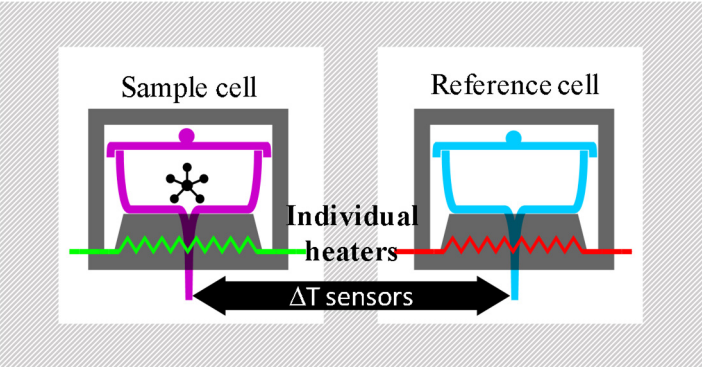

Figure 3.13 Schematic representation of a typical differential scanner calorimeter

With this technique, it is possible to observe and quantify transitions of first order like fusion or crystallization, percentage of crystallinity, thermal conductivity, heat capacity and transitions of second order like the glass transitions temperature. The main principle of the instrument is to measure the temperature difference through the electrical signal of the thermocouples. The difference is proportional to the heat flow rate. A real-time control unit to run, record, calibrate, compensate and display the actual results are required elements of the machine (Figure 3.14) where φ_m is the heat flow rate, Ts and Tr are the temperature of the sample and the reference respectable, $\Delta T = Ts-Tr$, ΔP it the compensation heating power and Pav is the average heating power [20].

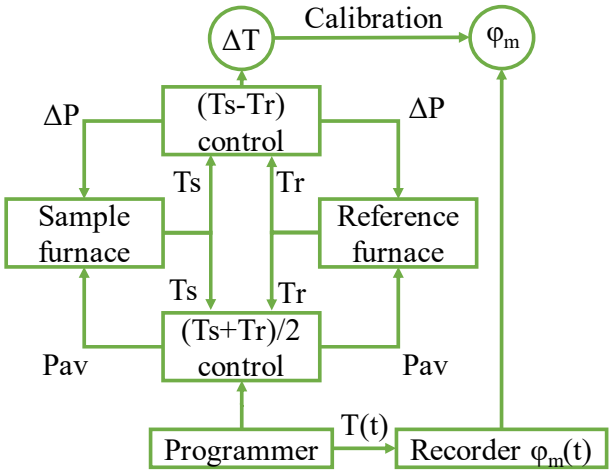

Figure 3.14 Block diagram of power compensation DSC instrument, adapted from Höhne [20]

3.7 Molecular modelling

3.7.1 Topology method Synthia.

There are many software programs developed to predict properties of polymers that use different methods. The program named Synthia [21] is similar to traditional group additive contribution methods,

but the calculated properties are expressed in terms of topological variables called connectivity indices. These indices combined with geometrical variables and structural descriptors, allowing the prediction of properties of truly novel types of polymer structures. This method transcends the limitations of traditional group contribution techniques, where the use of pre-existing experimental thermophysical data banks for its calculations are often missing, this is more evident in the design of candidate polymers for cutting-edge applications, where structural units are often considered exotic.

Synthia predicts properties of isotropic linear polymers (amorphous or amorphous phases of semicrystalline) constituted of nine elements: carbon, hydrogen, oxygen, nitrogen, silicon, chlorine, sulphur, fluorine and bromide, but the method allows prediction for polymers containing more elements using databases and extended corrections available in the Bicerano book [21]. The main topological starting point formalism for this quantitative structure properties relationship (QSPR) program is based on graph theory and connectivity indices that are calculated exactly from valence bond theory. The program includes a calculation for arbitrary bond lengths and a variable number of atoms, conformational properties of polymer chains and the distinction between intensive and extensive properties - how the properties change when the size of the system varies and distinction between backbone and side-group contributions.

The final correlation of each property uses indices, geometrical constants related to the composition, and some experimental data (normally in the range of hundreds) to fine-tune the correlation, where a typical standard deviation is in the range of 1 % to no more than 13 % and in some few cases above 25 %. The general forms of correlations in terms of connectivity indices are shown by equation (18) for intensive properties (IP) and equation (19) for extensive properties (EP).

$$IP = \sum b\frac{\chi}{N} + \begin{matrix} structural\ parameter\ and atomic\ or \\ group\ corrections + constant \end{matrix} \qquad (18)$$

$$EP = \sum a\,\chi + structural\ parameter\ and\ atomic\ or\ group\ corrections \qquad (19)$$

Where N is the non-hydrogen atoms in the system, a and b are the regression coefficients and χ represents the connectivity indices.

3.7.1.1 Topological indices calculation example

Once the repetitive unit is defined, for every non-hydrogen atom the simple atomic index (δ) is calculated as the number of non-hydrogen atoms bonded to a given non-hydrogen as well as the second atomic index (δ^v), using the equation (20) where Z^v is the number of valence electrons, N_H is the number of bonded hydrogens and Z is the atomic number.

$$\delta^v = \frac{Z^v - N_H}{Z - Z^v - 1} \quad (20)$$

Later for each non-hydrogen bond, it is calculate the bond indices β and β^v as the product of δ and δ^v respectable for each pair of atoms that form the bond, see equations (21) and (22)

$$\beta_{ij} = \delta_i \delta_j \quad (21)$$

$$\beta_{ij}^v = \delta_i^v \delta_j^v \quad (22)$$

These tasks can be better exemplified by identifying the hybridisation of each non-hydrogen atom over the diagram of the structure (Figure 3.15 a) and use a pre-calculated table as in Figure 3.15 b) to substituted the non-hydrogen atoms by their corresponding values for the vertices (δ_i, δ^v_i) and edges (β_{ij}, β^v_{ij}) in a hydrogen-suppressed diagram (Figure 3.15 c to f). Notice that only numbers into the brackets will be considered for further calculations avoiding redundancy due to the periodic structure notation and the number and symbols outside are just indicative in Figure 3.15.

With the atom and bond indices it is calculated the zeroth-order ($^0\chi$, $^0\chi^v$) and first-order ($^1\chi$, $^1\chi^v$) connectivity indices using equation (23) to (26) (Figure 3.15 g and h).

$$^0\chi = \sum \left(\frac{1}{\sqrt{\delta_i}} \right) \quad (23)$$

$$^0\chi^v = \sum \left(\frac{1}{\sqrt{\delta^v{}_i}} \right) \quad (24)$$

$$^1\chi = \sum \left(\frac{1}{\sqrt{\beta_i}} \right) \quad (25)$$

$$^1\chi^v = \sum \left(\frac{1}{\sqrt{\beta^{v_i}}} \right) \quad (26)$$

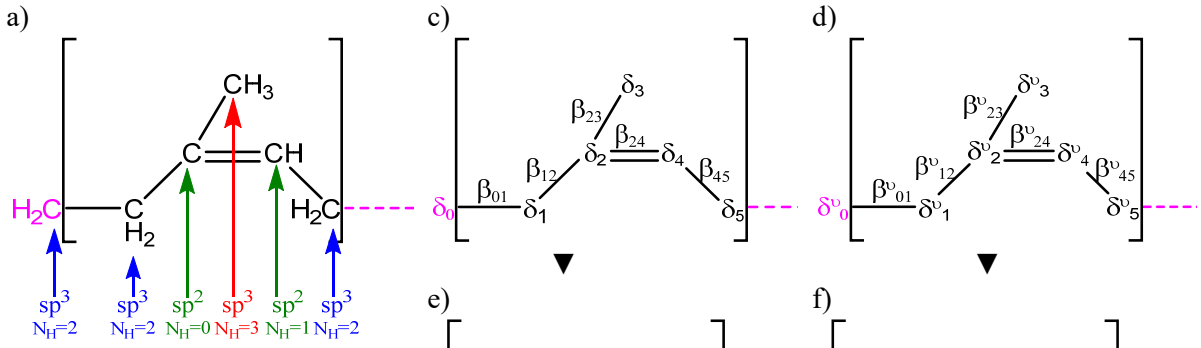

b)

Carbon hybridisation	N_H	δ	δ^v
Sp^3	3	1	1
Sp^3	2	2	2
Sp^3	1	3	3
Sp^3	0	4	4
Sp^2	2	1	2
Sp^2	1	2	3
Sp^2	0	3	4
Sp	1	1	3
Sp	0	2	4

Figure 3.15 Schematic representation of connectivity indices calculations

3.7.1.2 Topological property predictions.

To predict a property, a correlation is needed, for example the equation (27) and (28) predicts directly the molar volume (V_m) in cm^3/mol at 298.15 K but for some other properties it is necessary to have extra information along with the previously calculated property like the density were molecular mass and V is necessary, see equation (29).

$$V_m = 3.642770\ {}^0\chi + 9.798697\ {}^0\chi^v + 8.542819\ {}^1\chi + 21.693912\ {}^1\chi^v + N_{MV} \qquad (27)$$

$$24N_{Si}\text{-}18N_{(\text{-}S\text{-})}\text{-}5N_{sulfone}\text{-}7N_{Cl}\text{-}16N_{Br}+2N_{\text{-}ester\text{-}}+3N_{ether}+5N_{carbonate}+5N_{C=C}\text{-}11N_{cyc}\text{-}7\,N_{fus} \qquad (28)$$

Where N_{MV} is a correction index for the molar volume estimation of the contribution in the repeating unit associated with the number of silicon, sulphur, chlorine and bromide atoms in the lowest oxidation state (N_{Si}, $N_{(\text{-}S\text{-})}$, N_{Cl}, N_{Br} respectively), sulfone atoms in the highest oxidation state ($N_{sulfone}$), ether and carbonate groups (N_{ether}, $N_{carbonate}$, respectively), non-aromatic rings with no double bond (N_{cyc}), carbon-carbon double bonds ($N_{C=C}$), 2 o more ring containing at least one

aromatic ring which shares at least one edge with another ring ($N_{fused-1}$) and esters in the backbone-chain (N_{-ester}).

$$\rho = \frac{M_{mero}}{V_m} \tag{29}$$

Thus, the predicted *Vm* can be write as equation (30):

$$V_m = 3.64(3.70)+9.80(3.49)+8.54(2.39)+21.69(2.05)+5=76.61\ [cm^3/mol] \tag{30}$$

And the expression predicting the density is given by equation (31).

$$\rho = \frac{68.12}{76.61} = 0.89\ [g/cm^3] \tag{31}$$

3.7.2 Molecular mechanics/dynamics

Regardless of the great advantages of the topological method and its low computational time/cost, is not possible to predict properties for physical composites, where the addition of non-covalent bounded molecules into a polymer has been made. For this reason, other computational means to estimate the properties of novel nano-composites are utilized. One of these methods is molecular mechanics and dynamics which is an application of the Newtonian mechanics. It uses a force field to represent the equilibrium and time-averaged effects of electrons and nucleus with reasonable accuracy. Most commonly, a three-dimensional structure of the molecules, with periodic boundary conditions, is constructed and entities such as bond stretching-compression, valence angle deformation, torsion or rotation about the bond and non-bonded interactions [22] are calculated and correlated to physical, thermal and chemical properties. Although this method offers a more flexible design than a topological method it increases the computational time, but not as much as an ab initio method.

There are different levels of atomistic computational modelling or approximations, the most accurate of all is the ab initio (Latin term meaning "from the beginning") follow by semiempirical Molecular orbital calculations, molecular mechanics, meso scale and finite element (Figure 3.16). The more accurate the model, the more time it will cost to and per se the smaller is the timescale of simulation.

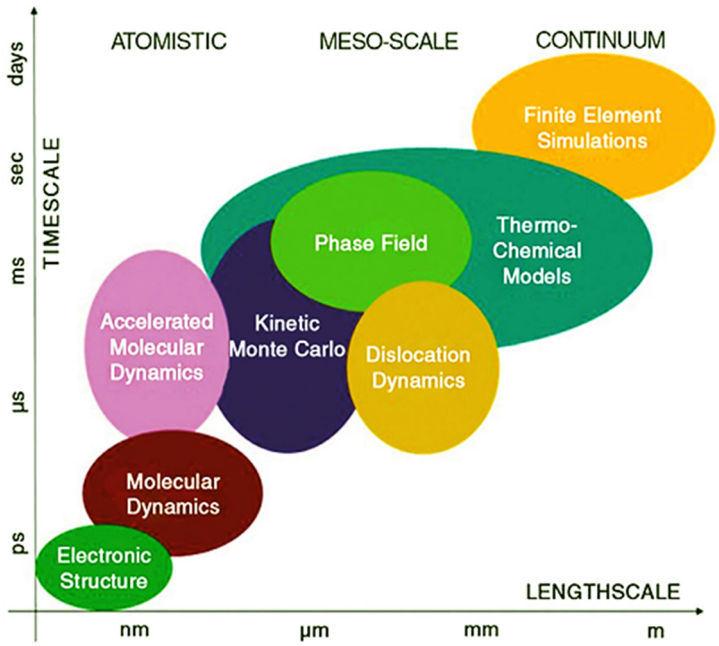

Figure 3.16 Multi-scale theoretical and computational methods used for materials model development and computer simulations, took from Stan [23]

Computational performance increases each year, this implies that materials can gain complexity and molecular mechanics/dynamics has emerged as an attractive tool [24] because it becomes more accessible. A classical procedure of molecular mechanics/dynamics modelling polymers is shown in Figure 3.17.

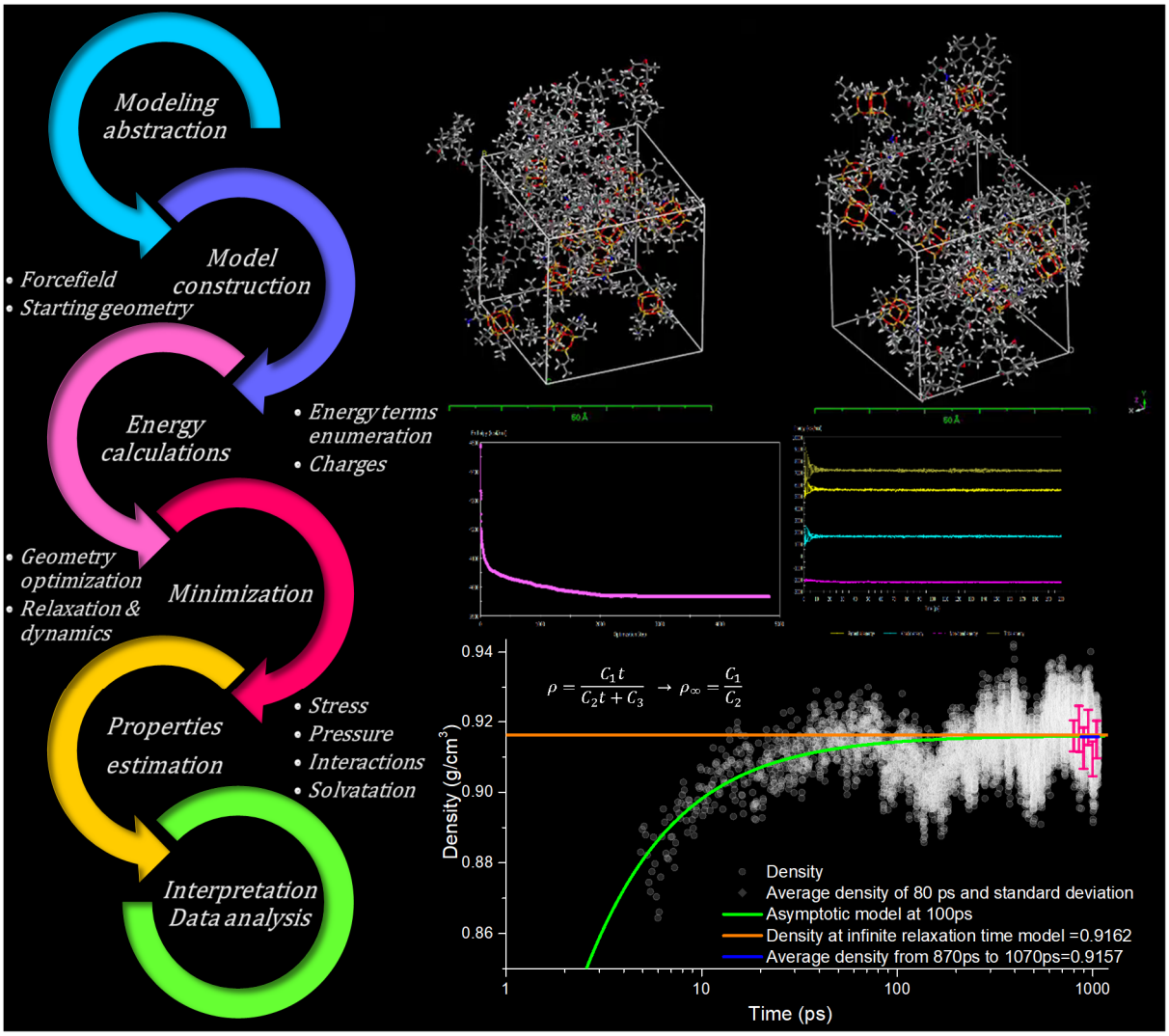

Figure 3.17 Schematic procedure of molecular mechanical molecular modelling

3.7.2.1 Modelling abstraction

The Oxford dictionary of computer science [25] define modelling as "The act of creating a model of something for a particular purpose, such as to describe it, understand it, or derive some properties. The process involves deciding which simplifications, idealizations, or abstractions to make, what kinds of representations to adopt, and how to express the selected properties of the referent".

A polymeric matrix has a high degree of complexity, due to a series of different aspects like molecular weight distribution, composition, tacticity, nanostructure, inter and intra molecular interactions, micro and macro structure and regularity among other characteristics. For this reason, making a simplification or an abstraction of all this variable sometimes present a challenge and is the first step to create an accurate mode.

3.7.2.2 Model construction

All the constrains and simplification during the modelling abstraction have to be translate into useful set of data that represent all the information. Normally a computer software is used to draw the molecules to be simulated in a three-dimensional unit cell (crystalline or amorphous, see Figure 3.18) with periodic boundary conditions. mechanics/dynamics. In this stage it is necessary to select the type of force field like the condensed-phase optimized molecular potentials for atomistic simulation studies (COMPASS), consistent valence forcefield (CVFF), among many others. Also, it is necessary to select the lattice type (cubic, tetragonal or orthogonal) and an initial estimate of the density.

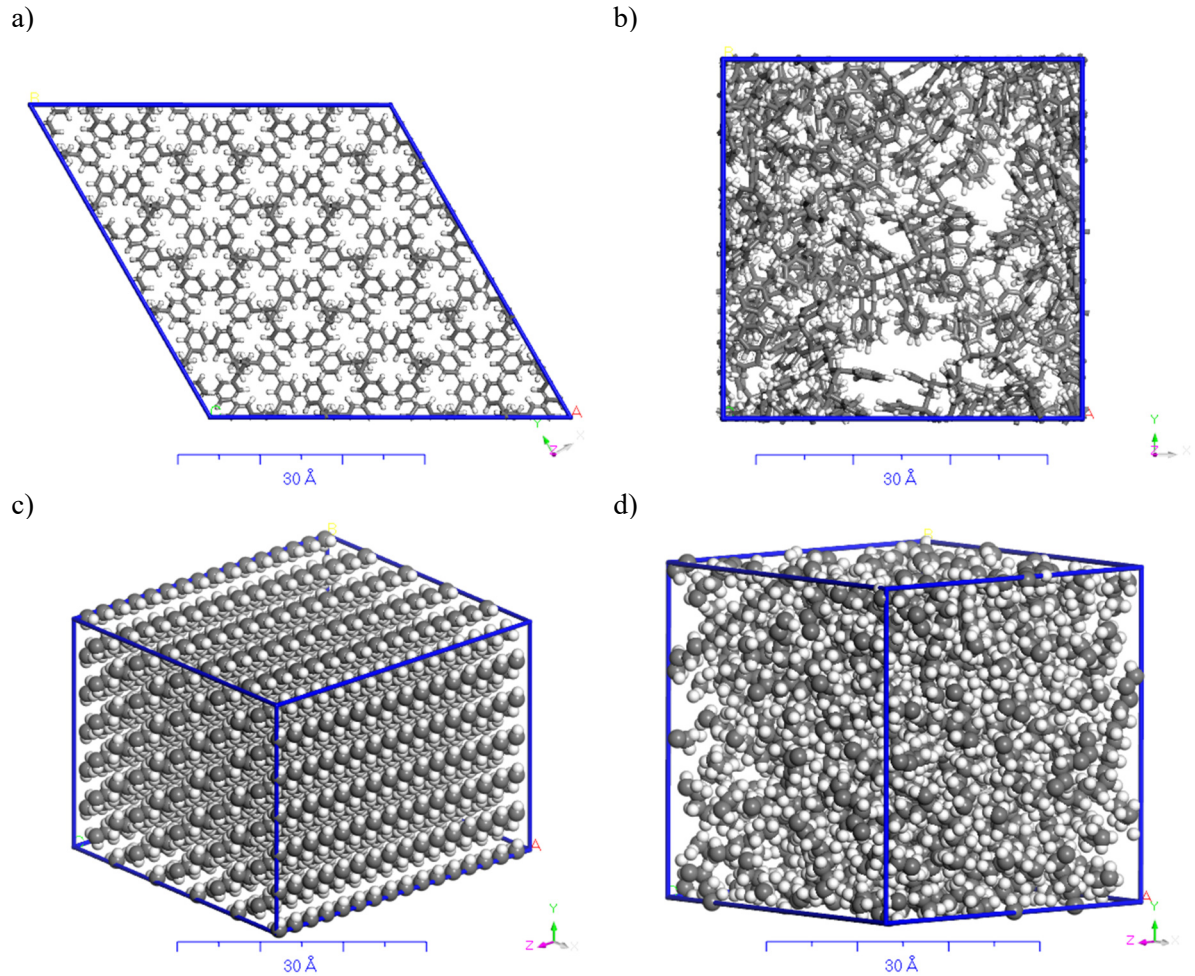

Figure 3.18 Different cells for a) crystalline isotactic styrene, b) amorphous styrene, c) crystalline poly(ethylene) and d) amorphous poly(ethylene)

3.7.2.3 Energy calculation

Once all the geometrical factors are set up, is necessary to select temperature, type of charges (e.g. Gasleiger) and summation method for the electrostatic and van der Waals forces. With all geometric

and energy parameter set in place it is possible to calculate an initial state of energy. The model in this stage at the given temperature is at its maximum due the lack of optimization.

3.7.2.4 Geometry and energy minimization

In order for the model to be reliable its geometry and energy have to be minimized with different sets of stages or techniques in order to get a global minimum and not just a local minimum state of energy (Figure 3.19).

Normally a reiterative geometry optimization is set prior or after energy optimization, dynamic or property calculation. A geometry optimization requires to select a solving algorithm (e.g. step descent, Newton) a long with a minimum convergence tolerance.

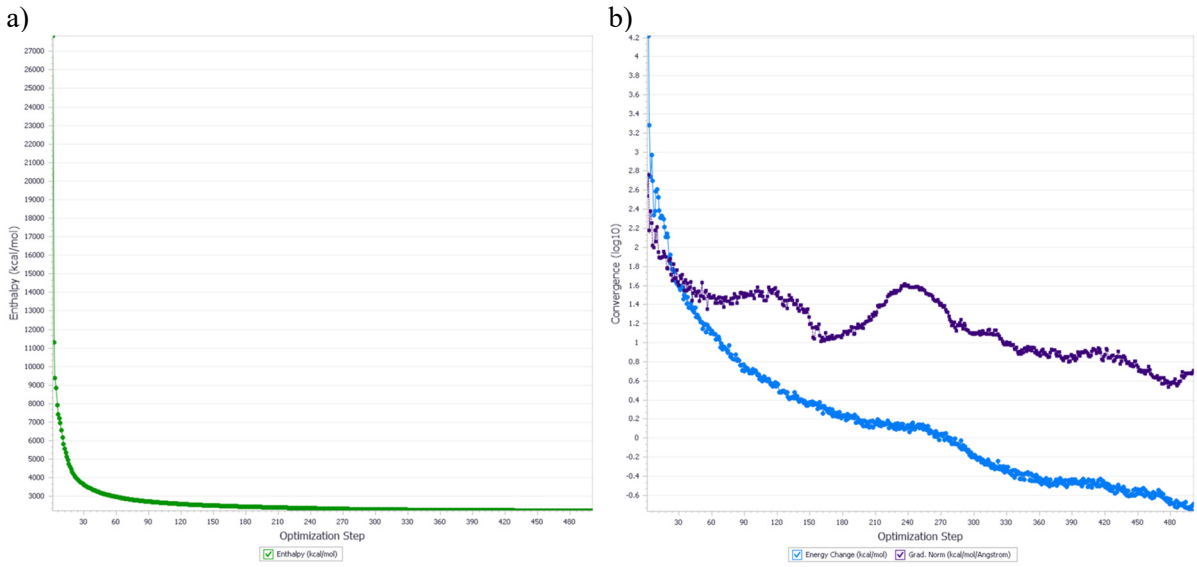

Figure 3.19 Geometry optimization data change over steps for a) energy and b) its convergence parameters

There are many dynamic techniques for energy minimizations like quenching and annealing (Figure 3.20) among others where there is orientation playing between pressure, volume, energy, enthalpy or temperature to relax as much as possible the cell to the desirable condition, please notice that the only variable that remain constant is the number of moles or N. To control the pressure and temperature is necessary to configure barostat, thermostat and run the dynamics under different ensemble. These ensembles are mean to keep constant some variables and change the others over time, for example a NPT test keeps the number of mole, temperate and pressure constants, a NVE keeps the number of mole, volume and the energy constant.

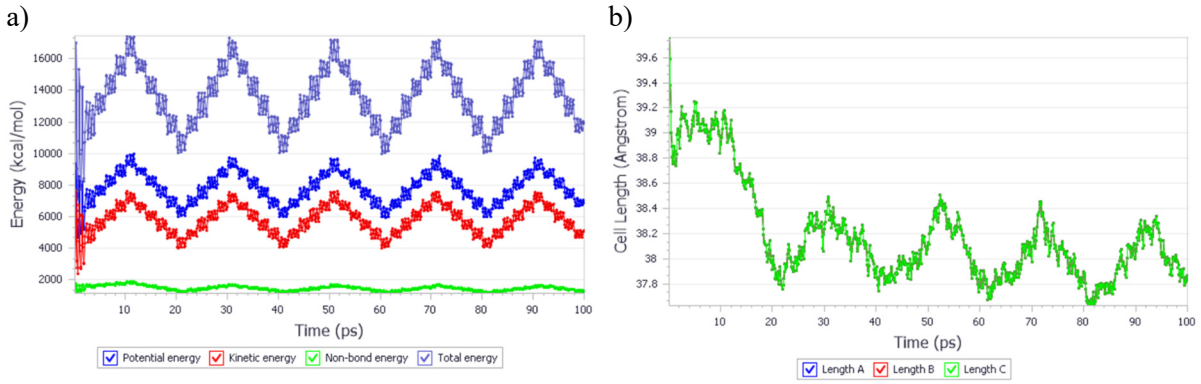

Figure 3.20 Anneal dynamic data change over time for a) energy and b) cell length

3.7.2.5 Properties estimation

Once the cell is relaxed, the geometry and all energies are at their global minimum, experiments can be conducted to understand, describe, calculate or derive properties or behaviours such as mechanical properties, solvation energy, density, glass transition temperature and more of the material can be measured.

3.8 References

1. *A Nanophotonic Comeback for Incandescent Bulbs?* Optik & Photonik, 2016. **11**(1): p. 12-12.
2. Freise, A. and K. Strain, *Interferometer Techniques for Gravitational-Wave Detection.* Living Rev. Relativ., 2010. **13**(1).
3. Bindig, U., et al., *Fiber-optical and microscopic detection of malignant tissue by use of infrared spectrometry.* Journal of biomedical optics, 2002. **7**(1): p. 100.
4. Sungho, K., et al., *Midwave FTIR-Based Remote Surface Temperature Estimation Using a Deep Convolutional Neural Network in a Dynamic Weather Environment.* Micromachines, 2018. **9**(10): p. 495.
5. Hardesty, L. *Explained: The Discrete Fourier Transform*. 2009.
6. Rohankar, T. and A. Ingle, *Enhanced the Infrared Image Using Wavelet Transform.* International Journal of Advanced Research in Computer Science, 2012. **3**(3).
7. Pardo, I.R.M., *Efecto de la hidrogenacion catalitica homogena de copolimeros model lineales y en forma de estrella sobre su microesturctura y comportamiento termico*, in *Chemistry department*. 2007, National Autonomous University of Mexico: Mexico City. p. 71.
8. Ida, R., *Adaptability of a Moisture Analyzer Equipped with a Halogen Heater to the Measurement of Water Content of Unhulled Rice.* Japanese Journal of Crop Science, 2016. **85**(2): p. 173-177.
9. Ratha, S.K., et al., *A rapid and reliable method for estimating microalgal biomass using a moisture analyser.* Journal of applied phycology, 2016. **28**(3): p. 1725-1734.
10. Kwok, D.Y., et al., *Contact angle measurements and contact angle interpretation. 1. Contact angle measurements by axisymmetric drop shape analysis and a goniometer sessile drop technique.* Langmuir, 1997. **13**(10): p. 2880-2894.
11. Lander, L.M., et al., *A systematic comparison of contact angle methods.* Langmuir, 1993. **9**(8): p. 2237-2239.
12. Chou, P.C. and N.J. Pagano, *Elasticity Tensor, Dyadic, and Engineering Approaches*. Elasticity, ed. N.J. Pagano. 2013, Newburyport: Dover Publications.
13. Menard, K.P., *Dynamic mechanical analysis a practical introduction*. 2nd ed. ed. 2008, Boca Raton, FL: CRC Press.

14. Wu, P.-H., et al., *A comparison of methods to assess cell mechanical properties.* Nature methods, 2018. **15**(7): p. 491.
15. Macosko, C.W.A. and C.W. Macosko, *Rheology: Principles, Measurements, and Applications*, ed. C.W.C. Macosko. 1994, Place of publication not identified: Published by - Wiley VCH Imprint.
16. Heijboer, J., *Secondary Loss Peaks in Glassy Amorphous Polymers.* International Journal of Polymeric Materials, 1977. **6**(1-2): p. 11-37.
17. Menard, K.P. and N.R. Menard, *Dynamic Mechanical Analysis in the Analysis of Polymers and Rubbers.* Encyclopedia of Polymer Science and Technology, 2002: p. 1-33.
18. Kawak, B.J., B.H. Cabon, and G.S. Aglietti, *Innovative viscoelastic material selection strategy based on dma and mini-shaker tests for spacecraft applications.* Acta Astronautica, 2017. **131**: p. 18-27.
19. Klančnik, G., J. Medved, and P. Mrvar, *Differential thermal analysis (DTA) and differential scanning calorimetry (DSC) as a method of material investigation Diferenčna termična analiza (DTA) in diferenčna vrstična kalorimetrija (DSC) kot metoda za raziskavo materialov.* RMZ–Materials and Geoenvironment, 2010. **57**(1): p. 127-142.
20. Höhne, G.W.H.a., W.F. Hemminger, and H.J. Flammersheim, *Differential Scanning Calorimetry*. 2nd revised and enlarged edition. ed, ed. W.F.a. Hemminger and H.J.a. Flammersheim. 2003, Berlin, Heidelberg: Springer Berlin Heidelberg : Imprint: Springer.
21. Bicerano, J., *Prediction of polymer properties*. 2002: CRC Press.
22. Gelin, B.R., *Molecular modeling of polymer structures and properties*. 1994: Hanser Publishers.
23. Stan, M., *Discovery and design of nuclear fuels.* Materials Today, 2009. **12**(11): p. 20-28.
24. Wu, C., *Multiscale Modeling Scheme for Simulating Polymeric Melts: Application to Poly (Ethylene Oxide).* Macromolecular Theory and Simulations, 2018. **27**(1): p. 1700066.
25. Butterfield, A. and G.E. Ngondi, *A Dictionary of Computer Science*. 7 ed. 2016: Oxford University Press.

4 THERMOPLASTIC STARCH NANOHYBRID FILMS MODIFIED WITH POS

4.1 Introduction

Since starch is biodegradable, is widely available, have the ability to convert into thermoplastic material, transparent in its thermoplastic form[1] is gaining attention as a viable alternative to polymeric petroleum-based material.

The three basic steps to produce casted thermoplastic starch films are gelatinization, casting and drying.

As mention in 2.1, the gelatinization of starch granules is carried out using heat, plasticizers (normally water and glycerol) and agitation to disrupt its crystalline structure.

This disruption involves the unentangle of amylose double helix and therefore the intra molecular hydrogen bonds between hydroxyl groups are loss and given rise to intermolecular interactions. These intermolecular interactions occur mainly with water or glycerol during gelatinization and once the film is dry with the remaining water, glycerol and other hydroxyl groups.

The exposed hydroxyl groups of amyloses polymeric chains (Figure 4.1 a) are the reason for which is possible the gelatinization, this is positive because allows the thermoplastic films making but at the same time are the cause of the two mayor concerns in making this kind of materials. The first concern is related to retrogradation (see 2.1.4) where the hydroxyl groups of adjacent amylose chains get their way recoiling them self in double helix gaining. The second concern and main focus of this work is the hydrophilic nature of the films where all the hydroxyl groups are susceptible and eager to interact with water (Figure 4.1 b) which ultimates greatly limits its application.

For this reason, increasing the hydrophobicity of thermoplastic starch films is a priority. It is hypnotised that a custom POS can bring hydrophobicity (Figure 4.1 c). The main complexity in designing the hybrid is to achieve a balance between compatibility and hydrophobicity. The approach to this design was to take a POS substituted with isobutyl in seven of its vertices and change the remaining vertex with a substitute different in nature (more hydrophobic, more hydrophilic, or chemically oppose like glycidyl and amino).

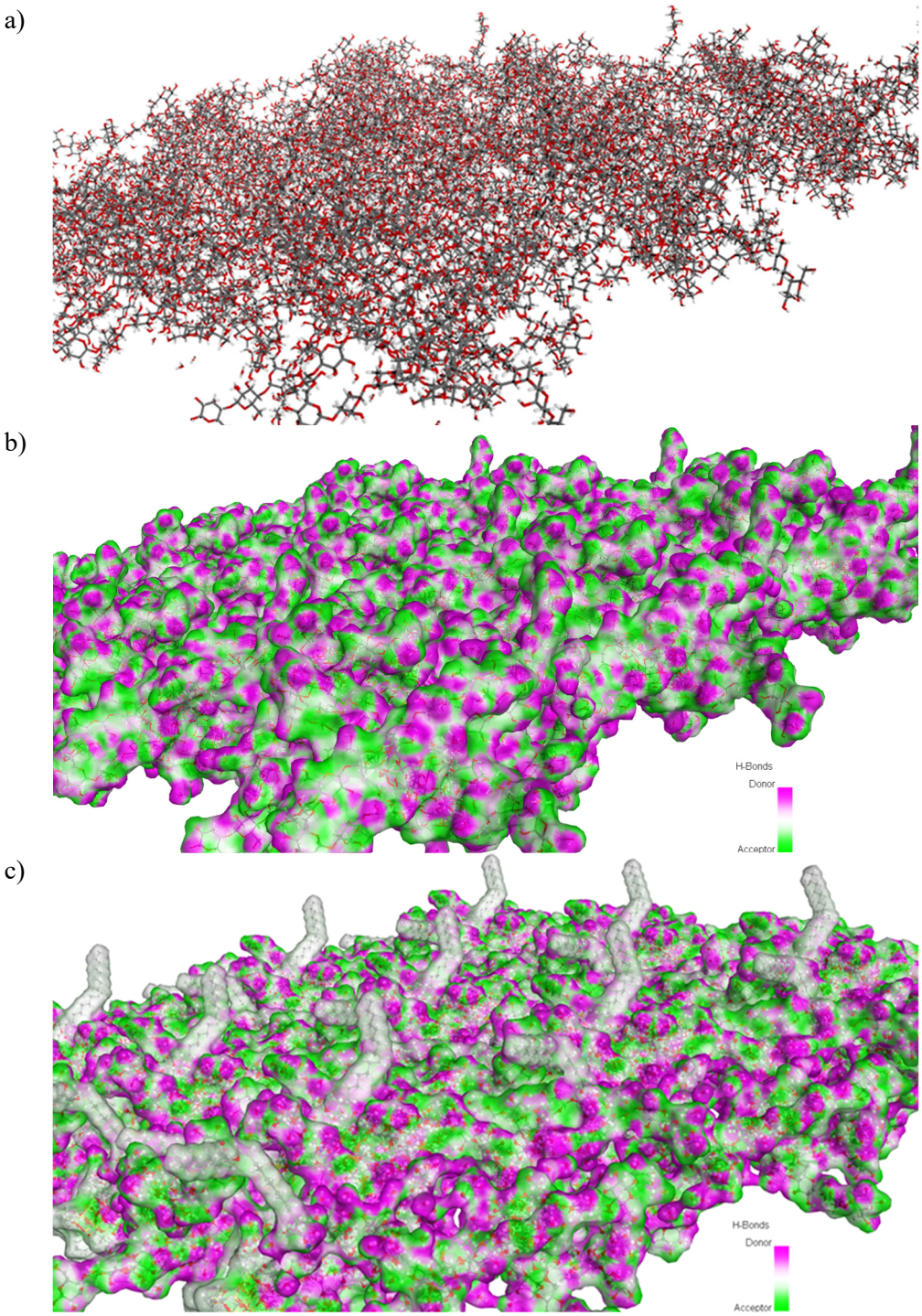

Figure 4.1 Molecular illustrations of thermoplastic films, the surface is coloured accordin to its hydrogen bonding nature, green for acceptor, pink for donor and pure white for neither. a) molecules of starch, glycerol and water, b) Van der Waals surface of starch, glycerol and water molecules, c) Van der Waals surface of POS, starch, glycerol and water molecules.

4.2 Materials

Pre-gelatinised hydroxypropylated corn starch (Penford™ A939) was used as the starch. According to the manufacturer it contained ~80 of high-amylose and 6.5% by weight of hydroxypropyl substitution. Distilled water was used as solvent or dispersant. Propane-1,2,3-triol (glycerol) was purchased from

Sigma-Aldrich (Sydney, Australia) was used as plasticizer. Glycerol contained less than 1 % w/w moisture.

1-(3-Glycidyl)propoxy-3,5,7,9,11,13,15-isobutylpentacyclo[9.5.1.1^{3,9}.1^{5,15}.1^{7,13}] octasiloxane (epoxy-POS) was used to modify the starch films as well as to produce the novel functionalized POS. The 1-(3-amino) propyl-3,5,7,9,11,13,15- isobutylpentacyclo[9.5.1.1.^{3,9}.1^{5,15}.1^{7,13}] octasiloxane (NH_2-POS) was used to modify the starch films. These two chemicals were purchased from Hybrid Plastics Inc. (Hattiesburg, USA). O-(2-Aminopropyl)-O′-(2-methoxyethyl)poly(propylene glycol) 500 (Jeffamine) was used to chemically functionalize the POS and was purchased from Sigma-Aldrich (Sydney, Australia). Anhydrous and inhibitor-free oxolane (tetrahydrofuran, THF) was used as solvent in all reactions. THF was purchased from Science Supply Australia Limited (Melbourne, Australia). docos-13-enoic acid (Erucamide) was obtained from Croda International (Hull, United Kingdom).

All materials were used as received and the moisture content of each material was measured and compensated for while determining the concentration of each chemical and preparing starch slurries for gelatinisation.

4.3 Methods

4.3.1 Functionalization of nanohybrid POS

Epoxy-POS was functionalized either with Erucamide or Jeffamine at a molar stoichiometric ratio of 1:1. The solvent (THF)-reactants (epoxy-POS) mixture was stirred at 40 °C for 24 h (Figure 4.2). The THF-epoxy-POS molar ratio was maintained at 35:1 during reaction and the product was collected after evaporation of the THF under vacuum at 40 °C.

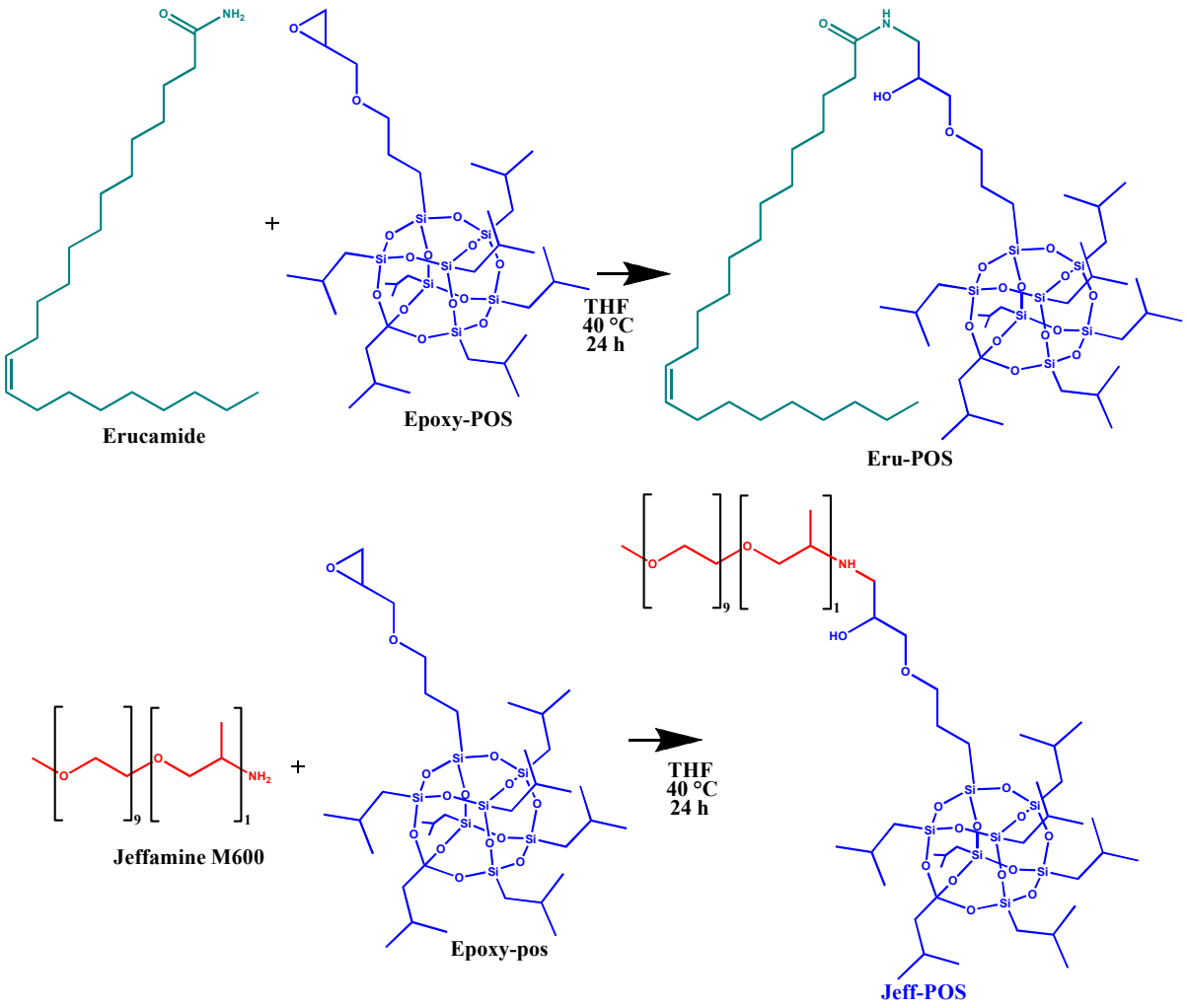

Figure 4.2. Epoxy-POS functionalization reaction with either Erucamide or Jeffamine to produce POS nanohybrids

4.3.2 Identification of functional and reactive groups

Fourier transform infrared (FTIR) spectra were acquired using a PerkinElmer Spectrum 100 spectrophotometer to identify the key functional and reactive groups during reactions. A universal diamond attenuated reflectance (ATR) was used to scan wavenumber from 4000 cm^{-1} to 650 cm^{-1}, 10 scans per spectrum were recorded with a resolution of 4 cm^{-1}.

4.3.3 Preparation of starch-plasticizer, starch-plasticizer-nano additive slurries

A master batch starch-plasticizer slurry was prepared by dissolving 4.03 % w/w starch, 1.21 % w/w glycerol in 94.88 % w/w water. This master batch was used throughout to avoid discrepancy in preparing the exact concentrations of formulations. This slurry was heated (IKA RH-digital hotplate, Staufen, Germany) at 95 ±3 °C for about 20 min.

The progress and completion of gelatinization and homogeneity of the dispersion was monitored using an optical microscope (Nikon Labophot II, Japan). The progress and completion of the gelatinization was monitored using both plain and polarized optical microscopy.

4.3.3.1 Addition of nano-additives to the gelatinized starch slurry

Four aqueous slurries of monohybrids from the master batch were prepared, NH_2-POS, Epoxy-POS, Eru-POS and Jeff-POS by dissolving 1.3 % w/w of each hybrid in 98.7 % w/w of master batch; the master batch alone was considered as the control. Then each slurry was individually homogenized using a high-shear disperser (Bamix, Australia).

4.3.3.2 Degassing, film casting and conditioning

The air entrapped during agitation was removed by degassing the slurries for 5 min in a vacuum chamber. After degassing, 20 mL of each slurry was transferred onto a polystyrene Petri dish (90 mm diameter) using a syringe. Drying was carried out in a custom-built isothermal drying box with gentle fan forced air circulation at 30 ±1 °C for 48 h. Temperature within the chamber was controlled using a digital proportional–integral–derivative (PID) controller unit. After drying, the films were stored in a desiccator containing a saturated solution of magnesium nitrate (about 54 % relative humidity) at ambient temperature (20 °C) for at least 48 h prior to further tests.

Figure 4.3 General schematic representation of thermoplastic starch film production after gelatinization

4.3.4 Determination of moisture content

The moisture content of films was determined by a gravimetric method using a Mettler-Toledo HG63 (Australia) halogen moisture analyser. The measurements were terminated when the mass change was < 1 mg over 140 s.

4.3.5 Determination of wettability kinetics

The wettability kinetics [2, 3] were measured as the change of the contact angle (θ_c) of the films with time. A sessile droplet method was used, and the measurements were made using a Data-Physics OCA20 instrument (Germany). Contact angles were measured in triplicate on the top surface (the surface that had not been in direct contact with the polystyrene Petri dish during the drying process). Contact angles were automatically calculated by fitting an ellipse to the surface of the drop method using OCA20 software. Two drops of water obtained from a Milli-Q system were deposited on each film. Apparent contact angle (θ) was measured in 1 s interval for about 5min.

4.3.6 Determination of mechanical properties

Stress–strain analysis was performed and Young modulus, maximum tensile stress, tensile strain and toughness were determined from data acquired using an Instron 4465 Universal Test Instrument in tensile mode, in accordance with ASTM 882 [4]. A grip distance of 26.5 mm and a cross-head speed of 2.65 mm/s were used for these tests. The specimen dimensions were measured in three different places using a Duratool DC150 digital calliper. In order to ensure that the specimens would break at about the centre, they were die-cut into dumbbell shape as specified in ASTM D638 [5]. The Young modulus was calculated from the stress-strain curve between a stress value of 0.005 MPa and a stress value below the proportional limit and preload tensile modulus ASTM E111 [6].

4.3.7 Determination of glass transition temperature by dynamic mechanical analysis

Specimens were cut to 9.6 mm (wide) × 45 mm (long) × 0.10 mm (thick) and coated with petroleum jelly to reduce moisture evaporation. A sweep pre-treatment (temperature-frequency) was carried out before each scan to remove any pre-existing thermal or mechanical history. Scans were performed in tensile mode using synthetic multi-frequency (0.5, 1, 2, 5, 10 Hz) where all frequencies were applied simultaneously, and Fourier transform resolved by the instrument software. Pre-treatments were

performed at a rate of 20 K/min from -60 °C to 80 °C then returned to -60 °C. Tests were carried out from -60 °C to 90 °C at a rate of 5 K/min.

4.3.8 Statistical analysis

At least triplicate tests were carried out, except when indicated otherwise, for each parameter and the results are reported as average values ±standard deviation from a mean value. If a difference was to be considered statistically significant or not a Student t-test was performed assuming two tail distribution and unpaired two sample equal variance with a confidence interval of 95 % ($p > 0.05$)

4.4 Results and Discussion

At first appraisal the nanohybrids were essentially hydrophobic, but due to polar nitrogen and oxygen atoms interactions with other molecules in the starch films were feasible. Sites of interaction were visualized using molecular modelling (Discovery Studio, Dassault Systemes Biovia Corporation, France) by calculating hydrogen bonding receptor surfaces of the molecules using a probe radius of 0.13 nm (Figure 4.4).

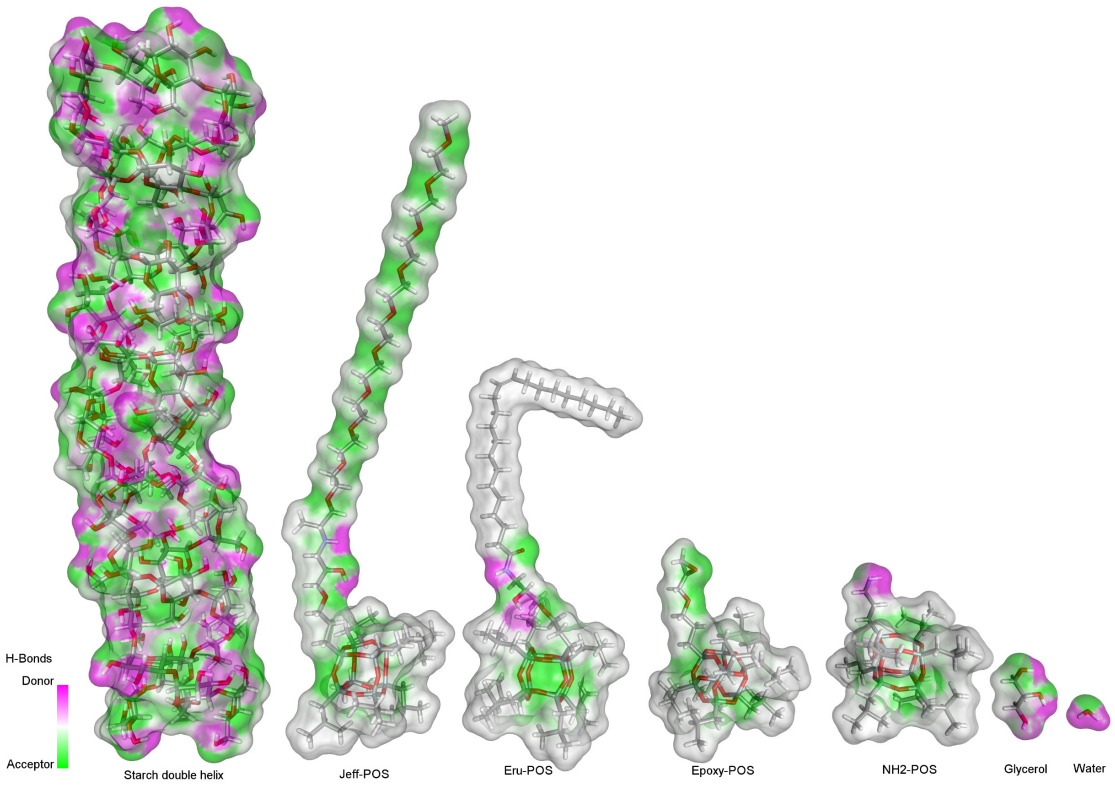

Figure 4.4 Hydrogen bonding receptor surface of molecules in the starch film systems, their Van der Waals surface coloured according to its hydrogen bonding nature, green for acceptor, pink for donor and pure white for neither

4.4.1 Identification of functional and reactive groups and indication of reaction completion

FTIR spectra of the products and the reactants are compared in Figure 4.5 to confirm reactions shown in Figure 4.2.

In the FTIR spectra of Eru-POS system in Figure 4.5 b) the most important peaks are those that almost disappear or shift in the range 3300 to 3450 cm^{-1} and 1650 to 1675 cm^{-1} (see expanded detail in Figure 4.5 d), these peaks correspond to the amine group and the C=O stretching next to it respectively (both forming an amide group) and are evidence that the primary amide change to a secondary amide, these changing peaks indicate that an addition reaction occurred.

In the case of the Jeff-POS system (Figure 4.5 a) the previous peaks are not useful because lacks of the C=O stretching, but the spectra product shows additional peaks respect to its precursors (epoxy-POS and Jeffamine), these peaks are in the range of 1600 to 1700 cm^{-1} and 3050 to 3600 cm^{-1} (see expanded detail in Figure 4.5 c) corresponding mostly to hydroxyl group but also to amine group, the appearance of hydroxyl groups coupled with a decrease of the whole epoxy ring stretching peak at 1250 cm^{-1} [7] is indicative of the ring reaction.

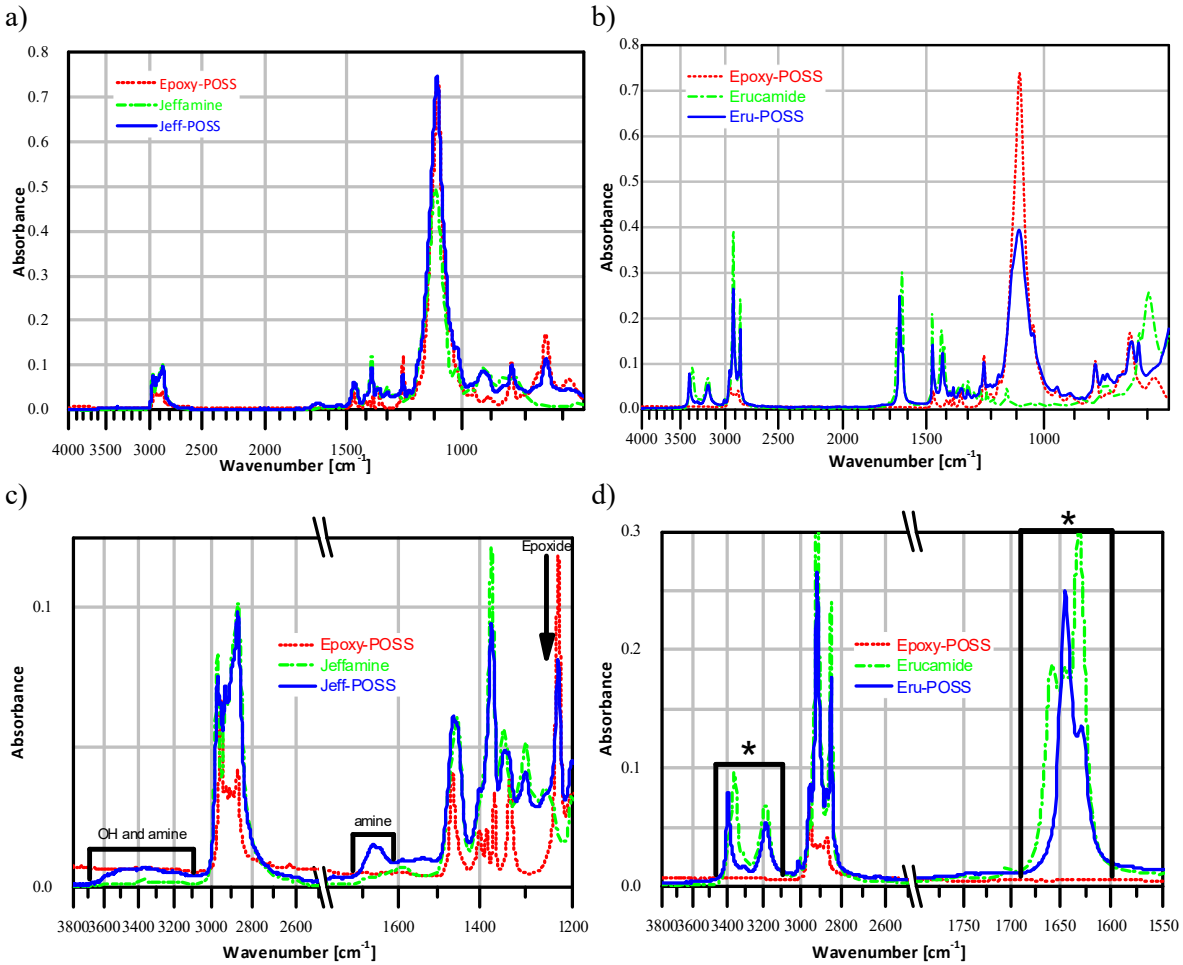

Figure 4.5 FTIR spectra of Eru-POS and Jeff-POSS and their precursors a) Jeff-POSS, b) Eru-POS, c) expanded details of Jeff-POSS and d) expanded details of Eru-POS

4.4.2 Moisture content in the films

The moisture content control, NH_2-POS, Epoxy-POS, Eru-POS and Jeff-POS were 6.04±0.38, 5. 35±0.41, 5.95±0.88, 5.89±0.08 and 6.13±0.35, respectively. There was no significant difference in moisture content compared with the control which indicates that within the bulk starch hydrophilicity was maintained.

4.4.3 Contact angle of the films

Water spreading over the starch film is a dynamic condition where equilibrium would be achieved after it was no longer possible to read the contact angle. It is not only a function of instantaneous surface energy, but over time, absorption increased interactions, until a time when it was no longer possible to read the contact angle due a deformation of the film or the water drop. This occurred after 5 min, until

then contact angles were able to be measured. The contact angle profiles are shown in Figure 4.6, in order to present smooth curves of the data, a 10th degree polynomial was used to fit it.

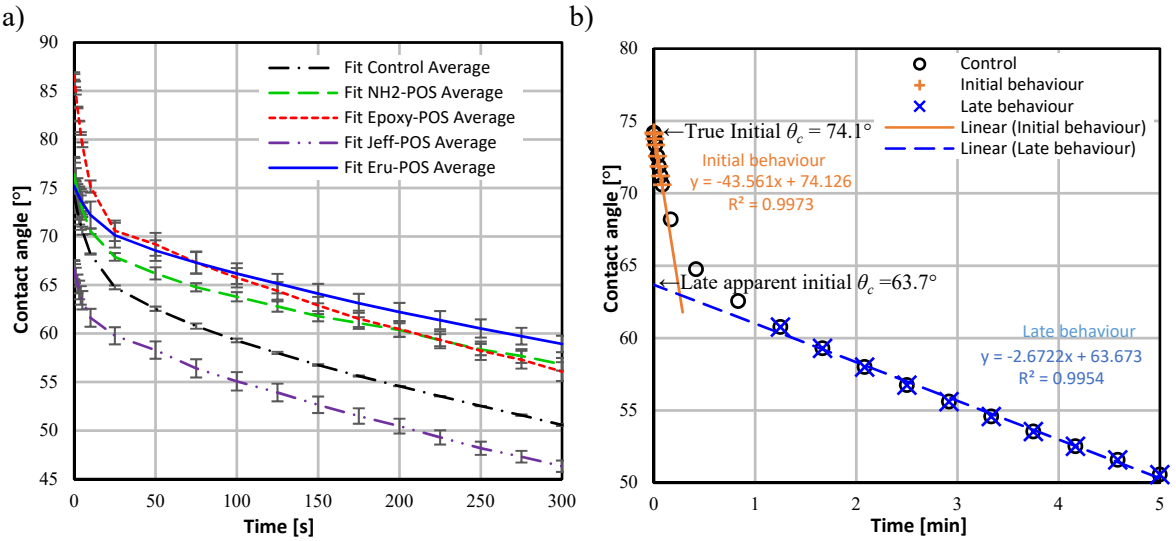

Figure 4.6 a) 10th order polynomial fitting of the average wettability profile of the films; the error bars represent the standard deviation and b) characterization of the initial and late behaviour of the control film by linear fitting

The contact angle data presented in Figure 4.6 shows that representation of wettability of these films by a single contact angle (θ_c) is not possible as θ_c varied with time. Some films had similar initial θ_c values; however, they diverged over time before conserving to a more or less stable difference between their θ_c values.

As the variation of θ_c over time showed two distinct regimes (Figure 4.6 a), hence, two linear equations were used to represent the variation of θ_c at initial and later stages. The slope of both equations represents the rate of change of θ_c respect to time [°/min]. The intercepts in abscissa of these linear lines represent the initial θ_c (initial stage) and an apparent initial θ_c for the later stage as shown in Figure 4.6 b and Table 4.1. All films containing the nanohybrid additives had higher contact angle compared with the starch–glycerol only (control) film except for the film that contained Jeff-POS. The Jeff-POS films had lower initial contact angle values than that of the control film due to the hydrophilic nature of Jeffamine. It appears that a single substituted hydrophilic Jeffamine in the POS cage predominated over the other seven hydrophobic substituted groups, imparting more hydrophilic nature to the film.

The control and Jeff-POS films shared the similar variation of θ_c over time in the later rate. This observation indicated that the Jeff-POS at this concentration does not contribute to or modify the wettability (θ_c versus time) characteristics of films at later stage. Although the Control, NH_2-POS and Eru-POS films had similar initial θ_c the latter two films had much higher θ_c values in later stage indicating higher hydrophobicity in NH_2-POS film and Eru-POS film compared with that in the control.

The most water resistant (hydrophobic) film was the one with largest initial θ_c and smallest variation over time. For that reason, it was assumed that the way to compare hydrophobic/water resistance (wr) nature of these materials was to calculate the area under θ_c versus time plot, the larger the area [°·min] the more water resistant was the film. The other approach to determine the hydrophobicity was to use the area of the control film as a reference and normalise the area ratio using this reference (Nwr), see Table 4.1.

The starch (control) and NH_2-POS films share similar initial θc and initial rate [°/min] which indicated that theNH_2-POS did not affect the wettability or hydrophobic/hydrophilic behaviour in the film at this concentration in the initial stage. The Eru-POS film, Epoxy-POS film and NH_2-POS film were the material with higher water resistance at 5 min respectably, which indicates that the longer the hydrophobic group the higher was the wr.

Table 4.1 Film wettability (θc) and water resistance from 0 to 5 min.

Film name	Control	NH_2-POS	Epoxy-POS	Jeff-POS	Eru-POS
Initial rate [°/min]	-43.6	-44.2	-86.2	-38.3	-21.2
True initial θ_c [°]	74.1	76.3	86.4	66.5	75.2
Initial R^2	0.997	0.996	0.996	0.995	0.998
Later rate [°/min]	-2.67	-2.1	-2.95	-2.69	-2.22
Later apparent θ_c [°]	63.7	67.2	70.5	59.5	69.8
Later R^2	0.995	0.998	0.994	0.998	0.997
wr [°·min]	288.6	306.5	309.7	274	312.7
Nwr [%]	0	6.2	7.3	-5.1	8.4

4.4.4 Tensile stress–strain behaviour of the films

The tensile mechanical properties (Young modulus, maximum stress and strain) of the starch and starch–additive films are presented in Figure 4.7 and tensile properties are compiled in Table 4.2. It is important to note that only the NH_2-POS film showed a first offset yield strength, which is an

uncommon behaviour and was attributed to a secondary smaller molecular arrangement due to the intrinsic interaction of the nano-hybrid with the glycerol plasticized starch films. The toughness was calculated as the area under the stress-strain curve and is reported as [MJ/m^3] that is equivalent to [M(Pa)·(m/m)] or [M(N m)/(m^2 m)]. Comparing the control film with NH_2-POS film it is found similar maximum tensile stress and comparing the control film to Jeff-POS film it is found similar maximum strain, but when the toughness is compared the control is at least 8 and 3 times tougher. All the mechanical properties of the films with respect to the control film decreased except for the maximum tensile stress of the NH_2-POS where there was not a statistically significant difference. The NH_2-POS and Eru-POS films share about the same Young modulus with insignificant statistical difference and they are about 25 % less than the control film. Although the nanohybrids are not entirely hydrophobic thanks to the nitrogen and oxygen atoms of the molecules, the decrease of the mechanical properties could be due the introduction of hydrophobicity into the films and not just at the surface.

Table 4.2 Tensile mechanical properties of films

Film	Control	NH_2-POS	Jeff-POS	Eru-POS	Epoxy-POS
Maximum tensile stress [MPa]	12.5±1.7	10.5±1.1	7.0±1.6	8.1±0.7	5.4±0.4
Maximum tensile strain [m/m]	0.348±0.054	0.060±0.009	0.177±0.029	0.0322±0.0004	0.117±0.053
Young modulus [MPa]	869.0±4.3	645.0±120.5	468.8±135.7	653.7±99.6	387.7±77.1
Toughness [MJ/m^3]	3.544±0.314	0.406±0.029	1.080±0.141	0.206±0.008	0.531±0.005
First offset yield stress [MPa]	-	6.60±0.24	-	-	-

a) b)

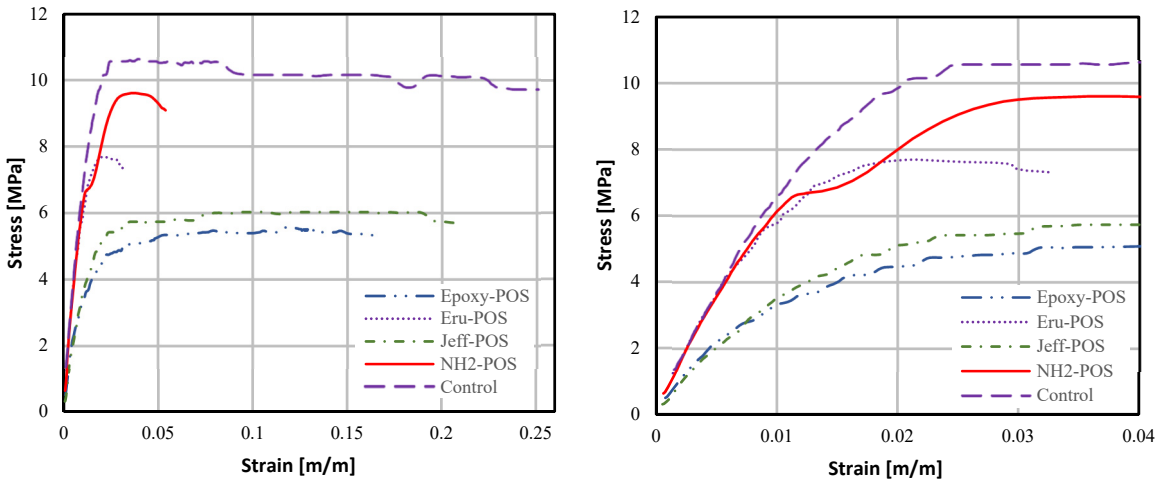

Figure 4.7 a) Stress-strain curves of starch–additive films b) expanded view of the NH_2-POS first offset yield

4.4.5 Thermomechanical transition of the films

It was possible to detect transitions by testing the materials at one frequency, however without complementary tests or prior knowledge of the system the type of transition could not be validated. To interpret the type of transition using only DMA; is necessary to test the material at several frequencies and under modulated temperature cycles, with the objective to determine if the transition was frequency dependent, or if the transition temperature was conserved with frequency. If the transition was conserved and frequency dependent it is a glass transition because it is a kinematic change. If the transition is conserved and it is not frequency dependent, it is a melting temperature, which is a thermodynamic change. If the material has transitions that are not conserved, this is an indication of previous thermo-mechanical history.

Elastic modulus (E'), viscous modulus (E'') and tan(δ) (Figure 4.8 a) were measured at different frequency, in order to determine the thermo-mechanical transition temperatures presented in Table 4.3, the estimations were done by fitting a 10^{th} order linear polynomial equation to the tan(δ) region of the transition along with a linear baseline (Figure 4.8 b), the temperature that corresponded the maximum vertical distance between the polynomial curve and the baseline is reported as the transition temperature.

The first transition is the glass transition temperature (T_g) because it was found at the lowest temperature, was frequency dependent and reversible. The second transition was considered a melting temperature (T_m) because it was found at the highest temperature (before the boiling temperature of water), was not frequency dependent and was reversible. Only the control film exhibited an intermediate transition between T_g and T_m, which was small, frequency independent and semi-reversible. This intermediate transition may be due to starch regaining crystallinity after gelatinization (retrogradation) [8].

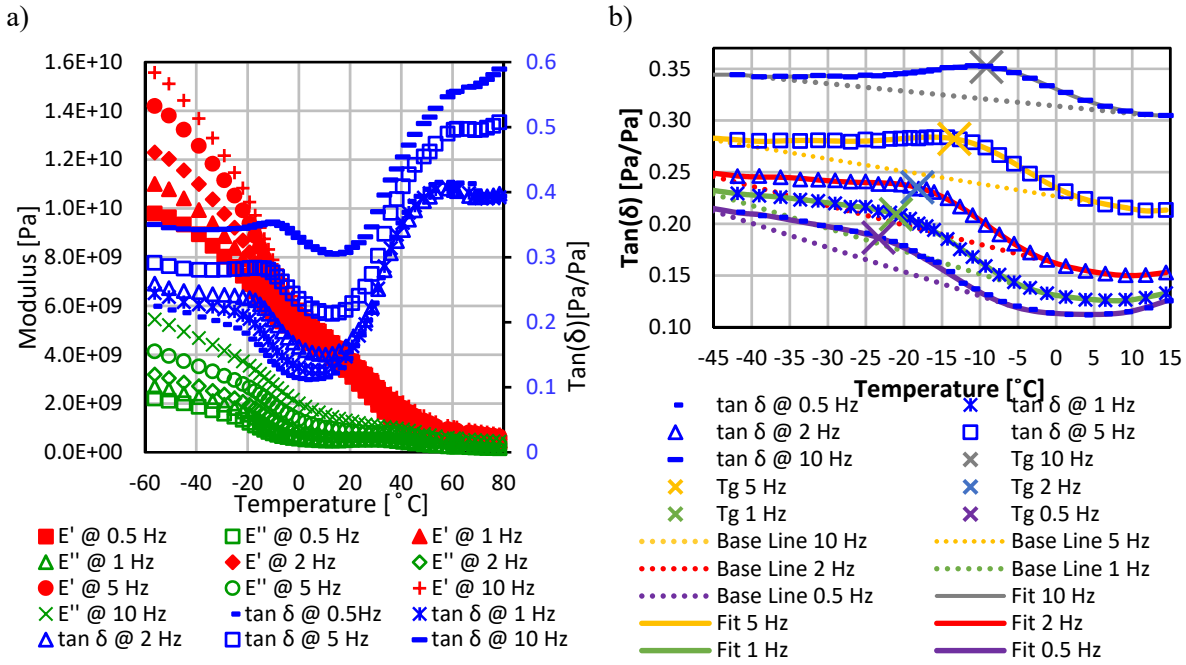

Figure 4.8 a) E', E'' and tan(δ) of Jeff-POS film. b) Schematic representation of the calculated T_g at different frequencies

The control film had the lowest T_g and the highest T_m, which means it remained flexible with consistent mechanical properties in a wider range of temperatures than the other films follow by the NH_2-POS, Epoxy-POS, Eru-POS and Jeff-POS films. There is not significant difference in the T_m of Eru-POS and the Jeff-POS films.

Table 4.3 Thermo-mechanical transition temperatures of the films

Property	Control film	NH_2-POS film	Epoxy-POS film	Eru-POS film	Jeff-POS film
T_g at 10 Hz [˚C]	-18.1	-8.2	-9.9	-7.0	-9.2
T_g at 5 Hz [˚C]	-20.8	-12.3	-14.1	-11.2	-13.4
T_g at 2 Hz [˚C]	-25.2	-17.6	-19.8	-17.2	-18.2
T_g at 1 Hz [˚C]	-28.2	-20.9	-24.2	-20.1	-21.0
T_g at 0.5 Hz [˚C]	-32.1	-23.8	-28.7	-23.1	-23.3
Intermediate transition [˚C]	51.3±0.47	-	-	-	-
Average T_m [˚C]	80.1±0.2	71.5±0.5	57.7±5.4	47.5±0.3	47.2±2.1

4.5 Conclusion

The nanohybrid Erucamide-POS and Jeffamine-POS were dispersed with glycerol plasticized starch films and synthesized by substituting a single pendant group of a POS cage either by Erucamide or Jeffamine 600 respectively. This novel nanohybrids along with the other two commercial ones (epoxy-POS and NH_2-POS) were incorporated individually to glycerol plasticized starch films obtaining films

with different contact angle and mechanical properties compared with those of the control, glycerol plasticized starch film.

The POS nanohybrids increased or promoted the re-association of amylose molecules in gelatinised starch films (retrogradation) as indicated by the highest melting temperature (T_m) and the lowest glass transition temperature (T_g) with respect to the control film. Only the control film exhibited an intermediate transition between T_g and T_m, which was small, frequency independent that may be due to starch regaining crystallinity after gelatinization.

The control film had the highest ultimate tensile strain and the highest tensile modulus, and consequently it was the toughest film, followed by NH_2-POS and Erucamide-POS.

Hydrophobicity of the films as indicated by the contact angle (θ_c) was time dependent, having two distinct regimes. The initial θ_c of the first regime and the apparent θ_c of the second regime depended on the type of nanohybrids used. The initial θ_c was always larger than the apparent θ_c by 10°. Initial rate of decrease of θ_c was always larger than that in second stage by almost 18 times. All the films with nanohybrids had higher contact angle (7.8 %) with respect to the control film except in the case of Jeff-POS film. The longer the hydrophobic mono-substituted pendant group in the POS cage the higher the water resistance is, by the contrary if the hydrophilic Jeffamine is used the water resistance decrease.

4.6 References

1. Javanbakht, S. and H. Namazi, *Solid state photoluminescence thermoplastic starch film containing graphene quantum dots.* Carbohydrate Polymers, 2017. **176**: p. 220-226.
2. Li, X., et al., *Wettability of colloid-imprinted carbons by contact angle kinetics and water vapor sorption measurements.* Carbon, 2015. **87**: p. 44-60.
3. Wiącek, A.E., *Effect of surface modification on starch biopolymer wettability.* Food Hydrocolloids, 2015. **48**: p. 228-237.
4. ASTM, *D882–02, Standard test method for tensile properties of thin plastic sheeting.* Annual Book of ASTM Standards, American Society for Testing Materials, Philadelphia, PA, 2001.
5. ASTM, *D638-03, Standard test method for tensile properties of plastics.* Annual Book of ASTM Standards, American Society for Testing Materials, Philadelphia, PA, 2003.
6. ASTM, *E111-04, Standard Test Method for Young's Modulus.* Annual Book of ASTM Standards, American Society for Testing Materials, Philadelphia, PA, 1997.
7. Ratnam, C.T., et al., *Electron beam irradiation of epoxidized natural rubber: FTIR studies.* Polymer international, 2000. **49**(12): p. 1693-1701.
8. Wang, S. and L. Copeland, *Molecular disassembly of starch granules during gelatinization and its effect on starch digestibility: a review.* Food & function, 2013. **4**(11): p. 1564-1580.

5 RHEOLOGICAL CHARACTERIZATION OF THERMOPLASTIC STARCH FILMS MODIFIED WITH POS

5.1 Introduction

There is an increasing interest in finding alternative materials to replace non-renewable petroleum-based polymeric materials. One of these alternative materials used in food industry is thermoplastic starch. It is derived from sustainable sources, it is produced worldwide in large quantities [1], is non-toxic, biodegradable and possesses attractive mechanical properties. However, it lacks suitable water resistance and impermeability. For these reasons most research focuses on solving the hydrophilicity issue, but the development of methodologies to understand the thermo-mechanical properties that determine applications and processability of thermoplastic starch materials is equally important.

A very important factor that determines the usability and processability of starch films is their thermo-mechanical behaviour. During deformation, starch films, exhibit time-temperature dependent viscose-elastic behaviour. This behaviour depends upon polymer characteristics such as composition, crystallinity, topology and thermo-mechanical history, which is explained as molecular rearrangements to lessen intra- and inter-molecular stresses.

In practice this means that evaluation of viscose-elastic behaviour needs to be performed under rigorous time-temperature conditions, which in many instances is beyond the capability of DMA instruments. However, it is possible to extend the observational window (time and temperature) of a DMA instrument using the time-temperature superposition principle (TTSP). The principle states that equivalent changes in temperature (or pressure), have the same proportional time response and can be expressed as the temperature shift function ($a_{T_0}(T)$) as given in equation (32).

$$a_{T_0}(T) = \frac{\tau_i(T)}{\tau_i(T_0)} \quad \therefore \quad \tau_i(T) = a_{T_0}(T) \cdot \tau_i(T_0) \tag{32}$$

where, T is the temperature, T_0 is the reference temperature, τ_i are the respondance times.

In practice, the TTSP master-curves are constructed to extend the observational window. First, viscoelastic properties (e.g., modulus) are measured at different temperatures, then shift factors are calculated and finally isothermal curves are superimposed by shifting to a chosen reference temperature.

Strictly speaking, this implies that each frequency is measured at a constant temperature, then the temperature is incremented to provide a series of isothermal temperatures, under the tolerance of the instrument though any temperature fluctuations are more evident at sub-zero temperatures. In this work, this source of error was removed by instantaneously measuring the properties using a synthetic simultaneous multifrequency scans (SSMS).

SSMS instantaneously measures the storage and loss modulus at all frequencies simultaneously at a given single temperature resolving them using Fourier transformation. In this way, the moduli are measured at larger number of temperatures, with a smaller number of frequencies, in contrast to the traditional TTSP method. Traditional, measurements are performed over a small number of temperatures and a wide range and a large number of frequencies.

The most important step in the construction of the master-curve is the estimation of the shift factors to consecutively splice the sets of isothermal data by superposition building a continuous time/frequency series called the master-curve. Sometimes this shifting is performed manually, using arbitrary shift factor values until visual confirmation is obtained; a more traditional method is to use one or more isothermal sets and the sum of squared residuals (SSR) as reference to achieve approximate overlapping between the selected isothermal data sets. This work proposes and describes an integrational method that virtually takes a large number of isothermal data sets in the splice section to achieve the closest possible overlapping of the sections.

After determining the experimental shift factors, it is possible to model them to obtain more information about the materials. The most used models for this shifting are Arrhenius equation (33) and Williams, Landel, and Ferry (WLF) equation (34).

$$ln(a_T) = -\frac{\Delta E a_T}{R}\frac{1}{T} + ln(Aa_{\mathrm{T}}) \tag{33}$$

$$ln(a_T) = \frac{-C_1^r(T - T_r)}{C_2^r + (T - T_r)} \tag{34}$$

where a_T is the shift factor at a given temperature (T), $\Delta E a_T$ is the apparent shifting activation energy, Aa_{T} is the preexponential Arrhenius constant, R is the universal gas constant, C_1^r and C_2^r are the WLF constants or viscoelastic coefficients, and T_r is the reference temperature.

The Arrhenius equation provides a model analogous to the temperature response chemical reactions, where the transition is measured from one stage to another, and increasing temperature decreases the response increment and is related to the relaxation time for local motions of polymer chains.

The WLF model elucidates behaviour due to retardation-relaxation from segmental or backbone motions (micro-Brownian motion) of the polymeric chains in the bulk and it can be derived from free volume theory [2] that it is intimately related to T_g and the coefficient of thermal expansion.

The TTSP equation, applies in theory only to thermorheologically simple materials that involve unbranched polymers, since branches can have different relaxation processes to the main-chain, and it should not be used to model mixtures that could have more than one characteristic time–temperature response. For those reasons, the TTSP must be selectively applied [3], if higher-order transitions (transitions below the T_g) are being considered, though such materials do not exist in practice. Thus, this principle can be applied to complex materials such as block copolymers, graft polymers, hybrids or multiphase materials and specially carbohydrates with complex architectures. By introducing one or more extra distinct distributions of temperature (or time/frequency) dependence respondance parameters across defined ranges according to Fesko and Tschoegl (FT) empirical shift function [4] in equation (35).

$$ln(a_T) = -\frac{C_1^r(T - T_r)}{C_2^r + T - T_r}\theta(T) + \frac{\Delta E_{a_T}}{R}\left(\frac{1}{T} - \frac{1}{T_o}\right)\theta(T - T_o) \qquad (35)$$

They combine the WLF and Arrhenius equations in a continuous additive function in which the WLF parameters fit and are valid only below a characteristic temperature T0, the Arrhenius equation fits and is valid only above T0, and both models contribute to an average at exactly T0, because of the use of the Heaviside step functions $\theta(T)$ and $\theta(T\text{-}T_0)$ with temperatures in degree Celsius.

It is hypothesized that; the proposed integrational method can be used to construct master curves of thermo-rheologically complex starch–nanohybrid films under certain constraints that can be found using properties predicted by models. These methodologies can lead to a better thermo-mechanical analysis of carbohydrate polymers, which are by their nature rheologically complex materials, a valuable objective, especially given these types of films have great potential in the bioplastic, food science and packaging industries.

5.2 Material and methods

5.2.1 Materials

High amylose (>50 %) hydroxypropylated [5] corn starch Penford™ A939 was used [6]. Distilled water was used as the solvent or dispersant and glycerol (propane-1,2,3-triol) with less than 1 % moisture (w/w) from Sigma-Aldrich (Sydney, Australia) was used as plasticizer.

To modify the starch films, functionalized polyhedral oligomeric silsesquioxanes (POS) 1-(3-Glycidyl) propoxy-3,5,7,9,11,13,15-isobutylpentacyclo[9.5.1.1^{3,9}.1^{5,15}.1^{7,13}] octasiloxane (epoxy-POS) was used. The 1-(3-amino) propyl-3,5,7,9,11,13,15- isobutylpentacyclo[9.5.1.1.^{3,9}.1^{5,15}.1^{7,13}] octasiloxane (NH_2-POS) was used only to modify films. Both POS samples were acquired from Hybrid Plastics Inc. (Hattiesburg, USA). The epoxy-POS was functionalized using Erucamide (docos-13-enoic acid) from Croda Int. plc (Hull, United Kingdom) or Jeffamine™ M-600 (O-(2-aminopropyl)-O′-(2-methoxyethyl)poly(propylene glycol) 500) purchased from Sigma-Aldrich (Sydney, Australia). The solvent used for all reactions was anhydrous and inhibitor-free oxolane (tetrahydrofuran or THF) purchased from Science Supply Australia Limited (Melbourne, Australia). The materials were used as received; the moisture of glycerol, starch and all the POS were measured and taken into consideration to calculate the concentration of each material and preparing different slurries.

5.2.2 Preparation of starch films and functionalization of POS nanohybrids

The process of preparation of starch films as well as the identification of reaction completion (functionalization of nanohybrid POS) were described in the previous section 4.3.3. The most important aspects of both are briefly summarized in the following sections.

5.2.2.1 Functionalization of nanohybrid POS

Erucamide and Jeffamine were reacted separately with epoxy-POS in 1:1 stoichiometrically ratio in THF (molar ratio of 35:1). The reactants were stirred for 24 h at 40 °C to obtain Eru-POS and Jeff-POS, respectably after complete evaporation of THF under vacuum at 40 °C. All chemical structures used in the films are represented in Figure 4.4.

5.2.2.2 Preparation of starch films

A slurry master batch (4.03 % w/w starch, 1.21 % w/w glycerol, and 94.88 % w/w water) was prepared by heating at 95 ±3 °C for 20 min (IKA RH-digital hotplate, Staufen, Germany). Equal amounts of master batch were individually added to 1.3 % w/w of each hybrid NH_2-POS, epoxy-POS, Eru-POS and Jeff-POS. The film prepared only by the master batch was used as the control. Each slurry was individually homogenized using a high-shear disperser (Bamix, Australia) for 30 s. The completion of gelatinization was monitored with an optical microscope (Nikon Labophot II, Japan) with polarized light filters. The entrapped air was removed from the slurries by applying vacuum for 5 min. Twenty millilitres of each slurry was cast onto a Petri dish with a 9 cm diameter and dried at 30 ±1 ° C for 48 h in a customised temperature control drying box (proportional–integral–derivative controller) and gently forced air circulation was used. All samples were conditioned in a desiccator using a saturated solution with 54 % relative humidity at 20 °C (magnesium nitrate) for 48 h before testing.

5.2.3 Determination of dynamic mechanical properties

Viscoelastic analysis of the films was performed using a PerkinElmer Diamond Dynamic Mechanical Analyser. Specimens were die-cut to dimensions of 45 mm long, 9.6 mm wide, 0.10 mm thick and coated with petroleum jelly to avoid loss of water during tests. To remove any pre-existing thermal or mechanical history (due to casting, peeling and die-cutting), a fast sweep pre-treatment was set in the instrument before each scan. Tensile measurements were made using synthetic simultaneous multi-frequency (10, 5, 2, 1 and 0.5 Hz) scans. Pre-treatment was performed from -60 °C to 80 °C, returning to -60 °C at 20 K/min to begin the scan at 5 K/min to 90 °C. This temperature range was chosen to reveal the glass transition region with plateau. The upper temperature was limited to 93 °C to avoid the boiling temperature of the water in the specimens.

5.2.3.1 Construction of master curves

A range of temperatures were selected to test the material. A multi-frequency measurement of the modulus was performed over a reasonable time scale at each selected temperature to obtain different isothermal modulus-versus-time curves (logarithmic time scale).

The isothermal modulus-versus-time curve obtained at the temperature close to 25 °C was selected as the reference isotherm (T_r) and was used as the initial pivot. It was necessary to multiply the time values of each isothermal curve (f) by a different unique single scalar number (a_T) to horizontally shift all remaining isotherm curves toward this reference). The remaining isothermal curves were sequentially shifted to obtain a superimposed continuous curve called master curve (Figure 5.1).

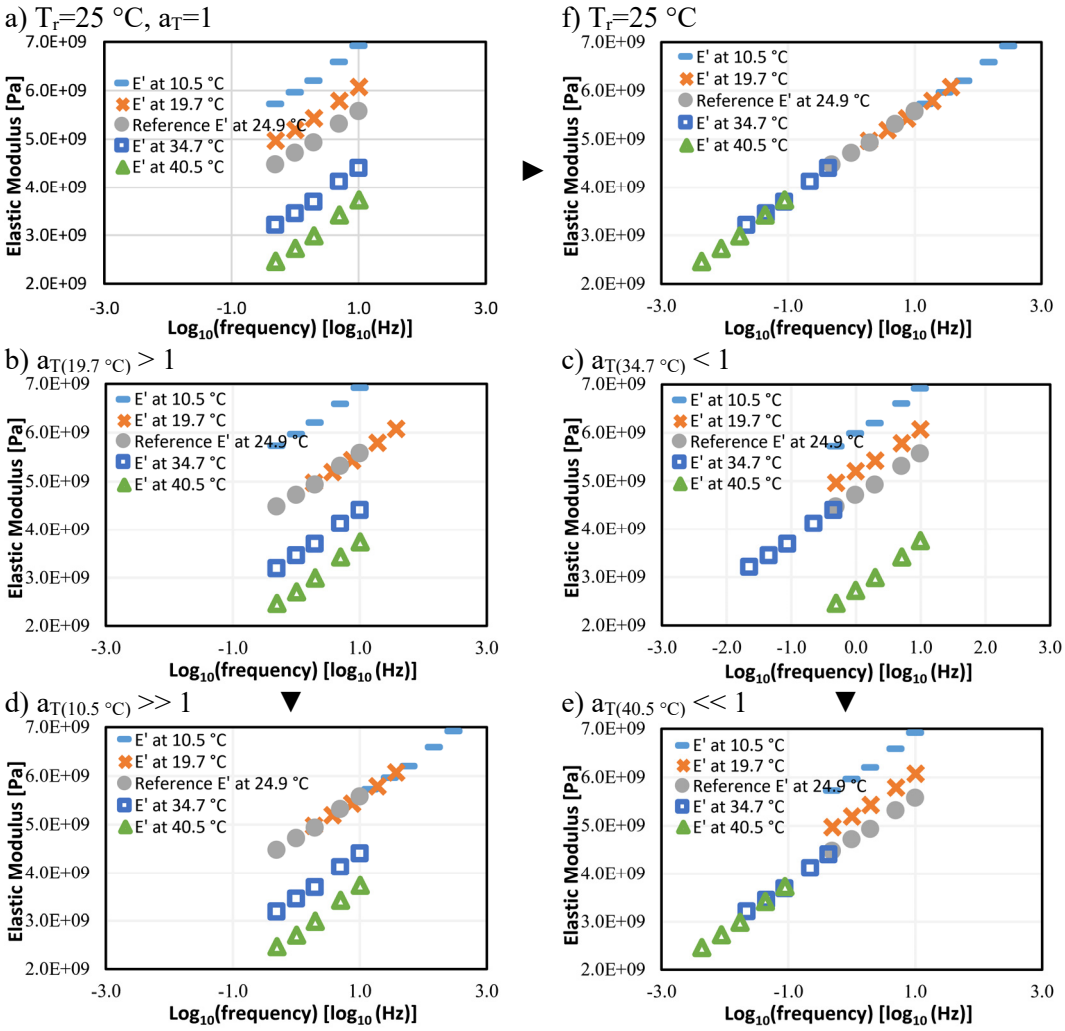

Figure 5.1 Sequential shifting of selected isothermal modulus-versus-time curves of the control film, a) Initial experimental data T_r of 25 °C (a_T = 1); b) first shift below T_r, from left to right (a_T > 1); c) first shift above T_r from right to left (a_T < 1); d) consecutive shift below T_r; e) consecutive shift above the T_r; f) resulting master curve

Each shift factor (a_T) must be such that the difference along the overlap region is as low as possible to obtain a best superposition of the curves to obtain the most representative master curve. The calculation of a_T is the most important element in the construction of a master curve. For this reason, we proposed an integrational method to calculate a_T in this section.

The limit of the overlap region was defined by the maximum and minimum elastic modulus (E') of the two curves to be paired. The difference along the overlap region was evaluated as an area between the fitting functions (Figure 5.2 a), which can be evaluated using an integration optimization function (Figure 5.2 b). It is important to note that calculated area can be a negative value. For this reason, and to simplify the evaluation, the absolute value of the area is used.

It is possible to use fitting functions with a physical meaning only if it is practical while fitting the experimental data; otherwise, a polynomial fitting would be preferred.

As explained earlier in this section, it is necessary to multiply the frequency values ($\log_{10}(f)$) of the curve by a scalar number to shift the curve. Each scalar number produces a different fitting curve and a different fitting function with a different area between the curves. Thus, an optimization calculation is needed to automatically update the fitting functions. The scalar that produces the minimum area is the a_T chosen for that specific temperature, as shown in Figure 5.2 c. Finally, all the shift factors were calculated sequentially in both directions, to construct the master curve (Figure 5.3).

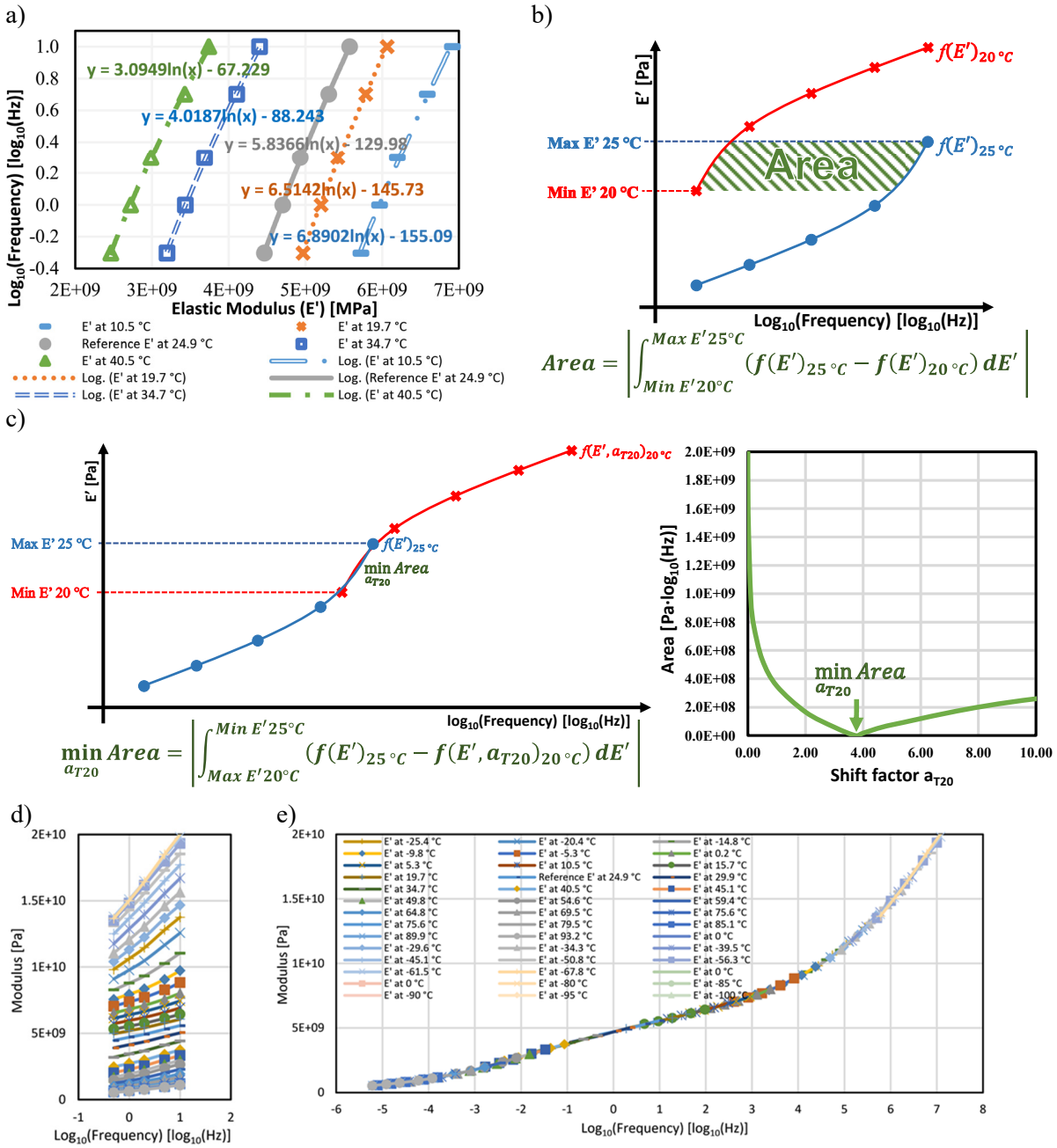

Figure 5.2 a) example of fitting equivalent to a power law model of the control film; b) original area between fitting functions within the limits of the overlapping region and area optimization function; c) shift factor obtained for the control film at a reference temperature of 20 ˚C. Comparison between: d) original isothermal modulus-versus-time curves from -100 ˚C to 93 ˚C and e) all the curves shifted throw 25 ˚C that construct a single master curve

5.2.3.2 Estimation of T_g and other transition temperatures

The transitions were estimated by fitting a 10-degree polynomial, to the experimental data and a linear equation as baseline. The transition temperature corresponds to the temperature at which the maximum vertical distance exists between the baseline and the polynomial (Figure 5.3 a).

The functional dependence of the frequency ν_g [Hz] on the T_g can be represented by the Arrhenius model given by equation (36):

$$\nu_g = A_g e^{-\frac{\Delta E_g}{R\,T_g}} \;\rightarrow\; ln(\nu_g) = -\frac{\Delta E_g}{R}\frac{1}{T_g} + ln(A_g) \qquad (36)$$

where A_g [Hz] is the temperature-independent pre-exponential factor, ΔE_g [J mol^{-1}] is the apparent activation energy of glass transition [7], T_g [K] is the glass transition temperature at the respective frequency, and R [J K^{-1} mol^{-1}] is the universal gas constant. The ΔE_g indicates the onset of polymer segmental motions in the matrix of the composites [7].

The value of ΔE_g was calculated as the negative product of R times the value of the slope of plot of natural logarithm of frequency versus the reciprocal of the absolute temperature. The values of T_g, ΔE_g, and A_g were calculated and are reported in Table 5.1.

5.2.3.3 Calculation of Arrhenius and WLF constants, free volume fraction and thermal expansion coefficients.

Similar to section 5.2.3.2, the Arrhenius parameters were calculated for aT_n (Figure 5.3 c). The WLF constants or viscoelastic coefficients C_1^r and C_2^r were calculated at the reference temperature with the equation given in Figure 5.3 b ([8-10]).

The WLF constants, C_1^g and C_2^g, free volume fraction (f_g) and thermal expansion coefficients (α_g) were calculated at given T_g (at 1 Hz) and at the reference temperature (T_r). The values of C_1^r, C_2^r, f_r and α_r were calculated using equations (37) to (40), assuming that Doolittle constant B is equal to 1 [11], and are reported in Table 5.3.

$$T_g - C_2^g = T_r - C_2^r \;\rightarrow\; C_2^g = T_g + C_2^r - T_r \qquad (37)$$

$$C_1^r C_2^r = C_1^g C_2^g \;\rightarrow\; C_1^g = \frac{C_1^r C_2^r}{C_2^g} \qquad (38)$$

$$C_1^g = \frac{B}{f_g} \;\; with \;\; B = 1 \;\rightarrow\; f_g = \frac{1}{C_1^g} \qquad (39)$$

$$C_2^g = \frac{f_g}{\alpha_g} \;\rightarrow\; \alpha_g = \frac{f_g}{C_2^g} \;\rightarrow\; \alpha_g = \frac{1}{C_1^g C_2^g} \;\therefore\; \alpha_r = \frac{1}{C_1^r C_2^r} \qquad (40)$$

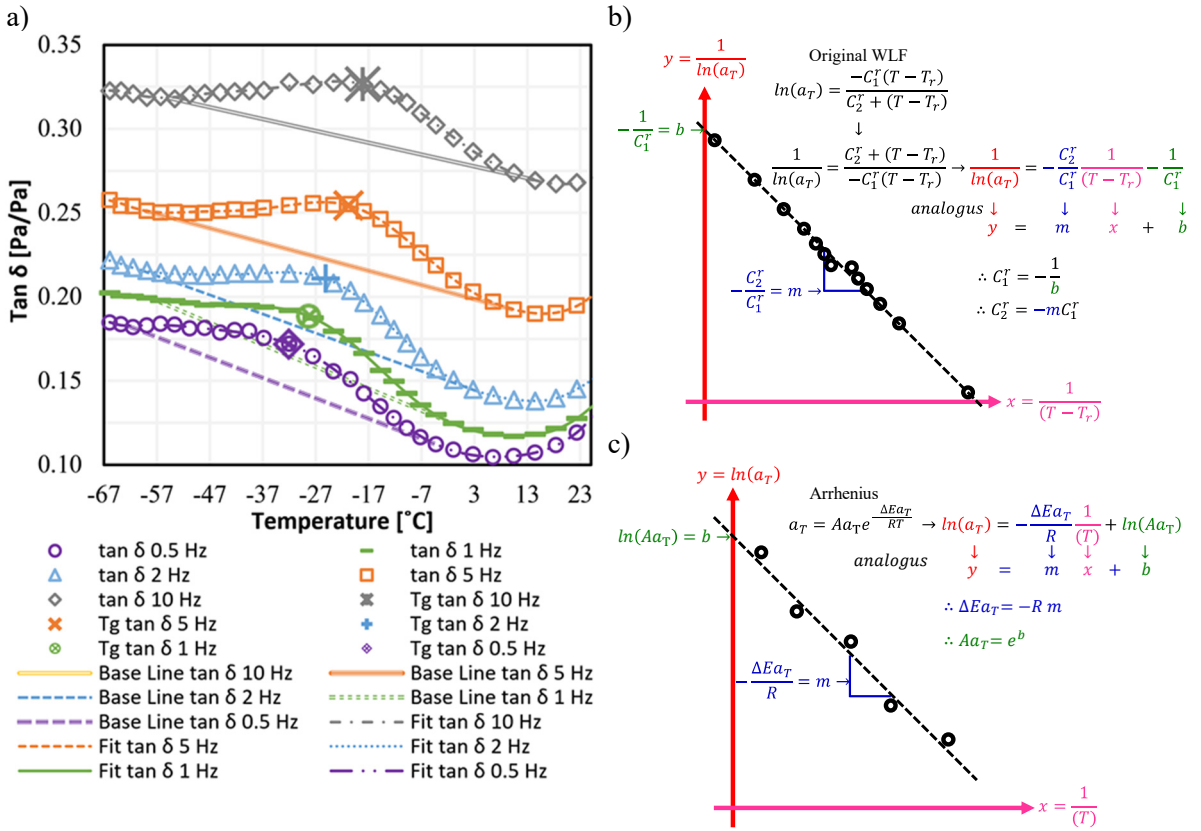

Figure 5.3 a) calculation of T_g for the control film using tan(δ) at different frequency scans with polynomial fitting and base lines. Schematic aT modelling for b) WLF and c) Arrhenius equations

5.2.4 Main differences between the proposed and conventional methods.

In conventional methods each frequency is measured at different temperatures and this measurement becomes the source of major error for the construction of master curves. This error is particularly pronounced in sub-ambient and sub-zero temperatures where liquid nitrogen is used to control the temperature. The synthetic frequency approach proposed in this work avoids this error.

Most conventional methods scan a wide range of frequencies with a small number of isothermal temperature steps; by the contrary our method enables to test materials over a much large temperature number of isothermals with fewer frequencies depending on the selection of the synthetic frequency.

The calculation of the shift factors is at the core of any master-curve construction; for this reason, the new method proposed in this work is easy to use and can readily optimised. There is a dearth of publications that can guide the practitioners from acquisition of data right to the calculation of properties. Most importantly the conventional TTSP method cannot be applied to rheologically complex materials.

5.2.5 Generalized time temperature superposition models

Similar to the Fesko and Tschoegl equation describe in the introduction, empirical models can be stablished for *n* number of characteristic temperatures, and because the models are independent at each interval delimited by a characteristic temperature, it is possible to establish generalised models (Figure 5.4) incorporating one or more types of model with independent parameter per interval.

The Fesko and Tschoegl model divides the full set of data into two independent sets or regions (before and after T_1). Then this model uses the WLF equation to fit the first set of data (before T_1) and uses Arrhenius model to fit the second set of data. The simplified version of Fesko and Tschoegl model can be expressed as equation (41).

$$Ln(a_T) = WLF\ \theta 1(T_1) + Arrhenius\ \theta 2(T_1) \tag{41}$$

Where $\theta 1(T_1)$ is a Heaviside function in terms of the characteristic temperature T_1.

In the case the first half set of data is better represented by Arrhenius and the second half by WLF, equation (41) can be written as equation (42).

$$Ln(a_T) = Arrhenius\ \theta 1(T_1) + WLF\ \theta 2(T_1) \tag{42}$$

Similarly, there can be a case where the data could be better described by two independent WLF equations as given by equation (43).

$$Ln(a_T) = WLF1\ \theta 1(T_1) + WLF2\ \theta 2(T_1) \tag{43}$$

Following this line of reasoning, if the data set can be divided into three regions with two characteristic temperatures T_1 and T_2, a generalised WLF equation (gWLF) with n=2 can be written equation (44).

$$Ln(a_T) = WLF1\ \theta 1(T_1) + WLF2\ \theta 2(T_1, T_2) + WLF3\ \theta 3(T_{02}) \tag{44}$$

Or all Arrhenius

$$Ln(a_T) = Arrhenius\ \theta 1(T_1) + Arrhenius\ \theta 2(T_1, T_2) + Arrhenius\ \theta 3(T_{02}) \tag{45}$$

Or a combination of both gWLF and Arrhenius models as given by equation (46).

$$Ln(a_T) = Arrhenius\ \theta 1(T_1) + WLF1\ \theta 2(T_1, T_2) + Arrhenius\ \theta 3(T_{02}) \tag{46}$$

For example, equations (47) and (48) present the empirical, respectively, empirical generalised Arrhenius and WLF (gWLF) models for thermorheologically complex materials. Where T_1 to T_n are the characteristic temperatures, $T_0 = T\text{-}1$, $T_{n+1}=T+1$ and temperatures are on Kelvin.

$$ln(a_T) = \sum_{i=0}^{n} \langle \left[\frac{-\Delta E a_{T,i+1}}{R} \frac{1}{T} + ln\left(A_{a_{Ti+1}}\right) \right] \{\theta[(T - T_i)(T_{i+1} - T)]\} \rangle \qquad (47)$$

$$ln(a_T) = \sum_{i=0}^{n} \langle \left[\frac{-C^r_{1,i+1}(T - T_r)}{C^r_{2,i+1} + (T - T_r)} \right] \{\theta[(T - T_i)(T_{i+1} - T)]\} \rangle \qquad (48)$$

where T_1 to T_n are the characteristic temperatures, $T_0 = T\text{-}1$ and $T_{n+1} = T+1$.

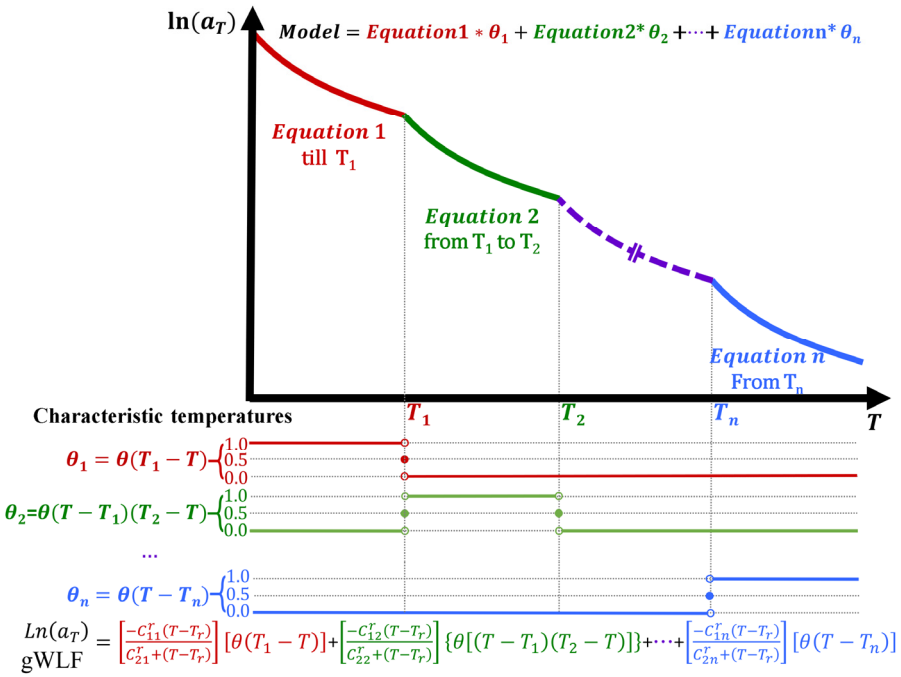

Figure 5.4 Schematic representation of generalised time-temperature superposition model for thermorheologically complex materials.

5.3 Results and Discussion

The phase angle (tan(δ)) at various frequencies showed at least two transitions (see result in Table 5.1). Second-order transitions are kinetic phenomena. They are derived from intermolecular mobility due to variation in temperature, pressure or mechanical stress [12]. It is considered that transition occurring at the lowest temperature is glass transition because it is frequency dependent and reversible. The transition at the highest temperature (but below the boiling temperature of water) was reversible and frequency independent, for these reasons it was considered as the melting temperature (T_m). There was another intermediate transition between the above two (Table 5.1), but only in the case of the control

film. This intermediate transition was independent to frequency and was reversible or pseudo-reversable (it decreased in magnitude depending on time). This intermediate transition can be attributed to melting of retrograded starch upon heating, where starch recrystallised after gelatinization [13]. It is also worth mentioning that it was found that the average ratio between the T_g and the T_m is about 0.75, with a standard deviation of 0.04 among the materials tested, which indicated that similar factors affected both T_g and T_m even when the films were different.

Table 5.1 Dynamic mechanical properties of different films. Mean (standard deviation)

Film	Eru-POS	Jeff-POS	Epoxy-POS	NH_2-POS	Control
T_g (0.5 Hz) [˚C]	*-23.1*	*-23.3*	*-28.7*	*-23.8*	*-32.1*
T_g (1 Hz) [˚C]	*-20.1*	*-21.0*	*-24.2*	*-20.9*	*-28.2*
T_g (2 Hz) [˚C]	*-17.2*	*-18.2*	*-19.8*	*-17.6*	*-25.2*
T_g (5 Hz) [˚C]	*-11.2*	*-13.4*	*-14.1*	*-12.3*	*-20.8*
T_g (10 Hz) [˚C]	-7.0	-9.2	-9.9	-8.2	-18.1
Average T_m [˚C]	*47.5 (0.3)*	*47.2 (2.1)*	*57.7 (5.4)*	*71.5 (0.5)*	*80.1 (0.2)*
Intermediate transition [˚C]	-	-	-	-	*51.3 (0.47)*
T_g (1 Hz) /T_m [K K^{-1}]	*0.79*	*0.79*	*0.75*	*0.73*	*0.69*
ΔE_g [J mol^{-1}]	*101 186*	*114 828*	*85 276*	*104 288*	*109 465*
A_g [Hz]	*6.11×10^{20}*	*3.97×10^{23}*	*$7.61E\times10^{17}$*	*3.4×10^{21}*	*2.41×10^{23}*
Arrhenius R^2	*0.9786*	*0.9958*	*0.9742*	*0.9686*	*0.9362*

The value of T_g can be calculated at any given frequency with the Arrhenius equation and experimental data (Figure 5.5 a), using the equation (50) derived from equation (36). This allows an increase in the observation frequency window of the instrument. For instance, the Diamond Dynamic Mechanical Analyser used in this experiment, operates in a frequency range between 0.01 and 100 Hz, but with the model, one can expand the observation window by orders of magnitude (Figure 5.5 b).

$$T_g = -\frac{\Delta E_g}{R\left(\ ln(\nu_g) - n(A_g)\right)} \qquad (49)$$

The rubbery and glassy state regions can be determined using the value of T_g and the melting temperatures (Figure 5.5 c). According to Gordon–Taylor equation, polymers with higher crystallinity or higher T_g are related to lower capacity of moisture sorption [14], lower storage temperature and increased risk of recrystallisation [15]. In starch films, it ultimately leads to retrogradation and these factors are critical for the design of films for food packaging applications.

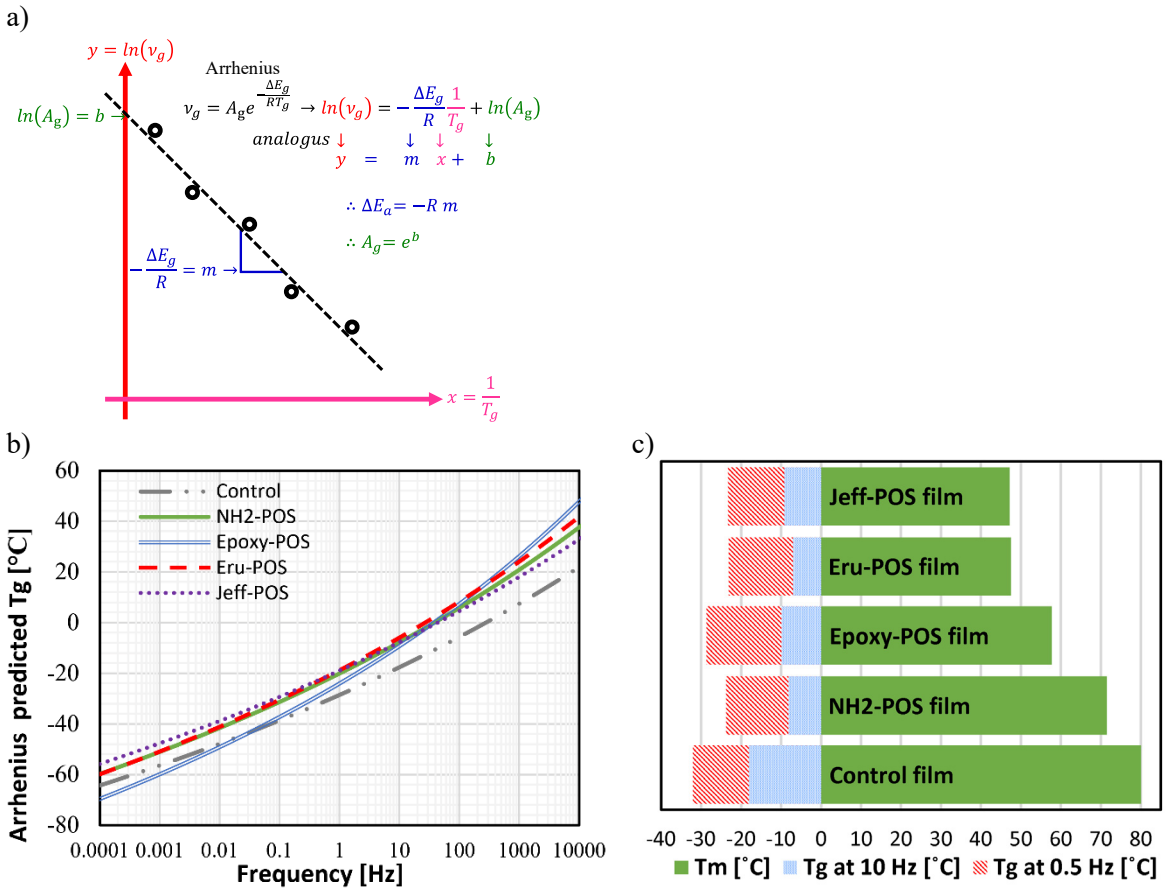

Figure 5.5 a) Schematic plot and equations used to model T_g, b) Predicted T_g at an expanded interval of frequencies and c) rubbery state temperature range

Due to the brittle nature of starch at the glassy state, it is not recommended to process or stress the starch films with epoxy-POS over 480 Hz, Eru-POS over 560 Hz, NH_2-POS over 890 Hz, Jeff-POS above 1300 Hz and the control (starch) over 7300 Hz at the normal temperature condition (20 °C). As shown in Figure 5.5 b, the control film had the lowest T_g but at frequencies below 0.04 Hz the epoxy-POS film had the lowest T_g.

The resulting master curves for the elastic modulus (E') are shown in Figure 5.6 a. Feather-like master curves or pseudo-master curves are observed for the viscous modulus (E'') in all the films (Figure 5.6 b). It can be considered the feather-like curves as evidence of thermorheologically complex behaviour. Various relaxation processes can occur [16] due to complex networking, presence of amylopectin branches or polymer-nanohybrid interactions, all of which determine the films' dynamic properties [17].

All master curves of the starch nanohybrid films with the exception of the Jeff-POS begin at higher frequencies than the control, indicating that nanohybrid films were recovered before the next higher

deformation (frequency). Jeff-POS behaves in a manner similar to the control; suggesting that the cage effect of POS diffused into the polymeric matrix due the long and highly hydrophilic substituent group that Jeffamine provided to the POS cage.

The master curves of the NH_2-POS and epoxy-POS films show elastic and viscous moduli higher than those of the control by about one order of magnitude, indicating that the nanohybrids are acting as reinforcements. It is also important to note that the curve for NH_2-POS and epoxy-POS films terminated at lower frequencies compared to other films.

The resulting a_T of the films are shown in Figure 5.6 c. By fitting a_T values to WLF or Arrhenius model it was found that they cannot described the temperature dependence of a_T in the entire experimental temperature (Figure 5.6 d). This is another indication that all the films are not rheologically simple materials.

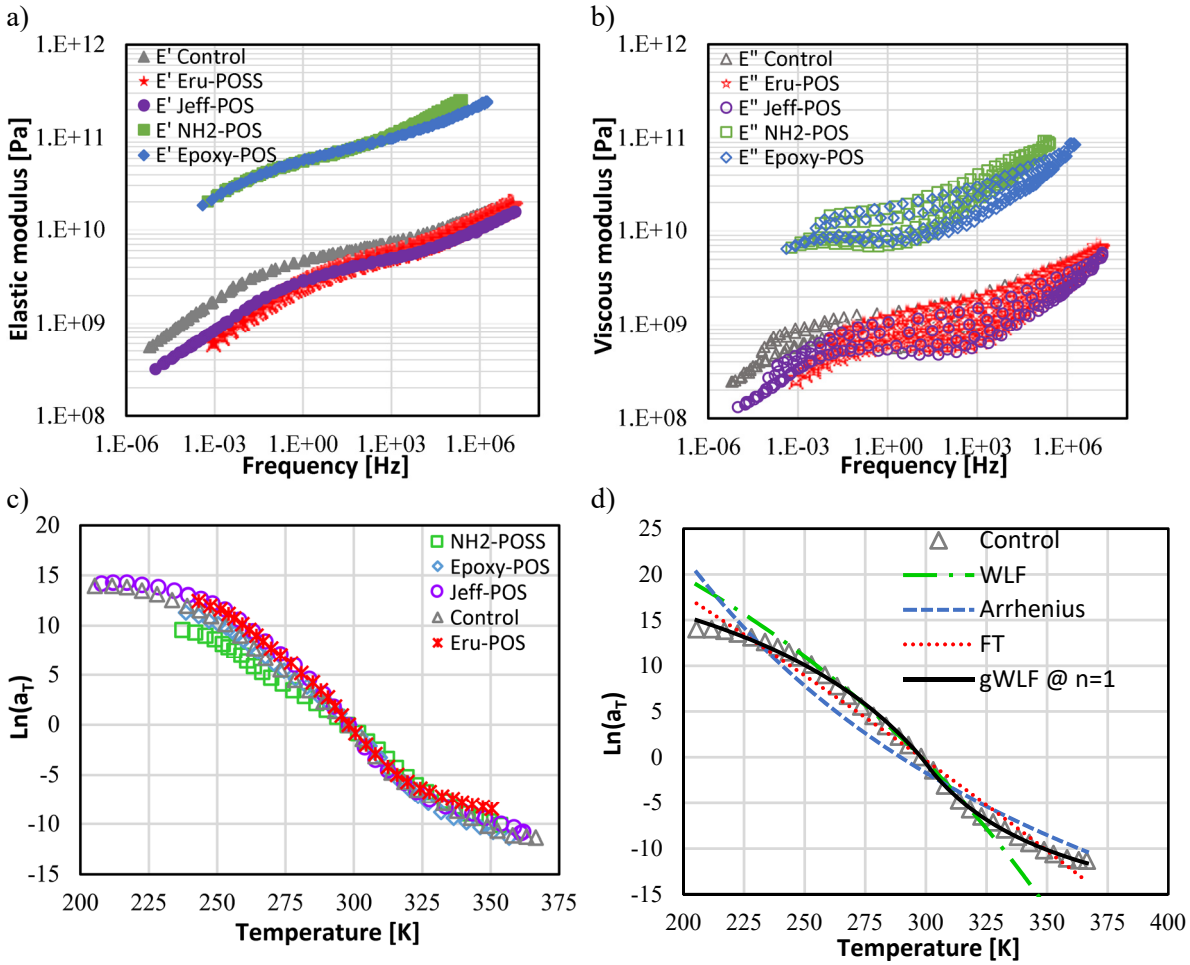

Figure 5.6 Master curves of the different films for the a) elastic modulus and b) viscous modulus. Resulting shift factors c) for the different films, d) comparison of the shift factors of the control film and models

The WLF constants at T_r (C_1^r and C_2^r,) and T_g (C_1^g and C_2^g) are useful parameters to predict important properties such as free volume fraction (f) and the thermal coefficient of expansion (α). The coefficients of Arrhenius equation (ΔEa_T and Aa_T) correlate with the variation (magnitude and trend) of a_T with respect to temperature (equation (50)).

$$ln(a_T) = \frac{\Delta Ea_T}{R}\frac{1}{T} + ln\left(A_{a_T}\right) \quad (50)$$

While useful, neither WLF or Arrhenius model can be utilised if its correlation is low or it predicts unrealistic values. In our case, the films are not rheologically simple materials in the full range of the master curve. Thus, it was necessary to find a range of temperatures in which the models are valid. The initial intervals limits for the non-complex material models were chosen using T_r and the T_g. In later calculations using complex material models, tracking every temperature and almost every possible interval, it was found the same results as in the case of non-complex material models.

For all tested materials except for the Jeff-POS film, the temperature interval in which the models correlate to an R^2 of at least 0.99 and do not predict unrealistic values was above the T_r. Table 5.2 shows that for the control film, even if both models have R^2 values above 0.9, they predict negative values of free volume fraction and absolute temperatures. Only by taking temperatures above the T_r do both models produced acceptable correlation without unrealistic predictions.

Table 5.2 WLF constants, f and α at the T_g and Tr of the control film at different temperatures intervals (inadequate values predicted by the model and R2 below 0.9 are between parenthesis)

Interval	Full range	Below T_r	Above T_r	Below T_g	Above T_g	Between T_g and T_r
ΔEa_T [J mol^{-1}]	-118 864	-75 670	-139 873	-28 095	-156 764	-133 839
Aa_T [Hz]	3.6×10^{-22}	1.1×10^{-12}	5.7×10^{-26}	1.4×10^{-1}	1.7×10^{-28}	5.7×10^{-24}
Arrhenius R^2	(0.3716)	(0.5025)	0.9969	(0.8946)	0.9446	0.9677
T_r	298.0	298.0	298.0	298.0	298.0	298.0
C_1^r	-82.2	-46.5	31.8	-21.6	-119.7	-51.53
C_2^r [K]	(-310.4)	(-178.7)	100.5	(-47.0)	(-450.7)	(-198.8)
f_r	(-0.0122)	(-0.0215)	0.0315	(-0.0462)	(-0.0084)	(-0.0194)
α_r [K^{-1}]	3.9×10^{-5}	1.2×10^{-4}	3.1×10^{-4}	9.8×10^{-4}	1.9×10^{-5}	9.8×10^{-5}
C_1^g	-70.2	-35.9	67.4	-10.2	-107.1	-40.7
C_2^g [K]	(-363.5)	(-231.8)	47.4	(-100.0)	(-503.8)	(-251.9)
f_g	(-0.0143)	(-0.0279)	0.0148	(-0.0985)	(-0.0093)	(-0.0246)
α_g [K^{-1}]	$3.9E\times10^{-5}$	1.2×10^{-4}	3.1×10^{-4}	9.8×10^{-4}	1.9×10^{-5}	9.8×10^{-5}
WLF R^2	(0.5961)	(0.7266)	0.99995	0.9484	0.9860	0.9985

All parameters of and realistic properties predicted by the models, at the chosen interval, are presented in Table 5.3.

A gWLF with a value of n=1 was also fitted to the full range of a_T for all the films. Characteristic temperatures (T_l) of gWLF were very close to their T_r and providing similar results of WLF. This is because a gWLF model segments data as required using characteristic temperatures and treat each segment independently. For this reason, redundant results are omitted in Table 5.3.

For the FT model, the correlation of the model using the calculated parameters for the non-complex models and its characteristic temperature T_o was estimated using a simple sum of squared residuals (SSR) method. The gWLF used for all tested materials, except for Jeff-POS film, highlights the possibility to use either a numerical, analytical (Figure 5.3 b) or a SSR method to estimate its characteristic temperature (T_l) and both pair of constants ($C_{11}^r, C_{21}^r, C_{12}^r \; and \; C_{22}^r$).

*Table 5.3 Arrhenius and WLF constants, f and α at the T_g and Tr at their valid interval. * indicates that the full range of data was used for calculation*

Film	Control	Eru-POS	Epoxy-POS	Jeff-POS	NH_2-POS
Interval	*Above T_r*	*Above T_r*	*Above T_r*	*Above T_g*	*Above T_r*
ΔEa$_T$ [J/mol]	*-139 873*	*-127 946*	*-168 737*	*-170 210*	*-157 711*
Aa$_T$	*5.7×10^{-26}*	*8.6×10^{-24}*	*8.6×10^{-31}*	*1.6×10^{-30}*	*1.1×10^{-28}*
Arrhenius R^2	*0.996916*	*0.989839*	*0.994976*	*0.967096*	*0.999215*
T_r [K]	*298.0*	*298.1*	*298.5*	*297.9*	*297.8*
C_1^r	*31.8*	*17.5*	*52.3*	*64.8*	*108.4*
C_2^r [K]	*100.5*	*48.1*	*166.9*	*192.8*	*458.9*
f_r	*0.0315*	*0.0573*	*0.0191*	*0.0154*	*0.0092*
α_r [K^{-1}]	*3.1×10^{-4}*	*1.2×10^{-3}*	*1.1×10^{-4}*	*8.0×10^{-5}*	*2.0×10^{-5}*
C_1^g	*67.4*	*281.9*	*74.4*	*84.9*	*120.4*
C_2^g [K]	*47.4*	*3.0*	*117.4*	*147.1*	*413.4*
f_g	*0.0148*	*0.0035*	*0.0134*	*0.0118*	*0.0083*
α_g [K^{-1}]	*3.1×10^{-4}*	*1.2×10^{-3}*	*1.1×10^{-4}*	*8.0×10^{-5}*	*2.0×10^{-5}*
WLF R^2	*0.999954*	*0.999998*	*0.999990*	*0.900495*	*0.999986*
T_0	*341.2*	*335.1*	*330.3*	*306.1*	*332.5*
FT R^2	*0.999954*	*0.999998*	*0.999990*	*0.900495*	*0.999986*
****T_l gWLF @ n=1 [k]***	*298.1*	*295.6*	*298.5*	*297.9*	*297.8*
****gWLF R^2***	*0.9985*	*0.9997*	*0.9992*	*0.9986*	*0.9989*
****SSE***	*4.151*	*0.6476*	*1.501*	*4.153*	*1.525*

5.4 Conclusions

It is possible to identify T_g, T_m and other transitions using dynamic mechanical analysis using simultaneous multifrequency scans. It was found a consistent ratio of 0.75 between the T_g and T_m. The

Arrhenius equation was able to predict the T_g at any frequency-deformation, which is useful to determine if the materials is in rubbery or glassy state.

The incorporation of POS into the starch films increased the T_g which in principle decreased moisture sorption [14, 18], a beneficial feature for storage of food materials. The presence of POS decreased T_m, indicating that less energy is required for their processing.

Smooth master curves can be produced using the integrational method for a_T proposed. The master curves of the NH_2-POS and Epoxy-POS films exhibited an increase in both moduli (E', E'') by an order of magnitude respect to the starch control film. The increased muduli, indicates that the different chemical nature of the amine and epoxy was not as important as their stereochemical configuration.

Even though the films like most of the carbohydrate are rheologically complex materials, it is possible to model their behaviour using WLF and Arrhenius equations using appropriate temperature constraints, which can be found by calculating ΔEa_T, C^r_2, f, α *and* R^2. Complex and non-complex models can be used with the understanding that their parameters are independent and only valid within intervals defined by their characteristic temperatures. At some intervals the complex model's predicted properties could be unrealistic, and in those, the models shall not be used. In all cases the proposed generalised complex models had coefficient of determinations greater than 0.99 for the a_T.

It wasn't found more than one characteristic temperature for each material, but the generalized models can model materials with more than one characteristic temperature.

The addition of POS in starch increased the inner order of the material, led to more compact molecular arrangement and made them more resilient to deformation due to change in temperature.

5.5 References

1. Kim, J.R. and A.N. Netravali, *Self-healing starch-based 'green'thermoset resin.* Polymer, 2017. **117**: p. 150-159.
2. Tschoegl, N.W., W.G. Knauss, and I. Emri, *The effect of temperature and pressure on the mechanical properties of thermo-and/or piezorheologically simple polymeric materials in thermodynamic equilibrium–A critical review.* Mechanics of Time-Dependent Materials, 2002. **6**(1): p. 53-99.
3. Malkin, A.Y. and A.I. Isayev, *Rheology: concepts, methods, and applications*. 2017: Elsevier.
4. Fesko, D. and N. Tschoegl. *Time-temperature superposition in thermorheologically complex materials*. in *Journal of Polymer Science Part C: Polymer Symposia*. 1971. Wiley Online Library.
5. Halley, P., S. McGlashan, and J. Gralton, *Biodegradable polymer*. 2006, Google Patents.
6. Khemani, K., et al., *Starch nanocomposite materials*. 2008, Google Patents.

7. Karbhari, V.M. and Q. Wang, *Multi-frequency dynamic mechanical thermal analysis of moisture uptake in E-glass/vinylester composites.* Composites Part B: Engineering, 2004. **35**(4): p. 299-304.
8. Williams, M.L., R.F. Landel, and J.D. Ferry, *The temperature dependence of relaxation mechanisms in amorphous polymers and other glass-forming liquids.* Journal of the American Chemical society, 1955. **77**(14): p. 3701-3707.
9. Maidannyk, V. and Y. Roos, *Modification of the WLF model for characterization of the relaxation time-temperature relationship in trehalose-whey protein isolate systems.* Journal of Food Engineering, 2016. **188**: p. 21-31.
10. Yasutomi, S., S. Bair, and W. Winer, *An application of a free volume model to lubricant rheology I—dependence of viscosity on temperature and pressure.* Journal of tribology, 1984. **106**(2): p. 291-302.
11. Olmos, D., et al., *The effect of surface modification of silica microfillers in an epoxy matrix on the thermo-mechanical properties.* Journal of Adhesion Science and Technology, 2008. **22**(13): p. 1443-1459.
12. Kasapis, S., *Building on the WLF/free volume framework: Utilization of the coupling model in the relaxation dynamics of the gelatin/cosolute system.* Biomacromolecules, 2006. **7**(5): p. 1671-1678.
13. Wang, S. and L. Copeland, *Molecular disassembly of starch granules during gelatinization and its effect on starch digestibility: a review.* Food & function, 2013. **4**(11): p. 1564-1580.
14. Bley, O., J. Siepmann, and R. Bodmeier, *Importance of glassy-to-rubbery state transitions in moisture-protective polymer coatings.* European Journal of Pharmaceutics and Biopharmaceutics, 2009. **73**(1): p. 146-153.
15. Royall, P.G., D.Q. Craig, and C. Doherty, *Characterisation of moisture uptake effects on the glass transitional behaviour of an amorphous drug using modulated temperature DSC.* International journal of pharmaceutics, 1999. **192**(1): p. 39-46.
16. Villar, M.A., et al., *Rheological characterization of molten ethylene–α-olefin copolymers synthesized with Et [Ind] 2ZrCl2/MAO catalyst.* Polymer, 2001. **42**(22): p. 9269-9279.
17. Wang, M.J., S.X. Lu, and K. Mahmud, *Carbon–silica dual-phase filler, a new-generation reinforcing agent for rubber. Part VI. Time–temperature superposition of dynamic properties of carbon–silica-dual-phase-filler-filled vulcanizates.* Journal of Polymer Science Part B: Polymer Physics, 2000. **38**(9): p. 1240-1249.
18. Hancock, B.C. and G. Zografi, *Characteristics and significance of the amorphous state in pharmaceutical systems*. 1997: New York. p. 1-12.

6 MOLECULAR MODELING OF POS-NATURAL RUBBER AND ENR50

6.1 Introduction

As mention in 2.2 in order for the NR to have a commercial use it is necessary modify it using additives and fillers. Besides sulphur, among all different additives and filler carbon black is the most preferred reinforcing filler [1]; however clays and nano-silica (same composition than POS) are gaining popularity because some have increased reinforcement more than traditional carbon black. In any mature fields as in the case of rubber, the use of novel filler that could enhance the performance is worthy to investigate.

Despite the worthy investigation for enhanced properties of NR by incorporation POS as many literatures suggest [2-5], few scientific works have reported grafting or mixing POS onto NR or epoxidized NR (ENR) [6] and even less research has been reported contrasting hybrids and composites as mention in 2.4.2.

Computational performance increases each year and in novel modelled synthetic methods, materials can gain complexity and molecular dynamics has emerged as an attractive tool [7]. The use of molecular modelling and simulation becomes more accessible, and this is especially true in the nano-composite field, where design rules allow modelling of engineering materials by combining the desirable properties of nanoparticles and polymers for potential commercialisation [8].

For these reasons, it was important to construct models to compare structures and properties using molecular modelling and simulation, which give a unique comparative perspective with fewer confounding variables than traditional experiments, for example the complex process of mixing [9]. It can be hypothesised that hybrids are more effective than composites in transferring stress from the polymeric matrix to the nanoparticles.

6.2 Methods

6.2.1 Topology method

All topology calculations were performed using Synthia, which significantly simplified the task, while minimising errors. To give an overview of how the method predicts properties, we describe in general the calculations of indices, molar volume (V) and density (ρ) for polyisoprene at 298.15 K

6.2.2 Modelling size selection

An important factor to consider when modelling is the number of atoms because there is a compromise with computational time. For this reason, it was necessary to identify a minimum number of atoms for each material or degree of polymerisation (DP) that could predict representative and consistent properties. As a reference, the ENR50 had a weight average molar mass (Mw) of 700,000 g/mol [10] [11], about 124,000 atoms or to compare with the other materials a degree of DP of 9,200. An equivalent precursor of ENR50 would be NR with the same DP of 9,200 but with different Mw of 627,000 g/mol and number of atoms = 120,000.

The topology method was used to predict mechanical properties of the polymers at discrete temperatures to choose the least but representative DP. In Figure 6.1, we observed that above a DP of 123, mechanical properties such as bulk and tensile modulus were similar and representative of those at higher DP; for the sake of having an even DP fraction, a DP of 128 was chosen for all the materials. This reduced the computational time by about 72 times.

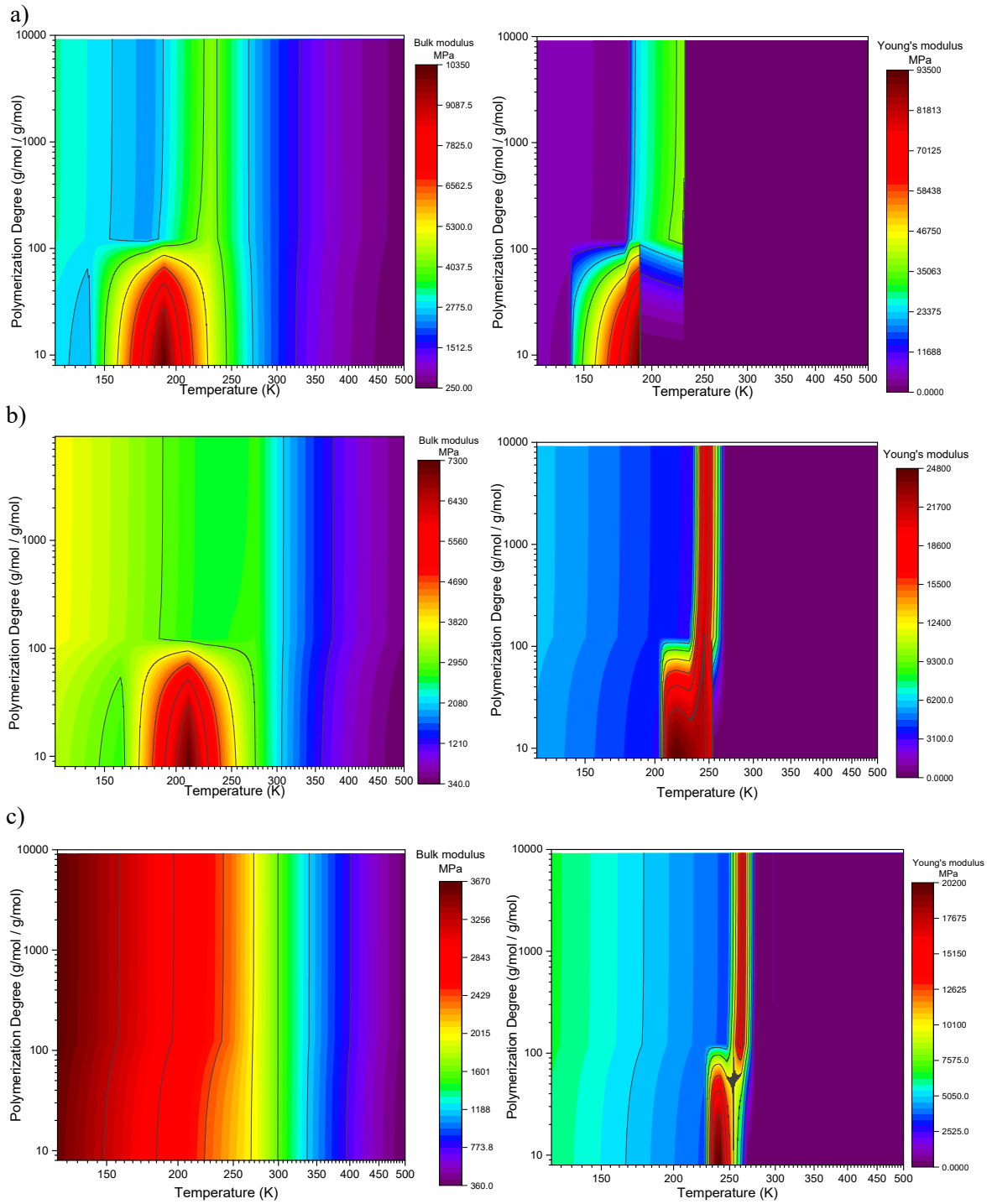

Figure 6.1. Mechanical properties predicted by the group contribution method, a) NR, b) ENR50 and c) ENR50 reacted with 50 phr of POS

6.2.3 Geometry optimisation of repeating units and molecules

All the repeat units (mer) of polyisoprene, EN50, hybrids (EN50Chem and NRChem) and POS (aminopropylisobutyl-POS) were geometrically optimised prior to any further steps using the COMPASSII forcefield [12] with atom-based charges (electrostatic and Van der Waals) using a smart algorithm (a cascade algorithm of steepest descent, adjusted basis set, Newton-Raphson [ABNR] and

quasi-Newton [Broyden-Fletcher-Goldfarb-Shanno]) until convergence was achieved for thresholds of 0.00002 kcal mol^{-1}, 0.001 kcal·mol^{-1}·$Å^{-1}$, 0.001 GPa and 0.00001 Å that are reasonable for energy, force, stress and displacement.

6.2.4 Polymers and amorphous cell constructions

Using BIOVIA Material Studio (Dassault Systèmes) a series of 18 linear polymers were constructed with DP = 128, shown in Table 6.1, and they are the number of random concatenated atactic mers and molecules used to construct amorphous cells (AC) for each polymer, hybrid and nanocomposite. The polyisoprene mers consist of random atactic 1,4-cis-polyisoprene isomer; the ENR50Chem materials have aminopropylisobutyl-POS molecules attached randomly via the epoxy groups; in NRChem the aminopropylisobutyl-POS molecules were attached randomly via epoxy groups.

Ten amorphous cells were generated for each material and the cell with the lowest energy after 500 steps of geometric optimisation was selected. All the amorphous cells were constructed with periodic boundary conditions (PBC) in all three-orthogonal directions of a cubic lattice, using COMPASSII forcefield, Ewald electrostatic charge, atom-based Van der Waals forces, checking for ring spearing, avoiding close contacts smaller than 0.25 Å, an initial density of 1 g/cm^3, a composition of one polymer chain and for the physical composite series, an additional number of aminopropylisobutyl-POS molecules.

Table 6.1 Structure and composition of the materials and code names

Polymeric structure schematic	Codename	n	m	q	r
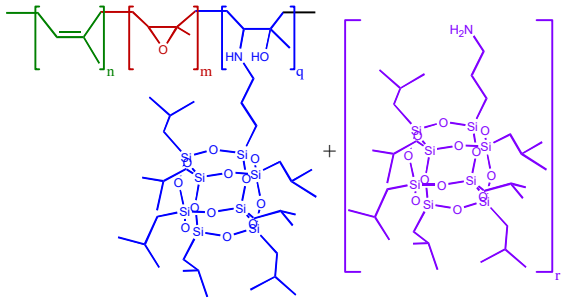	NR	128	0	0	0
	NRChem01	127	0	1	0
	NRChem03	125	0	3	0
	NRChem06	122	0	6	0
	NRChem11	117	0	11	0
	NRPhy01	128	0	0	1
	NRPhy03	128	0	0	3
	NRPhy06	128	0	0	6
	NRPhy11	128	0	0	11
	ENR50	64	64	0	0
	ENR50Chem01	64	63	1	0
	ENR50Chem03	64	61	3	0
	ENR50Chem06	64	58	6	0
	ENR50Chem11	64	53	11	0
	ENR50Phy01	64	64	0	1
	ENR50Phy03	64	64	0	3
	ENR50Phy06	64	64	0	6
	ENR50Phy11	64	64	0	11

6.2.5 Relaxation of the amorphous cells

6.2.5.1 After cell construction.

The cells were geometrically optimised in two steps; the first was using the Universal forcefield with a pre-set quality of ultra-fine. The second method was using the COMPASSII forcefield with a quality set to fine. Both steps were calculated using a quasi-Newton algorithm until convergence, an Ewald method for electrostatic interactions, an atom-based method for Van der Waals interactions and an external pressure of 0.1 MPa (approximately 1 atm).

6.2.5.2 Dynamics.

After the geometrical optimisation two dynamics were performed using COMPASII forcefield with a pre-set quality of fine, an Ewald method for electrostatic interactions and an atom-based method for Van der Waals interactions.

6.2.5.3 The first molecular dynamics.

It was run with a Nosé–Hoover thermostat to maintain constant temperature (Q ratio: 0.01) of 298 K and a Berendsen barostat to maintain a constant pressure at 0.1 MPa with a decay constant of 0.1 ps was performed for 200 ps with a time step or 1.0 fs and recording 1001 equidistant frames.

6.2.5.4 The second molecular dynamics.

It was run with fixed volume using a Berendsen thermostat to maintain a constant temperature of 298 K with a decay constant of 0.1 ps and it was performed for 200 ps with a time step or 1.0 fs and a recording frame of 200 steps.

6.2.5.5 Final geometrical optimisation.

Before calculation of the mechanical properties, another two steps of geometrical optimisation, as described in 6.2.5.1, were performed on the last ten frames of the second molecular dynamics (6.2.5.4).

6.2.6 Mechanical Properties Calculation

The mechanical properties were calculated in the ten geometrically optimised frames described in 6.2.5.5 using a constant strain method, in four steps for each strain, with a maximum strain amplitude of 0.003, using COMPASII forcefield with a pre-set quality of fine, Ewald method for electrostatic interactions and an atom based method for Van der Waals interactions.

6.2.7 Estimation of the glass transition temperature and melting temperature

6.2.7.1 Density estimation.

It was necessary to estimate the density of each material at increasing temperatures to calculate the transition temperatures. The last frame of the final geometrical optimisation was used (6.2.5.5) to perform an extra dynamic process as described in 6.2.5.3 (NPT), but for 100 ps at each specific temperature. The densities were estimated at least for 12 different temperatures between 100 K and 400 K. All densities used to calculate the transitions were estimated as the density at infinity relaxation time by fitting an empirical asymptotic model between 5 and 100 ps of the NPT dynamics as shown in Figure 6.4 a and in the equation (60).

$$\lim_{t\to+\infty}\left(\frac{C_1 t}{C_2 t + C_3}\right) = \rho_\infty = \frac{C_1}{C_2} \qquad (51)$$

Extended simulation for some representative materials were run to corroborate the feasibility of the method. Very similar results at 1000 ps were obtained to those obtained at 100 ps. As example the NRPhy01 presented in the Figure 6.4, the density has an initial student change followed by a distribution of densities. This distribution have an average standard deviation of 0.005 [g/cm^3] benign no more than

0.0065 [g/cm^3] if it is compare the predicted density at infinite relaxation time (ρ_∞) using the asymptotic model within the first 100 ps of simulation (100 000 steps) It be can see how there is just a difference of 0.0005 [g/cm^3] respect to the last 200 ps of the extended simulation of 1000 ps (1 073 000 steps) which is statistically insignificant (if it is assume same standard deviation and sample size and a 95% of confidence).

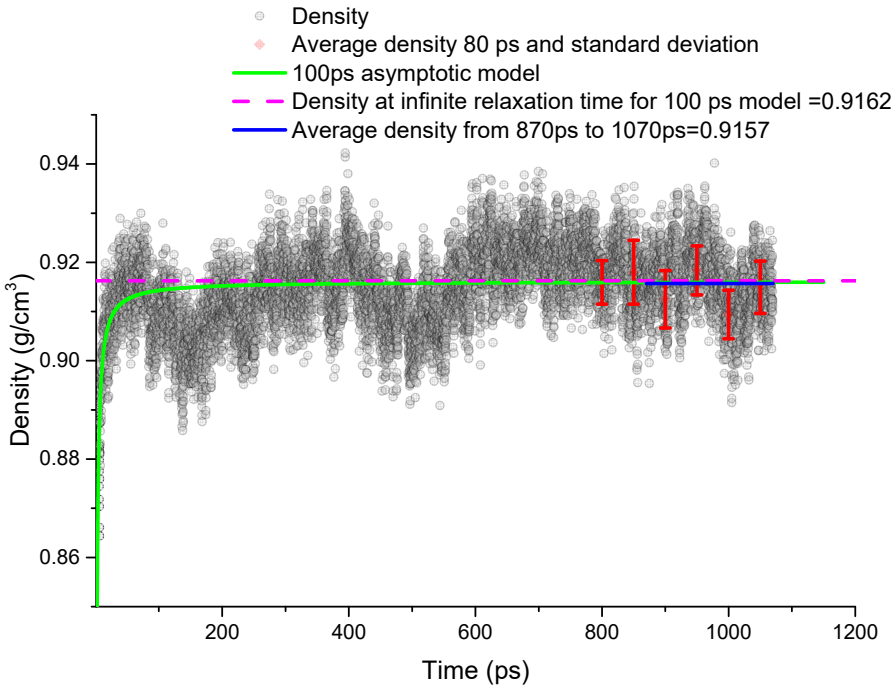

Figure 6.2 Extended simulation for the NRPhy01 density

In view of the later result it can be say that an asymptotic function can predict the density at longer relaxation times which can be use as computational savings. It is possible to think that the model gives fairly accurate predictions because it takes more in consideration the initial changes in the density than the later changes as can be observed in more detail in the Figure 6.3 using a logarithmic (base 10) time scale instead of a linear one.

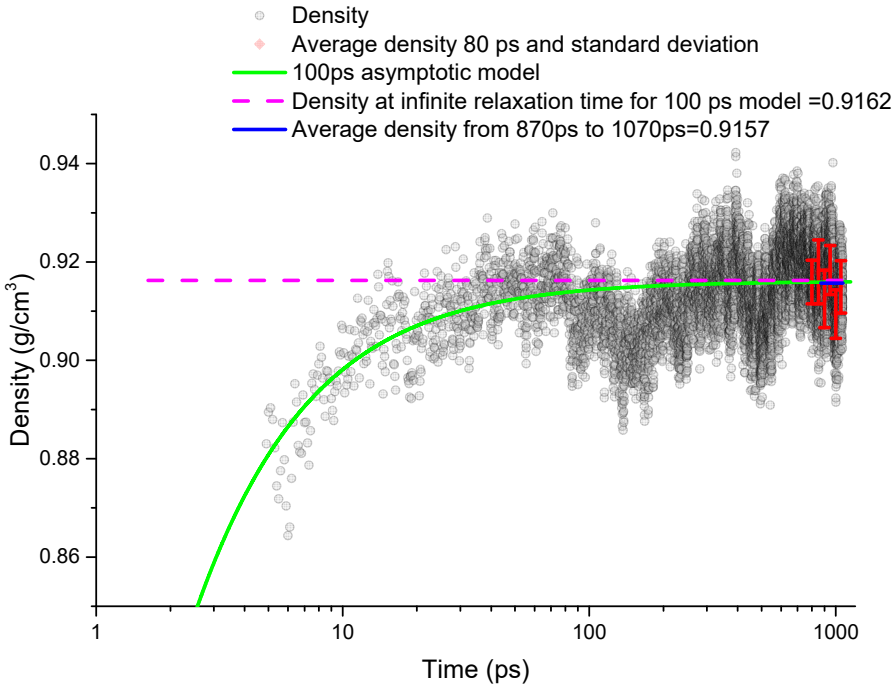

Figure 6.3 Extended simulation for the NRPhy01 (time scale in log_{10})

6.2.7.2 Transition calculation.

The transitions were calculated from the intersection of two quadratic equations fitted in the vicinity of the transitions as shown Figure 6.4 b.

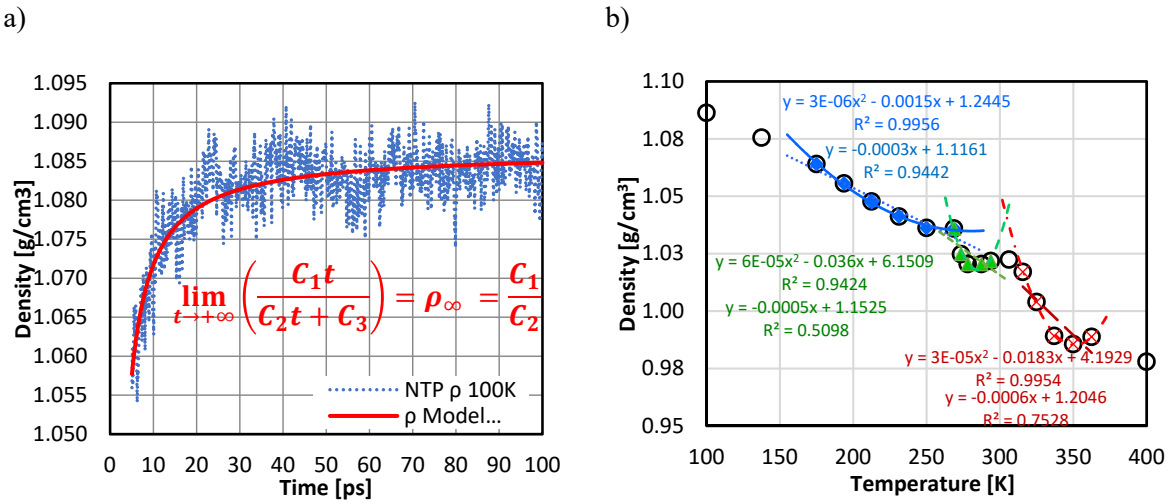

Figure 6.4. Estimation of T_g, a) single temperature ρ_∞ calculation using the frames dynamic relaxation fitting an asymptotic function, b) estimation of T_g by solving the intersection of two fitting functions

I believe that the authors normally use linear correlation to simplify the task to find the T_g when the intervals searching for the T_g are small but if it is use linear fitting in the Figure 6.4 b it would be over-simplified given that the intervals are around hundreds of Kelvins and it was possible to use less data

to get similar T_g to the reported. Furthermore, if density varies with temperature for smaller molecules, we will find that this relation it is not linear.

Using the definition of density (equation (52)) and some basic equations

$$\rho = \frac{Mass}{Volumen} = \frac{M}{V} \tag{52}$$

Let's consider equation (53) a change in volume dV

$$dV = Final\ volume - Initial\ volume = V_F - V_0 \tag{53}$$

If this change of volume is due a change in the temperature it can be expressed as equation (54) in terms of its volumetric thermal coefficient of expansion

$$dV = V_0\ \alpha_v\ (T_F - T_0) \tag{54}$$

Substituting the last two equations (53) and (54) it is possible to have equation (55):

$$V_F - V_0 = V_0\ \alpha_v\ (T_F - T_0) \tag{55}$$

Keeping V_F just in one side one can write equation (56).

$$V_F = V_0\ \alpha_v\ (T_F - T_0) + V_0 \tag{56}$$

Equation (56) can be rearranged as (57) taking the common term V_0 out of the bracket.

$$V_F = V_0\ [1 + \alpha_v\ (T_F - T_0)] \tag{57}$$

Dividing in both sides of equation (57) by mass and applying the mass conservation law ($M = M_0 = M_F$) the equation (58) is derived.

$$\frac{M}{V_F} = \frac{M}{V_0} \frac{1}{[1 + \alpha_v (T_F - T_0)]} \tag{58}$$

Using the definition of density, it is found

$$\rho_F = \frac{\rho_0}{1 + \alpha_v (T_F - T_0)} \tag{59}$$

Is possible to observe that this relation is non-linear and if for example if a polymer with a "initial" density of 0.98 g/cm^3 at 298.15 K with a volumetric thermal coefficient of expansion equals to 0.0004

[K^{-1}] it is possible to plot a density-temperature diagram (Figure 6.5) to find that a linear equation will have R^2=0.9959 but a quadratic fitting correlates perfect to the same data (R^2=1.00000).

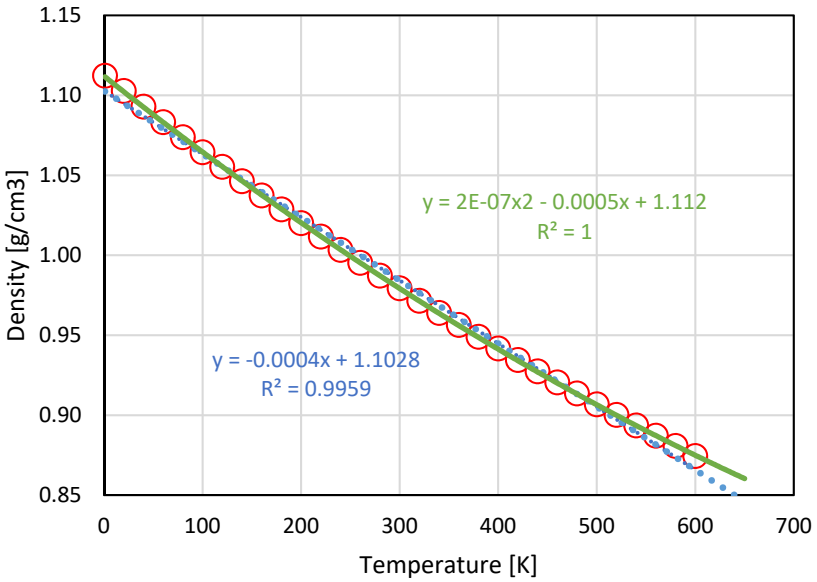

Figure 6.5 Linear and quadratic curve fitting of a diagram density vs Temperature for a exemplified material

Finally, same trend was observed in correlations of density predicted by topology method before and after the T_g, as presented in Figure 6.6.

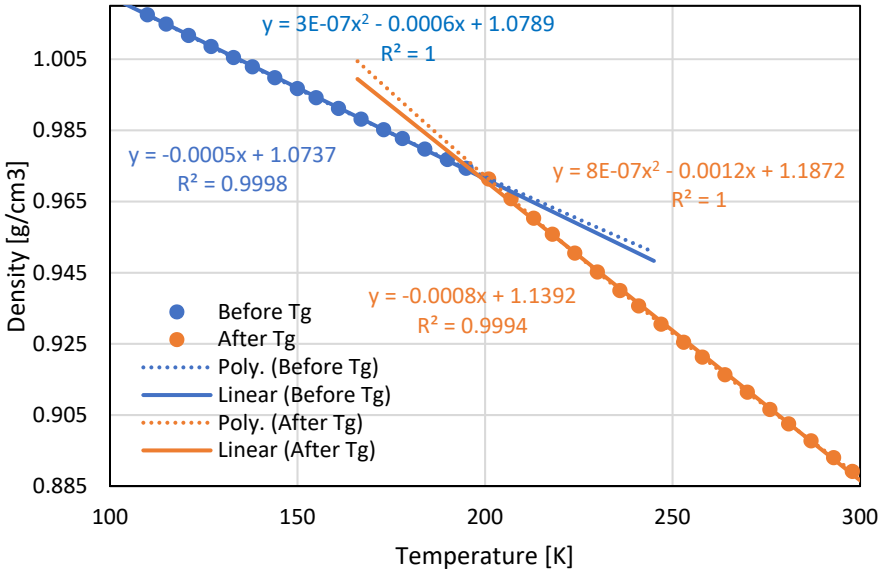

Figure 6.6 Linear and quadratic fitting comparation to determine a thermal transition in a diagram density vs temperature for natural rubber predicted by Synthia

6.2.8 Estimation of the Coefficient of Thermal Expansion

By definition, α_v is the reciprocal of the volume multiplied by the volume change with temperature at constant pressure (equation (60))

$$\alpha_V = \frac{1}{V}\left(\frac{\partial V}{\partial T}\right)_P \qquad (60)$$

The volumes were calculated at incremented temperatures using the density at infinite relaxation time and the mass of the cell. The volumes with respect to temperature were fitted with first and sixth order linear polynomial functions (Figure 6.7 a)), but only the results of the first-degree polynomial were reported because it more accurately represents the data at the edge of the initial and final evaluated temperature as Figure 6.7 b) shows. The derivatives of this functions were evaluated at each temperature and multiplied by the reciprocal volume at that temperature to obtain α_V (Figure 6.7 b).

a) b)

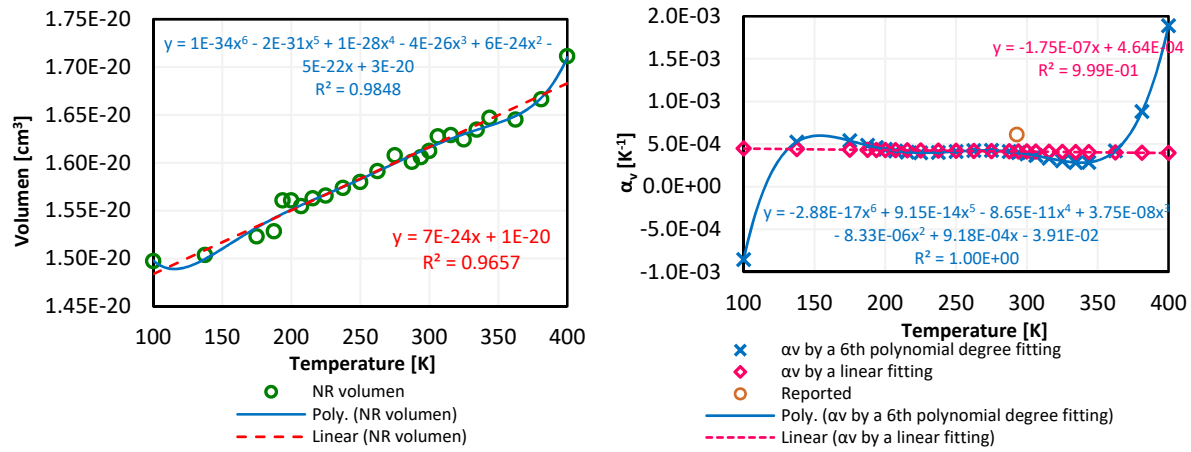

Figure 6.7 Change due temperature of a) calculated volumes for NR, b) α_v for NR

6.3 Results and Discussion

All T_g of the vinyl groups of ENR50 are higher than those of NR (Figure 6.8 a)), if the T_g is below the intended use temperature, a material can be considered of interest for manufacture. For this reason, lower T_g is preferred. Under this consideration, ENR50Chem06, ENR50Chem11 and ENR50Phy06 are considered to have T_g above 273.15 K and the series of NRChem had lower T_g. This increase is correlated with the increase of the free volume (Table 6.2), being proportional to the number or grafted POS attached to the polymeric chain.

Table 6.2 Complementary predicted properties from amorphous cell molecular dynamics

Material	POS Molecules	Average velocity of sound [km/s]	Lambda Lame constant [GPa]	Mu Lame constant [GPa]	Occupied volume [Å^3]	Free volume [Å^3]	Surface Area [Å^2]	Compressibility [1/TPa]
NR AC	0	1.374	1.685	1.020	13626.1	2277.7	3879.0	494.0
NRPhy01 AC	1	1.497	1.728	1.265	14586.9	2747.2	4530.2	401.4
NRPhy03 AC	3	1.414	1.536	1.181	16652.6	3202.0	5060.2	436.6
NRPhy06 AC	6	1.199	0.653	0.873	19837.9	4557.1	6846.8	690.0
NRPhy11 AC	11	1.331	1.210	1.139	25271.1	5119.2	7915.7	471.6
NRChem01 AC	1	1.587	1.841	1.438	14485.1	2909.8	5409.9	329.8
NRChem03 AC	3	1.500	0.999	1.420	16529.4	3801.9	6606.7	439.0
NRChem06 AC	6	1.488	1.271	1.403	19752.5	4477.6	7823.9	423.3
NRChem11 AC	11	2.315	2.824	3.419	24792.4	7278.1	10025.3	226.7
ENR50 AC	0	1.342	1.548	1.046	11683.4	5164.9	9103.3	476.7
ENR50Phy01 AC	1	1.310	1.856	0.969	12601.0	5363.6	9033.4	432.3
ENR50Phy03 AC	3	1.311	1.563	1.041	14401.7	6182.5	10910.9	484.1
ENR50Phy06 AC	6	1.209	1.651	0.843	17062.6	7548.3	12969.4	549.2
ENR50Phy11 AC	11	1.082	0.913	0.696	21397.5	12452.2	16774.2	976.6
ENR50Chem01 AC	1	1.218	0.844	0.979	12595.7	5370.3	9484.2	698.7
ENR50Chem03 AC	3	1.350	1.252	1.182	14381.3	5970.6	10681.4	454.9
ENR50Chem06 AC	6	1.281	1.202	1.074	17020.5	7323.8	12816.0	573.5
ENR50Chem11 AC	11	1.236	1.701	0.931	21431.5	9346.3	16008.6	471.2

A suitable parameter to evaluate the stiffness is the tensile or Young modulus (*E*) and because it has a direct association with the stress-strain relationship, it is an indication of toughness in the linear elastic region. The incorporation of POS decreased *E* for ENR50 series. In the case of the NRChem series, most *E* did not change above 5 %, but the NRChem11 had significant increments of about 200 %; in the case of the NRPhy series at the lowest POS concentration (NRPhy01) had a higher *E* than its chemical counterpart (NRChem01) but the rest for the series were below the NRPhy series (Figure 6.8 b).

The bulk modulus (*B*) indicates the resistance of the material to compression, in this context It is found that the NR series was more resistant than the ENR50 series because most of them had a higher *B* (except for NRPhy06 and ENRPhy11, see Figure 6.8 c). Only the physical mixture at the lowest concentration of POS increased *B* above 10 % for the ENR50 series. In the case of the NR series, there is a non-monotonical increase of *B*, having a remarkable 50 % increase at the lowest POS concentration and a 110 % increase at the highest POS concentration.

The shear modulus (*G*) is analogous to *E* or *B* but calculated over a “cut-off” stress and for this reason, an increase of *G* is desirable. The NR series, in general, have greater *G* than the precursor (NR), and this increase is more evident in the chemical hybrids than the physical mixtures, especially at the

greatest concentration where it increased more than 200 %. On the contrary, almost all ENR50 materials had *G* decreased compared with the precursor ENR50 (Figure 6.8 d).

The Poisson ratio (ν) is a measure of material lateral expansion or contraction due to elongation, a lower value means less deformation under the same stress and hence a lower value is preferred. Addition of POS, either physical or chemical increased or did not change significantly (change below 5 %) ν, except for the highest physical POS concentration (Figure 6.8 e).

The volumetric thermal expansion (α_v) is an important parameter for the design and manufacture of large products or where materials are sensitive to small changes of dimension with temperature. Under this premise, it is desirable to keep α_v as low as possible to maintain dimensional stability during fabrication, for most of the ENR50 series addition of POS decreased α_v but it is found a compromise between POS concentration and α_v for the NR series (Figure 6.8 f).

All ENR50 materials have greater density than the NR series, and density increased proportional to the number of POS, from a manufacturing consideration it is desirable to have a lower density to produce more items with the same mass. Therefore, similar products with lower density and the same mechanical properties are preferred. For these reasons, the NR series materials are more desirable than the ENR50 series (Figure 6.8 g).

Epoxidation of NR increased properties, such as half-decomposition temperature, oil resistance[13] and decreased oxygen, carbon dioxide and nitrogen permeability (Table 6.3).

Table 6.3 Complementary predicted properties from the topological method

Material	POS Molecules	Secondary relaxation temperature [K]	Temperature of half decomposition [K]	Permeability of O_2 [(cm^3 mm)/(m^2 day atm)]	Permeability of N_2 [(cm^3 mm)/(m^2 day atm)]	Permeability of CO_2 [(cm^3 mm)/(m^2 day atm)]
NR Synthia	0	115.3	658.8	1044.5	336.6	6146.6
NRChem01 Synthia	1	121.9	663.4	988.0	316.9	5785.1
NRChem03 Synthia	3	135.2	670.4	904.2	288.0	5252.6
NRChem06 Synthia	6	153.2	677.5	821.9	259.8	4733.8
NRChem11 Synthia	11	180.8	684.8	741.3	232.4	4230.8
ENR50 Synthia	0	140.0	660.9	419.4	125.6	2275.0
ENR50Chem01 Synthia	1	143.5	664.8	427.3	128.1	2321.6
ENR50Chem03 Synthia	3	152.2	671.0	432.8	129.9	2395.5
ENR50Chem06 Synthia	6	164.7	677.6	453.1	136.5	2474.5
ENR50Chem11 Synthia	11	185.7	684.5	467.2	141.1	2558.6

In the context of the above results, at the lowest concentration of POS in ENR50, it is concluded that the use of a physical mixture is preferred over a chemical hybrid because it gives more desirable characteristics (or the same for the same ρ). At the highest POS concentration, the hybrid materials performed better than the composites, but in most cases when compared with the ENR50 alone, hybrids were less convenient.

For the NR series, at the highest concentration of POS, it was found that chemical hybrids performed better than physical mixtures; the same applied to the lowest POS concentration excluding ν and α_v.

Results from the topology method gave a monotonical increase or decrease of the evaluated property by increments of POS concentration with the only exception being the ENR50Chem Synthia series with a minimum global concentration of 6 POS molecules. While this difference was small (5 % with respect to 11 POS molecules), it is explained by increments in the tensile and shear modulus since they correlated as $2G(1+\nu)=E=3B(1-2\nu)$. These results suggest that at these concentrations of POS the topology method did not produce adequate results (Figure 6.8) just for this case.

6.3.1 Comparison of reported properties, amorphous cells and the group contribution method

Figure 6.8 h suggests AC results in a better match of the reported natural rubber properties in 4 out of the 7 evaluated properties. It is pertinent to note that the AC calculation takes significantly more time to predict properties, but it has an advantage over the group contribution method in predicting physical mixture properties.

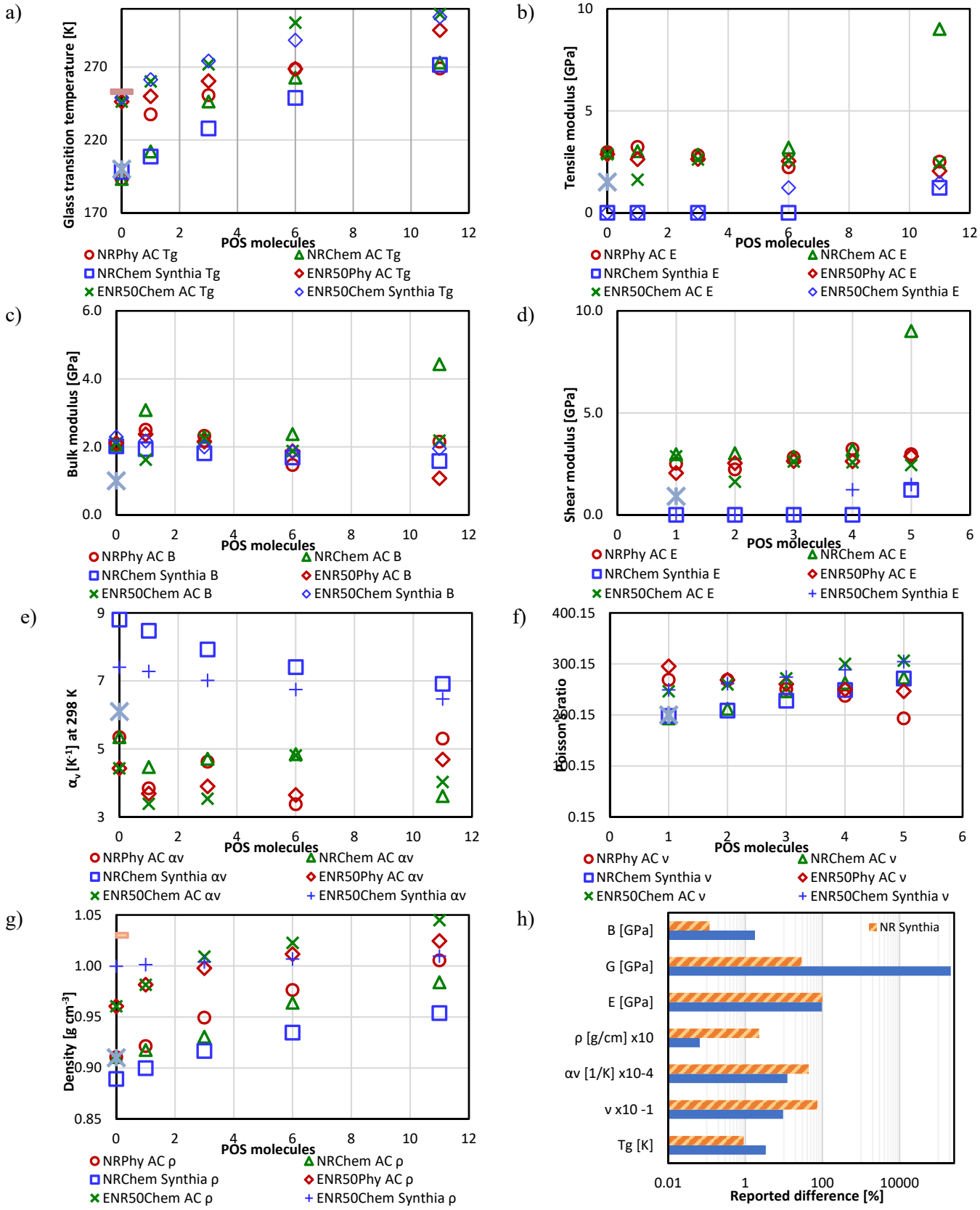

Figure 6.8 a) to g) Topology method and amorphous cell calculated properties, h) difference of the properties with respect to the reported properties; all reported B, E, ρ, T_g, αv, v and G for NR are found at [14-16]; the reported ENR50 ρ, T_g are found at [17-19]

6.3.2 T_g comparison of amorphous cell and group contribution method

As for many temperature dependent transitions, T_g occurs over a temperature range, using the density of the topology method shows a single T_g, but all other properties exhibit an interval (Figure 6.9); the density of the amorphous cell shows an interval for T_g as well as other transitions, which indicate realistic modelling. It was found that a second-degree polynomial better described the density between thermo-mechanical transitions than a linear correlation (Figure 6.4 b).

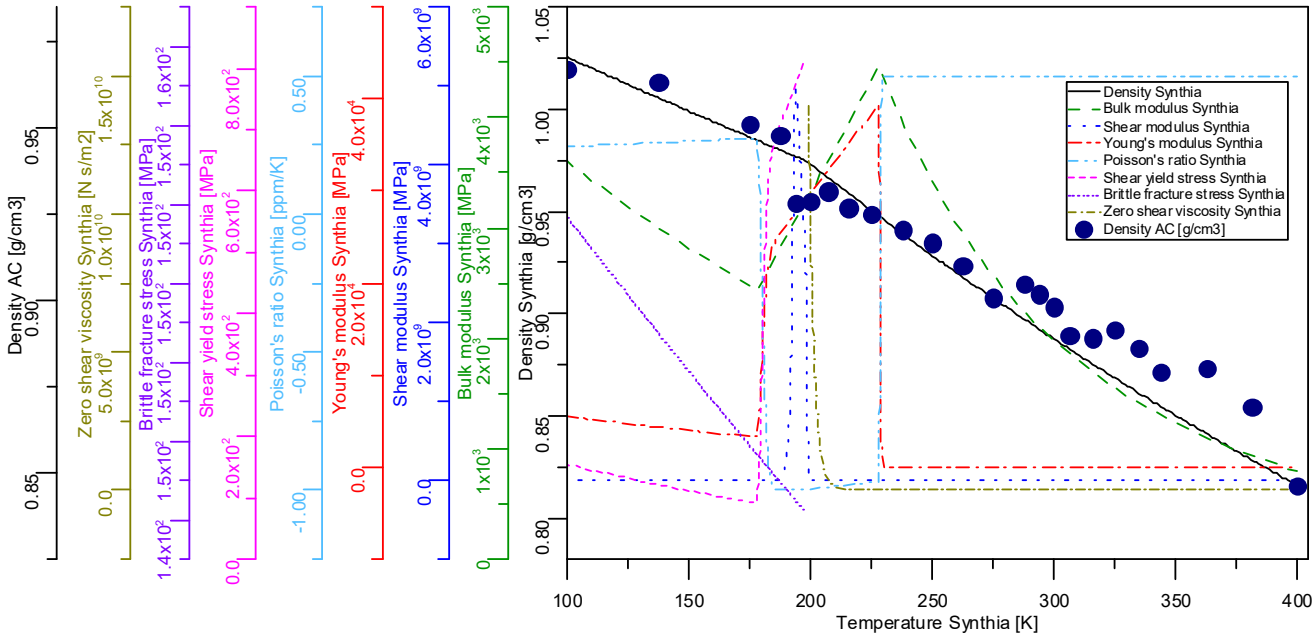

Figure 6.9. NR temperature dependency of some topology method properties and density from AC

6.4 Conclusions

Pre-calculations to determine a minimum polymerisation degree were used to predict equivalent thermo-mechanical properties to the realistic scale experimental system were proven to agree with most mechanical properties by comparing our results with those reported in the literature. It was found that the AC dynamics method matched closer most of the reported properties compared with the topology method for NR. These pre-calculations were of great advantage in allowing reduction of computational time/cost. Another way to reduce computational cost was the use of an asymptotic function to calculate density at infinite relaxation time.

Diagrams of density versus temperature were used to calculate the glass transition temperatures and other thermal transitions. It was found that second-degree polynomials better described the density

between thermo-mechanical transitions rather than a linear correlation, being the correlation most used in the literature [14, 20-24], the latter is true for the topology method where the correlation coefficient (R^2) was equal to 1.000.

While most of the changes were desirable, it was found a compromise with mechanical properties, density and glass transition temperature. Although it was necessary to epoxidize NR to graft chemically with POS (hybrid formation), the epoxidation degree was preferred to be low.

It can be stay that when choosing between nano-composites and hybrids for natural rubber, hybrids are preferred because they have more desirable properties than the nano-composites. In the case of ENR50, consideration must be taken before choosing between hybrids or nano-composites; for instance, hybrids are preferred over nano-composites at high concentration of POS, but the glass transition temperatures were above standard temperature-pressure conditions (STP). At the lowest POS concentration, ENR50-nanocomposites are preferred over hybrids, but the addition of POS decreased most of the mechanical properties.

6.5 References

1. Zhao, G., et al., *Synergistic effect of nanobarite and carbon black fillers in natural rubber matrix.* Materials & Design, 2012. **35**: p. 847-853.
2. Pothen, L., C.H. Chan, and S. Thomas, *Natural Rubber Materials, Volume 2-Composites and Nanocomposites*. 2013: Royal Society of Chemistry.
3. Kodal, M. and G. Ozkoc, *Micro and Nanofillers in Rubbers*. 2013 ed, ed. P.M. Visakh, A.K. Chandra, and A.P. Mathew. Vol. 11. 2013, Berlin, Heidelberg: Berlin, Heidelberg: Springer Berlin Heidelberg. 303-356.
4. Strankowski, M., *Nonlinear viscoelasticity in Three Dimensional filler reinforced rubber composites and nanocomposites*, in *Non-Linear Viscoelasticity of Rubber Composites and Nanocomposites*. 2014, Springer. p. 59-83.
5. Stephen, R. and S. Thomas, *Nanocomposites: state of the art, new challenges and opportunities.* Rubber Nanocomposites: Preparation, Properties, and Applications, S. Thomas and R. Stephen Eds., John Wiley & Sons, singapore, 2010: p. 1.
6. Lin, Q., et al., *The grafting reaction of epoxidized natural rubber with carboxyl ionic liquids and the ionic conductivity of solid electrolyte composites.* RSC Advances, 2015. **5**(109): p. 90031-90040.
7. Wu, C., *Multiscale Modeling Scheme for Simulating Polymeric Melts: Application to Poly (Ethylene Oxide).* Macromolecular Theory and Simulations, 2018. **27**(1): p. 1700066.
8. Balazs, A.C., T. Emrick, and T.P. Russell, *Nanoparticle polymer composites: where two small worlds meet.* Science, 2006. **314**(5802): p. 1107-1110.
9. Lloyd, D., *Additives in rubber processing.* Materials & Design, 1991. **12**(3): p. 139-146.
10. Chan, C. and H. Kammer, *Properties of solid solutions of poly (ethylene oxide)/epoxidized natural rubber blends and LiClO4.* Journal of applied polymer science, 2008. **110**(1): p. 424-432.

11. Chan, C.H. and H.-W. Kammer, *Polymer electrolytes—relaxation and transport properties.* Ionics, 2015. **21**(4): p. 927-934.
12. Sun, H., et al., *COMPASS II: extended coverage for polymer and drug-like molecule databases.* Journal of molecular modeling, 2016. **22**(2): p. 1-10.
13. Johnson, T. and S. Thomas, *Effect of epoxidation on the transport behaviour and mechanical properties of natural rubber.* Polymer, 2000. **41**(20): p. 7511-7522.
14. Sharma, P., S. Roy, and H.A. Karimi-Varzaneh, *Validation of Force Fields of Rubber through Glass-Transition Temperature Calculation by Microsecond Atomic-Scale Molecular Dynamics Simulation.* The Journal of Physical Chemistry B, 2016. **120**(7): p. 1367-1379.
15. Afifi, H. and A. El-Wakil, *Study of the effect of natural rubber-graft-maleic anhydride (NR-g-MA) on the compatibility of NR-NBR blends using the ultrasonic technique.* Polymer-Plastics Technology and Engineering, 2008. **47**(10): p. 1032-1039.
16. Yoon, J.H., et al., *Investigation on variable shear modulus of magnetorheological elastomer based on natural rubber due to change of fabrication design.* Polymer Engineering & Science, 2013. **53**(5): p. 992-1000.
17. Ellis, B. and R. Smith, *Polymers: a property database*. 2008: CRC Press.
18. Wanchart, P., *Bonding of natural rubber and epoxidized natural rubber to poly (ethylene terephthalate)*, in *Department of Polymer Science*. 2000, University of Akron: Ohio, USA. p. 180.
19. Ang, D.T.C., Y.K. Khong, and S.N. Gan, *Novel approach to enhance film properties of environmentally friendly UV-curable alkyd coating using epoxidised natural rubber.* Progress in Organic Coatings, 2013. **76**(4): p. 705-711.
20. Sul, J.-H., B.G. Prusty, and D.W. Kelly, *Application of molecular dynamics to evaluate the design performance of low aspect ratio carbon nanotubes in fibre reinforced polymer resin.* Composites Part A: Applied Science and Manufacturing, 2014. **65**: p. 64-72.
21. Soldera, A. and N. Metatla, *Glass transition phenomena observed in stereoregular PMMAs using molecular modeling.* Composites Part A: Applied Science and Manufacturing, 2005. **36**(4): p. 521-530.
22. Patrone, P.N., et al., *Uncertainty quantification in molecular dynamics studies of the glass transition temperature.* Polymer, 2016. **87**: p. 246-259.
23. Sarangapani, R., S.T. Reddy, and A.K. Sikder, *Molecular dynamics simulations to calculate glass transition temperature and elastic constants of novel polyethers.* Journal of Molecular Graphics and Modelling, 2015. **57**: p. 114-121.
24. Chantawansri, T.L., I.-C. Yeh, and A.J. Hsieh, *Investigating the glass transition temperature at the atom-level in select model polyamides: A molecular dynamics study.* Polymer, 2015. **81**: p. 50-61.

7 SYNTHESIS AND CHARACTERIZATION OF POS-ENR50 HYBRID

7.1 Introduction

Nanofillers are playing an increasingly important role in rubber industry as the performance of classical fillers is inferior to that of nano scale. As mention in 1.1 one of the reasons for their superior performance is large specific surface area which facilitates their incorporation. The most popular way to incorporate nanofillers into NR or ENR is through physical mixing (emulsion, melt, solution or latex) [1], Incorporation of nanofillers through physical mixing is simple but it can lead to problems such as agglomeration, precipitation or unstable dispersion. In some cases, these problems can be avoided or minimised by using additives such as surfactants and thickeners or simply using more intense agitation. Another way of incorporate nanofillers is trough chemical reactions. However, this method is avoided because both NR and filler have to be chemically modified prior to enable them to react. Sometimes these modifications are complex involving several steps coupled with well-defined reactions and purifications. The yield of these reactions is also low which makes it hard to scale up. The application of POS as nanofillers can avoid above problems as they are chemically versatile, have specific sites of reactions, have discreet molecular mass and can be easily modified to facilitate their reaction with ENR even *in-situ*.

Since ENR is commercially available and POS can be readily customized, a “click reaction” can be designed between these two. The hypothesized click reaction is a nucleophilic ring opening reaction of epoxy ring with the amino group in the ENR.

The concept of click reaction was introduced by Kolb, Finn and Sharpless [2] they were inspired in discreet reactions between heteroatoms links (C-X-C) and other small molecular units which result in to substances that occurs in nature. According to these authors a click reaction has the follow characteristics, modular, high yield, wide scope, do not generate “offensive” by-products, solvents or by-products can be separate without the need of chromatographic methods, have simple reaction conditions (are not too sensitive to water and oxygen) and lastly be stereospecific (not necessarily enantioselective).

This concept of click reaction has moved from this philosophy inspired by nature but applicable to limited set of organic reactions that produce conjugate molecules to any type of generic reactions that are modular, selective, efficient, produce single product which does not require chromatographic purification [3].

As mention in 2.4.2, there are many books about elastomers and fillers marking as a possible and promising the use of POS into NR [4-7], but never the less there are few related peer review works, for this reason our objective is to make a grafting reaction with a designed polyhedral oligomeric silsesquioxane and ENR evaluating if it is possible to called it a click reaction.

7.2 Materials and Methods

7.2.1 Materials

The natural rubber used was STR5L (Standard Thai Rubber 5L) obtained from Srijareon Rubber Co. Ltd (Thailand). The liquid natural rubber was a cis-polyisoprene, made from natural rubber and was purchased from Sigma-Aldrich Co. LLC. (Australia). The ENR50 was obtained from the Malaysian Rubber Board (Malaysian). 1-(3-amino) propyl-3,5,7,9,11,13,15- isobutylpentacyclo [9.5.1.1.^{3,9}.1^{5,15}.1^{7,13}] octasiloxane (NH_2-POS) was purchased from Hybrid Plastics Inc. (USA).

7.2.2 Synthesis and characterisation of NR, ENR50 and ENR50 hybrid

7.2.2.1 Synthesis of hybrid (ENR50 + NH_2-POS)

The schematic diagram of the proposed synthesis is shown in Figure 7.1. Equal parts in of ENR50 and 1-(3-amino) propyl-3,5,7,9,11,13,15- isobutyl pentacyclic [9.5.1.13,9.15,15.17,13] octasiloxane (NH_2-POS) were dissolved into oxolane (THF) and heated on reflux at 313 K for 24 h. Later the polymer was precipitated using ethanol (analytical reagent grade) and dried under vacuum at 313 K for 24 h. the yield of reaction product (POS-ENR50 hybrid) was at least 85 % mass basis.

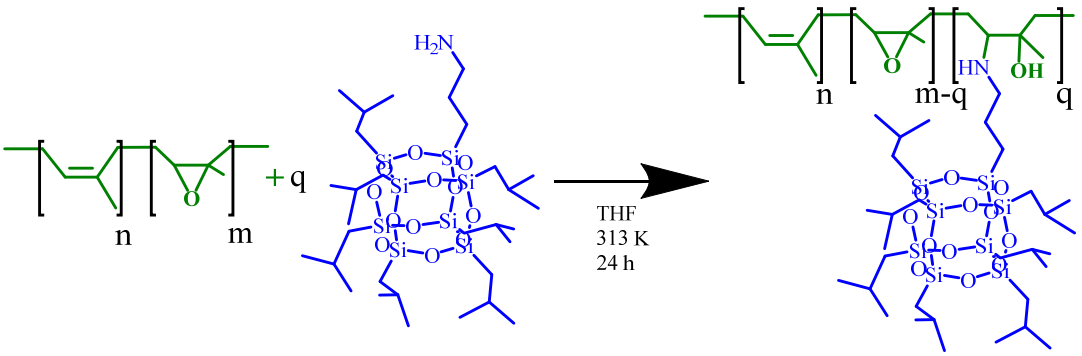

Figure 7.1 Reaction between ENR50 and NH_2POS to produce the hybrid

7.2.2.2 Identification of functional and reactive groups

A PerkinElmer Spectrum 100 spectrophotometer with a universal diamond attenuated reflectance (ATR) was used to acquire Fourier transform infrared (FTIR) spectra of the synthesised materials and their precursors. Ten scans were performed at a wavenumber from 4000 cm^{-1} to 650 cm^{-1} with a resolution of 4 cm^{-1}.

7.2.2.3 Determination of thermal behaviour by differential scanning calorimetry

A differential scanning calorimeter (DSC) (Mettler Toledo DSC 1) with liquid nitrogen cooling unit was used to determine the thermal transition. Temperature sweep pre-treatments were performed first from room temperature to 333 K and then to 173 K at a rate of 10 K/min before each scan to remove pre-existing thermal history. The reported scans were performed at 10 K/min from 174 K to 424 K.

7.2.2.4 Determination of thermo-mechanical behaviour by dynamic mechanical analysis

A Perkin Elmer Diamond dynamic mechanical analyser (DMA) with liquid nitrogen cooling unit was used. A temperature-frequency sweep pre-treatment was carried out before each scan to remove any pre-existing thermo-mechanical history. Scans were performed with synthetic multi-frequency (0.5, 1, 2, 5, 10 Hz) in compression mode, where all frequencies were applied simultaneously and Fourier transform was resolved by the instrument software. Pre-treatments were performed at a rate of 20 K/min from room temperature to 213 K and then to 353 K followed by cooling to approximately 115 K. The tests were carried out from 120 K to 495 K at a rate of 5 K/min and the tan(δ) at 10 Hz frequency are reported because the thermal transitions are more clearly observed at this frequency.

7.2.3 Epoxidation of natural rubber

The chemical transformation of double bounds into epoxy ring is normally a simple reaction that can be carried out at room temperature using chloroform as the solvent (Figure 7.2). It was intended, in the early stage, to epoxidate the natural rubber; however, as commercial ENR with 50% molar epoxidation was available, it was decided to utilize it to achieve more consistent results.

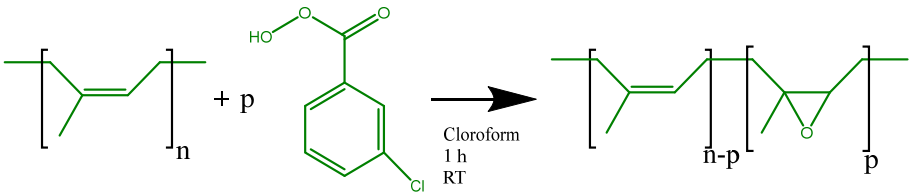

Figure 7.2 Chemical reaction between NR and 3-chlorobenzene-1-carboperoxoic acid yielding ENR

7.3 Results and Discussion

7.3.1 Confirmation of reaction through FTIR

FTIR spectra were used to confirm the reaction between ENR50 and the NH_2-POS. Many peaks of interest are transposed or difficult to read (Figure 7.3), firstly due the nature of the materials having similar signals for their functional groups and second because it is a partial reaction by design where the NH_2-POS is the limiting reagent. Never the less, the most important peaks that can be used to follow the reaction are the characteristic absorption peak of C–O–C stretching from the epoxy ring at 873 cm^{-1} and the produced pendant hydroxyl at 3300 cm^{-1} [8]. When the FTIR spectra of ENR50 (on of the precursors) and the hybrid (product) are compared (Figure 7.3), It can be observed that the signal at 873cm^{-1} decreased and the signal at 3300 cm^{-1} increased. This is a definitive indication that a ring opening mono-substitution reaction of the epoxy group with the amino group of the POS had taken place.

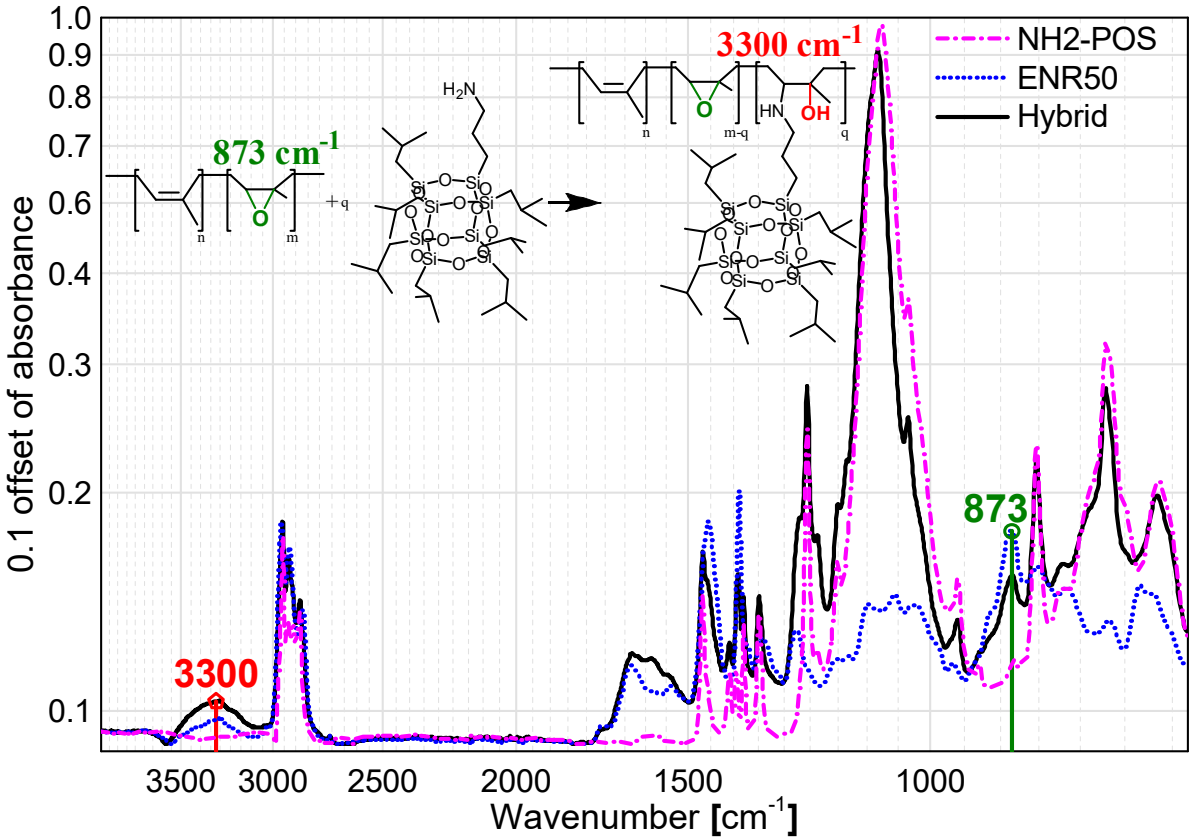

Figure 7.3. Fourier transform infrared (FTIR) spectra of precursors (NH_2-POS and ENR50) and hybrid (product)

7.3.2 Thermal transitions estimated by DSC

Figure 7.4 shows that the liquid NR and solid Standard Thai Rubber L5 (STRL5) polymer have almost identical thermal behaviour. NH_2-POS show a very characteristic sharp melting temperature at 326 K.

As expected, the hybrid formed between the ENR50 and the NH_2-POS inherited some of their thermal characteristics (T_g and T_m) from their precursors with smaller magnitude and slight shifts. This conservation of transitions, together with the fact that after the reaction the produced polymer was precipitated while NH_2-POS is still soluble in THF give us further evidence to conclude that the reaction between ENR50 and NH_2-POS had indeed taken place.

All the samples were thermally pre-treated in order to remove as much as possible pre-existing thermal history acquired by the materials during the manufacture process or storage. But even with this pre-treatment small deviations from the base line can be observed and are marked with numbers in the Figure 7.4.

The T_g of ENR50 appeared at about 40 K higher than the T_g of NR. This is an indication that ENR50 have a higher level of order than NR and that requires more energy to move from its glassy state to its rubbery state. This change can be correlated to the transformation of double bound to epoxy rings (Figure 7.4).

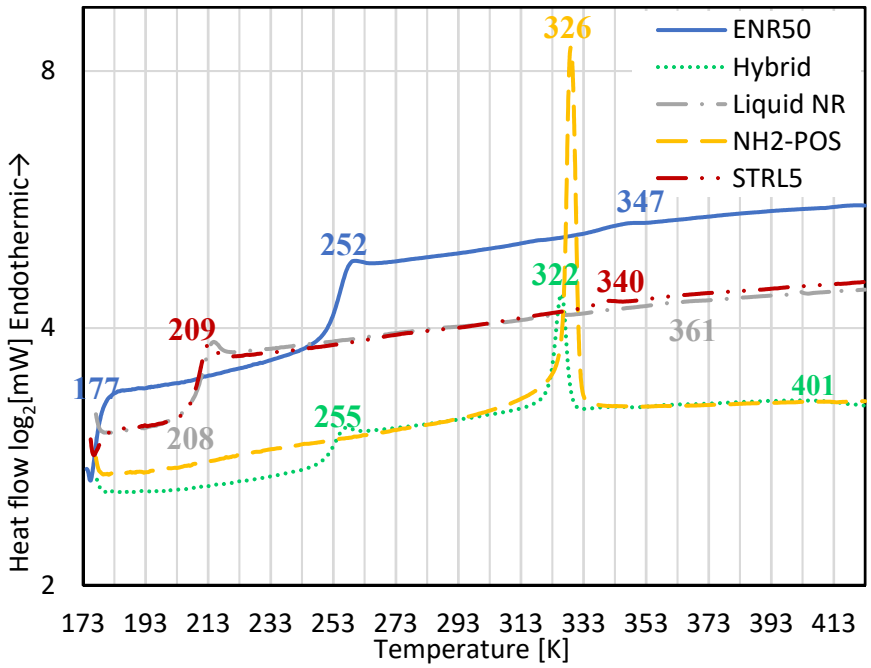

Figure 7.4. DSC thermograms of precursors and hybrid nano-composite materials

There is plenty evidence that the reaction between ENR and NH_2-POS can be consider a click reaction:

1. The reaction occurred in heteroatoms of the type C-X-C, in this case the epoxy ring (C-O-C).
2. It is modular as POS are discreet molecules.
3. It has a high yield (85%).
4. It does not generate "offensive" by-products.
5. It was carryout at simple conditions, 40 ºC, without a catalyst and was insensitive to oxygen and relative humidity at ambient condition.
6. It can be separate from solvent without using chromatographic methods, isopropyl alcohol was used to precipitate the polymer.

7.3.3 Thermo mechanical characteristics obtained by DMA.

It is possible to estimate the T_g of the materials and the higher order transition betta (T_β) by using tan(δ) curves from the DMA (Figure 7.5).

The T_g of STR5L, ENR50 and hybrid were 239, 286 and 209 K, respectively. T_β were observed at 223 and 233 K in ENR50 and the hybrid respectably. It is expected for NR (STR5L) to have a T_β; however, due its low value it did not appear in the tan(δ) curve. As expected, the T_g values obtained from DSC and DMA do not match, however, they do indicate similar trends. For example, it is possible to be observed from Figure 7.5 that all materials had their T_g and that only the NR lacks T_β. However, the E' curve of the STR5L shows that the material possesses a T_β with a small plateau (Figure 7.6). Another attribute that can be observed from DMA curves is a likely melting point (T_m) observed at 484, 487, 484 K for ENR50, STR5 and hybrid, respectably, observed towards the end of the scans. The last yet important attribute that can be observed in the hybrid DMA curve is a possible crystallization or recrystallization occurring at 409 K. This possible recrystallisation can be attributed to the grafting of POS into polymeric chain.

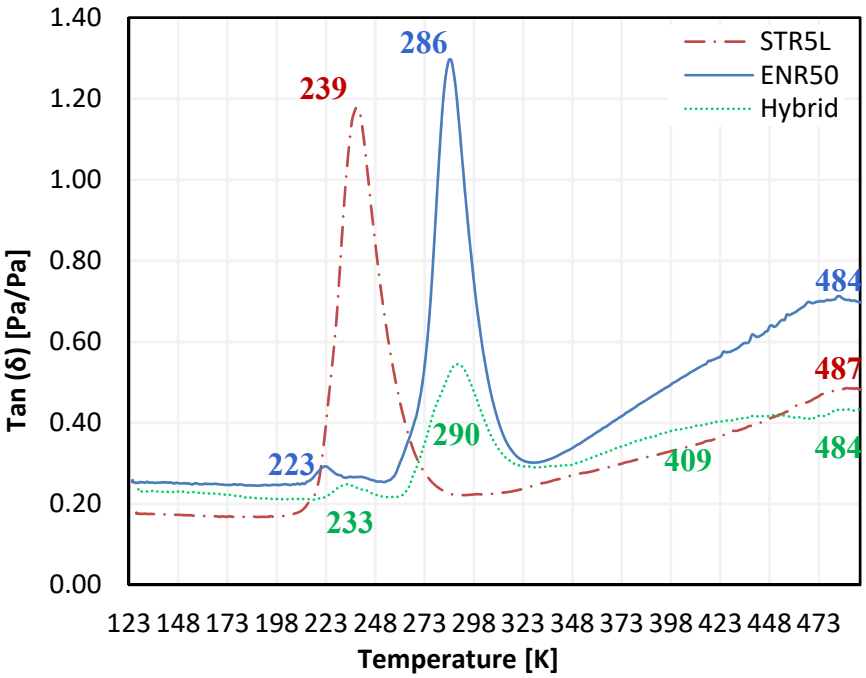

Figure 7.5 Tan(δ) DMA curve of NR (STR5L), ENR50 and Hybrid material.

The elastic modulus presented in Figure 7.6 reveals that at glassy state of ENR50 has a considerably bigger modulus than rest of the materials. In rubbery state the hybrid material possesses a higher modulus than STR5L and ENR50 (Figure 7.7 a).

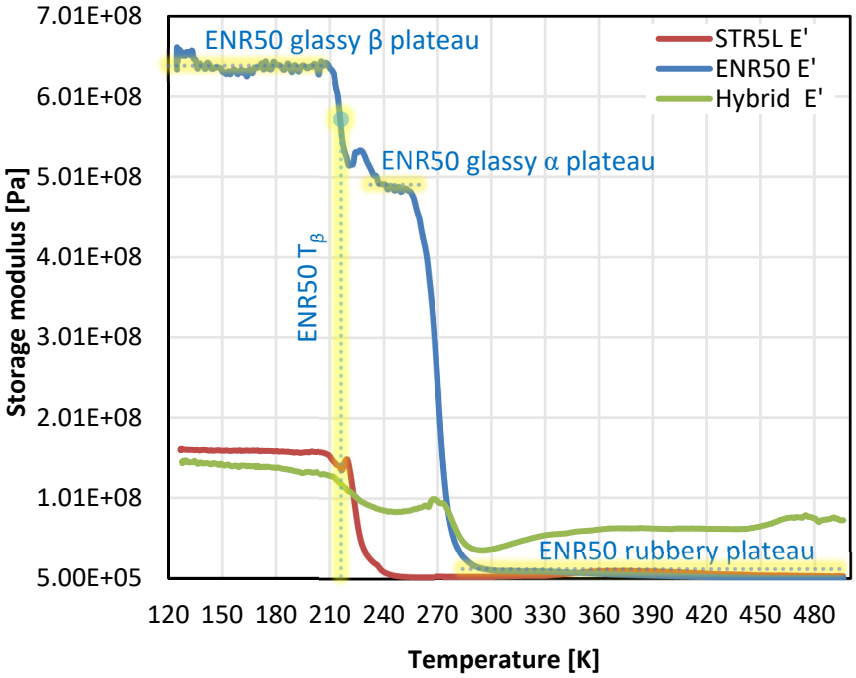

Figure 7.6 Elastic modulus (E') for STR5L, ENR50 and the Hybrid. The blue dash line highlighted in yellow marks the ENR50 main thermo-mechanical characteristics of ENR50.

It is important to note that the value of T_β in all the test materials were very similar, but its magnitude followed ENR50 > STRL > hybrid trend. Since T_β is closely related to the movements of the side groups in the polymeric chain, it can be said that the side groups of the hybrid material have higher intermolecular order than in the ENR50. This means that the hybrid material needs less energy to relax to another state (from β to α glassy state). The hybrid material needs even less energy than STRL5 that have almost none lateral groups. This is also applicable to the T_g, but in this case the hybrid has a higher order in its main polymeric chain compared to its precursors.

The difference in magnitude between two plateaus of hybrid material is smaller than in STRL5 and the ENR50, this is an indication that the product (hybrid) is more thermally stable than its precursors within the temperature range tested. Achieving higher thermal stability is one of the main reasons for incorporating POS into a polymeric matrix.

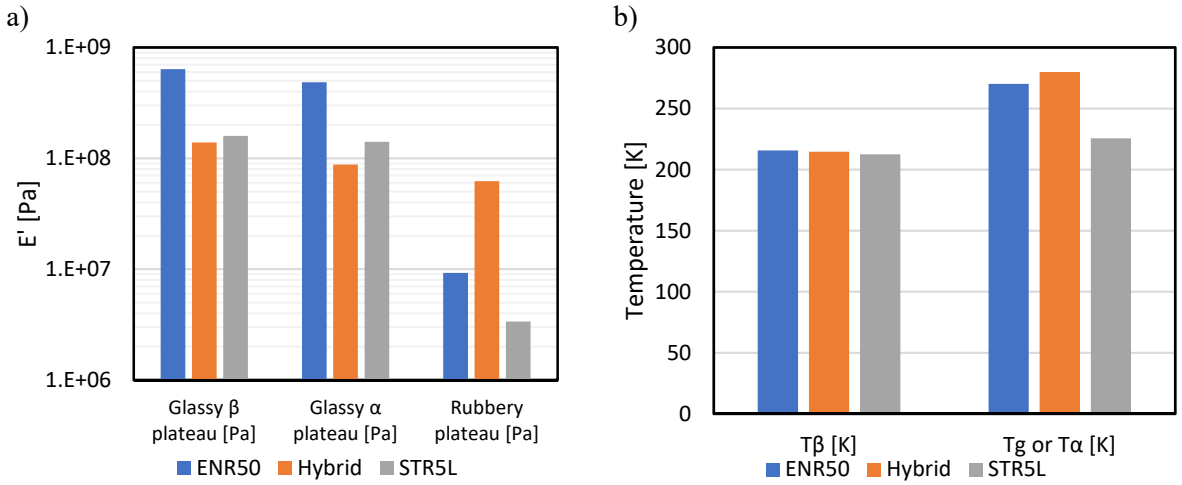

Figure 7.7 a) Characteristic β, α and rubbery plateaus comparison in log_{10} scale for all the materials and b) values of T_g and T_β from E' curves from DMA for all materials

The loss (E") and complex (E^*) moduli of the precursor and their hybrid product corroborate the discussion presented earlier because they show similar trends (Figure 7.8 a). As shown in Figure 7.8 b, the E' values of all the test materials are much higher than their corresponding E'' values in the temperature range tested and consequently the E* is very similar to E'.

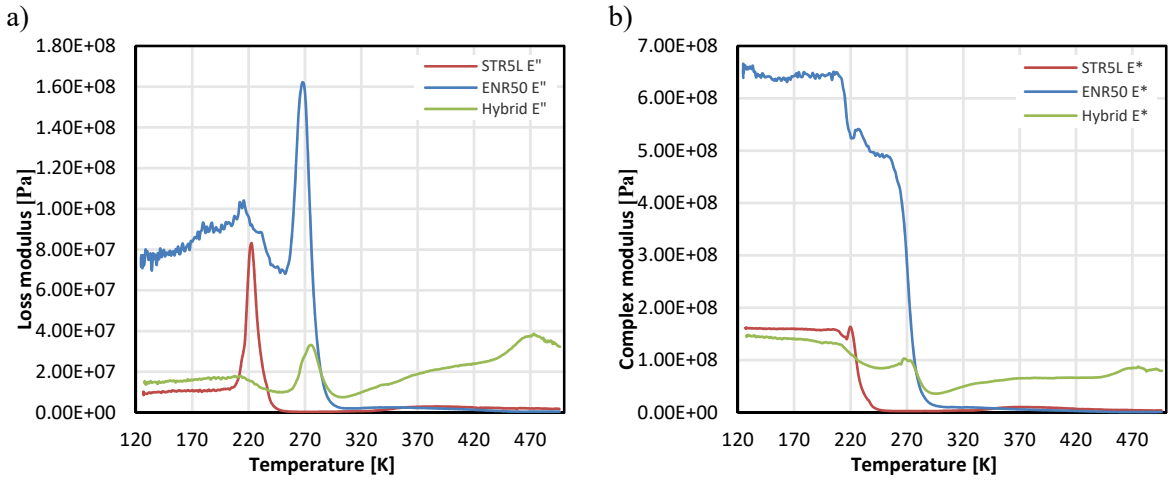

Figure 7.8 The a) loss modulus (E") and b) complex modulus (E^*) of NR, ENR50 and their hybrid product

Although the E'' values of hybrid product is smaller than its E' value, in fact it is not remarkably low when compared with E' values of the precursor materials in their rubbery state (Figure 7.9).

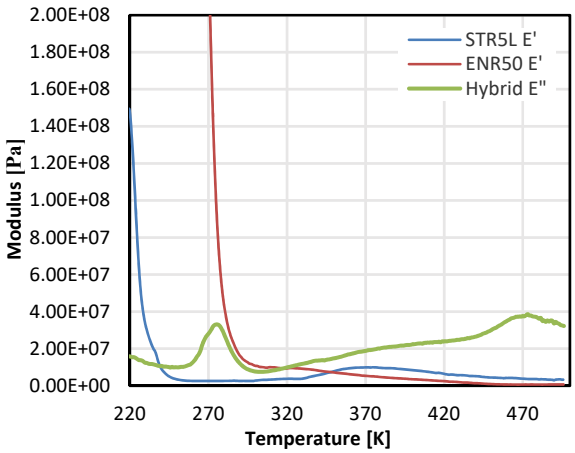

Figure 7.9 Scaled detailed comparation of the loss modulus (E'') of hybrid product to the storage modulus (E') of precursor materials (STR5L and ENR50)

All the above documented results clearly match the experimental results predictions presented in chapter 6 qualitatively. For example, the T_g was increased (both DSC and DMA measurements) which can be correlated to the free volume. This match the increase in parallel of density and T_g (both correlated to the free volume too) of the topological method as seen in Figure 7.10. Another example is the decrease of the coefficient of volumetric thermal expansion that match the higher intermolecular order and thermal stability correlated to DMA analysis.

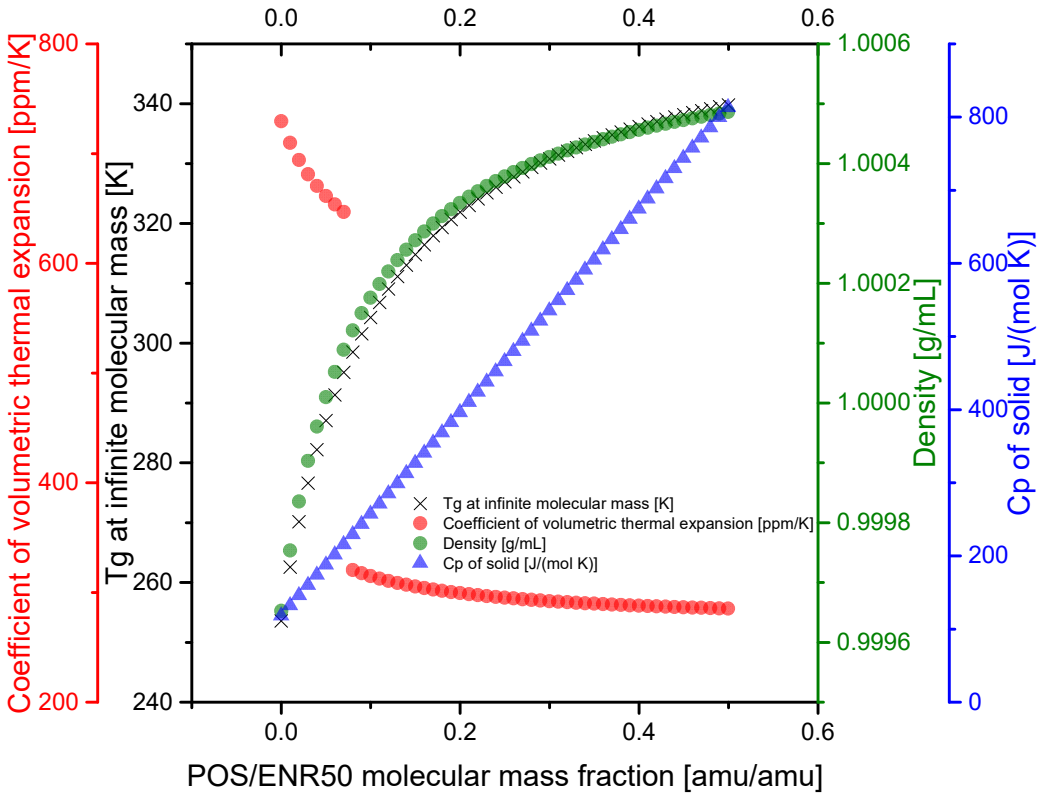

Figure 7.10 Properties change due to the POS content

7.4 Conclusions

The reaction between ENR50 and POS was successfully carried out producing its hybrid material. This reaction can be considered a 'click reaction'. Addition of POS increased the density and T_g and that optimisation of concentration of POS in the mixture was found to be the most important step in synthesising ENR50-POS hybrid nanocomposite.

This work shows that incorporation of POS into ENR50 brings a higher intermolecular order promoted by the addition of POS, a like system with higher order could mean more compacted structure that is a translation of more mass per volume or higher density.

This work shows that incorporation of POS into ENR50 brings about a higher intermolecular order (higher T_g, less free volume, more density) and produces hybrid material with compacted structure and higher density.

The hybrid material had less difference in magnitude between plateaus of glassy and rubbery states indicating to its higher thermal stability. The hybrid material also required less energy to relax from β to α glassy states, this energy is rated to the energy side groups in the polymeric chain which can be correlated to a lower stearic energy configuration.

Result on this chapter can be correlated to the predictions on Chapter 6.

7.5 References

1. Thomas, S. and R. Stephen, *Rubber nanocomposites: preparation, properties, and applications*. 2010: John Wiley & Sons.
2. Kolb, H.C., M.G. Finn, and K.B. Sharpless, *Click Chemistry: Diverse Chemical Function from a Few Good Reactions*. 2001: Weinheim. p. 2004-2021.
3. Chansekaran, S., *Click reactions in organic synthesis*, ed. S.e. Chansekaran. 2016, Weinheim, Germany: Wiley-VCH.
4. Pothen, L., C.H. Chan, and S. Thomas, *Natural Rubber Materials, Volume 2-Composites and Nanocomposites*. 2013: Royal Society of Chemistry.
5. Kodal, M. and G. Ozkoc, *Micro and Nanofillers in Rubbers*. 2013 ed, ed. P.M. Visakh, A.K. Chandra, and A.P. Mathew. Vol. 11. 2013, Berlin, Heidelberg: Berlin, Heidelberg: Springer Berlin Heidelberg. 303-356.
6. Strankowski, M., *Nonlinear viscoelasticity in Three Dimensional filler reinforced rubber composites and nanocomposites*, in *Non-Linear Viscoelasticity of Rubber Composites and Nanocomposites*. 2014, Springer. p. 59-83.
7. Stephen, R. and S. Thomas, *Nanocomposites: state of the art, new challenges and opportunities.* Rubber Nanocomposites: Preparation, Properties, and Applications, S. Thomas and R. Stephen Eds., John Wiley & Sons, singapore, 2010: p. 1.

8. Lin, Q., et al., *The grafting reaction of epoxidized natural rubber with carboxyl ionic liquids and the ionic conductivity of solid electrolyte composites.* RSC Advances, 2015. **5**(109): p. 90031-90040.

8 CONCLUSIONS, REMARKS AND FUTURE WORK

8.1 Conclusions and remarks

This work examined the effect of incorporation of polyhedral oligomeric silsesquioxanes (POS) into two distinctly different natural polymeric matrices: starch and natural rubber. The starch was transformed into thermoplastic by removing the crystalline granule structure during the gelatinisation process using glycerol and water as plasticizers which made possible to cast it into films. The natural rubber was transformed by a wet epoxidation reaction into epoxidized natural rubber (ENR50) and was chemically grafted with POS through a click reaction at room temperature without a catalyst. In both systems new materials were produced, characterized and studied through classical experimental and modelling techniques as well as newly developed methods and models.

Specifically, Chapter 4 documents the succeeded in increasing the surface water resistance of the glycerol plasticised high amylose starch films using nano-silica hybrids (POS). This is important for packaging where water repellency on the surface and barrier to water vapour transmission are essential but difficult to achieve. Wettability kinetics of starch films containing POS was quantified and found to be a function of two distinct mechanisms each with independent linear behaviour. The increase in water repellence in starch-POS films is attributed to the preferential localisation of POS derivatives at the surface. The inherent hydrophobicity of POS increased water repellence of the starch-POS films. The thermomechanical transition of the films suggested that the presence of POS nanohybrids increased or promoted the re-association (retrogradation) of amylose molecules in gelatinised starch films. This is the reason why the starch-POS films had higher melting temperature and higher T_g compared to the starch-only film. In the presence of POS, the starch-POS film required less energy to transit to the glassy state.

Chapter 5 documents the science and procedure of constructing a time-temperature master curve (moduli or phase angle versus time) for starch-nanohybrid films using a new integrational method developed in this study. This new method provides more accurate shift factors than that provided by classical methods such as least square fit or numerical analysis.

Master curves are useful where it is essential to measure the rheologically complex behaviour at very long or short time-frames and experiments at actual time-temperature condition are impractical. Because most carbohydrate polymers are thermo-rheologically complex materials, it is generally accepted that the time-temperature superposition principle (TTSP) cannot be used to construct a master curves, for example, in the case of high amylose thermoplastic starch films.

The chapter 5 proceeded by hypothesising that it is possible to apply TTSP in rheologically complex materials under certain constrains. The experimental data and model predictions showed that thermoplastic starch film indeed showed complex rheological behaviour and that, in classical sense, the TTSP could not be used to construct a master curve. However, based on properties predicted by the Arrhenius and Williams–Landel–Ferry (WLF) models, it was possible to establish temperature constraints where the time-temperature principle was valid. The hypothesis of applicability of TTSP for rheologically complex materials under certain constrains was proven by determining and applying temperature constrains.

As a simple and rigorous approach, this thesis proposed simple generalised customisable models based on combining currently available models and characteristic temperatures. The models proposed in this work have higher coefficient of determination (R2) and much lower error during fitting of the shift factors than those achieved by the WLF or Arrhenius models. Therefore, the approach of generalized TTSP models for rheologically complex materials is highly beneficial to carbohydrates and other biomaterials commonly encountered in food and packaging industry.

The addition of POS increased the internal order of the film leading to more compact molecular arrangement. The starch-POS films were more resistant to deformation compared to starch-only films and their master curves started at higher frequencies.

Chapters 6 and 7 it is document synthesis and modelling of physically blended (nanocomposites) and chemically reacted nanohybrids of natural rubber (NR) and epoxidized natural rubber (ENR) with POS at different concentrations. Physicochemical characteristics of these materials were compared using amorphous cell molecular dynamics (ACMD) and a topological method. These methods of synthesis

and predictive models are important in the NR industry where there is a continuous demand for innovative composites which enhanced properties. The properties of NR, ENR and a synthetized hybrid predicted by the models and the experimental data reported in the literature were very close to each other.

The modelling work undertaken in this thesis also covers two approaches to reduce computational time and cost. The first approach consists of pre-calculations using topology methods to determine the optimum/minimum number of atoms in ACMD that predicts the experimental thermo-mechanical properties. The second approach makes use of an asymptotic function to estimate densities at infinite relaxation time. Various thermo-mechanical transitions were calculated using asymptotic and quadratic polynomial functions which agreed with the experimental data.

The incorporation of POS increased the density, T_g and mechanical properties at an optimal concentration. The results showed that NR hybrids were preferred to nanocomposites in terms of mechanical properties. In the case of ENR, an increase of T_g can be problematic and must be considered when choosing between composites and hybrids.

8.2 Future work

During the course of this thesis, I realised that there were some interesting and worthwhile research avenues or aspects to pursue further. Due to time and resource constraints, it was not possible for me to pursue those avenues in this thesis. Thus, I recommend those aspects as worthwhile future work.

- In the formulation used in Chapter 4 for control starch film, one can incorporate weak organic acids such as prop-1-ene-1,2,3-tricarboxylic acid (aconitic acid), citric acid or poly(carboxylic acids). Incorporation of these acids is expected to increase ultimate stress, decrease the permeability and increase the water repellence by a crosslinking within the main matrix. Also, the use of POS containing the similar type of functional groups than the weak acid could have the same effect and in addition increase of thermo-mechanical properties.
- The generalized time-temperature superposition models, proposed in Chapter 5, can be applied to other rheologically complex materials. It is recommended to apply these models to custom

or purpose designed polymers (for example isotactic propylene or polymethylmethacrylate) as well as more complex materials such as asphalts to broaden their applicability.

- Further dedicated studies are recommended for both methods that decrease the computational time in Chapter 6.A series of model polymers with previous real scale independent experimental results must be used in order to validate the method for a wider range of polymers.
- It is recommended that industrial functionality tests such as abrasion or rolling resistance on the hybrid materials synthetised in this study (Chapter 7).

9 APPENDIX

9.1 Thermoplastic starch-nanohybrid films with polyhedral oligomeric silsesquioxane

Carbohydrate Polymers 173 (2017) 170–177

Contents lists available at ScienceDirect

Carbohydrate Polymers

journal homepage: www.elsevier.com/locate/carbpol

Thermoplastic starch-nanohybrid films with polyhedral oligomeric silsesquioxane

I. Martinez-Pardo[a], Robert A. Shanks[a,*], Benu Adhikari[a], Raju Adhikari[b]

[a] School of Science, RMIT University, Melbourne, VIC 3000, Australia
[b] CSIRO Manufacturing, Clayton South, VIC 3169, Australia,

a r t i c l e i n f o

Article history:
Received 1 February 2017
Received in revised form 2 May 2017
Accepted 2 May 2017
Available online 10 May 2017

Chemical compounds studied in this article:
Hydroxypropyl starch (PubChem CID: 24847857)
1-(3-Glycidyl)propoxy-3,5,7,9,11,13,15-isobutylpentacyclo [9.5.1.13,9.15,15.17,13] octasiloxane (PubChem CID: 4126588)
O-(2-aminopropyl)-O′-(2-methoxyethyl)poly(propylene glycol)500 (PubChem SID: 24846306)
oxolane (PubChem CID: 8028)
(Z)-docos-13-enamide (PubChem CID: 5365371)
propane-1,2,3-triol (PubChem CID: 753)

Keywords:
Nanohybrids
Starch film
Gelatinization
Contact angle
Polyhedral oligomeric silsesquioxanes
Water-resistant

a b s t r a c t

Thermoplastic starch forms packaging films that have low gas permeability, but they are more permeable to water vapour and they are attacked by water. Our approach was to create surface and internal localised hydrophobicity using added reactive nano-materials to form nano-silica hybrids with emphasis on enhancing surface water resistance. Functionalization was via epoxy-POS, that were further linked to hydrophobic erucamide or an amphiphilic poly(oxyethylene-co-oxypropylene) mono-amine. High amylose thermoplastic starch was combined with mono-functionalised hepta-isobutyl polyhedral oligomeric silsesquioxane (POS). POS modified thermoplastic starch increased water resistance of TPS film. Wettability kinetics was a function of two distinct mechanisms each with independent linear behaviour. Surface water resistance increased and is proposed to be due to preferential location of the POS derivatives at the surface with associated increase of hydrophobicity due a surface change.

1. Introduction

Thermoplastic starch (TPS) has hardness and strength, though lacks water resistance. Surface hydrophobicity is proposed to increase surface water resistance while attempting to minimize changing bulk properties responsible for mechanical properties and biodegradability. An additional attribute is expected to be decreased retrogradation, which typically leads to embrittlement. Starch is a natural energy storage substance that can be modified to give a readily biodegradable renewable material with suitable mechanical properties for some packaging applications. A high amylose content is preferred for thermoplastic starch due to processability of the linear amylose, while the highly branched amylopectin with higher molar mass contributes to material properties. Starch compositions have been applied in food, paper and pharmaceutical preparations, where they are resistance to gas permeation (Stevens & Kabasci, 2013), but permeable to water

Abbreviations: ASTM, American Society for Testing and Materials; Control film, modified thermoplastic glycerol plasticized starch film; Epoxy-POS film, modified thermoplastic glycerol plasticized starch film with Epoxy-POS; Epoxy-POS, 1-(3-glycidyl)propoxy-3,5,7,9,11,13,15-isobutylpentacyclo[9.5.1.1^{3,9}.1^{5,15}.1^{7,13}] octasiloxane; Eru-POS film, modify thermoplastic glycerol plasticized starch film with Eru-POS; Eru-POS, functionalized of Epoxy-POS with erucamide in the epoxy ring; Jeff-POS film, modified thermoplastic glycerol plasticized starch film with Jeff-POS; Jeff-POS, functionalized of Epoxy-POS with Jeffamine M-600 in the epoxy ring; NH_2-POS film, modified thermoplastic glycerol plasticized starch film with NH_2-POS; NH_2-POS, 1-(3-amino) propyl-3,5,7,9,11,13,15-isobutylpentacyclo[9.5.1.1.^{3,9} .1^{5,15} .1^{7,13}] octasiloxane; N_{wr}, normalise water resistance ratio respect to the control film; p, p-value of statistics hypothesis test; POS or POSS®, polyhedral oligomeric silsesquioxanes; Tanδ, loss angle or dissipation factor; T_g, glass transition temperature; T_m, melting temperature; wr, water resistant as area under a θ_c *versus time plot*; θc, contact angle.

*Corresponding author.
E-mail addresses: issac.rubens@gmail.com (I. Martinez-Pardo), robert.shanks@rmit.edu.au (R.A. Shanks), benu.adhikari@rmit.edu.au (B. Adhikari), raju.adhikari@csiro.au (R. Adhikari).

http://dx.doi.org/10.1016/j.carbpol.2017.05.009
0144-8617/

vapour (Wiącek, 2015). TPS packaging provides a barrier to external elements such as atmosphereic gases, moisture, oil and microorganisms.

Starch is an abundantly available biomaterial in nature and is a renewable resource from plants. Starch consists of linear amylose α(1,4)-glucopyranoside and amylopectin that has additional α(1,6) branches. Starch is the energy storage material found in plants in the form of granules (Rindlav-Westling & Gatenholm, 2003) and is primarily used as food. About half of starch production is for non-food applications such bioplastics, papers, adhesives and biofuels (Ceseracciu, Heredia-Guerrero, Dante, Athanassiou, & Bayer, 2015). This widespread use of starch is due to its desirable barrier and mechanical characteristics, biodegradability, non-toxic nature and its being a renewable resource. Native starch is usually modified by physical and chemical means to meet industrial needs (Chen, Shen, & Yeh, 2010); with one of these applications being manufacture of flexible packaging films.

Starch granular and crystal structure must be disrupted by gelatinization to convert it into a thermoplastic material (see supplementary data video 1). Extrusion and solution casting methods are most commonly used to prepare flexible films from thermoplastic starch (Jiménez, Fabra, Talens, & Chiralt, 2012). In their extrusion method, starch and appropriate amounts of plasticizers are extruded into films. In solution casting, a water dispersion containing gelatinized starch containing appropriate amounts of plasticizers is cast to form a film. Finally, extruded and solution cast films are dried at mild temperature and air flow. Gelatinization involves heating, hydration and dissolution of granular–crystalline starch with plasticization (Ebnesajjad, 2013). Initially, there is a hydration of amorphous amylose and irreversible disruption of the double helical structure of amylopectin. Loss of semicrystalline initial molecular organization is referred to as melting of starch crystals and dissociation of starch–lipid complexes. V-type crystals of amylose can then be formed in a process called retrogradation, ageing or staling, causing the thermoplastic starch to become brittle. Plasticizers, co-solvents and derivative formation, such as hydroxypropylation, are added to avoid or minimize retrogradation.

When the fully gelatinised and plasticised starch is cast and dried a transparent, smooth films that are thermally processable are obtained. Nevertheless, due the hydrophilic nature of amylopectin and amylose, hydrogen bonds are formed when starch interacts with atmospheric humidity and starch re-associates into a partially ordered (retrograded) structure (Yao, Zhang, & Ding, 2003). Retrogradation is one of the main causes of quality deterioration such as brittleness in starch and starch-based films.

Plasticizers are able to retard retrogradation because a single helical structure of amylose tends to form helical inclusion complexes with adequate complexing agents. These inclusion complexes prevent or minimize formation of a new double helical structure of amylose; thus, the formation of semicrystalline structure is prevented. Plasticizers reduce the glass transition temperature (T_g), increase the flexibility and retard ageing of films all of which are desirable for good films. Although xylitol and glycerol are most commonly used to produce starch films (Muscat, Adhikari, Adhikari, & Chaudhary, 2012); however, additives such as monoacyl lipids, emulsifiers, alcohols induce formation of left-handed amylose single helices (Pérez & Bertoft, 2010).

Starch based films are less permeable to gases such as oxygen and carbon dioxide which is desirable attribute for packaging materials (Stevens & Kabasci, 2013). However; water vapour readily permeates through the starch-based packaging films as water molecules have good affinity with the abundant and free hydroxyl groups in its chemical structure (Wiącek, 2015). Thus, the water barrier property and water repellency or surface hydrophobicity of starch and starch-based packaging films needs to be substantially increased to increase their application as stand-alone packaging films. An approache to increase the water vapour barrier properties and surface hydrophobicity in starch films is to use nanomaterials that are capable of modifying the surface characteristics of these films. The advantage of nanomaterials as surface modifying agents is that their physicochemical properties are substantially different than those of their macroscale or bulk counterparts. Among these, polyhedral oligomeric silsesquioxanes (POSS®), which are silica based molecular nanoparticles, are shown to increase modulus and strength of starch films while maintaining low density and flexibility (Bastola & Vaidyanathan, 2015). The POSS nanoparticles have greater versatility as they allow alteration or tailoring of their pendant groups.

There are many types of POS and the mono-substituted POS type is one of the most versatile nano-additives used in surface modification of polymers. This so called mono-substituted POS are an octa-functionalized POS that contain seven identical and a different reactive mono-substituents that can be chemically customized by using standard chemical reactions to improve compatibility between many materials such as polymers, fillers, catalyst, solvents, composites and biomaterials (Hartmann-Thompson, 2011). POS are used to impart desirable properties such as light-emission (Singh et al., 2009) and hydrophobicity (Jerman, Koželj, & Orel, 2010). POS are used as indicating (marking) materials for magnetic resonance imaging (Tanaka & Chujo, 2012).

The aim was to incorporate octa-functionalized POS in glycerol plasticized thermoplastic starch films to increase or tune the hydrophobicity or water resistance of the film surface. For this purpose, four different octa-functionalized POS nanohybrids having in common seven hydrophobic isobutyl groups were tested. First, a commercially available POS having an aminopropyl as its eight substituted group; second, a POS with a glycidyl as its eight substituted group, this one was also used to synthetise the third and fourth, via its epoxy ring with the widely used food grade hydrophobic slip agent erucamide and the amphiphilic poly(oxyethylene-co-oxypropylene) respectively.

2. Material and methods

2.1. Materials

Pre-gelatinised hydroxypropylated corn starch (Penford™ A939) was used as the starch. According to the manufacturer it contained ~80 of high-amylose and 6.5% by weight of hydroxypropyl substitution. Distilled water was used as solvent or dispersant. Propane-1,2,3-triol (glycerol) was purchased from Sigma-Aldrich (Sydney, Australia) was used as plasticizer. Glycerol contained less than 1 %w/wmoisture.

1-(3-Glycidyl)propoxy-3,5,7,9,11,13,15-isobutylpentacyclo[9.5.1.1^{3,9}.1^{5,15}.1^{7,13}] octasiloxane (epoxy-POS) was used to modify the starch films as well as to produce the novel functionalized POS. The 1-(3-amino) propyl-3,5,7,9,11,13,15-isobutylpentacyclo[9.5.1.1.^{3,9}.1^{5,15}.1^{7,13}] octasiloxane (NH_2-POS) was used to modify the starch films. These two chemicals were purchased from Hybrid Plastics Inc. (Hattiesburg, USA). O-(2-Aminopropyl)-O^1-(2-methoxyethyl)poly(propylene glycol) 500 (Jeffamine) was used to chemically functionalize the POS and was purchased from Sigma-Aldrich (Sydney, Australia). Anhydrous and inhibitor-free oxolane (tetrahydrofuran, THF) was used as solvent in all reactions. THF was purchased from Science Supply Australia Limited (Melbourne, Australia). (Z)-docos-13-enamide (*cis*-13-docosenoamide or Crodamide ER) was obtained from Croda International (Hull, United Kingdom).

All materials were used as received and the moisture content of each material was measured and was compensated for while

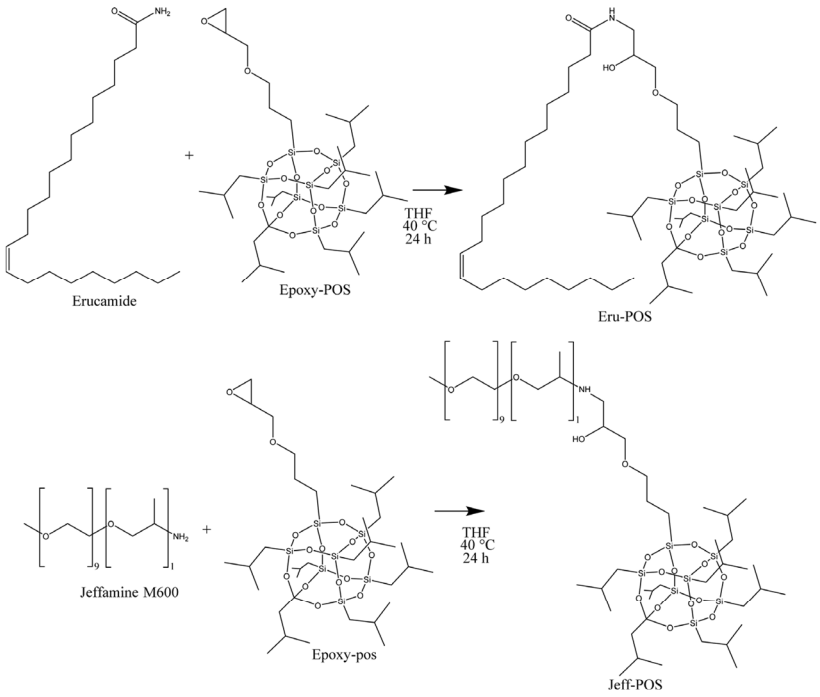

Fig. 1. Epoxy-POS functionalization reaction with either erucamide or Jeffamine to produce POS nanohybrids.

determining the concentration of each chemical and preparing starch slurries for gelatinisation.

2.2. Functionalization of nanohybrid POS

Epoxy-POS was functionalized either with erucamide or Jeffamine at a molar stoichiometric ratio of 1:1. The solvent (THF)-reactants (epoxy-POS) mixture was stirred at 40 °C for 24 h (Fig. 1). The THF-epoxy-POS molar ratio was maintained at 35:1 during reaction and the product was collected after evaporation of the THF under vacuum at 40 °C.

2.3. Identification of functional and reactive groups

Fourier transform infrared (FTIR) spectra were acquired using a PerkinElmer Spectrum 100 spectrophotometer to identify the key functional and reactive groups during reactions. A universal diamond attenuated reflectance (ATR) was used to scan wavenumber from 4000 cm^{-1} to 650 cm^{-1}, 10 scans per spectrum were recorded with a resolution of 4 cm^{-1}.

2.4. Preparation of starch-plasticizer, starch-plasticizer-nano additive slurries

A master batch starch-plasticizer slurry was prepared by dissolving 4.03 % w/w starch, 1.21 % w/w glycerol in 94.88 % w/w water. This master batch was used throughout to avoid discrepancy in preparing the exact concentrations of formulations. This slurry was heated (IKA RH-digital hotplate, Staufen, Germany) at 95 ±3 °C for about 20 min.

The progress and completion of gelatinization and homogeneity of the dispersion was monitored using an optical microscope (Nikon Labophot II, Japan). The progress and completion of the gelatinization was monitored using both plain and polarized optical microscopy.

2.4.1. Addition of nano-additives to the gelatinized starch slurry

Four aqueous slurries of monohybrids from the master batch were prepared, NH_2-POS, Epoxy-POS, Eru-POS and Jeff-POS by dissolving 1.3 % w/w of each hybrid in 98.7 % w/w of master batch; the master batch alone was considered as the control. Then each slurry was individually homogenized using a high-shear disperser (Bamix, Australia).

2.4.2. Degassing, film casting and conditioning

The air entrapped during agitation was removed by degassing the slurries for 5 min in a vacuum chamber. After degassing, 20 mL of each slurry was transferred onto a polystyrene Petri dish (90 mm diameter) using a syringe. Drying was carried out in a custom-built isothermal drying box with gentle fan forced air circulation at 30 ±1 °C for 48 h. Temperature within the chamber was controlled using a digital proportional–integral–derivative (PID) controller unit. After drying, the films were stored in a desiccator containing a saturated solution of magnesium nitrate (about 54% relative humidity) at ambient temperature (20 °C) for at least 48 h prior to further tests.

2.5. Determination of moisture content

The moisture content of films was determined by a gravimetric method using a Mettler-Toledo HG63 (Australia) halogen moisture analyser. The measurements were terminated when the mass change was <1 mg over 140 s.

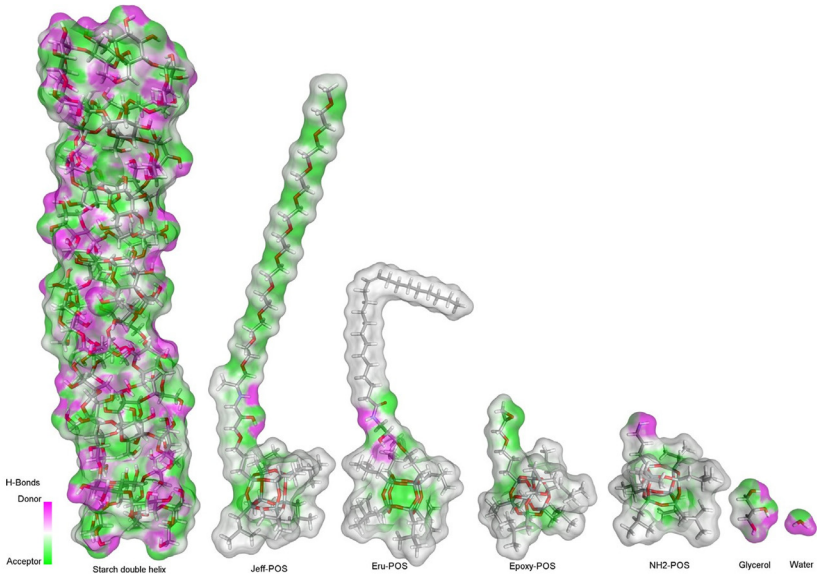

Fig. 2. Hydrogen bonding receptor surface of molecules in the starch film systems.

2.6. Determination of wettability kinetics

The wettability kinetics (Li et al., 2015; Wia¸cek, 2015) were measured as the change of the contact angle (θ_c) of the films with time. A sessile droplet method was used and the measurements were made using a Data-Physics OCA20 instrument (Germany). Contact angles were measured in triplicate on the top surface (the surface that had not been in direct contact with the polystyrene Petri dish during the drying process). Contact angles were automatically calculated by fitting an ellipse to the surface of the drop method using OCA20 software. Two drops of water obtained from a Milli-Q system were deposited on each film. Apparent contact angle (θ) was measured in 1 s interval for about 5 min.

2.7. Determination of mechanical properties

Stress–strain analysis was performed and Young modulus, maximum tensile stress, tensile strain and toughness were determined from data acquired using an Instron 4465 Universal Test Instrument in tensile mode, in accordance with ASTM 882(ASTM, 2001). A grip distance of 26.5 mm and a cross-head speed of 2.65 mm/s were used for these tests. The specimen dimensions were measured in three different places using a Duratool DC150 digital caliper. Specimens were die-cut into dumbbell shapes as specified by ASTM D638 (ASTM, 2003). The Young modulus was calculated from the stress-strain curve between a stress value of 0.005 MPa and a stress value below the proportional limit and preload tensile modulus ASTM E111(ASTM, 1997).

2.8. Determination of glass transition temperature by dynamic mechanical analysis

Specimens were cut to 9.6 mm (wide) × 45 mm (long) × 0.10 mm (thick) and coated with petroleum jelly to reduce moisture evaporation. A sweep pre-treatment (temperature-frequency) was carried out before each scan to remove any pre-existing thermal or mechanical history. Scans were performed in tensile mode using synthetic multi-frequency (0.5, 1, 2, 5, 10 Hz) where all frequencies were applied simultaneously and Fourier transform resolved by the instrument software. Pre-treatments were performed at a rate of 20 K/min from −60 °C to 80 °C then returned to −60 °C. Tests were carried out from −60 °C to 90 °C at a rate of 5 K/min.

2.9. Statistical analysis

At least triplicate tests were carried out, except when indicated otherwise, for each parameter and the results are reported as average values ±standard deviation from a mean value. If a difference was to be considered statistically significant or not a Student *t*-test was performed assuming two tail distribution and unpaired two sample equal variance with a confidence interval of 95% ($p > 0.05$)

3. Results and discussion

At first appraisal the nanohybrids were essentially hydrophobic, but due to polar nitrogen and oxygen atoms interactions with other molecules in the starch films were feasible. Sites of interaction were visualized using molecular modelling (Discovery Studio, Dassault Systemes Biovia Corporation, France) by calculating hydrogen bonding receptor surfaces of the molecules using a probe radius of 0.13 nm (see Fig. 2).

3.1. Identification of functional and reactive groups and indication of reaction completion

FTIR spectra of the products and the reactants are compared in Figure to confirm reactions shown in Fig. 1.

In the FTIR spectra of Eru-POS system in Fig. 3b) the most important peaks are those that almost disappear or shift in the range 3300–3450 cm^{-1} and 1650–1675 cm^{-1} (see expanded detail in Fig. 3d), these peaks correspond to the amine group and the ⋹O stretching next to it respectively (both forming an amide group) and are evidence that the primary amide change to a secondary amide, these changing peaks indicate that an addition reaction occurred.

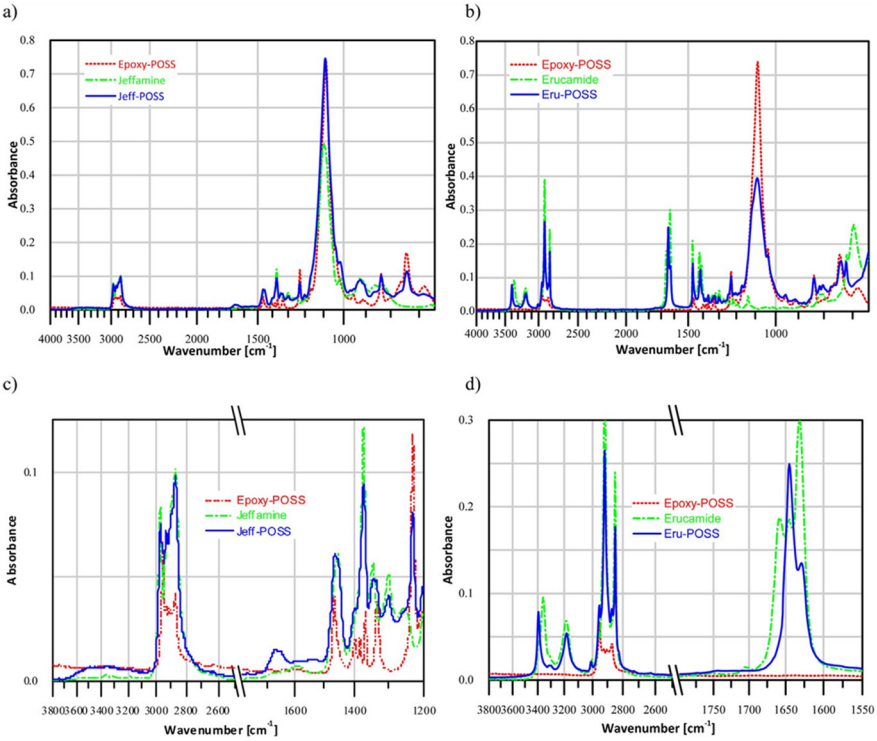

Fig. 3. FTIR spectra of Eru-POS and Jeff-POSS and their precursors a) Jeff-POSS, b) Eru-POS, c) expanded details of Jeff-POSS and d) expanded details of Eru-POS.

In the case of the Jeff-POS system (Fig. 3a) the previous peaks are not useful because lacks of the C=O stretching, but the spectra product shows additional peaks respect to its precursors (epoxy-POS and Jeffamine), these peaks are in the range of 1600–1700 cm^{-1} and 3050–3600 cm^{-1} (see expanded detail in Fig. 3c) corresponding mostly to hydroxyl group but also to amine group, the appearance of hydroxyl groups coupled with a decrease of the whole epoxy ring stretching peak at 1250 cm^{-1} (Ratnam, Nasir, Baharin, & Zaman, 2000) is indicative of the ring reaction.

3.2. Moisture content in the films

The moisture content control, NH_2-POS, Epoxy-POS, Eru-POS and Jeff-POS were 6.04 ± 0.38, 5.35 ± 0.41, 5.95 ± 0.88, 5.89 ± 0.08 and 6.13 ± 0.35, respectively. There was no significant difference in moisture content compared with the control which indicates that within the bulk starch hydrophilicity was maintained.

3.3. Contact angle of the films

Water spreading over the starch film is a dynamic condi- tion where equilibrium would be achieved after it was no longer possible to read the contact angle. It is not only a function of instantaneous surface energy, but over time, absorption increased interactions, until a time when it was no longer possible to read the contact angle due a deformation of the film or the water drop. This occurred after 5 min, until then contact angles were able to be measured. The contact angle profiles are shown in Fig. 4, in order to present smooth curves of the data, a 10th degree polynomial was used to fit it.

The contact angle data presented in Fig. 4 shows that representation of wettability of these films by a single contact angle (θ_c) is not possible as θ_c varied with time. Some films had similar initial θ_c values; however, they diverged over time before conserving to a more or less stable difference between their θ_c values (See supplementary data video 2).

As the variation of θ_c over time showed two distinct regimes (Fig. 4a), hence, two linear equations were used to represent the variation of θ_c at initial and later stages. The slope of both equations represents the rate of change of θ_c respect to time [°/min]. The intercepts in abscissa of these linear lines represent the initial θ_c (initial stage) and an apparent initial θ_c for the later stage as shown in 4b) and Table 1. All films containing the nanohybrid additives had higher contact angle compared with the starch–glycerol only (control) film except for the film that contained Jeff-POS. The Jeff-POS films had lower initial contact angle values than that of the control film due to the hydrophilic nature of Jeffamine. It appears that a single substituted hydrophilic Jeffamine in the POS cage predominated over the other seven hydrophobic substituted groups, imparting more hydrophilic nature to the film.

The control and Jeff-POS films shared the similar variation of θ_c over time in the later rate. This observation indicated that the Jeff-POS at this concentration does not contribute to or modify the wettability (θ_c versus time) characteristics of films at later stage. Although the Control, NH_2-POS and Eru-POS films had similar initial θ_c the latter two films had much higher θ_c values in later stage indicating higher hydrophobicity in NH_2-POS film and Eru-POS film compared with that in the control.

The most water resistant (hydrophobic) film was the one with largest initial θ_c and smallest variation over time. For that reason, it was assumed that the way to compare hydrophobic/water

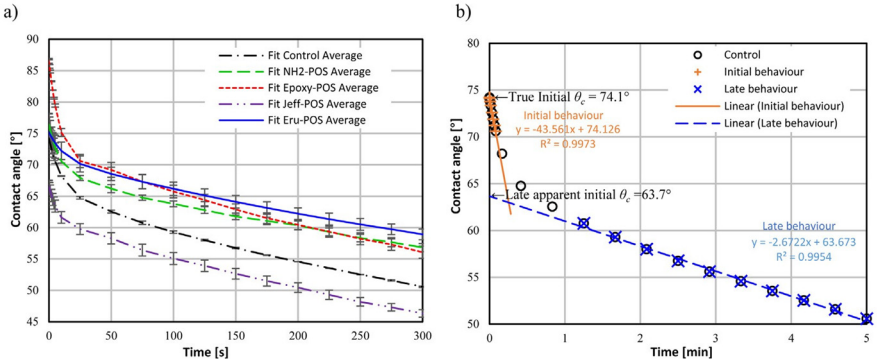

Fig. 4. a) 10th order polynomial fitting of the average wettability profile of the films; the error bars represent the standard deviation and b) characterization of the initial and late behaviour of the control film by linear fitting.

Table 1
Film wettability (δ_c) and water resistance from 0 to 5 min.

Film name	Initial rate [°/min]	True initial θ_c [°]	Initial correlation coefficient^2	Later rate [°/min]	Later apparent θ_c [°]	Later correlation coefficient^2	wr [°·min]	Nwr [%]
Control	−43.6	74.1	0.997	−2.67	63.7	0.995	288.6	0.0
NH_2-POS	−44.2	76.3	0.996	−2.10	67.2	0.998	306.5	6.2
Epoxy-POS	−86.2	86.4	0.996	−2.95	70.5	0.994	309.7	7.3
Jeff-POS	−38.3	66.5	0.995	−2.69	59.5	0.998	274.0	−5.1
Eru-POS	−21.2	75.2	0.998	−2.22	69.8	0.997	312.7	8.4

resistance (wr) nature of these materials was to calculate the area under θ_c versus time plot, the larger the area [°·min] the more water resistant was the film. The other approach to determine the hydrophobicity was to use the area of the control film as a reference and normalise the area ratio using this reference (Nwr), see Table 1.

The starch (control) and NH_2-POS films share similar initial θ_c and initial rate [°/min] which indicated that the NH_2-POS did not affect the wettability or hydrophobic/hydrophilic behaviour in the film at this concentration in the initial stage. The Eru-POS film, Epoxy-POS film and NH_2-POS film were the material with higher water resistance at 5 min respectably, which indicates that the longer the hydrophobic group the higher was the wr.

3.4. Tensile stress–strain behaviour of the films

The tensile mechanical properties (Young modulus, maximum stress and strain) of the starch and starch-additive films are presented in Fig. 5 and tensile properties are compiled in Table 2. It is important to note that only the NH_2-POS film showed a first offset yield strength, which is an uncommon behaviour and was attributed to a secondary smaller molecular arrangement due to the intrinsic interaction of the nano-hybrid with the glycerol plasticized starch films. The toughness were calculated as the area under the stress-strain curve and is reported as [MJ/m^3] that is equivalent to [M(Pa)·(m/m)] or [M(N m)/(m^2 m)]. Comparing the control film with NH2-POSS film we found similar maximum tensile stress and comparing the control film to Jeff-POS film we found similar maximum strain, but when the toughness is compared the control is at least 8 and 3 times tougher. All the mechanical properties of the films with respect to the control film decreased except for the maximum tensile stress of the NH_2-POS where there was not a statistically significant difference. The NH_2-POS and Eru-POS films share about the same Young modulus with insignificant statistical difference and they are about 25 % less than the control film. Although the nanohybrids are not entirely hydrophobic thanks to the nitrogen and oxygen atoms of the molecules, the decrease of the mechanical properties could be due the introduction of hydrophobicity into the films and not just at the surface

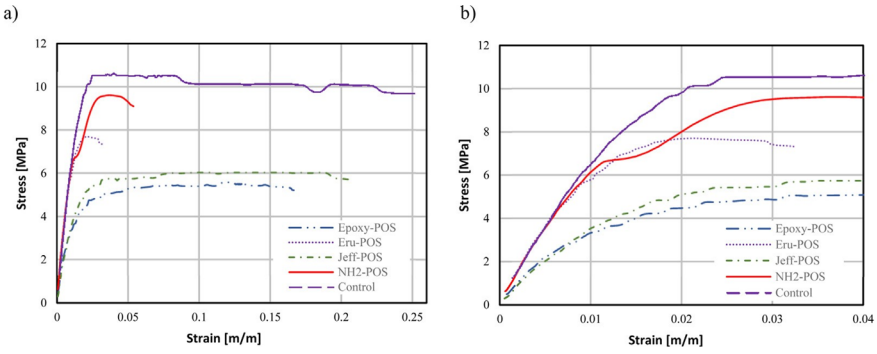

Fig. 5. a) Stress-strain curves of starch–additive films b) expanded view of the NH_2-POS first offset yield.

Table 2
Tensile mechanical properties of films.

Property	Control flim	NH_2-POS film	Jeff-POS film	Eru-POS film	Epoxy-POS film
Maximum tensile stress [MPa]	12.54 ± 1.71	10.52 ± 1.05	6.98 ± 1.57	8.06 ± 0.69	5.38 ± 0.35
Maximum tensile strain [m/m]	0.3481 ± 0.0541	0.0603 ± 0.0090	0.1773 ± 0.0285	0.0322 ± 0.0004	0.1171 ± 0.0527
Young modulus [MPa]	868.98 ± 4.28	645.00 ± 120.51	468.75 ± 135.65	653.71 ± 99.64	387.66 ± 77.08
Toughness [MJ/m^3]	3.5442 ± 0.3138	0.4059 ± 0.0293	1.0800 ± 0.1408	0.2055 ± 0.0081	0.5309 ± 0.0053
First offset yield stress [MPa]	–	6.60 ± 0.24	–	–	–

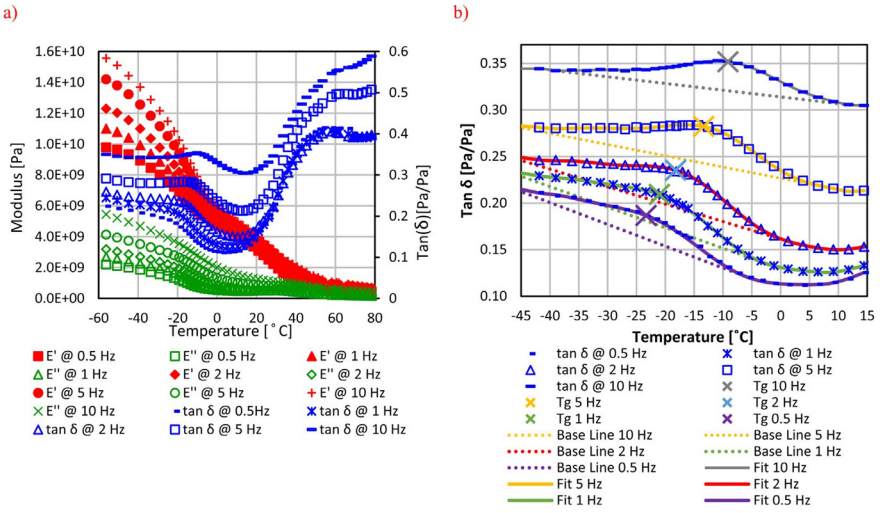

Fig. 6. a) E′, E″ and tan ○ of Jeff-POS film. b) Schematic representation of the calculated Tg at different frequencies.

3.4.1. Thermomechanical transition of the films

It was possible to detect transitions by testing the materials at one frequency, however without complementary tests or prior knowledge of the system the type of transition could not be validated. To interpret the type of transition using only DMA; is necessary to test the material at several frequencies and under modulated temperature cycles, with the objective to determine if the transition was frequency dependent, or if the transition temperature was conserved with frequency. If the transition was conserved and frequency dependent it is a glass transition because it is a kinematic change. If the transition is conserved and it is not frequency dependent, it is a melting temperature, which is a thermodynamic change. If the material has transitions that are not conserved, this is an indication of previous thermo-mechanical history.

Elastic modulus (E′), viscous modulus (E″) and tan ○ (See Fig. 6a)) were measured at different frequency, in order to determine the thermo-mechanical transition temperatures presented in Table 3, the estimations were done by fitting a 10th order linear polynomial equation to the Tan ○ region of the transition along with a linear baseline (See Fig. 6b)), the temperature that corresponded the maximum vertical distance between the polynomial curve and the baseline is reported as the transition temperature.

The first transition is the glass transition temperature (T_g) because it was found at the lowest temperature, was frequency dependent and reversible. The second transition was considered a melting temperature (T_m) because it was found at the highest temperature (before the boiling temperature of water), was not frequency dependent and was reversible. Only the control film exhibited an intermediate transition between T_g and T_m which was small, frequency independent and semi-reversible. This intermediate transition may be due to starch regaining crystallinity after gelatinization (retrogradation) (Wang & Copeland, 2013).

The control film had the lowest T_g and the highest T_m, which means it remained flexible with consistent mechanical properties in a wider range of temperatures than the other films follow by the NH_2-POS, Epoxy-POS, Eru-POS and Jeff-POS films. There is not significant difference in the T_m of Eru-POS and the Jeff-POS films.

Table 3
Thermo-mechanical transition temperatures of the films.

Property	Control film	NH_2-POS film	Epoxy-POS film	Eru-POS film	Jeff-POS film
T_g at 10 Hz [°C]	−18.1	−8.2	−9.9	−7.0	−9.2
T_g at 5 Hz [°C]	−20.8	−12.3	−14.1	−11.2	−13.4
T_g at 2 Hz [°C]	−25.2	−17.6	−19.8	−17.2	−18.2
T_g at 1 Hz [°C]	−28.2	−20.9	−24.2	−20.1	−21.0
T_g at 0.5 Hz [°C]	−32.1	−23.8	−28.7	−23.1	−23.3
Intermediate transition [°C]	51.3 ± 0.47	–	–	–	–
Average T_m [°C]	80.1 ± 0.2	71.5 ± 0.5	57.7 ± 5.4	47.5 ± 0.3	47.2 ± 2.1

4. Conclusion

The nanohybrid erucamide-POS and Jeffamine-POS were dispersed with glycerol plasticized starch films and synthesized by substituting a single pendant group of a POS cage either by erucamide or Jeffamine 600 respectively. This novel nanohybrids along with the other two commercial ones (epoxy-POS and NH2-POS) were incorporated individually to glycerol plasticized starch films obtaining films with different contact angle and mechanical properties compared with those of the control, glycerol plasticized starch film.

The POS nanohybrids increased or promoted the re-association of amylose molecules in gelatinised starch films (retrogradation) as indicated by the highest melting temperature (T_m) and the lowest glass transition temperature (T_g) with respect to the control film. Only the control film exhibited an intermediate transition between T_g and T_m, which was small, frequency independent that may be due to starch regaining crystallinity after gelatinization.

The control film had the highest ultimate tensile strain and the highest tensile modulus, and consequently it was the toughest film, followed by NH2-POS and erucamide-POS.

Hydrophobicity of the films as indicated by the contact angle (θ_c) was time dependent, having two distinct regimes. The initial θ_c of the first regime and the apparent θ_c of the second regime depended on the type of nanohybrids used. The initial θ_c was always larger than the apparent θ_c by 10°. Initial rate of decrease of θ_c was always larger than that in second stage by almost 18 times. All the films with nanohybrids had higher contact angle (7.8 %) with respect to the control film except in the case of Jeff-POS film. The longer the hydrophobic mono-substituted pendant group in the POS cage the higher the water resistance is, by the contrary if the hydrophilic Jeffamine is used the water resistance decrease.

Appendix A. Supplementary data

Supplementary data associated with this article can be found, in the online version, at http://dx.doi.org/10.1016/j.carbpol.2017.05.009.

References

ASTM. (1997). *E111-04, standard test method for young's modulus. annual book of ASTM standards.* Philadelphia, PA: American Society for Testing Materials.

ASTM. (2001). *D882-02, Standard test method for tensile properties of thin plastic sheeting. Annual Book of ASTM Standards.* Philadelphia, PA: American Society for Testing Materials.

ASTM. (2003). *D638-03, Standard test method for tensile properties of plastics. Annual Book of ASTM Standards.* Philadelphia, PA: American Society for Testing Materials.

Bastola, K. P., & Vaidyanathan, R. K. (2015). System and method for synthesis of poss-starch derivatives as effective fillers for developing high performance composites. Google Patents.

Ceseracciu, L., Heredia-Guerrero, J. A., Dante, S., Athanassiou, A., & Bayer, I. S. (2015). Robust and biodegradable elastomers based on corn starch and polydimethylsiloxane (PDMS). *ACS Applied Materials & Interfaces, 7*(6), 3742–3753.

Chen, C.-J., Shen, Y.-C., & Yeh, A.-I. (2010). Physico-chemical characteristics of media-milled corn starch. *Journal of Agricultural and Food Chemistry, 58*(16), 9083–9091.

Ebnesajjad, S. (2013). *Handbook of biopolymers and biodegradable plastics: properties, processing and applications.*

Hartmann-Thompson, C. (2011). *Applications of polyhedral oligomeric silsesquioxanes.* Springer.

Jerman, I., Koz˘elj, M., & Orel, B. (2010). The effect of polyhedral oligomeric silsesquioxane dispersant and low surface energy additives on spectrally selective paint coatings with self-cleaning properties. *Solar Energy Materials and Solar Cells, 94*(2), 232–245.

Jiménez, A., Fabra, M. J., Talens, P., & Chiralt, A. (2012). Edible and biodegradable starch films: a review. *Food and Bioprocess Technology, 5*(6), 2058–2076.

Li, X., Banham, D., Feng, F., Forouzandeh, F., Ye, S., Kwok, D. Y., et al. (2015). Wettability of colloid-imprinted carbons by contact angle kinetics and water vapor sorption measurements. *Carbon, 87*, 44–60.

Muscat, D., Adhikari, B., Adhikari, R., & Chaudhary, D. (2012). Comparative study of film forming behaviour of low and high amylose starches using glycerol and xylitol as plasticizers. *Journal of Food Engineering, 109*(2), 189–201.

Pérez, S., & Bertoft, E. (2010). The molecular structures of starch components and their contribution to the architecture of starch granules: a comprehensive review. *Starch-Stärke, 62*(8), 389–420.

Ratnam, C. T., Nasir, M., Baharin, A., & Zaman, K. (2000). Electron beam irradiation of epoxidized natural rubber: FTIR studies. *Polymer International, 49*(12), 1693–1701.

Rindlav-Westling, Å., & Gatenholm, P. (2003). Surface composition and morphology of starch, amylose, and amylopectin films. *Biomacromolecules, 4*(1), 166–172.

Singh, M., Chae, H. S., Froehlich, J. D., Kondou, T., Li, S., Mochizuki, A., et al. (2009). Electroluminescence from printed stellate polyhedral oligomeric silsesquioxanes. *Soft Matter, 5*(16), 3002–3005.

Stevens, C., & Kabasci, S. (2013). *Bio-based plastics: Materials and applications.* John Wiley & Sons.

Tanaka, K., & Chujo, Y. (2012). Advanced functional materials based on polyhedral oligomeric silsesquioxane (POSS). *Journal of Materials Chemistry, 22*(5), 1733–1746.

Wang, S., & Copeland, L. (2013). Molecular disassembly of starch granules during gelatinization and its effect on starch digestibility: a review. *Food & Function, 4*(11), 1564–1580.

Wia¸cek, A. E. (2015). Effect of surface modification on starch biopolymer wettability. *Food Hydrocolloids, 48*, 228–237.

Yao, Y., Zhang, J., & Ding, X. (2003). Partial β-amylolysis retards starch retrogradation in rice products. *Journal of Agricultural and Food Chemistry, 51*(14), 4066–4071.

9.2 Natural rubber with polyhedral oligomeric silsesquioxane, nanocomposites, and hybrids compared by molecular modeling

9.2.1 Cover

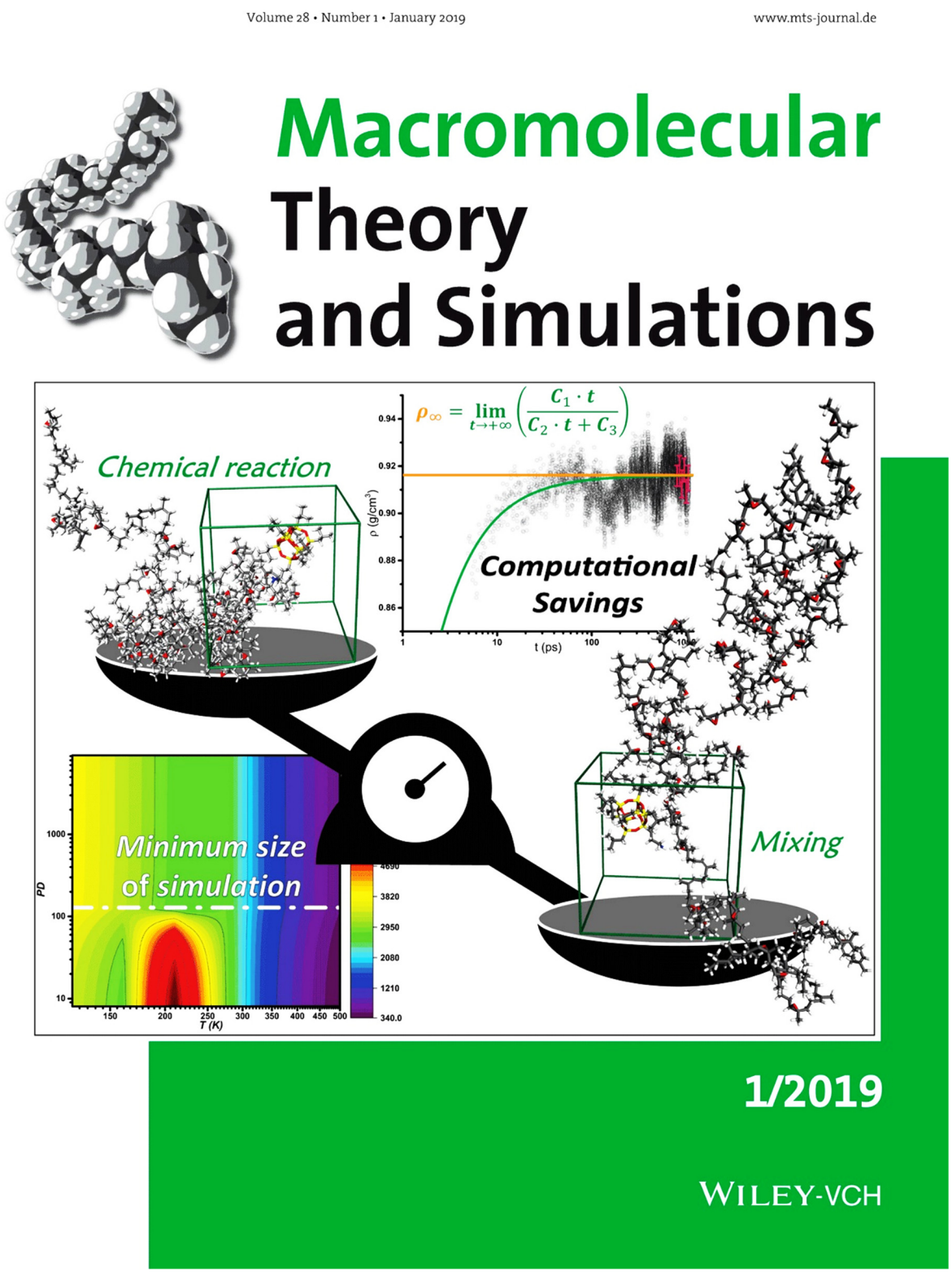

Full PaPer

Nanocomposite

Macromolecular Theory and Simulations
www.mts-journal.de

Natural Rubber with Polyhedral Oligomeric Silsesquioxane, Nanocomposites, and Hybrids Compared by Molecular Modeling

Isaac Martinez-Pardo, Robert A. Shanks, Raju Adhikari, and Benu Adhikari*

Physical and chemical blends, that is nanocomposites and hybrids, respectively, of natural rubber (NR) and epoxidized natural rubber (ENR) with polyhedral oligomeric silsesquioxane (POS) at different concentrations are modeled and compared using amorphous cell molecular dynamics (ACMD) and a topology method similar to group additivity contribution methods. Pre-calculations using topology methods are proven useful to determine the optimum number of atoms in ACMD that will predict equivalent reported experimental thermo-mechanical properties. Densities at infinite relaxation time are used to estimate various thermo-mechanical transitions using asymptotic and quadratic polynomial functions. Incorporation of POS increases the density and glass transition temperature (T_g). The results demonstrate that NR hybrids are preferred to nanocomposites for mechanical properties, though with ENR, T_g increase may be problematic and must be considered before choosing between composites or hybrids.

1. Introduction

Natural rubber (NR) is a versatile elastomer with well-balanced mechanical properties.[1] Due to its large strain at break and low stress–strain hysteresis, NR has applications in the automotive,[2] electronics,[3] rubber goods industries[4] as well as in pressure sensitive adhesives.[5,6] Carbon black is the most preferred reinforcing filler;[7] however, clay and silica are used for increased reinforcement. Polyhedral oligomeric silsesquioxanes (POS or POSS) are molecular forms of silica that are chemically functionalized to adjust polar and nonpolar characteristics and chemical reactivity. POS are known to be promising fillers compared with particulate silicas and carbon black, as they offer better processability and dispersion, and avoid agglomeration.[8,9]

I. Martinez-Pardo, Prof. R. A. Shanks, Prof. B. Adhikari
School of Science
RMIT University
124 La Trobe St, Melbourne, VIC 3000, Australia
E-mail: robert.shanks@rmit.edu.au
Prof. R. Adhikari
CSIRO Manufacturing
Clayton South, VIC 3169, Australia
The ORCID identification number(s) for the author(s) of this article can be found under https://doi.org/10.1002/mats.201800026.

DOI: 10.1002/mats.201800026

While a physical mixture of inorganic-organic materials can change NR properties by transferring some characteristics of the filler to the material, this depends upon their intrinsic compatibility and their surface interactions.[10] Regardless, the use of nanoparticles to maximize surface interactions or to increase chemical compatibility by adding pendant groups gives less physical interaction between the materials than that obtained with chemical bonding.

The use of nanofillers to reinforce NR has high expectation because nanofillers have shown in many cases an enhancement of the mechanical properties;[11] conventional inclusion of inorganic fillers by dispersion is more widely used over organic fillers, where carbon black and silica are the most used[12] that have comparable tensile strength, but lower tensile modulus (E) than exhibited by silica composites.[13] With the current demand for fillers from renewable resources, organic fillers have become more widely used, especially in the form of fibers, although lower performance than the inorganic fillers has been reported.[14] There are several studies where a synergetic contribution using hybrid fillers (organic–inorganic) appears to enhance mechanical properties as well as increase thermal and physico-chemical properties.[15–17]

Physical or chemical addition of nano-fillers onto polymers may lead to changes in T_g that is the most significant transition or relaxation observed for amorphous polymers;[18] even small changes in T_g lead to considerable changes in density, bulk modulus, tensile modulus, and shear modulus.[19] Therefore, property prediction is an important factor to consider in the design, modification, and production of polymer composites for existing or novel applications. Hence, a comparison of the mechanical and thermal properties using molecular dynamics of physical mixtures compared with chemical hybrids is important for design and production of nanocomposites, where both possibilities are of interest and estimation of properties such as T_g is essential.

In addition to its industrial importance, NR is dynami- cally flexible, which is an advantage for simulations because local dynamics occur under 100 ps.[20] While experimental results for mixtures are preferred, modeling is used to predict structure and properties of similar materials because it eliminates the need for synthesis of each material composition,

confirming proposed hypotheses, while obtaining principally new results.[21] Computational performance increases each year and in novel modeled synthetic methods, materials can gain complexity, and molecular dynamics has emerged as an attractive tool.[22] The use of molecular modeling and simulation becomes more accessible, and this is especially true in the nanocomposite field, where design rules allow modeling of engineering materials by combining the desirable properties of nanoparticles and polymers for potential commercialization.[23]

There are many software programs developed to predict properties of polymers that use different methods; the program Synthia[24] is similar to traditional group additive contribution methods, but the calculated properties are expressed in terms of topological variables, (connectivity indices) combined with geometrical variables and structural descriptors, allowing the prediction of properties of truly novel types of polymer structures. This method transcends the limitations of traditional group contribution techniques, where the use of pre-existing experimental thermophysical data banks for its calculations is often missing; this is more evident in the design of candidate polymers for cutting-edge applications, where structural units are often considered exotic.

Synthia predicts properties of isotropic linear polymers (amorphous or amorphous phases of semicrystalline) constituted of nine elements: carbon, hydrogen, oxygen, nitrogen, silicon, chlorine, sulphur, fluorine, and bromide, but the method allows prediction for polymers containing more elements using databases and extended corrections available in the Bicerano book.[24] The main topological starting point formalism for this quantitative structure properties relationship (QSPR) program is based on graph theory and connectivity indices that are calculated exactly from valence bond theory. The program includes a calculation for arbitrary bond lengths and a variable number of atoms, conformational properties of polymer chains, and the distinction between intensive and extensive properties—how the properties change when the size of the system varies and distinction between backbone and side-group contributions.

The final correlation of each property uses indices, geometrical constants related to the composition, and some experimental data (normally in the range of hundreds) to fine-tune the correlation, where a typical standard deviation is in the range of 1% to no more than 13% and in some few cases above 25%. The general forms of correlations in terms of connectivity indices are shown by Equation (1) for intensive properties (IP) and Equation (2) for extensive properties (EP).

$$IP = \sum b \frac{\chi}{N} + \text{structural parameter and atomic or group corrections} + \text{constant} \quad (1)$$

$$EP = \sum a\ \chi + \text{structural parameter and atomic or group corrections} \quad (2)$$

where N is the non-hydrogen atoms in the system, a and b are the regression coefficients and χ represents the connectivity indices.

Regardless of the great advantages of the topological method and its low computational time, is not possible to predict properties for physical composites, where the addition of non-covalent bounded molecules into a polymer has been made. For this reason, other computational means to estimate the properties of novel nanocomposites are utilized. One of these methods is molecular mechanics and dynamics, which use a force field to represent the equilibrium and time-averaged effects of electrons and nucleus with reasonable accuracy. Most commonly, a 3D structure of the molecules, with periodic boundary conditions, is constructed and entities such as bond stretching-compression, valence angle deformation, torsion or rotation about the bond, and non-bonded interactions[25] are calculated and correlated to physical, thermal, and chemical properties. Although this method offers a more flexible design than a topological method it increases the computational time, but not as much as an ab initio method.

Despite the worthy investigation for enhanced properties of NR by incorporation POS,[12] few works have reported grafting POS onto NR or epoxidized NR (ENR)[26] and even less research has been reported contrasting hybrids and composites. For these reasons, it was important to construct models to compare structures and properties using molecular modeling and simulation, which give a unique comparative perspective with fewer confounding variables than traditional experiments, for example, the complex process of mixing.[27] We hypothesize that hybrids are more effective than composites in transferring stress from the polymeric matrix to the nanoparticles.

2. Experimental Section

1. Materials

The natural rubber used was STR5L (Standard Thai Rubber 5L) obtained from Srijareon Rubber Co. Ltd, Thailand; the liquid natural rubber was a cis-polyisoprene, made from natural rubber purchased from Sigma-Aldrich Co. LLC. Melbourne Australia; the natural rubber with a 50% mol of random epoxidized natural rubber (ENR50) was obtained from the Malaysian Rubber Board.

2.2. Topology Method

All topology calculations were performed using Synthia, which significantly simplified the task, while minimizing errors. To give an overview of how the method predicts properties, the calculations of indices, molar volume (V_m), and density (ρ) for polyisoprene at 298.15 K are described in general.

2.2.1. Topological Indices Calculation

Once the repetitive unit is defined, for every non-hydrogen atom, the simple atomic index (δ) is calculated as the number of non-hydrogen atoms bonded to a given non-hydrogen as well as the second atomic index (δ^v), using Equation (3) where Z^v is the number of valence electrons, N_H is the number of bonded hydrogens, and Z is the atomic number.

$$\delta^v = \frac{Z^v - N_H}{Z - Z^v - 1} \quad (3)$$

Later for each non-hydrogen bond, the bond indices simple bond index (β) and and second bond index ($\beta\upsilon$) were calculated as the product of δ and δ^{υ} respectable for each pair of atoms that form the bond, see equations (4) and (5).

$$\beta_{ij} = \delta_i \delta \tag{4}$$

$$\beta^{\upsilon}_{ij} = \delta^{\upsilon}_i \, \delta^{\upsilon}_j \tag{5}$$

These tasks can be better exemplified by identifying the hybridization of each non-hydrogen atom over the diagram of the structure (see **Figure 1**a) and use a pre-calculated table as in Figure 1b to substitute the non-hydrogen atoms by their corresponding values for the vertices (δ_i, δ^{υ}) and edges ($\beta_{ij}\beta^{\upsilon}$)$_{ij}$ in a hydrogen-suppressed diagram (see Figure 1c–f). Notice that only the numbers in brackets will be considered for further calculations, avoiding redundancy due to the periodic structure notation, and the number and symbols outside brackets are only indicative in Figure 1.

With the atom and bond indices the zeroth-order ($^0\chi$, $^0\chi^{\upsilon}$) and first-order ($^1\chi$, $^1\chi^{\upsilon}$) connectivity indices were calculated using Equations (6–9), see Figure 1g,h.

$$^0\chi = \sum\left(\frac{1}{\sqrt{\delta_i}}\right) \tag{6}$$

$$^0\chi^{\upsilon} = \sum\left(\frac{1}{\sqrt{\delta^{\upsilon}_i}}\right) \tag{7}$$

$$^1\chi = \sum\left(\frac{1}{\sqrt{\beta_i}}\right) \tag{8}$$

$$^1\chi^{\upsilon} = \sum\left(\frac{1}{\sqrt{\beta^{\upsilon}_{ij}}}\right) \tag{9}$$

2.3. Topological Property Predictions

To predict a property, a correlation is needed, for example, Equations (10) and (11) predict directly the V_m in $cm^3\,mol^{-1}$ at 298.15 K but for some other properties extra information is necessary, along with the previously calculated property, such as density, where molar mass and V are necessary, see Equation (12).

$$V_m = 3.642770\,^0\chi + 9.798697\,^0\chi^{\upsilon} + 8.542819\,^1\chi + 21.693912\,^1\chi^{\upsilon} + N_{MV} \tag{10}$$

$$N_{MV} = 24N_{Si} - 18N_{(-S-)} - 5N_{sulfone} - 7N_{Cl} - 16N_{Br} + 2N_{ester} + 3N_{ether} + 5N_{carbonate} + 5N_{C=C} - 11N_{cyc} - 7N_{fused\text{-}1} \tag{11}$$

where N_{MV} is a correction index for the V_m estimation of the contribution in the repeating unit associated with the number of silicon, sulphur, chlorine, and bromide atoms in the lowest oxidation state (N_{Si}, $N_{(-S-)}$, N_{Cl}, N_{Br}, respectively), sulfone atoms in the highest oxidation state ($N_{sulfone}$), ether, and carbonate groups (N_{ether}, $N_{carbonate}$, respectively), non-aromatic rings with no double bond (N_{cyc}), carbon–carbon double bonds ($N_{C=C}$),

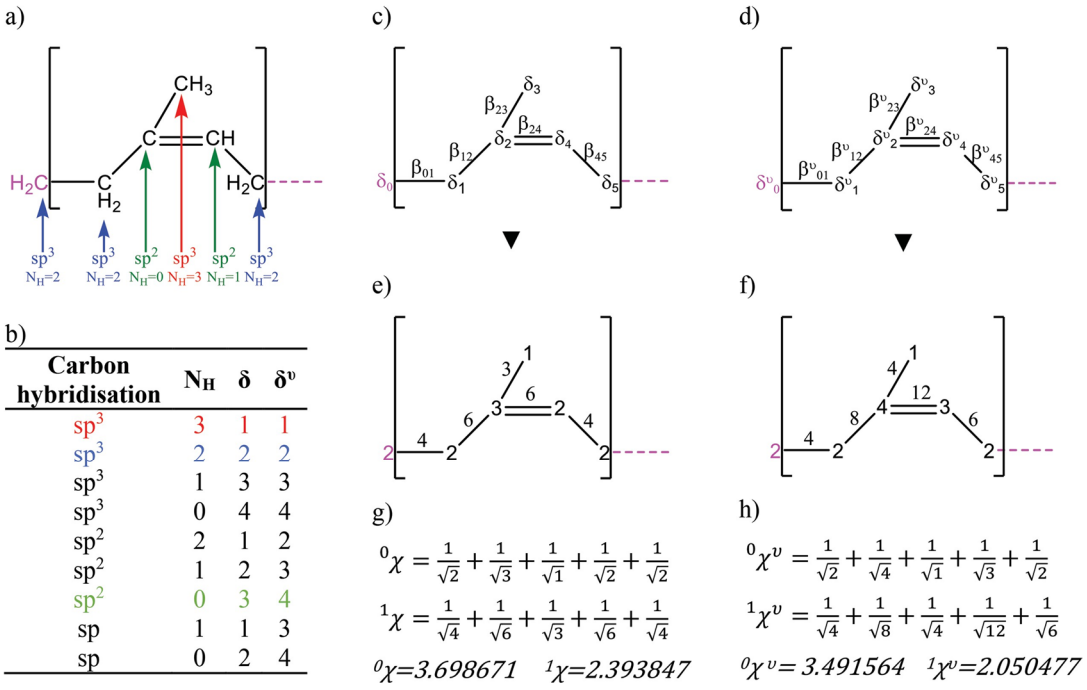

Figure 1. Schematic representation of calculations of connectivity indices.

two or more rings containing at least one aromatic ring which shares at least one edge with another ring ($N_{fused-1}$) and esters in the backbone-chain (N_{ester}).

$$\rho = \frac{M_{mero}}{V_m} \quad (12)$$

Thus the predicted V_m = 3.64(3.70) + 9.80(3.49) + 8.54(2.39) + 21.69(2.05) + 5 = 76.61 [cm^3 mol^{-1}] and ρ = (68.12/76.61) = 0.89 g cm^{-3}.

2.4. Modeling Size Selection

An important factor to consider when modeling is the number of atoms because there is a compromise with computational time. For this reason, it was necessary to identify a minimum number of atoms for each material or degree of polymerization (DP) that could predict representative and consistent properties. As a reference, the ENR50 had a weight average molar mass (M_w) of 7 00 000 g mol^{-1},[28,29] about 1 24 000 atoms or to compare with the other materials a degree of DP of 9200. An equivalent precursor of ENR50 would be NR with the same DP of 9200 but with different M_w of 6 27 000 g mol^{-1} and number of atoms = 1 20 000.

The topology method was used to predict mechanical properties of the polymers at discrete temperatures to choose the least but representative DP. In **Figure 2**, it was observed that above a DP of 123, mechanical properties such as bulk and tensile modulus were similar and representative of those at higher DP; for the sake of having an even DP fraction, a DP of 128 was chosen for all the materials. This reduced the computational time by about 72 times.

2.5. Geometry Optimization of Repeating Units and Molecules

All the repeat units (mer) of polyisoprene, EN50, hybrids (EN50Chem and NRChem), and POS (aminopropylisobutyl-POS) were geometrically optimized prior to any further steps using the COMPASSII forcefield[30] with atom-based charges (electrostatic and Van der Waals) using a smart algo- rithm (a cascade algorithm of steepest descent, adjusted basis set, Newton–Raphson [ABNR] and quasi-Newton [Broyden–Fletcher–Goldfarb–Shanno]) until convergence was achieved for thresholds of 0.00002 kcal mol^{-1}, 0.001 kcal mol^{-1} Å^{-1}, 0.001 GPa, and 0.00001 Å that are reasonable for energy, force, stress, and displacement.

2.6. Polymers and Amorphous Cell Constructions

Using BIOVIA Material Studio (Dassault Systèmes) a series of 18 linear polymers were constructed with DP = 128, shown in **Table1**, and they are the number of random concatenated atactic mers and molecules used to construct amorphous cells (AC) for each polymer, hybrid, and nanocomposite. The polyisoprene mers consist of random atactic 1,4-cis-polyisoprene isomer; the ENR50Chem materials have aminopropylisobutyl-POS molecules attached randomly via the epoxy groups; in NRChem the aminopropylisobutyl-POS molecules were attached randomly via epoxy groups.

Ten amorphous cells were generated for each material and the cell with the lowest energy after 500 steps of geometric optimization was selected. All the amorphous cells were constructed with periodic boundary conditions (PBC) in all three orthogonal directions of a cubic lattice, using COMPASSII forcefield, Ewald electrostatic charge, atom-based Van der Waals forces, checking for ring spearing, avoiding close contacts smaller than 0.25 Å, an initial density of 1 g cm^{-3}, a composition of one polymer chain and for the physical composite series, an additional number of aminopropylisobutyl-POS molecules.

2.7. Relaxation of the Amorphous Cells

1. After cell construction, the cells were geometrically optimized in two steps; the first was using the Universal forcefield with a pre-set quality of ultra-fine. The second method was using the COMPASSII forcefield with a quality set to fine. Both steps were calculated using a quasi-Newton algorithm until convergence, an Ewald method for electrostatic interactions, an atom-based method for Van der Waals interactions, and an external pressure of 0.1 MPa (approximately 1 atm).
2. Dynamics. After the geometrical optimization, two dynamics were performed using COMPASSII forcefield with a pre-set quality of fine, an Ewald method for electrostatic interactions, and an atom-based method for Van der Waals interactions.
3. The first molecular dynamics was run with a Nosé–Hoover thermostat to maintain constant temperature (Q ratio: 0.01) of 298 K and a Berendsen barostat to maintain a constant pressure at 0.1 MPa with a decay constant of 0.1 ps was performed for 200 ps with a time step or 1.0 fs and recording 1001 equidistant frames.
4. The second molecular dynamics was run with fixed volume using a Berendsen thermostat to maintain a constant temperature of 298 K with a decay constant of 0.1 ps and it was performed for 200 ps with a time step or 1.0 fs and a recording frame of 200 steps.
5. Final geometrical optimization. Before calculation of the mechanical properties, another two steps of geometri- cal optimization, as described in item 1, were performed on the last ten frames of the second molecular dynamics (item 4).

2.8. Mechanical Properties Calculation

The mechanical properties were calculated in the ten geometrically optimized frames described in item 5 on the list in Section 2.7 using a constant strain method, in four steps for each strain, with a maximum strain amplitude of 0.003, using COMPASSII forcefield with a pre-set quality of fine, Ewald method for electrostatic interactions, and an atom-based method for Van der Waals interactions.

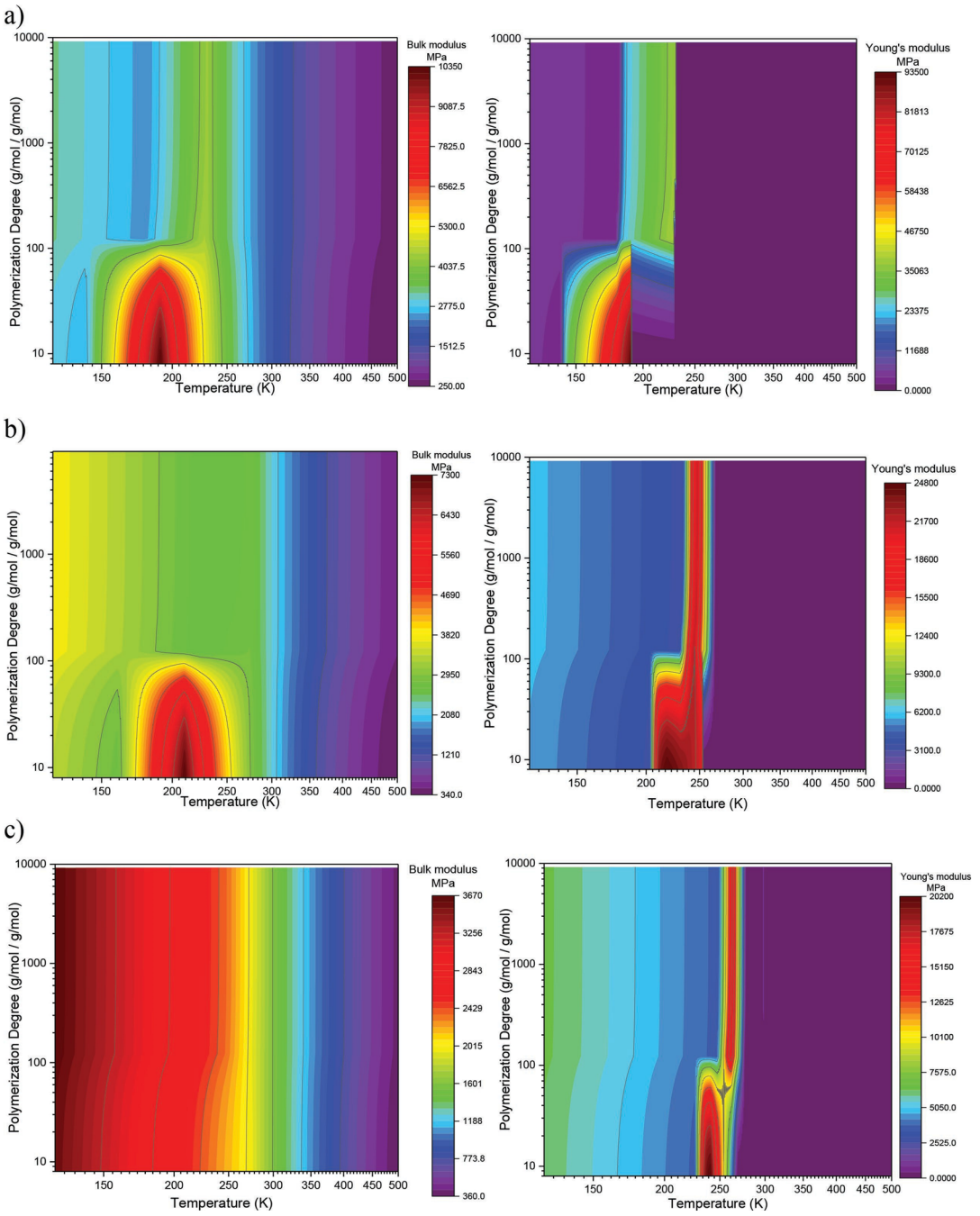

Figure 2. Mechanical properties predicted by the group contribution method, a) NR, b) ENR50, and c) ENR50 reacted with 50 phr (part per hundred) of POS.

Table 1. Structure and composition of the materials and code names.

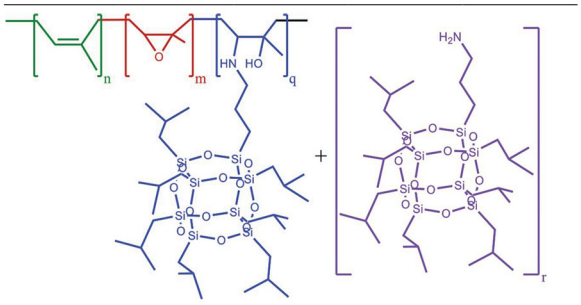

Codename	n	m	q	r
NR	128	0	0	0
NRChem01	127	0	1	0
NRChem03	125	0	3	0
NRChem06	122	0	6	0
NRChem11	117	0	11	0
NRPhy01	128	0	0	1
NRPhy03	128	0	0	3
NRPhy06	128	0	0	6
NRPhy11	128	0	0	11
ENR50	64	64	0	0
ENR50Chem01	64	63	1	0
ENR50Chem03	64	61	3	0
ENR50Chem06	64	58	6	0
ENR50Chem11	64	53	11	0
ENR50Phy01	64	64	0	1
ENR50Phy03	64	64	0	3
ENR50Phy06	64	64	0	6
ENR50Phy11	64	64	0	11

2.9. Estimation of the Glass Transition Temperature and Melting Temperature

1. Density estimation. It was necessary to estimate the density of each material at increasing temperatures to calculate the transition temperatures. The last frame of the final geometrical optimization was used (see item 5 on the list in Section 2.7) to perform an extra dynamic process as described in item 3 on the list in Section 2.7 (NPT), but for 100 ps at each specific temperature. The densities were estimated at least for 12 different temperatures between 100 and 400 K. All densities used to calculate the transitions were estimated as the density at infinity relaxation time by fitting an empirical asymptotic model between 5 and 100 ps of the NPT dynamics as shown in **Figure 3**a.
2. Transition calculation. The transitions were calculated from the intersection of two quadratic equations fitted in the vicinity of the transitions as shown in Figure 3b.

2.10. Estimation of the Coefficient of Thermal Expansion

The coefficient of volumetric thermal expansion (α_v) is the reciprocal of the volume multiplied by the volume change with temperature at constant pressure, see Equation (13)

$$\alpha_V = \frac{1}{V}\left(\frac{\partial V}{\partial T}\right)_P \tag{13}$$

The volumes were calculated at incremented temperatures using the density at infinite relaxation time and the mass of the cell. The volumes with respect to temperature were fitted with first and sixth order linear polynomial functions (see **Figure 4**a), but only the results of the first-degree polynomial were reported because it more accurately represents the data at the edge of the initial and final evaluated temperature as Figure 4b shows. The derivatives of this function were evaluated at each temperature and multiplied by the reciprocal volume at that temperature to obtain α_V (see Figure 4b).

3. Synthesis and Characterization of NR, ENR50, and ENR50 Hybrid

1. Synthesis of Hybrid (ENR50 + POS-NH2)

Equal parts of ENR50 and 1-(3-amino) propyl-3,5,7,9,11,13,15-isobutyl pentacyclic [9.5.1.13,9.15,15.17,13] octasiloxane (POS-NH2) were dissolved into oxolane (THF) and heated on reflux at 313 K for 24 h. Later, the polymer was precipitated using ethanol (analytical reagent grade) and dried under vacuum at 313 K for 24 h.

2. Identification of Functional and Reactive Groups

A PerkinElmer Spectrum 100 spectrophotometer with a universal diamond attenuated reflectance (ATR) was used to acquire the Fourier transform infrared (FTIR) spectra of the synthesized materials and its precursors, 10 scans were performed at a wavenumber from 4000 to 650 cm^{-1}, with a resolution of 4 cm^{-1}

3.3. Determination of Thermal Transition by Differential Scanner Calorimeter

A Mettler Toledo differential scanning calorimeter 1 was used with liquid nitrogen cooling unit. Sweep temperature pre-treatments from room temperature to 333 to 173 K at a rate of 10 K min^{-1} were performed before each scan to remove any pre-existing thermal history. The reported scans were performed at 10 K min^{-1} from 174 to 424 K; see **Figure 5**a.

3.4. Determination of Thermal Transitions by Dynamic Mechanical Analysis

A Perkin Elmer Diamond DMA with liquid nitrogen cooling unit was used. A temperature-frequency sweep pre-treatment

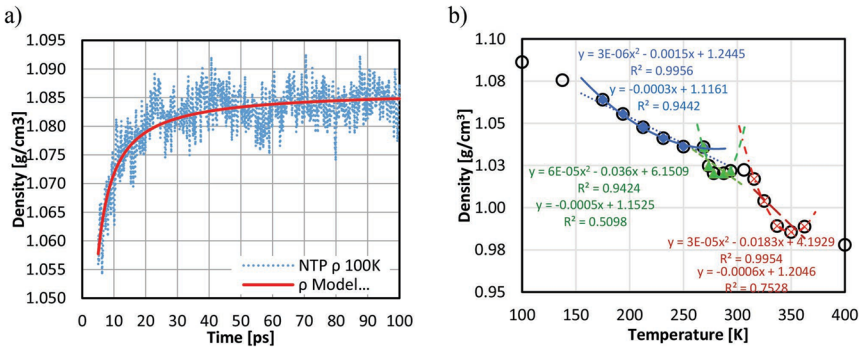

Figure 3. Estimation of T_g, a) single temperature ρ_∞ calculation using the frames dynamic relaxation fitting an asymptotic function, b) estimation of T_g by solving the intersection of two fitting functions.

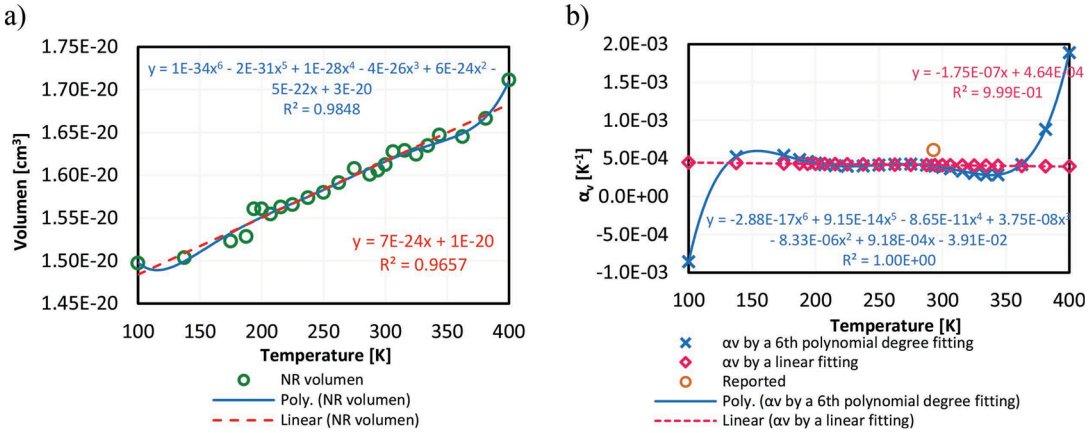

Figure 4. a) calculated volumes for NR, b) α_v for NR.

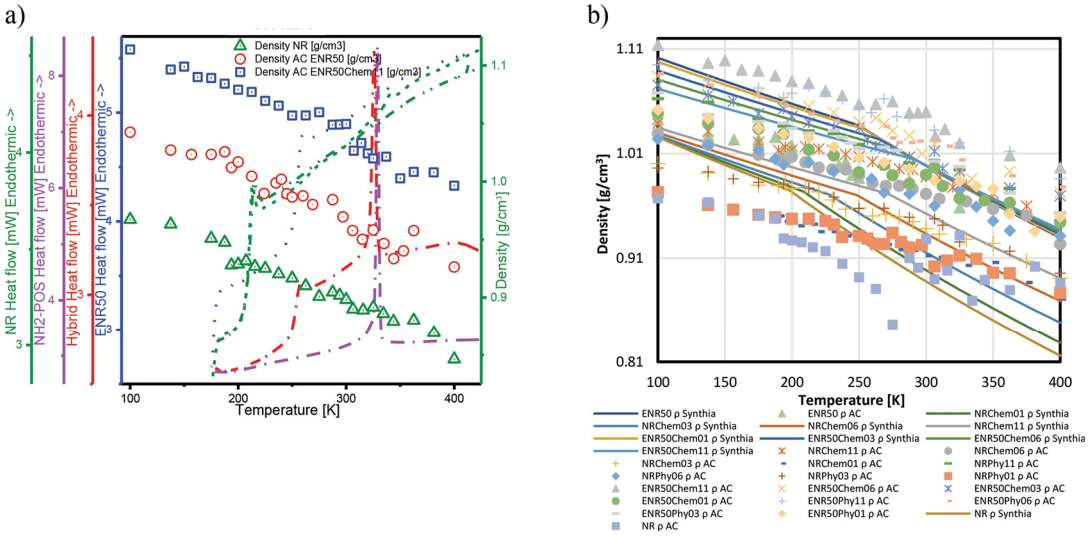

Figure 5. a) Amorphous cell density and DSC versus temperature plots for some selected materials and b) comparison of the density between AC and the topology method.

was carried out before each scan to remove any pre-existing thermo-mechanical history. Scans were performed with synthetic multi-frequency (0.5, 1, 2, 5, 10 Hz) compression mode, where all frequencies were applied simultaneously, and Fourier transform resolved by the instrument software. Pre-treatments were performed at a rate of 20 K min^{-1} from room temperature to 213 to 353 K and then cooled to approximately 115 K. The tests were carried out from 120 to 495 K at a rate of 5 K min^{-1} and the tan δ at 10 Hz frequency are reported because they more clearly show the transitions; see Figure 5b.

4. Results and Discussion

1. Indication of Reaction

Due to the nature of the materials and because it is a partial reaction, many peaks of interest are transposed or difficult to read (see **Figure 6**). The most important peaks that can be used to follow the reaction are the characteristic absorption peak of C–O–C stretching from the epoxy ring at 873 cm^{-1} and the 3300 cm^{-1}[26] that are attributed to the pendant hydroxyl. In Figure 6 from the ENR50 to the hybrid, it was observed that the signal 873 cm^{-1} decreased and the 3300 cm^{-1} increased; this is a good indication that a ring opening mono-substitution reaction of the epoxy group occurred and it was most likely due to the reaction with the amino group of the POS. These results combined with an increase in the glass transition temperature (T_g) observed in the DSC and DMA (See **Figure 7**) prove that a reaction between the ENR50 and the POS took place.

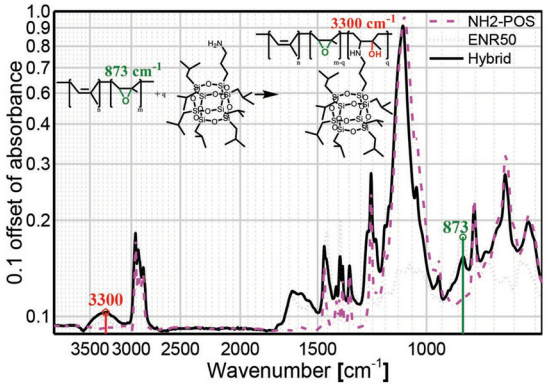

Figure 6. Fourier transform infrared (FTIR) spectra of precursors and hybrid.

4.2 Amorphous Cell

All T_g of the vinyl groups of ENR50 are higher than those of NR (see **Figure 8**a), if the T_g is below the intended use temperature, a material can be considered of interest for manufacture. For this reason, lower T_g is preferred. Under this consideration, ENR50Chem06, ENR50Chem11, and ENR50Phy06 are considered to have T_g above 273.15 K and the series of NRChem had lower T_g. This increase is correlated with the increase of the free volume (see **Table 2**) being proportional to the number or grafted POS attached to the polymeric chain.

A suitable parameter to evaluate the stiffness is the tensile or Young's modulus (E) and because it has a direct association with the stress–strain relationship, it is an indication of toughness in the linear elastic region. The incorporation of POS decreased E for ENR50 series. In the case of the NRChem series, most E did not change above 5%, but the NRChem11 had significant increments of about 200%; in the case of the NRPhy series at the lowest POS concentration (NRPhy01) had a higher E than its chemical counterpart (NRChem01) but the rest for the series were below the NRPhy series (see Figure 8b). The bulk modulus (B) indicates the resistance of the material to compression, in this context we found that the NR series was more resistant than the ENR50 series because most of them had a higher B (except for NRPhy06 and ENRPhy11, see

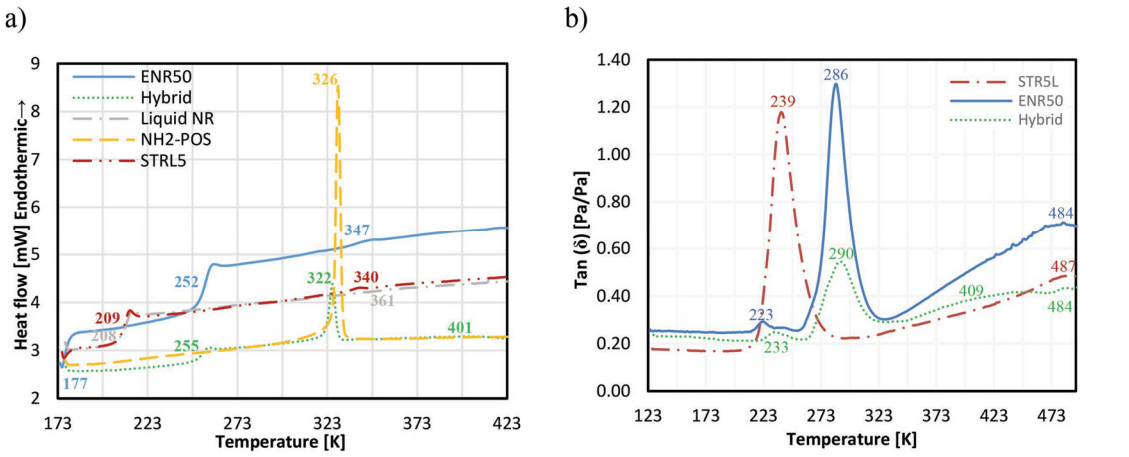

Figure 7. Precursor and hybrid nanocomposite data: a) DSC and b) DMA.

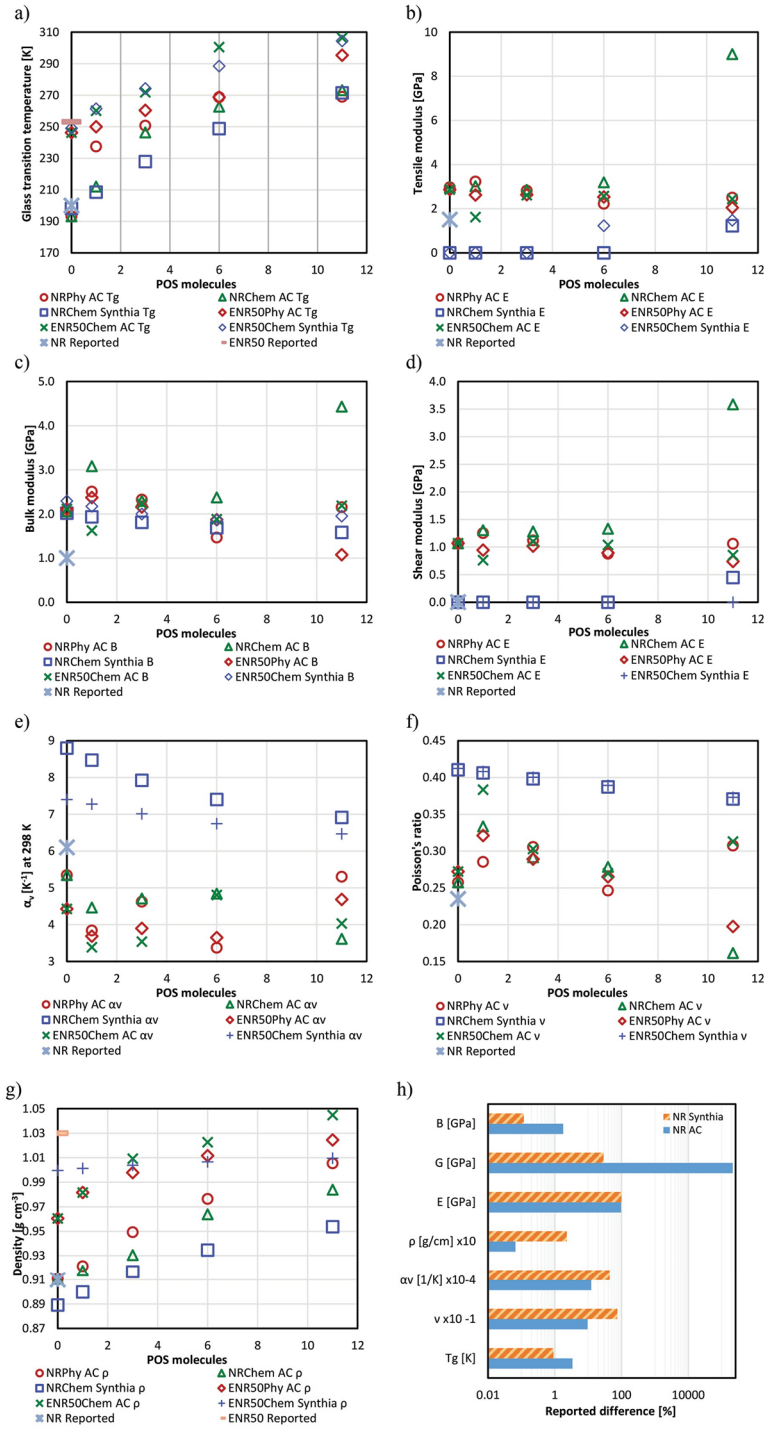

Figure 8. a–g) Topology method and amorphous cell calculated properties, h) difference of the properties with respect to the reported properties; all reported B, E, ρ, T_g, α_v, ν, and G for NR are found in refs. [19, 31, 32]; the reported ENR50 ρ, T_g are found in refs. .[33–35]

Figure 8c). Only the physical mixture at the lowest concentration of POS increased B above 10% for the ENR50 series. In the case of the NR series, there is a non-monotonical increase of B, having a remarkable 50% increase at the lowest POS concentration and a 110% increase at the highest POS concentration.

The shear modulus (G) is analogous to E or B but calculated over a "cut-off" stress and for this reason, an increase of G is desirable. The NR series, in general, has greater G than the precursor (NR), and this increase is more evident in the chemical hybrids than the physical mixtures, especially at the greatest concentration where it increased more than 200%. On the contrary, almost all ENR50 materials had G decreased compared with the precursor ENR50 (see Figure 8d).

The Poisson's ratio (ν) is a measure of material lateral expansion or contraction due to elongation, a lower value means less deformation under the same stress and hence a lower value is preferred. Addi- tion of POS, either physical or chemical increased or did not change significantly (change below 5%) ν, except for the highest physical POS concentration (see Figure 8e).

The volumetric thermal expansion (α_v) is an important parameter for the design and manufacture of large products or where materials are sensitive to small changes of dimension with temperature. Under this premise, it is desirable to keep α_v as low as possible to maintain dimensional stability during fabrication, for most of the ENR50 series addition of POS decreased α_v but we found a compromise between POS concentration and α_v for the NR series (see Figure 8f).

All ENR50 materials have greater density than the NR series, and density increased proportional to the number of POS, from a manufacturing consideration it is desirable to have a lower density to produce more items with the same mass. Therefore, similar products with lower density and the same mechanical properties are preferred. For these reasons, the NR series materials are more desirable than the ENR50 series (see Figure 8g).

In the context of the above results, at the lowest concentrations of POS into ENR50, we conclude that the use of a physical mixture is preferred over a chemical hybrid because it gives more desirable characteristics (or the same for the

Table 2. Complementary amorphous cell properties.

Material	POS molecules	Average velocity of sound [km s^{-1}]	λ Lamé constant [GPa]	μ Lamé constant [GPa]	Occupied volume [Å^3]	Free volume [Å^3]	Surface area [Å^2]	Compressibility [1/TPa]
NR AC	0	1.374	1.685	1.020	13 626.1	2277.7	3879.0	494.0
NRPhy01 AC	1	1.497	1.728	1.265	14 586.9	2747.2	4530.2	401.4
NRPhy03 AC	3	1.414	1.536	1.181	16 652.6	3202.0	5060.2	436.6
NRPhy06 AC	6	1.199	0.653	0.873	19 837.9	4557.1	6846.8	690.0
NRPhy11 AC	11	1.331	1.210	1.139	25 271.1	5119.2	7915.7	471.6
NRChem01 AC	1	1.587	1.841	1.438	14 485.1	2909.8	5409.9	329.8
NRChem03 AC	3	1.500	0.999	1.420	16 529.4	3801.9	6606.7	439.0
NRChem06 AC	6	1.488	1.271	1.403	19 752.5	4477.6	7823.9	423.3
NRChem11 AC	11	2.315	2.824	3.419	24 792.4	7278.1	10 025.3	226.7
ENR50 AC	0	1.342	1.548	1.046	11 683.4	5164.9	9103.3	476.7
ENR50Phy01 AC	1	1.310	1.856	0.969	12 601.0	5363.6	9033.4	432.3
ENR50Phy03 AC	3	1.311	1.563	1.041	14 401.7	6182.5	10 910.9	484.1
ENR50Phy06 AC	6	1.209	1.651	0.843	17 062.6	7548.3	12 969.4	549.2
ENR50Phy11 AC	11	1.082	0.913	0.696	21 397.5	12 452.2	16 774.2	976.6
ENR50Chem01 AC	1	1.218	0.844	0.979	12 595.7	5370.3	9484.2	698.7
ENR50Chem03 AC	3	1.350	1.252	1.182	14 381.3	5970.6	10 681.4	454.9
ENR50Chem06 AC	6	1.281	1.202	1.074	17 020.5	7323.8	12 816.0	573.5
ENR50Chem11 AC	11	1.236	1.701	0.931	21 431.5	9346.3	16 008.6	471.2

same ρ). At the highest POS concentration, the hybrid materials performed better than the composites, but in most cases when compared with the ENR50 alone, hybrids were less convenient.

For the NR series, at the highest concentration of POS, we found that chemical hybrids performed better than physical mixtures; the same applied to the lowest POS concentration excluding ν and α_v.

4.3. Topology Method

Results from the topology method gave a monotonical increase or decrease of the evaluated property by increments of POS concentration with the only exception being the ENR50Chem Synthia series with a minimum global concentration of six POS molecules. While this difference was small (5% with respect to 11 POS molecules), it is explained by increments in

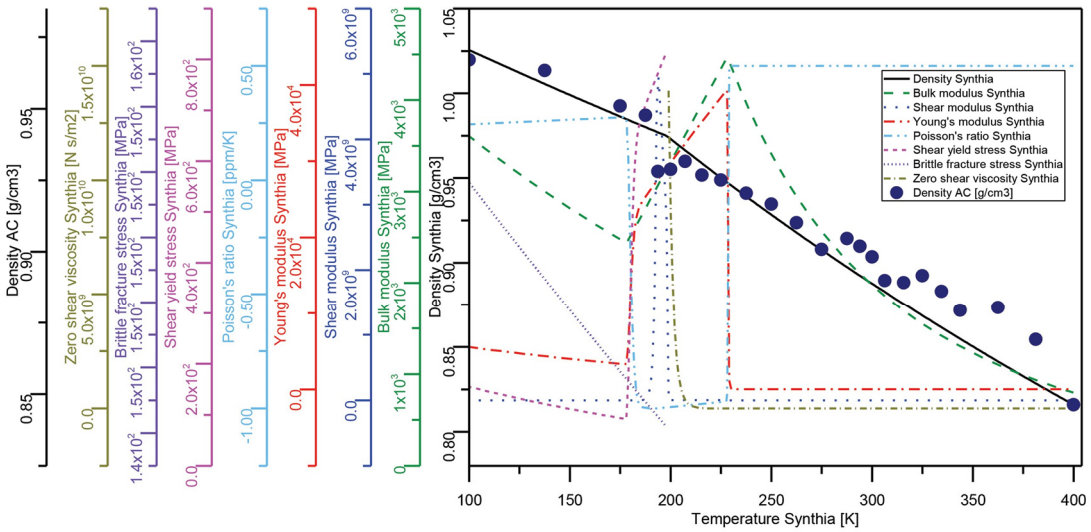

Figure 9. NR temperature dependency of some topology method properties and density from AC.

Table 3. Complementary topology method properties.

Material	POS molecules	Secondary relaxation temperature [K]	Temperature of half decomposition [K]	Permeability of O_2 [(cm^3 mm)/(m^2 day atm)]	Permeability of N_2 [(cm^3 mm)/(m^2 day atm)]	Permeability of CO_2 [(cm^3 mm)/(m^2 day atm)]
NR Synthia	0	115.3	658.8	1044.5	336.6	6146.6
NRChem01 Synthia	1	121.9	663.4	988.0	316.9	5785.1
NRChem03 Synthia	3	135.2	670.4	904.2	288.0	5252.6
NRChem06 Synthia	6	153.2	677.5	821.9	259.8	4733.8
NRChem11 Synthia	11	180.8	684.8	741.3	232.4	4230.8
ENR50 Synthia	0	140.0	660.9	419.4	125.6	2275.0
ENR50Chem01 Synthia	1	143.5	664.8	427.3	128.1	2321.6
ENR50Chem03 Synthia	3	152.2	671.0	432.8	129.9	2395.5
ENR50Chem06 Synthia	6	164.7	677.6	453.1	136.5	2474.5
ENR50Chem11 Synthia	11	185.7	684.5	467.2	141.1	2558.6

the tensile and shear modulus since they correlated as $2G(1+\nu) = E = 3B(1-2\nu)$. These results suggest that at these concentrations of POS the topology method did not produce adequate results (see Figure 8) just for this case.

4.4. Comparison of Reported Properties, Amorphous Cells, and the Group Contribution Method

Figure 8h suggests AC results in a better match of the reported natural rubber properties in four out of the seven evaluated properties. It is pertinent to note that the AC calculation takes significantly more time to predict properties, but it has an advantage over the group contribution method in predicting physical mixture properties.

4.5. T_g Comparison of Amorphous Cell and Group Contribution Method

As for many temperature dependent transitions, T_g occurs over a temperature range, using the density of the topology method shows a single T_g, but all other properties exhibit an interval (see **Figure 9**); the density of the amorphous cell shows an interval for T_g as well as other transitions, which indicate realistic modeling. We found that a second-degree polynomial better described the density between thermo-mechanical transitions than a linear correlation; see Figure 3b.

5. Conclusions

Pre-calculations to determine a minimum polymerization degree were used to predict equivalent thermo-mechanical properties to the realistic scale experimental system. They were proven to agree with most mechanical properties by comparing our results with those reported in the literature. It was found that the AC dynamics method matched most of the reported properties more than the topology method for NR. These pre-calculations were of great advantage in allowing reduction of computational time/cost. Another way to reduce computational cost was the use of an asymptotic function to calculate density at infinite relaxation time.

Diagrams of density versus temperature were used to calculate the glass transition temperatures and other thermal transitions. We found that second-degree polynomials better described the density between thermo-mechanical transitions rather than a linear correlation, the latter being the correlation most used in the literature,[36-40,19] the latter is true for the topology method where the correlation coefficient (R^2) was equal to 1.000.

Epoxidation of NR enhanced properties such as half-decomposition temperature, oil resistance[41] and decreased oxygen, carbon dioxide, and nitrogen permeability (see **Table 3**). While most of the changes were desirable, we found a compromise with mechanical properties, density, and glass transition temperature. Although it was necessary to epoxidize NR to graft chemically with POS (hybrid formation), the epoxidation degree was preferred to be low.

The reaction of ENR50 with POS was achieved. Addition of POS increased the density and glass transition temperature of all studied materials, and its concentration must be optimized for any intended use of hybrid or nanocomposite. When choosing between nanocomposites and hybrids for natural rubber, hybrids are preferred because they have more desirable properties than the nanocomposites. In the case of ENR50, consideration must be taken before choosing between hybrids or nanocomposites; for instance, hybrids are preferred over nanocomposites at high concentration of POS, but the glass transition temperatures were above standard temperature pressure conditions (STP). At the lowest POS concentration, ENR50-nanocomposites are preferred over hybrids, but the addition of POS decreased most of the mechanical properties.

Acknowledgements

The authors acknowledge Consejo Nacional de Ciencia y Tecnología de México (CONACYT) for a Ph.D. scholarship to Isaac Pardo 384575; Assoc. Prof. Winnie Kong Ing for kindly providing the ENR50 and CSIRO for the use of their software.

Conflict of Interest

The authors declare no conflict of interest.

Keywords

computer modeling, density, glass transition, nanocomposite, rubber

Received: April 26, 2018
Revised: September 11, 2018
Published online:

1 C.-W. Lee, T. Hwang, G.-Y. Nam, J.-P. Hong, D.-A. Lee, J.-S. Oh, S. B. Kwak, S.-H. Lee, W.-S. Lee, K.-M. Yang, *Composites, Part A* **2011**, *42*, 1826.
2 B. Omnès, S. Thuillier, P. Pilvin, Y. Grohens, S. Gillet, *Composites, Part A* **2008**, *39*, 1141.
3 D. Ponnamma, R. Ramachandran, S. Hussain, R. Rajaraman, G. Amarendra, K. Varughese, S. Thomas, *Composites, Part A* **2015**, *77*, 164.
4 J. O. Jo, P. Saha, N. G. Kim, C. C. Ho, J. K. Kim, *Mater. Des.* **2015**, *83*, 777.
5 I. Skeist, *Handbook of Adhesives*, Springer Science & Business Media New York, NY **2012**.
6 K. Gazeley, W. Wake, *Handbook of Adhesives*, Springer Boston, MA **1990**, p. 167.
7 G. Zhao, L. Shi, D. Zhang, X. Feng, S. Yuan, J. Zhuo, *Mater. Des.* **2012**, *35*, 847.
8 M. Arroyo, M. Lopez-Manchado, J. Valentin, J. Carretero, *Compos. Sci. Technol.* **2007**, *67*, 1330.
9 R. Ketkaew, Y. Tantirungrotechai, *Macromol. Theory Simul.* **2018**, *27*, 1700093.
10 R. Rajasekar, K. Pal, G. Heinrich, A. Das, C. Das, *Mater. Des.* **2009**, *30*, 3839.
11 H. Ismail, A. Ramly, N. Othman, *J. Appl. Polym. Sci.* **2013**, *128*, 2433.
12 L. Pothen, C. H. Chan, S. Thomas, *Natural Rubber Materials, Volume 2-Composites and Nanocomposites*, Royal Society of Chemistry UK **2013**.
13 A. S. Hashim, N. Kawabata, S. Kohjiya, *J. Sol-Gel Sci. Technol.* **1995**, *5*, 211.
14 N. Lopattananon, D. Jitkalong, M. Seadan, *J. Appl. Polym. Sci.* **2011**, *120*, 3242.
15 M. Haq, R. Burgueño, A. K. Mohanty, M. Misra, *Compos. Sci. Technol.* **2008**, *68*, 3344.
16 M. Huda, L. Drzal, A. Mohanty, M. Misra, *Composites, Part B* **2007**, *38*, 367.
17 Y. Zhao, X. Jiang, X. Zhang, L. Hou, *Polym. Compos.* **2015**.
18 D. Porter, *Group Interaction Modelling of Polymer Properties*, CRC Press USA **1995**.
19 P. Sharma, S. Roy, H. A. Karimi-Varzaneh, *J. Phys. Chem. B* **2016**, *120*, 1367.
20 N. E. Moe, M. Ediger, *Macromolecules* **1995**, *28*, 2329.
21 V. Mittal, *Modeling and Prediction of Polymer Nanocomposite Properties*, John Wiley & Sons Germany **2012**.
22 C. Wu, *Macromol. Theory Simul.* **2018**, *27*, 1700066.
23 A. C. Balazs, T. Emrick, T. P. Russell, *Science* **2006**, *314*, 1107.
24 J. Bicerano, *Prediction of Polymer Properties*, CRC Press USA **2002**.
25 B. R. Gelin, *Molecular Modeling of Polymer Structures and Properties*, Hanser Publishers Germany **1994**.
26 Q. Lin, Y. Lu, W. Ren, Y. Zhang, *RSC Adv.* **2015**, *5*, 90031.
[27] D. Lloyd, *Mater. Des.* **1991**, *12*, 139.
28 C. Chan, H. Kammer, *J. Appl. Polym. Sci.* **2008**, *110*, 424.
29 C. H. Chan, H.-W. Kammer, *Ionics* **2015**, *21*, 927.
30 H. Sun, Z. Jin, C. Yang, R. L. Akkermans, S. H. Robertson, N. A. Spenley, S. Miller, S. M. Todd, *J. Mol. Model.* **2016**, *22*, 1.
31 H. Afifi, A. El-Wakil, *Polym.-Plast. Technol. Eng.* **2008**, *47*, 1032.
32 J. H. Yoon, I. H. Yang, U. C. Jeong, K. H. Chung, J. Y. Lee, J. E. Oh, *Polym. Eng. Sci.* **2013**, *53*, 992.
33 B. Ellis, R. Smith, *Polymers: A Property Database*, CRC Press Boca Raton, FL **2008**.
34 P. Wanchart, Bonding of natural rubber and epoxidized natural rubber to poly (ethylene terephthalate). Department of Polymer Science. Ohio, USA, University of Akron. Doctor of Philosophy: 180 **2000**.
35 D. T. C. Ang, Y. K. Khong, S. N. Gan, *Prog. Org. Coat.* **2013**, *76*, 705.
36 J.-H. Sul, B. G. Prusty, D. W. Kelly, *Composites, Part A* **2014**, *65*, 64.
37 A. Soldera, N. Metatla, *Composites, Part A* **2005**, *36*, 521.
38 P. N. Patrone, A. Dienstfrey, A. R. Browning, S. Tucker, S. Christensen, *Polymer* **2016**, *87*, 246.
39 R. Sarangapani, S. T. Reddy, A. K. Sikder, *J. Mol. Graphics Modell.* **2015**, *57*, 114.
40 T. L. Chantawansri, I.-C. Yeh, A. J. Hsieh, *Polymer* **2015**, *81*, 50.
41 T. Johnson, S. Thomas, *Polymer* **2000**, *41*, 7511.